THE NONLINEAR SEISMIC RESPONSE OF TALL SHEAR WALL STRUCTURES

A thesis
submitted in partial fulfilment of the
requirements for the Degree of
Doctor of Philosophy in Civil Engineering
at the University of Canterbury

by

ROY GEORGE TAYLOR

University of Canterbury,
Christchurch, New Zealand
1977

ABSTRACT

New building codes are tending to place considerable value on the use of deterministic dynamic analyses as a means of assessing the ability of engineering structures to withstand severe seismic ground motions. An investigation of the more important factors affecting such an analysis, derived specifically for tall ductile shear walls, was undertaken. Initial considerations included the selection, and the derivation where necessary, of suitable structural idealisations, material constitutive relationships and numerical integration schemes, leading to an analysis which was sufficiently representative and economically viable. The basic problem of program verification followed. Difficulties in ensuring that reliable accurate results were being obtained arose when certain types of structural idealisation and integration procedures were used. When these problems, which initially handicapped confident application of the program, had been satisfactorily resolved a sensitivity study of a realistic structure was performed. Results presented illustrate important characteristics of structural behaviour and the capabilities of the implemented analysis. Because it is vital that theoretical idealisations of reinforced concrete components should be based on experimental evidence, the case of slab coupling of shear walls was investigated with a sequence of reinforced concrete models. Interest was first concentrated on aspects of slab design, especially the control of punching shear within the range of deformations likely to occur in a seismic disturbance. Limited attempts were made to match standard idealised hysteretic relationships to the experimental responses to allow an improved dynamic analysis of structures incorporating these components. Finally, a pilot test of a slab coupling unit with a monolithically cast shallow beam was performed.

ACKNOWLEDGEMENTS

The research for this report was carried out in the Department of Civil Engineering, University of Canterbury, of which Professor H.J. Hopkins is Head.

Grateful acknowledgement is made of the support and guidance given to the candidate by the supervisors of his studies, Professor T. Paulay and Dr. A.J. Carr, by members of the staff of the Department of Civil Engineering, and by fellow students.

Further assistance received from the following people is thankfully acknowledged:

Messrs. J. Sheard and G. Sims and the other technicians who worked on this project for their careful preparation of the test equipment and test specimens and for their assistance during testing.

Mr. H. Patterson for photographic work.

Mrs. A. Watt for typing this manuscript.

Mr. R. Powell for tracing many diagrams.

Mr. H. Watson for arranging for the purchase of materials and equipment.

The staff of the University's Computer Centre who made this project possible with their co-operation and friendly service.

This study was made possible by a generous financial contribution from the Ministry of Works and Development.

CONTENTS

LIST OF FIGURES

Page

LIST OF TABLES

LIST OF SYMBOLS

In the following list of symbols subscripts and/or superscripts have been left off some symbols. In these cases their use follows accepted patterns in signifying members of a series, the members of a vector or the elements of a matrix. Further definitions which relate to Appendix A are listed there.

Symbol	
b_c	variable thickness of concrete in section
b_s	variable thickness of steel in section
e_x	eccentricity of stiffness centroid from reference axis
f	spring stiffness
n	number of time steps
q	nodal displacement
$\bar{q}$	nodal displacement for linear increment
$\delta\bar{q}$	arbitrary displacement
q_1, q_2	nodal displacement for transformed system
t	time
u	displacement
$\dot{u}$	velocity
$\ddot{u}$	acceleration
$\ddot{u}_g$	base acceleration
v	transverse beam displacement used in element stiffness derivation
x	distance along length of beam element
y_e	distance from edge of section to stiffness centroid
z	dimensionless distance (z = x/H)
A	equivalent area of section
B	strain displacement relationship for element A
B_1	modified strain displacement relationship for element A
B_2	modified strain displacement relationship for element A
C	damping coefficient
C_o	tangent constitutive matrix
C_s	secant constitutive matrix
D	length of wall
E	Young's modulus of elasticity
E_c	Young's modulus of concrete
E_o	Young's modulus of elasticity relating to an equivalent section
E_s	secant modulus
	Young's modulus of steel

Symbol	
E_T	tangent modulus
Fe	predicted force at the end of an increment which is consistent with the linearisation
Fr	actually resisted forces computed from stresses
Fxs	excess force or out-of-balance force
H	plastic hinge length
I	moment of inertia
K	stiffness
K_o	tangent stiffness at beginning of increment
K_s	secant stiffness
$\bar{K}$	7 x 7 stiffness for original element A
K_2	simplified stiffness for element A
L	length of beam element
M	mass
N	element A displacement function
N_u	axial displacement function
N_v	transverse displacement function
P	initially applied external static loads
Q	dynamic force of the Newmark $\beta = \frac{1}{4}$ method
R	generalised forcing function
Se	predicted element force consistent with a linearised increment
Sr	actually resisted element force at end of an increment
T_i	transformation for i = 1,4
T_g	combined transformation to global system
U	potential energy
Z	first moment of area of the equivalent section
α	angle
	factor applied to mass to represent damping
β	Newmark's integration constant
	factor applied to stiffness to represent damping
δ	denotes a relatively small quantity
ϵ	angle of rotation of plastic hinge
	strain
ϵ_o	strain at beginning of current increment
θ	angle
ρ	radius of curvature of equivalent plastic hinge length
σ	stress
σ_c	concrete stress
σ_s	steel stress
ω	natural circular frequency
λ	fraction of critical damping

Symbols

Δ	denotes an incremental part of the quantity it precedes
$\dot{}, \ddot{}$	denote the first and second derivatives with respect to time
{ }	normally denotes a vector
[ ]	normally denotes a matrix

CHAPTER ONE

INTRODUCTION AND SCOPE OF RESEARCH

1.1 INTRODUCTION

Traditionally, rigid jointed frame structures have been accepted by engineers as most suitable for resisting seismic disturbances in a ductile manner. This was probably because their structural behaviour was more clearly understood and the analysis techniques were more fully developed for these than for other structural types.

More recently, interest in damage control, especially in the reduction of non-structural damage, has fostered increased interest in shear wall structures. One of the outstanding demonstrations of this was the performance of the Banco de America building, an 18-storey shear core structure, in comparison with a nearby similar size frame structure during the 1972 earthquake in Managua, Nicaragua [1,2]. The comparatively light total repair cost and the rational seismic behaviour of the coupled shear wall structure has resulted in a more general acceptance of these structures as highly efficient and reliable lateral load resisting components.

In 1965 a long term research project examining shear wall structures was initiated at the University of Canterbury. The experimental investigations consisted of a selective series of projects aimed at examining, understanding and improving the performance of various components of shear walls. Studies related to conventional deep coupling beams [3], diagonally reinforced deep coupling beams [3,4], shear strength of walls [5], diagonal cracking in tension walls [6], and construction joints in walls [7] have been undertaken. Numerous problems have been identified and improved solutions were suggested for the design of these individual components. In a major experimental program that followed the previous findings were combined to construct complete one-quarter scale structural models of seven-storey shear wall structures [8,9], the testing of which demonstrated their strength and ductility.

Significant progress has been made and is continuing with current similar tests [10]. However, at the end of any static testing program, no matter how comprehensive, the following three unanswered questions will remain:

i) What history of nonlinear deformation can be expected at critical locations during a major seismic disturbance?

ii) Which structural geometry, strength and stiffness configurations will give optimum performance when subjected to particular types of earthquakes?

iii) What design criteria, including limit state analysis procedures and detailing requirements, are necessary to ensure a design for a safe, reliable structure?

If a sufficiently refined and realistic structural idealisation for a time history dynamic analysis could be used it should provide valuable information regarding the above problems.

A theoretical study of the nonlinear structural dynamics of frame structures has led to the development of a general purpose computer program [12] which has provided a useful base on which to develop an analysis procedure for shear wall structures.

The research undertaken in this project has been directed towards answering the above three questions. It represents a continuation and merging of the two relevant fields of previous research as outlined above.

1.2 PHILOSOPHY OF DYNAMIC RESPONSE PREDICTION

The analysis of structural systems subjected to seismic loading may be said to be an empirical science; one based upon observation and experiment. As such, it is supposed to be verifiable, that is, capable of calculating beforehand results subsequently confirmed by observation and experiment. In fact it is only partially verifiable. That is to say, a certain displacement history will exist if a certain building, possessing certain mass, stiffness and damping characteristics, is subjected to a particular ground motion. In order to make absolute predictions of response, deterministic rather than probabilistic information relating the relevant structural variables is required.

In assessing the response results presented in this thesis scientific caution must be applied. It is important to avoid confusion between what is inferred and what is in fact determined. Although numerical values are presented for a number of analyses performed in the course of this study, only trends and characteristic behaviour patterns,

derived from a probabilistic assessment of a large body of results, should be accepted as reliable.

The role of approximate, but practical, analyses in understanding structural behaviour is a vital one. The importance of knowledge gained by mathematical model prediction is that it enables us to progress beyond the limits of our present experience. In view of the narrow range of our immediate experience (derived from model tests and actual seismic events) these analytical results are vital, but until the phenomena involved are more fully understood much of our knowledge must remain approximate.

1.3 THE DYNAMIC RESPONSE PROBLEM AND THE SCOPE OF THIS INVESTIGATION

It appears that three distinct problems, belonging to different studies and requiring different methods for their solution, require attention in any effort to predict nonlinear structural responses. There is a problem of determining an appropriate base acceleration function, a problem of selecting a representative structural idealisation and a problem of establishing a reliable piecewise numerical integration technique. Of these three, the base acceleration problem remains poorly defined and difficult to deal with; the numerical integration problem is partially solved in that reliable techniques are now available; the problem of structural idealisation, particularly the representation of shear walls, has often been oversimplified and consequently many models are of limited applicability.

In the above context the scope of this work is briefly outlined as follows:

a) Base acceleration

The selection of an earthquake record for a deterministic analysis is a highly subjective process and although about 15 strong motion historical records are available at the present time, ground motion intensity and characteristics for a particular shock vary widely with distance from the epicentre and differing geological conditions. Moreover, repeatability at a particular site cannot be assured so that an historical record may not be representative of a future event. Further brief reference is made to earthquake record selection in Chapter 9 where the analysis of a typical structure is undertaken.

b) Numerical integration

Newmark's constant average acceleration scheme [11] has been shown by many investigators to provide accurate, economical solutions for a wide range of problems. Most studies on numerical integration, however, examine elastic structures to gauge the techniques. In fact, it is probable that the effects of a variable structural stiffness upon the accuracy and stability of the integration scheme will be significant. Adaption and implementation of iterative and out-of-phase equilibrium correction procedures, to accommodate the highly interactive nonlinear effects, proved to be important developments in the integration of non-linear problems.

It has been suggested [12] that an explicit numerical integration scheme may provide a more efficient means of solution to continuously variable nonlinear problems than implicit integration schemes (see Chapter 5) which require numerous stiffness matrix operations. An exploratory study was performed to gauge the usefulness of explicit integration compared with implicit methods for the analysis of shear walls.

c) Structural idealisation

A range of structural models varying in detail of modelling and complexity may be considered. There are the simple and efficient pure elastic beam and lamina models which lead to economical solutions which have been extensively used in the past [13]. An elastic approximation, however, cannot always provide reliable results in a dynamic analysis. Nonlinear static analyses using refined isoparametric finite element models, with superimposed concrete and steel elements, have also been performed [14]. This extremely detailed modelling is considered to represent the forefront of present feasibility for nonlinear static analyses but is, because of the computational effort required, beyond the limits of practicability for a full scale dynamic analysis. However, it should be possible to find, somewhere between these extremes, a practical model which is sufficiently realistic in its idealisation of shear walls.

A major part of the research effort reported here was absorbed in identifying suitable elements, implementing them in a dynamic analysis program, and examining their merits. It must be recognised that any mathematical model, based on approximating assumptions, cannot be proved by experience with its use; only recourse to experimental evidence, not inhibited by approximating simplification but embodying all the complex

phenomena of the prototype, can provide verification. One example of such an experimental model investigation was undertaken here where the slab coupling of shear walls was considered.

1.4 FORMAT

Chapters 2 - 9 of this thesis present theoretical studies in which a refined analysis, intended for the dynamic analysis of shear walls, is discussed while in Chapters 10 - 12 the experimental investigation of shear wall coupling systems is described together with attempts to calibrate simplified mathematical models. A summary and suggestions for future research are presented in Chapter 13.

CHAPTER TWO

COMPUTER PROGRAM RELIABILITY AND VERIFICATION

2.1 INTRODUCTION

With the development of larger and more complex dynamic analysis computer programs, the problem of program verification [81] becomes increasingly more difficult. Even though a program is based on generally accepted theory it cannot be verified with just normal use and a review of the printout. Certainly any major errors will be detected with use of the program, but any perturbation which does not disturb the response results beyond the threshold of obvious error may not be detected by the user.

There are two relative situations which are widely recognised in program verification: One where the program has been written in-house and the programmer is in direct contact with all program use; the other where the program has been obtained externally and the users, typically, have only limited knowledge of the program structure and often do not fully appreciate any limitations of the mathematical models. The first situation is the one applicable to this development and it is, clearly, the most reliable, particularly when different structural types and newly developed models are considered. The second situation in the case of any nonlinear structural dynamics program must, with the knowledge available at present, be of limited reliability. The basic problems exposed by Sharpe [12] and the inherent but undefined approximations in recently published shear wall response studies [15,16], attest to this fact. This second situation is, unfortunately, the one in which most designers are likely to be placed when attempting nonlinear dynamic analyses.

2.2 VERIFICATION PROCEDURES

Many verification procedures, particularly those applied to programs written for theses, are haphazard processes at their best. The program is usually written to solve a problem of particular interest, but it may be computationally possible to apply the program to a wide range of problems. Meanwhile, it is probable that the program was verified only for the parameter ranges of interest, and therefore it is possible that the mathematical model, in conjunction with the solution technique, may only

be applicable to the original problem. Oversight of this second simple but fundamental principle would appear to be particularly prevalent in the application of nonlinear frame analyses to shear wall structures.

In an effort to ensure a high level of verification the following general procedures were involved:

i) Independent subroutine strings were used to compute the stiffness of different element types.

ii) Stiffness parameters were monitored to ensure that each element was functioning correctly as nonlinear excursions occurred.

iii) Cross checking was achieved by re-analysing a structure with five different elements available in the program.

iv) Convergence studies were carried out with refinement of the idealisation.

v) Convergence studies with time step reduction to examine the equilibrium correction techniques and overall integration accuracy were performed.

vi) Three different, completely independent programs were used to compare damped elastic responses computed by analytic explicit integration and implicit integration methods.

vii) Comparisons between analyses were made by matching accurately plotted graphs rather than by comparing point values. Many of the actual comparisons on which important conclusions are based are presented in this report.

More specific consideration in achieving these checks is given in the next section.

2.3 SELECTION OF TEST STRUCTURES

Program verification, idealisation accuracy and integration stability assessment are, by their nature, difficult when the proposed dynamic analysis (see Chapter 3) is undertaken. Only a carefully planned, methodical progression from simple verifiable examples to large scale analyses can produce a reliable program.

The procedure adopted commences with a highly simplified structure, used as a debugging tool, verifying the basic operation of the program. This was the simple elastic portal frame structure, used in Chapter 5 to confirm and test the numerical integration schemes. Different, specialised and

increasingly more complex structures were then used to examine various aspects of the integration process. As the structures became more complex, interpretation became more difficult and monitoring of parameters became more expensive.

Three further basic test structures (figures 2.1 to 2.4) were derived and analysed repetitively. Of these three, structure A was intended primarily for the numerical integration investigation and a single simple bilinear element was used exclusively; structure B, a modification of structure A, was derived specifically to allow comparison between the different idealisations, although a limited integration accuracy study was also performed; structure C was designed as a realistic example to investigate accuracy and stability criteria in the total analysis context.

A more detailed description of these structures is given as follows:

(a) Structure A

This structure (figure 2.1) comprises a single elasto-plastic element representing a cantilever with all yield occurring at the base. The following structural attributes represent an attempt to achieve simplicity of the response and confirmation of the numerical integration:

i) A single element structure was chosen for simplicity in result interpretation.

ii) Yield levels and stiffness values were selected so as to ensure a vigorous response in the nonlinear range.

iii) The longest natural period of the structure was shorter than is typical for tall shear wall structures.

iv) A short period mode was included to identify its role in the response.

v) Modification of the basic structure A was made to obtain structure A1 (figure 2.2) which possesses an identical first mode period with the higher translational mode suppressed.

(b) Structure B

This structure (figure 2.3) is similar to structure A with plastic hinging allowed only in the lower element and it retains most of the desirable features except i) and v) above. The additional features that were incorporated at the expense of some simplicity are as follows:

i) The two element idealisations with a small lower element was intended to be representative of an element in a refined idealisation environment.

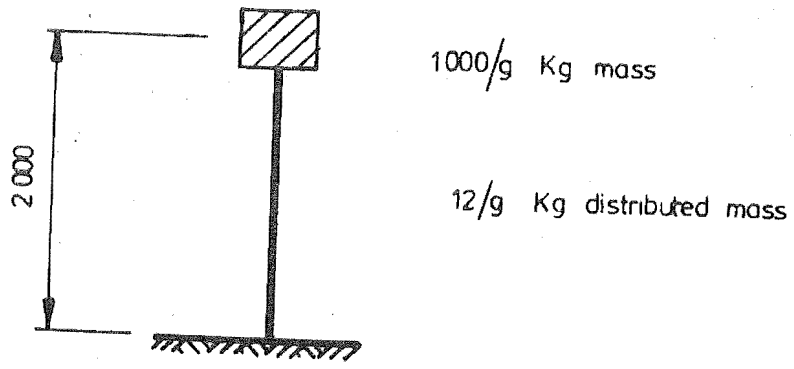

Details of Structure

i) Inertia $I = 3.6 \times 10^{-7}\ m^4$.

ii) Area $A = 4.8 \times 10^{-4}\ m^2$.

iii) Yield Moment 600 Nm.

iv) Damping - 10% of critical on first two modes.

v) Natural periods of two translational modes: 0.43 sec., 0.0062 sec.

FIGURE 2.1 : STRUCTURE A

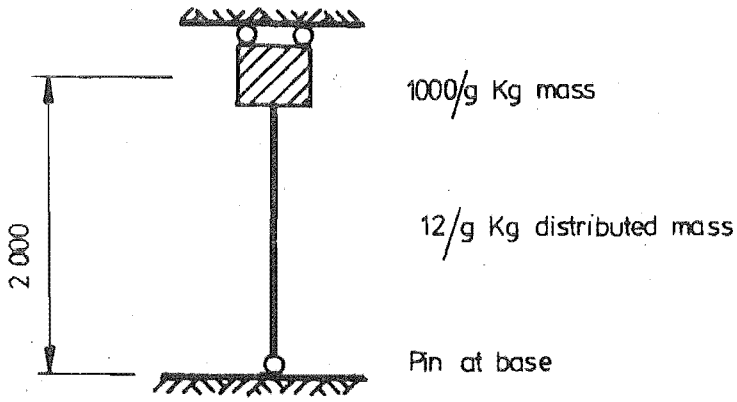

Details of Structure

i) Inertia $I = 3.6 \times 10^{-7}\ m^4$.

ii) Area $A = 4.8 \times 10^{-4} m^2$.

iii) Yield Moment 600 Nm.

iv) Damping - 10% on first mode.

v) Natural period 0.43 sec.

FIGURE 2.2 : STRUCTURE A1

ii) Additional short period modes were incorporated and these could be controlled, to some extent, by nodal mass assignment.

(c) Structure C

Finally, a ten-storey reinforced concrete cantilever was examined (figure 2.4). This structure, considered to be representative of a typical shear wall, was proportioned to make definite demands on the numerical technique in areas where weakness had previously been encountered. It has the following outstanding characteristics:

i) Only elements of the lower two floors allowed nonlinear behaviour. This resulted in a structure which was easily analysed and that provided an acceptable environment in which to test selected elements.

ii) Equal steel areas in each face of the wall were provided. In the absence of dead lead this can result in large and sudden changes in axial stiffness. Therefore, the model allows stringent testing of equilibrium correction techniques.

iii) The selected relatively long first mode period, together with a short period base motion, causes a series of nonlinear waves to propagate up the structure.

Although this structure has a long first natural period (2.46 seconds) consideration of alternative versions, with reduced masses and longest natural periods of 1.61 and 1.12 seconds, revealed the original structure to make the most severe demands on equilibrium correction techniques.

2.4 SELECTION OF BASE MOTIONS

For the most part, while testing the above three structures, the simple arbitrary ground motions I1 and I2, shown in figure 2.5, were used. They proved ideally suited to this portion of the investigation for the following reasons:

i) The cyclic but simple functions give an easily assessable response.

ii) A vigorous initial excitation of the structure into the nonlinear range required considerable equilibrium correction.

iii) Zero excitation is present during the final portion of the response so that, as inertial and damping forces diminished, a simple equilibrium check became available.

iv) Acceleration functions were shown to be capable of being accurately integrated with the time steps used.

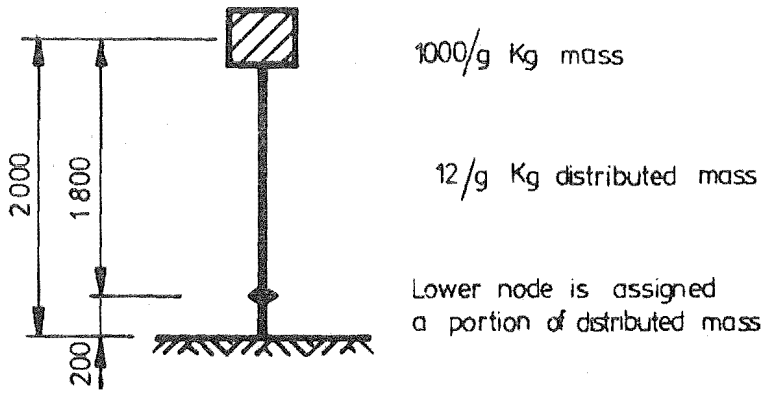

Details of Structure

i) Inertia $I = 3.6 \times 10^{-7}$ m^4.

ii) Area $A = 4.8 \times 10^{-4}$ m^2.

iii) Yield Moment 600 N-m.

iv) Damping - 10% of critical on first two modes.

v) Natural periods of translational modes - 0.43 , 0.098 , 0.0067 , 0.032 sec.

FIGURE 2.3 : STRUCTURE B

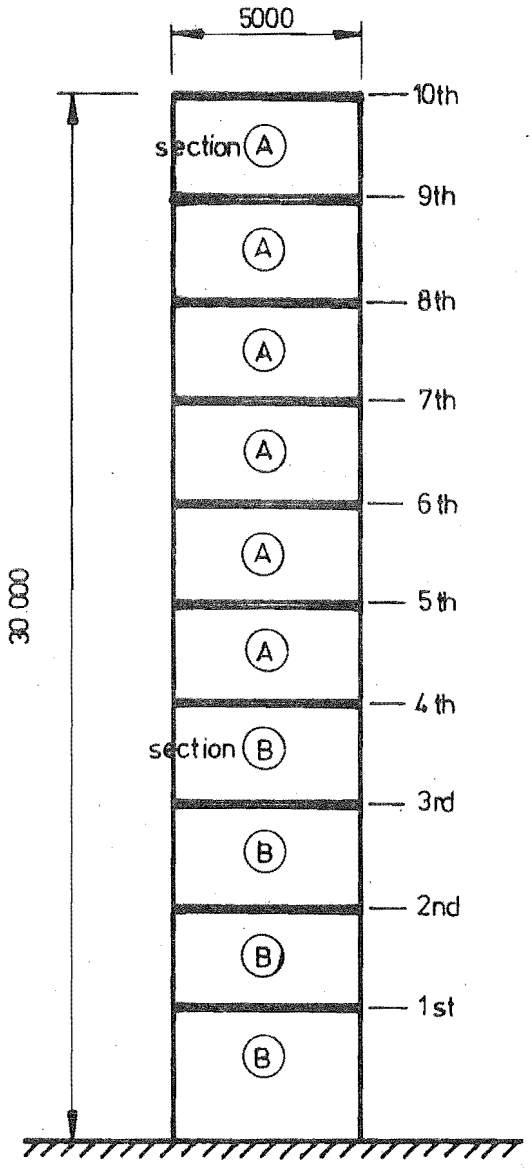

a) Properties of shearwall

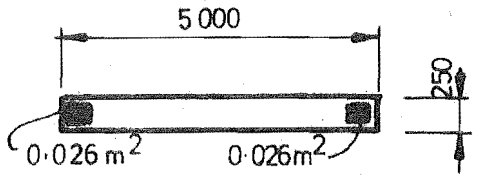

(b) Section (A)

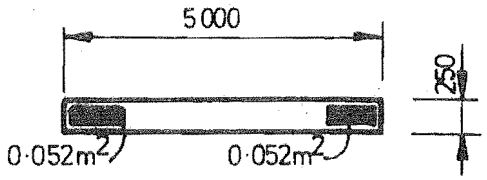

(c) Section (B)

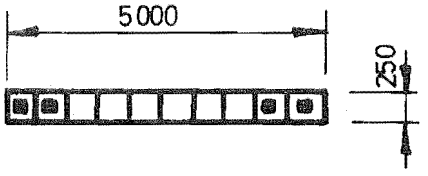

(d) Section (B) idealisation (Numerical integration on lower two floors only)

Details of Structure

i) Steel Properties:
Yield Stress = 280 MPa
Young's Modulus E = 200,000 MPa.

ii) Concrete Properties:
Crushing Strength f'_c = 21 MPa
Modular Ratio n = 10.

iii) Lumped Mass at Each Floor - 560 Mg.

iv) Damping - 10% of critical on first two natural modes.

v) Periods of first two natural modes:
2.46 sec., 0.42 sec.

FIGURE 2.4 : STRUCTURE C

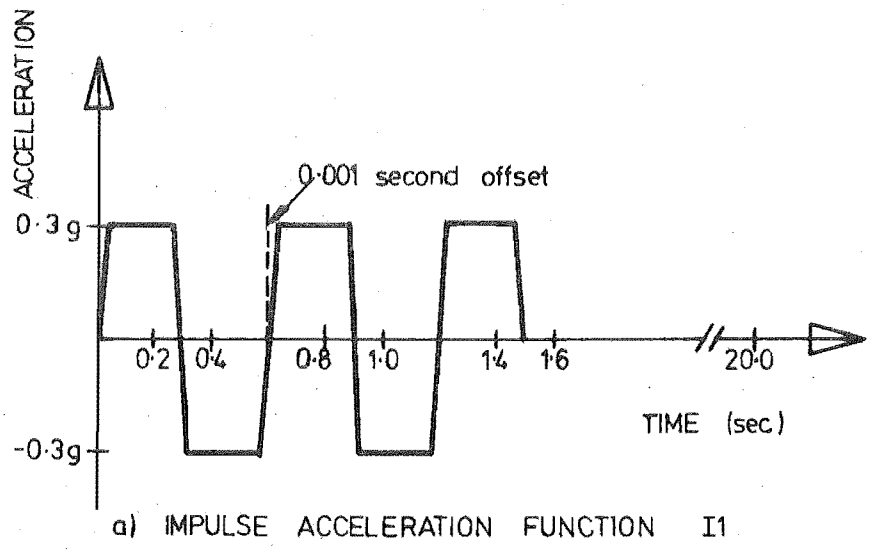

a) IMPULSE ACCELERATION FUNCTION I1

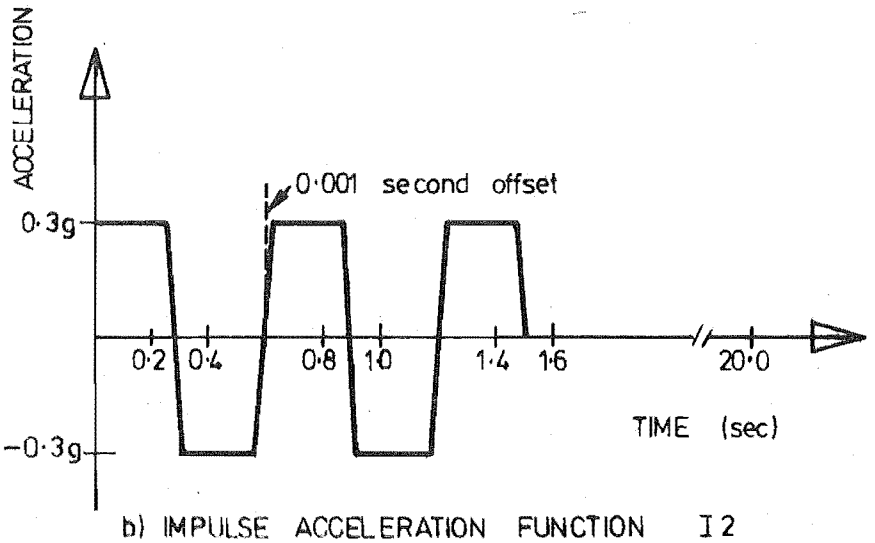

b) IMPULSE ACCELERATION FUNCTION I 2

FIGURE 2.5 : IMPULSE FUNCTIONS

v) Acceleration functions I1 and I2 were also found to be slightly more difficult to integrate with structure A and considerably more difficult with structure C than was the El Centro 1940 N-S ground motion. Thus conclusions drawn from the use of the acceleration functions I1 and I2 and applied to the integration of recorded ground motions should be conservative in most cases.

2.5 EXTENT OF VERIFICATION

Considerable efforts have been made to ensure that, using the program developed, reliable results could be obtained for any shear wall for which a flexural model is appropriate. The actual verification process is spread throughout the following six chapters of this thesis and is related to particular developments as they are discussed. The structures and acceleration functions described represent a small portion of the test runs actually performed, but they are considered to be sufficient to illustrate the approach taken in this study, some of the major problems encountered and, of course, to confirm any conclusions drawn. However, the program must still be strictly classified as a research tool and although it is based upon sound, versatile theory being highly suitable for future development, it is without the benefit of widespread application. Prospective users are warned that this, and other developmental nonlinear dynamic analysis programs, should be used with caution, preferably with understanding of the theory involved and with some knowledge of the program structure. Certainly, a critical assessment of any results is essential.

CHAPTER THREE

STRUCTURAL IDEALISATION OF A SLENDER SHEAR WALL

3.1 INTRODUCTION

The realistic determination of the response of reinforced concrete structures requires knowledge of the inelastic behaviour of the component materials, as well as the ability to incorporate this information into a rational analysis of real structures. Inevitably, an acceptable compromise between reality and computational simplicity is required.

While numerous successful nonlinear dynamic analyses have been performed with different structures, only a small portion of the literature on shear walls describes dynamic response determination. This is particularly true of nonlinear responses [1, 15, 16, 17] and in only one of these [15] is the structural model thoroughly described. Meanwhile, a considerable number of nonlinear static analyses, applicable to shear walls, have been performed, in some cases to quite high degrees of refinement [18,19,20,21,22,23,24,25].

The particular structural type of interest is the slender shear wall, defined in the following section, for which the selected elements have been specifically derived. Consideration has been given to a variety of idealisations, together with previous experimental and analytic work, to select a group of elements for further detailed investigations to achieve an improved idealisation of the structure [26,27].

3.2 FUNDAMENTALS OF STRUCTURAL BEHAVIOUR

For the purposes of this study the slender shear wall may be a single cantilever or it may consist of two or more coupled walls which in each case should have a height to length ratio of 3 or more so that flexural theory is directly applicable. Only those structures exhibiting a ductile moment failure mechanism, where shear, bond slip and other types of brittle failure are suppressed, are readily amenable to the proposed inelastic analysis.

The following distinctive features of the structural type are significant when a dynamic response investigation is contemplated:

i) Each wall tends to deform as a single cantilever exhibiting overall simplicity of structural action.

ii) Coupling beams exhibit antisymmetric deformation patterns such that nonlinear shear and flexural deformations may be uniquely allowed for with simple spring hinges.

iii) Substantial shear forces of alternating sense, transmitted from coupling beams, will have large and diverse effects on the moment-curvature relationships of complex wall sections.

iv) For elastic beam element solutions, very large wall lengths relative to the corridor width do not invalidate the assumptions of model application. It is possible, however, that large wall lengths combined with nonlinear behaviour may do so.

v) Rotational inertia associated with walls will be greater than for frames.

vi) Stress concentrations at the junction of walls and coupling beams may require consideration.

vii) Shear deformation due to sliding shear and diagonal cracking is likely to be significant in certain cases.

In the search for a suitable idealisation, attempts have been made to recognise these distinctive features, taking advantage of them where possible and incorporating capabilities in the model where necessary.

3.3 ASSESSMENT OF IDEALISATIONS : A UTILISATION OF PREVIOUS RESEARCH

3.3.1 General

In the following sections different types of structural idealisation are considered and their applicability to shear wall structures is examined. A nonlinear model is considered to be essential to gain a satisfactory understanding of the actual seismic response of shear wall structures. Previous experience with elastic models and indications of their accuracy provide a valuable basis on which to develop such a nonlinear model.

3.3.2 Elastic Analysis of Shear Wall Structures

a) Elastic beam element

Considering the approximation involved, suitably modified beam elements have been shown to provide remarkably accurate results in computing elastic displacements of tall coupled shear wall structures. In particular, MacLeod [28] investigated a wide variety of elastic structures and made comparisons between physical models, beam elements and constant strain triangles. In predicting displacements of these elastic structures for most practical purposes the beam idealisation is of adequate accuracy. Paulay [29] and Santhakumar [8] have presented long histories of beam type static analyses. A high level of acceptance has been engendered by the frequent use of this type of element. However, stress concentrations, particularly in the vicinity of coupling beams, remain undetected and the

use of general two-dimensional finite elements would yield superior results in this respect.

b) Elastic two-dimensional finite element

Some seemingly very accurate and intuitively sound analyses of elastic model structures have been performed using general finite elements, modelling structural behaviour in a very detailed manner [30,31]. In a real structure, however, even in its "elastic" range i.e. before coupling beams or walls yield, extreme hypothetical stress concentrations are non-existent. In their place nonlinear material behaviour occurs. It is possible that a model which depicts imaginary high stress concentration may be less representative than one which, in effect, ignores them.

3.3.3 Inelastic Analysis of Shear Walls

a) Nonlinear general finite elements

The continued application of constant strain triangles in the nonlinear range requires identification and empirical modelling of complex and detailed material behaviour. Because of different material characteristics the various physical phenomena occurring in reinforced concrete and requiring modelling may be summarised in three distinct groups: (a) concrete stress-strain properties including multiaxial compressional strain states and shear deformations in the cracked state; (b) steel stress-strain properties and (c) bond between the concrete and steel. Of these, two of the most intractable problems encountered in previous work and existing in our present state of knowledge, are the adequate modelling of the nonlinear concrete stress-strain relations and the allowance for bond-slip in anchorage regions.

Even if these phenomena could be adequately defined by mathematical functions (a requirement for the Finite Element method), the necessary computational effort is substantial. Feasibility estimates related to an optimised implementation of Gormack's [18] constant strain triangle idealisation of a 7-storey coupled shear wall and based on the explicit integration described in Chapter 5, are disappointing. A computational effort of at least 20 times that involved in the adopted approach was indicated. The combined effects of a large increase in the number of degrees of freedom for adequate accuracy and a corresponding increase in material parameters stored, together with a shorter time step to ensure stability, are responsible. Moreover, an implicit integration scheme (see Chapter 5) appears to show little improvement. Inference from Gormack's 25 solution steps, which strained computer facilities beyond present operational limitations, to a 1000 step dynamic solution indicates a factor of 40 in the increase of computational effort over the static

analysis. Nevertheless interesting work, leading to nonlinear static solutions for smaller problems, using a variety of refined finite elements, has been published [20,21]. It may well be that this is the approach of the future. For the present, however, a lower order of modelling, introducing the "plane sections remain plane" assumption, has been adopted.

b) Experimental basis for a nonlinear beam model

When considerable approximation is inherent in the model, direct or indirect experimental calibration is essential. Over recent years efforts have been made to relate experimental work for different shear wall components and, in most cases, results have been related to beam type models. A good example of such calibration is seen in the work of Paulay [3] and Binney [4] where coupling beams with complete anchorages were tested and overall results, suitable for dynamic modelling, are available. Of considerable interest is the observation of Santhakumar [8] that the primary flexural behaviour of the walls does not appear to be vitally disturbed by discrete introduction of coupling beam actions. It is reassuring to note that Santhakumar's monotonic nonlinear analysis, which is based on assumptions similar to those used in the flexural model of this study, showed "good agreement" with his shear wall experiments. Some interesting work is being done by Spurr [9] who also is using flexural elements based on similar structural assumptions. His incremental static solutions, incorporating refined stress-strain properties and considering shear deformations in some detail, were intended in the first instance to allow extensive and detailed comparison with experimental work.

3.4 A NONLINEAR FLEXURAL IDEALISATION OF WALLS

The extent of the nonlinear behaviour, related in some way to the deformation history, must be defined. The usual approach, which is highly successful in frame structures, is to relate a moment curvature hysteretic response criteria to the spring hinges. In this study a further consideration is that of axial load variation and interaction with moments (section 3.2(iii)). Immense practical difficulties are encountered in an attempt to create and use a reliable set of moment curvature axial force interaction curves, especially when cyclic loading is considered. Two additional, related and very significant phenomena were encountered and are, in retrospect, obvious: different strain histories of individual steel areas can significantly change the subsequent behaviour of complex sections and the effect of a variable instantaneous centre of stiffness

is to significantly change the structure's geometry.

The simplest and most satisfactory way in which these fundamental behavioural characteristics can be adequately modelled is to integrate current material properties across sections. Section parameters thus derived may be used in turn to compute element stiffnesses as described in the following section. Although a strict finite element approach has been followed, the use of section analyses throughout the wall, as a service to integration along the length, proved a convenient and familiar means of subdividing the process. With material property integration, even the most complex interactive behaviour is automatically allowed for in wall sections.

To recapitulate with particular reference to the overall simplicity of shear wall force distributions and the complexity of individual sections (see the list of distinctive properties of shear walls, section 3.2): The selected level of modelling is essential for a reliable assessment of behaviour and it is practical because of the relatively simple overall structural behaviour of shear walls. The normally separate considerations of distribution and extent of the nonlinearity are, in principle, embodied in a direct application of the Finite Element method.

3.5 FINITE ELEMENT MODEL A

3.5.1 General

A suitable displacement function, based on a flexural idealisation, was specified to represent walls. The finite element model A (figure 3.1) is based on a pure displacement model [33]. Because the element is reduced to one dimension and only end connectivity is present, then equilibrium is not violated across the boundaries as is the case with many two-dimensional elements. The internal degree of freedom at the mid point (figure 3.1) was introduced in order that the strain variation due to axial deformation be of the same degree as the strain variation due to flexure. This allows non-coincidence of the incremental neutral axis and the reference axis to be recognised within the element. It is assumed in this chapter that section properties at the required locations are available. The incremental stiffness of element A is derived using finite element techniques to integrate along the element length and is similar to the derivation by Aldstedt et al [22].

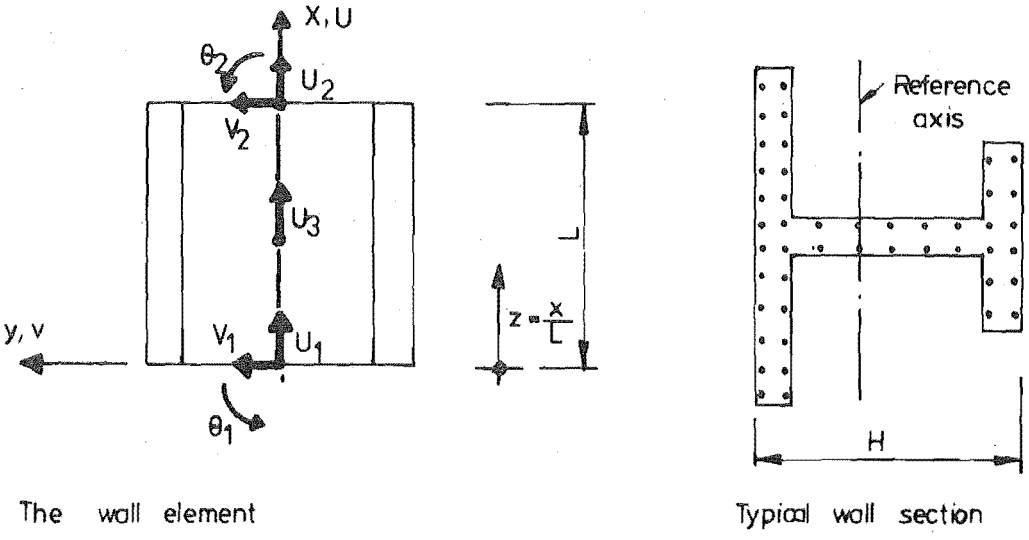

FIGURE 3.1 : ELEMENT A

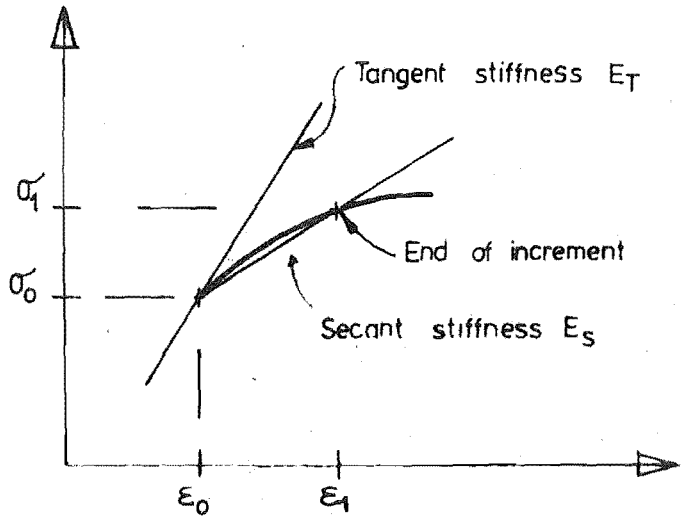

FIGURE 3.2 : INCREMENTAL TANGENT AND SECANT MATRIX DEFINITIONS

3.5.2 Displacement Functions

The following standard expressions relate to figure 3.1. Symbol definitions are listed at the beginning of this thesis.

a) Axial displacement along element u

$$u(z) = [N_u] \{u\} \tag{3.1}$$

where $[N_u] = [1 - z,\ z,\ 4z(1 - z)]$

$\{u\} = [u_1, u_2, u_3]^T$

$z = x/L$ and L is the beam length.

b) Transverse displacement along element v

$$v(z) = [N_v] \{v\} \tag{3.2}$$

where $[N_v] = [1 - 3z^2 + 2z^3,\ Lz(1 - z)^2,$

$1 - 3(1 - z)^2 + 2(1 - z)^3,\ - Lz^2(1 - z)]$

and $\{v\} = [v_1, \theta_1, v_2, \theta_2]^T$

c) Combined displacement function N

$$\{u(x,y)\} = \begin{Bmatrix} u(z) \\ v(z) \end{Bmatrix} = \begin{bmatrix} N_u & 0 \\ 0 & N_v \end{bmatrix} \begin{Bmatrix} u \\ v \end{Bmatrix} = [N] \{q\} \tag{3.3}$$

where $\{q\}$ is the nodal displacement vector.

3.5.3 Element Strains

Utilising Kirchhoff's hypothesis and assuming a uniaxial stress state, the strain $\{\varepsilon\}$ within the element is expressed as follows:

$$\begin{aligned} \{\varepsilon(x,y)\} &= \left[\frac{\partial N_u}{\partial x},\ - y \frac{\partial N_v}{\partial x} \right] \{q\} \\ &= \left[\frac{1}{L} \frac{dN_u}{dz},\ - \frac{y}{L^2} \frac{dN_v}{dz} \right] \{q\} \\ &= [B] \{q\} \end{aligned} \tag{3.4}$$

Performing the differentiations in equation 3.4 and substituting $x = Lz$ gives the strain displacement relationship [B] as a function of position.

$$[B] = \left[- \frac{1}{L},\ \frac{1}{L},\ \frac{4(L - 2x)}{L^2},\ \frac{6Y(L - 2x)}{L^3},\ \frac{2Y(2L - 3x)}{L^2},\ \frac{6Y(L - 2x)}{L^3},\ - \frac{2Y(L - 3x)}{L^2} \right] \tag{3.5}$$

This is the basic strain displacement relationship which is used to compute material strains at sections as the analysis progresses.

3.5.4 Constitutive Relationships

In physically nonlinear problems the material properties vary as functions of deformation and deformation history. An important aspect of the analysis is, therefore, the definition of stress-strain curves or constitutive relationships. At every stage of an iterative or incremental procedure, new element stiffness matrices must be computed and a prerequisite to this computation is the knowledge of current values of the material parameters [C]. Inelastic deformation is characterised by irreversible straining and is governed by a yield criteria of the form

$$F(\{\sigma\} , \{\varepsilon\}) = 0 \qquad (3.6)$$

which must be defined. The actual relationships, together with consideration of the two material composition of reinforced concrete, are dealt with in Chapter 4. In general, however, if $\{\sigma_o\}$ and $\{\varepsilon_o\}$ are the respective stress $\{\sigma\}$ and strain $\{\varepsilon\}$ values at the end of the previous increment then $[C_o(x,y)]$, the tangent constitutive matrix, may be defined.

$$\{\sigma\} = [C_o(x,y)] (\{\varepsilon\} - \{\varepsilon_o\}) + \{\sigma_o\} \qquad (3.7)$$

The terms $\{\sigma\}$ and $\{\varepsilon\}$ relate to the linearised increment to which conventional elastic analysis procedures apply and overall solutions comprise cumulative results. Since a state of plane uniaxial stress is assumed in this study and E_T is the Young's Modulus of the material computed at the commencement of an increment (tangent modulus), the following simplification is possible

$$[C_o] = \underset{1 \times 1}{[E_T]} \qquad (3.8)$$

Because of departures from linearity, actually resisted stresses $\{\sigma_1\}$, as distinct from stresses predicted in the linearised equation 3.7, must be computed at the end of the increment.

$$\{\sigma_1\} = [C_s(x,y)] (\{\varepsilon\} - \{\varepsilon_o\}) + \{\sigma_o\} \qquad (3.9)$$

where $[C_s(x,y)]$ is the local secant constitutive matrix. If E_s is defined as the local secant modulus then a simplification, as in equation

3.8, is possible, i.e.

$$[C_s] = \underset{1 \times 1}{[E_s]} \tag{3.10}$$

The secant and tangent moduli are illustrated in figure 3.2.

3.5.5 Energy Solution for a Single Element

A generalised method of computing the element stiffness matrix is to apply one of the variational principles of solid mechanics. Usually, when a compatible displacement element is considered, the principle of minimum potential energy is selected and it is used in the following derivation.

For a linearised increment, where $\{\Delta Se\}$ is the vector of incremental nodal forces associated with one element, the potential energy may be written in its general form, i.e.

$$\bar{U} = \frac{1}{2} \left[\int_{Vol} (\{\varepsilon\} - \{\varepsilon_o\})^T (\{\sigma\} - \{\sigma_o\}) \, d\,Vol \right.$$

$$\left. - \{\bar{q}\}^T \{\Delta Se\} \right] \tag{3.11}$$

where $\{\bar{q}\}$ is the incremental nodal displacement vector

and $\bar{U}$ is the strain energy associated with the increment.

By substitution into equation 3.11 from 3.4 and 3.7, it follows that:

$$\bar{U} = \frac{1}{2} \left[\int_{Vol} \{\bar{q}\}^T [B]^T [C_o] [B] \{\bar{q}\} \, d\,Vol \right.$$

$$\left. - \{\bar{q}\}^T \{\Delta Se\} \right] \tag{3.12}$$

Applying the principle of minimum potential energy, where $\{\delta\bar{q}\}$ is an arbitrary set of displacements, gives

$$\{\delta \bar{q}\}^T \left[\int_{Vol} [B]^T [C_o] [B] \, d\,Vol \; \{\bar{q}\} - \{\Delta Se\} \right] = 0 \tag{3.13}$$

and since $\{\delta \bar{q}\}$ is arbitrary and non-zero then

$$\int_{Vol} [B]^T [C_o] [B] \, d\,Vol \; \{\bar{q}\} = \{\Delta Se\} \tag{3.14}$$

By definition, the 7 x 7 incremental stiffness matrix $[\bar{K}]$ is given as follows:

$$\underset{7\times 7}{[\bar{K}]} = \int_{Vol} \underset{7\times 1}{[B]^T}\ \underset{1\times 1}{[C]}\ \underset{1\times 7}{[B]}\ d\,Vol \qquad (3.15)$$

The detailed evaluation of this integral is discussed in section 3.5.7. Formation of the total stiffness matrix is achieved using direct stiffness methods as described in section 3.9.

3.5.6 Force Computation

On completing the increment, predicted elastic forces $\{Se\}$ are easily computed using equation 3.14, since the integral has been evaluated previously. Strictly, the actual nodal forces $\{Sr\}$ should be computed by substitution of $[C_s]$ for $[C_o]$ in equation 3.14 and re-evaluation of the integral. However, for this particular element, considerable simplification is possible because of "end only" connectivity. Actual stress distributions may be simply integrated across boundary sections as outlined in Chapter 4, with the resultants expressed as standard beam actions.

3.5.7 Evaluation of Element A Stiffness

a) Simplification of the element stiffness matrix

In the interests of computational efficiency the numerical stiffness matrix operations within the program have been streamlined as much as possible. For instance, in transforming stiffness matrices to global systems, it is advantageous to operate on the minimum dimension stiffness matrix, obtained by eliminating rigid body modes. Transformation $[T_5]$, relating to figure 3.3, is useful in this respect and the resulting degrees of freedom are still adequate to define curvature and axial strain deformation patterns. Transformation $[T_5]$ is defined as follows:

$$\begin{Bmatrix} u_1 \\ u_2 \\ u_3 \\ \theta_1 \\ \theta_2 \end{Bmatrix} = \begin{bmatrix} 1 & . & . & . & . & . & . \\ . & 1 & . & . & . & . & . \\ . & . & 1 & . & . & . & . \\ . & . & . & -\frac{1}{L} & -1 & \frac{1}{L} & 0 \\ . & . & . & -\frac{1}{L} & 0 & \frac{1}{L} & 1 \end{bmatrix} \begin{Bmatrix} u_1 \\ u_2 \\ u_3 \\ v_1 \\ \theta_1 \\ v_2 \\ \theta_2 \end{Bmatrix} \qquad (3.16)$$

i.e. $\{q_1\} = [T_5]\{q\}$ where $\{q_1\}$ is defined in figure 3.3.

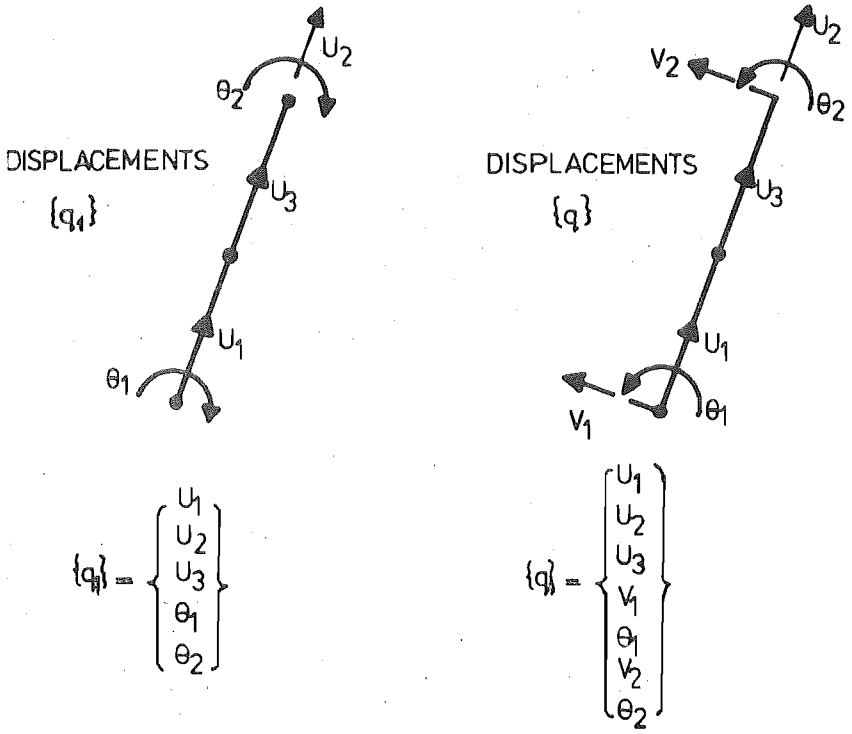

FIGURE 3.3 : DISPLACEMENT DEFINITIONS.

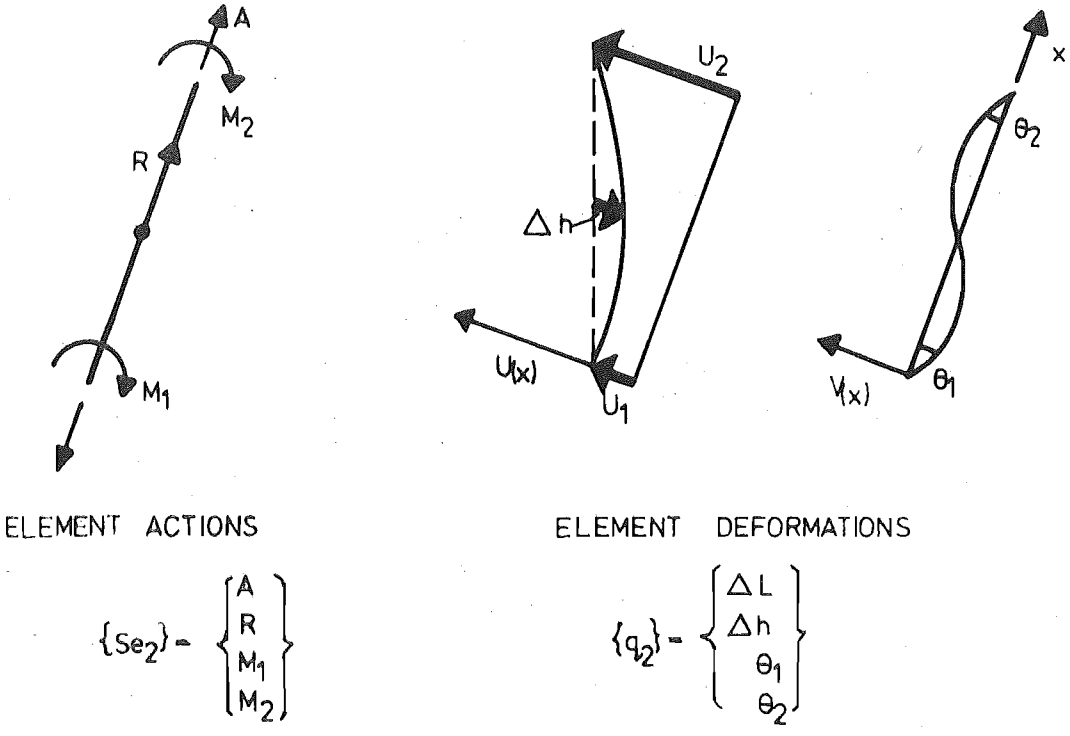

FIGURE 3.4 : FINAL SIMPLIFIED ACTIONS AND DEFORMATIONS.

Further, defining a new strain displacement relationship $[B_1]$ in equation 3.17 and combining with the original strain displacement relationship of equation 3.4 gives

$$\{\varepsilon\} = [B_1]\{q_1\} \tag{3.17}$$

$$\{\varepsilon\} = [B]\{q\} \tag{3.4}$$

$$[B_1] = [B][T_5]^T \tag{3.18}$$

On performing the matrix multiplication $[B_1]$ is obtained

$$(B_1] = [-\frac{1}{L}, \frac{1}{L}, \frac{4(L-2x)}{L^2}, \frac{-2y(2L-3x)}{L^2}, \frac{-2y(L-3x)}{L^2}] \tag{3.19}$$

The two constant components of equation 3.19 may be combined using the definitions of figure 3.4. A new length parameter ΔL expressing element elongation is used.

$$\Delta L = U_2 - U_1 \tag{3.20}$$

The middle node displacement is redefined, where Δh is defined as shown in figure 3.4.

$$\Delta h = U_3 - (U_1 + U_2)/2 \tag{3.21}$$

and the final strain displacement relationship $[B_2]$ is derived.

$$[B_2] = [\frac{1}{L}, \frac{4(L-x)}{L^2}, \frac{-2y(2L-3x)}{L^2}, \frac{-2y(L-3x)}{L^2}] \tag{3.22}$$

This departure from specifying all parameters, as is usual in the finite element method, in terms of nodal displacements or derivations of displacements, is possible in this case only because of the simplified nature of $[B_1]$.

The stiffness matrix $[K_2]$, relating to displacements $\{q_2\}$ of figure 3.4, may be expressed in integral form as follows:

$$\underset{4\times4}{[K_2]} = \int_{Vol} \underset{4\times1}{E_T} \underset{1\times4}{[B_2]^T} \underset{1\times4}{[B_2]} \, d\,Vol \tag{3.23}$$

Forces may be computed using the definition of a stiffness matrix, i.e.

$$\underset{4\times1}{\{Se_2\}} = \begin{Bmatrix} A \\ R \\ M_1 \\ M_2 \end{Bmatrix} = \underset{4\times4}{[K_2]} \; \underset{4\times1}{\{q_2\}} \qquad (3.24)$$

b) Choice of integration method

The stiffness matrix remains to be evaluated and an algebraic or a numerical integration of the strain energy gradient, which is expressed in the following form, is required.

$$\underset{4\times4}{[K_2]} = \int_{x=0}^{L}\int_{y=0}^{H} E_T \underset{4\times1}{[B_2]^T} \underset{1\times4}{[B_2]} \, dy \, dx$$

Note that E_T may vary in both x and y co-ordinate directions as shown in figure 3.1.

The usual integration evaluation techniques were considered: (i) analytic integration where a property variation is specified along the length, e.g. piecewise analytic integration where the integrand is evaluated over a number of subregions; (ii) Gaussian quadrature applied over either in-plane dimension and (iii) Newton-Cotes numerical integration, where equally spaced sample points are used.

Where it is practical analytic integration is usually the most efficient means of stiffness matrix evaluation and in this respect this element is probably no exception. However, if adequate accuracy is to be achieved piecewise analytic integration would probably require a minimum of three sections in each element - as many as for numerical integration. The specification of a linear variation in properties, as determined by end sections, over the length [28] and combined with analytic integration, is thought to be the most efficient means of stiffness evaluation. Furthermore, if elements idealised a wall with only two elements joining at each node, then, provided the necessary additional coding is incorporated, a common end section could be utilised for each adjacent element. In this manner maximum possible efficiency could be obtained, with section requirements reduced to one for each element.

Although Gaussian quadrature is usually the most efficient form of numerical integration, because a minimum number of strain energy gradient evaluations are involved, it is known to be inferior to some Newton-Cotes techniques when abrupt changes in the function are encountered. In the transverse direction of the flexural element, the presence of flanges

causes large abrupt changes in the area function and component areas are better treated as separate entities rather than defining points on some approximate function. The permissibility of non-sequential integration point numbering across a section is desirable, but not possible with Gaussian quadrature. In the longitudinal direction, the additional sections required to evaluate forces at element ends and the possibility of sudden changes in stiffness, when a strain reversal over a portion of the length is encountered, were the reasons for not investigating in detail Gaussian quadrature in this particular study.

Simpson's rule integration was applied in the longitudinal direction such that 3, 5, 7 or more sections could be used, representing ascending orders of integration. It is envisaged that in most cases integration with three sections should provide optimum accuracy in element stiffness evaluation.

It is interesting to note that a cubic displacement function was selected and that this corresponds to a linear (1st order) variation in curvature along the element length. Because third order integration of the strain energy gradient was used, a linear variation in flexural stiffness along the length will be evaluated precisely. Similarly, with the linear variation in axial strain present, a third order integration scheme will integrate a linear variation in axial stiffness precisely. Finally, a varying eccentricity may be present and may, because it appears in a product with area, cause a perturbation from exact integration. Nevertheless the indications are that third order integration should be efficient and sufficiently accurate for most purposes, while the availability of higher order integration provides the flexibility desirable in a preliminary study. The adequacy of third order integration is investigated in Chapter 8.

c) Static condensation

A 4 x 4 stiffness matrix has now been obtained and it is possible to simplify this further by the removal of the internal degree of freedom. Equation 3.24 was rewritten as follows:

$$\begin{Bmatrix} A \\ R \\ M_1 \\ M_2 \end{Bmatrix} = \begin{bmatrix} S_{11} & S_{12} & S_{13} & S_{14} \\ S_{21} & S_{22} & S_{23} & S_{24} \\ S_{31} & S_{32} & S_{33} & S_{34} \\ S_{41} & S_{42} & S_{43} & S_{44} \end{bmatrix} \begin{Bmatrix} \Delta L \\ \Delta h \\ \theta_1 \\ \theta_2 \end{Bmatrix} \qquad (3.25)$$

It was considered that only minor errors would be incurred by lumping longitudinal inertial masses at the ends of the member and performing a static condensation as in a static analysis. This gave the resulting 3 x 3 stiffness matrix to which 6 x 3 transformations, already existing in the coding and discussed later, could be applied, rather than the 6 x 4 or 7 x 7 transformations that are applicable to the original forms of the stiffness matrix of this element. The internal node deformations were recovered later using the relationship

$$\Delta h = -\frac{S_{22}}{S_{21}}\Delta L - \frac{S_{23}}{S_{21}}\theta_1 - \frac{S_{24}}{S_{21}}\theta_2 \qquad (3.26)$$

so that element strains could then be computed.

3.6 ELEMENT B : SIMPLIFIED INTEGRATION

3.6.1 Description

It was stated in preceding sections that third order integration should provide a stiffness matrix of adequate accuracy, particularly when a relatively refined idealisation is used. It was observed that a considerable proportion of the stiffness formation effort is absorbed in section integration. It would seem reasonable that, if element stiffness variation was restricted to be constant along the element length, which intuitively appears adequate for the analyses contemplated, then a single section could define a prismatic beam. Of course allowance must be made for the incremental eccentricity of the beam centreline. This may be handled easily with rigid end block transformations and any standard program requires only the addition of the section properties routines. The resulting element is extremely efficient as analytic integration of the strain energy gradient is possible. Strains may be computed using displacement function relationships or conventional force displacement relationships for beams, the conventional method having the advantage that an allowance for shear deformation is easily incorporated.

For the case of cracked elastic sections, where yielding never occurs, a further attempt to improve efficiency was made with an analytic treatment of section properties. Cracking, based on flange or extreme fibre conditions was allowed for and, because numerous point histories are no longer required, only curvatures and axial strains need be stored. Considerable efficiency is thus obtainable. A prerequisite for the use of this element is the foreknowledge that yield strains will not be exceeded.

3.6.2 Problems of Reduced Order Integration

Element B, when used in situations of severe stiffness deterioration, exhibited a major numerical stability problem. Typical behaviour of this element, when used in structure B, is seen in figure 8.6 in which a complete failure to model the physical situation has been observed. In practical terms, the instability stems from a basic inability of the element to detect reversal of curvature independently near one or other ends of the element. Instead, the entire element is considered by the analysis to conform to the state at a single, arbitrary section. In the example uncontrolled shear (sidesway) deformation occurred on yielding and, for as long as the sense of incremental curvature remained unchanged at the base section, complete reversal of curvature at the upper end of the beam passed undetected.

The problem is one of inadequate integration of the strain energy gradient. While the integration may be adequate for elastic solutions, it is inadequate to define a lst order variation of nonlinear curvature along the element length. The problem appears analogous to a difficulty encountered with reduced order numerical integration of strain energy gradients to compute elastic stiffness matrices [34]. If the integration order is too low, zero strain modes may arise, which in static solutions lead to singular stiffness matrices. In dynamic analyses the error may cause significant discrepancies in displacements.

Although Franklin [21] reports useful results obtained with this type of element, his sphere of operation imposed less demanding stability criteria in that solutions involving large inelastic deformations were not attempted and dynamic responses with highly variable cyclic loading were not considered. It does appear that element B may be satisfactory for monotonic loading, but that additional complexities, associated with unloading and direction dependent stiffness, initiate apparently insurmountable instabilities. Therefore element B was not considered suitable to represent plastic hinging in the walls in any of the analyses performed in this study.

It is suggested, however, that element B using a mid-height section may be ideal for an analysis in the cracked elastic state where large inelastic deformations do not occur and simple analytic integration is possible. No obvious difficulties were encountered in the development of this element but it was not used in these preliminary studies because typically designed walls were found to yield more freely at upper floors than was anticipated.

3.7 ELEMENTS C1 AND C2 : LOWER ORDER DISPLACEMENT FUNCTIONS

3.7.1 Description of Elements C1 and C2

In order to overcome the problems encountered with element B the order of the displacement function was reduced. The logical degeneration from a linear variation in curvature is to a constant curvature element. This still satisfies the convergence criteria of compatibility, constant strain states and rigid body modes [33]. An element identical to this, less rigorously derived but utilising existing coding very effectively, is one with a spring hinge at its mid-height. Both the mid-height hinge variation (element C2) and one with a spring at one end (element C1) were used. As with element B, one section for each element was used to define the nonlinear behaviour. To preserve, as far as possible, accuracy in the elastic range, a two component model was used in which elastic deformations on the original elastic beam occur while additional plastic deformations are lumped and constrained to occur at point hinges [35].

Of all the possibilities in which section analyses may be combined with spring hinges to model continua, element C2 is the only one which simultaneously satisfies the finite element convergence criteria and does not encounter serious conceptual difficulties in creating a strain displacement relationship and therefore models the physical situation directly. Some of the problems encountered with these elements are outlined in Chapter 8.

3.7.2 Stiffness of Elements C1 and C2

Stiffness matrices, incorporating variable spring hinge effects for a centrally or end located single hinge, were derived from first principles, based on the methods of Giberson [35] and Otani [36]. For a beam,2nd moment of area I, Young's Modulus E and length L the spring stiffness f is defined

$$M = \frac{4EI}{L} f \alpha \qquad (3.27)$$

where α is the rotation of the plastic hinge. Using this definition the stiffnesses were derived in the following manner. First, the flexibility matrix was computed by adding elastic and plastic deformations. Secondly, the stiffness matrix was derived by algebraic inversion of the flexibility matrix. To continue the analysis, spring rotations must be related to element curvatures such that section properties may be defined, section stiffness parameters computed and, in turn, new spring stiffnesses

defined, The parameters normally available are I, the basic elastic beam 2nd moment of area, and I_{new}, the incremental beam 2nd moment of area present after some deterioration. Typically, proportioning of the spring to achieve deformations as for a prismatic beam of inertia I_{new} is the object, and this can be achieved precisely for element C2 under a constant moment distribution. The best which can be achieved, however, for element C1 is to equalise rotations at member ends [15]. In both cases, where the hinge length is H, the spring stiffness may be redefined in terms of section inertia values.

$$f = \frac{L}{4H} \frac{I_{new}}{I - I_{new}} \tag{3.28}$$

The hinge length is usually chosen to be the beam length and this allows direct relationship of spring stiffnesses [12] to section derived properties. Alternatively, spring stiffnesses may be defined with a moment curvature relationship, useful examples of which are the bilinear rule and Clough's degrading stiffness model [37].

3.8 FURTHER ELEMENTS

The work of two very recent, relevant studies [15,16] was examined in some detail. In each case a basic prismatic beam was used with one [16] or two [15] spring hinges, concentrated at member ends, intended to allow nonlinear deformation. The element used in the single hinge model [16] was essentially element C1. The element used in the other study [15] was similar except that spring hinges were included at both ends. In each case a simple bilinear failure criteria was used rather than a section analysis. Although there are similarities to the elements derived here, these particular variations will be referred to as the PCA element [16] and the MWD element [15] because of different nonlinearity generation, and because specific reference is made to the two studies. The capabilities to define these variations already existed in Sharpe's [12] program.

3.9 TRANSFORMATIONS AND TOTAL STIFFNESS MATRIX FORMATION

To this stage the different local stiffness matrices have been derived. The transformations shown in figure 3.5 may be used to include end blocks, eccentricities and to translate stiffness matrices to a global system. In practice, all of the transformations were applied, combined into a single transformation $[T_g]$, and non-zero values were specified to activate the various options as required.

$$[T_g] = [T_1]\ [T_2]\ [T_3]\ [T_4] \tag{3.29}$$

The global stiffness $[K_g]$ is then computed as follows:

$$[K_g] = [T_g]^T\ [K_2]\ [T_g] \tag{3.30}$$

The total stiffness matrix may now be computed by simple addition of the component stiffnesses as in the direct stiffness method [38].

$[T_1]$

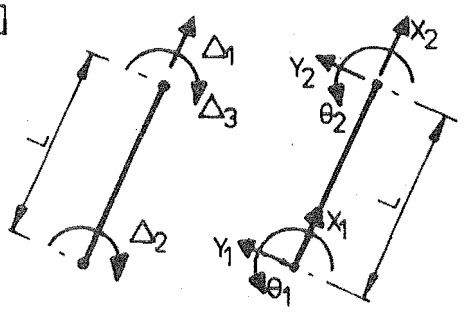

$$\begin{Bmatrix}\Delta_1\\ \Delta_2\\ \Delta_3\end{Bmatrix} = \begin{bmatrix} -1 & \cdot & \cdot & 1 & \cdot & \cdot \\ \cdot & -1/L & -1 & \cdot & 1/L & \cdot \\ \cdot & -1/L & \cdot & \cdot & 1/L & -1 \end{bmatrix} \begin{Bmatrix} X_1\\ Y_1\\ \theta_1\\ X_2\\ Y_2\\ \theta_2 \end{Bmatrix}$$

(a) Rigid body mode transformation

$[T_2]$

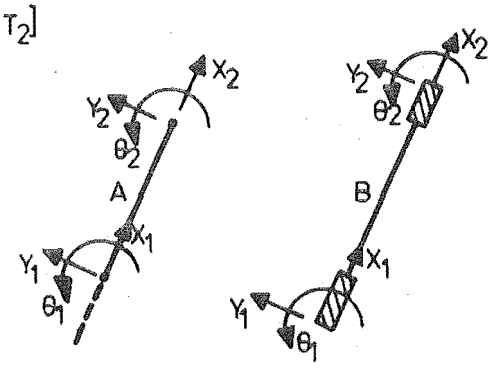

$$\begin{Bmatrix} X_1\\ Y_1\\ \theta_1\\ X_2\\ Y_2\\ \theta_2 \end{Bmatrix}^A = \begin{bmatrix} 1 & \cdot & \cdot & \cdot & \cdot & \cdot \\ \cdot & 1 & EX_1 & \cdot & \cdot & \cdot \\ \cdot & \cdot & 1 & \cdot & \cdot & \cdot \\ \cdot & \cdot & \cdot & 1 & \cdot & \cdot \\ \cdot & \cdot & \cdot & \cdot & 1 & -EX_2 \\ \cdot & \cdot & \cdot & \cdot & \cdot & 1 \end{bmatrix} \begin{Bmatrix} X_1\\ Y_1\\ \theta_1\\ X_2\\ Y_2\\ \theta_2 \end{Bmatrix}^B$$

(b) End block transformation

$[T_3]$

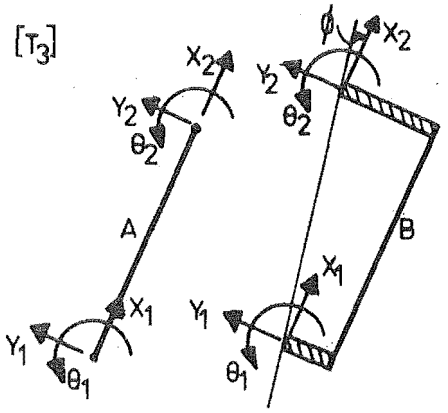

$$\begin{Bmatrix} X_1\\ Y_1\\ \theta_1\\ X_2\\ Y_2\\ \theta_2 \end{Bmatrix}^A = \begin{bmatrix} 1 & \cdot & \cdot & EY_1 & \cdot & \cdot \\ \cdot & 1 & \cdot & \cdot & \cdot & \cdot \\ \cdot & \cdot & 1 & \cdot & \cdot & \cdot \\ \cdot & \cdot & \cdot & 1 & \cdot & EY_2 \\ \cdot & \cdot & \cdot & \cdot & 1 & \cdot \\ \cdot & \cdot & \cdot & \cdot & \cdot & 1 \end{bmatrix} \begin{Bmatrix} X_1\\ Y_1\\ \theta_1\\ X_2\\ Y_2\\ \theta_2 \end{Bmatrix}^B$$

(c) Eccentricity transformation

$[T_4]$

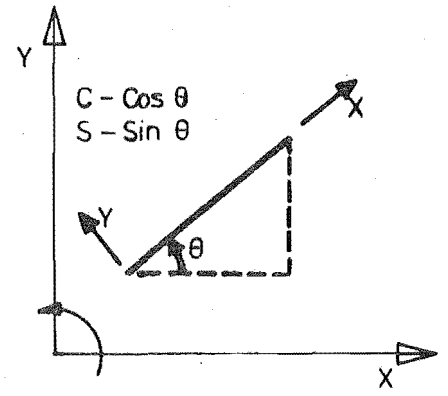

$$\begin{Bmatrix} X_1\\ Y_1\\ \theta_1\\ X_2\\ Y_2\\ \theta_2 \end{Bmatrix} = \begin{bmatrix} C & +S & \cdot & \cdot & \cdot & \cdot \\ -S & C & \cdot & \cdot & \cdot & \cdot \\ \cdot & \cdot & 1 & \cdot & \cdot & \cdot \\ \cdot & \cdot & \cdot & C & +S & \cdot \\ \cdot & \cdot & \cdot & -S & C & \cdot \\ \cdot & \cdot & \cdot & \cdot & \cdot & 1 \end{bmatrix} \begin{Bmatrix} X_1\\ Y_1\\ \theta_1\\ X_2\\ Y_2\\ \theta_2 \end{Bmatrix}$$

ϕ is included in transformation

(d) Co-ordinate rotation transformation

FIGURE 3.5 : TRANSFORMATIONS

CHAPTER FOUR

SECTIONAL ANALYSIS

4.1 INTRODUCTION

Although the inelastic flexural behaviour of reinforced concrete members has been recognised for some time, it is only relatively recently that nonlinear section analyses have been reported. Aoyama in his 1964 paper [39] claims to be the first to report a cyclic nonlinear section analysis. Standard procedures have since become established [40,41] and widespread use, particularly with single isolated sections,often involving complex material properties, has followed. The principal additional feature in this study is the inclusion of a large number of sections in a dynamic analysis. Instead of attempting beforehand to define the properties of a few typical sections, as in the majority of previous works, current deformations are computed and the analysis of all selected sections is performed as the overall response analysis progresses.

4.2 ASSUMPTIONS AND LIMITATIONS

In the application of sectional analyses to reinforced concrete flexural members certain standard approximations are inherent. They are:

i) Plane sections remain plane and shear deformation is not included.

ii) The effects of creep are ignored.

iii) Diagonal cracking is ignored.

iv) Further complexities in plastic hinge regions such as sliding shear, bond slip, spalling and buckling of reinforcement are ignored .

It is contended that, despite the above approximations affecting individual sections, the standard flexural element is applicable in an overall sense. The particular application to shear walls has been discussed in sections 3.3.3b and 3.4.

4.3 NONLINEAR SECTION THEORY

The concept of a section analysis is consistent with the flexural idealisation outlined in Chapter 3. The evaluation of standard parameters (inertia, area and eccentricity) corresponds to performing the integration of the strain energy gradient in the transverse direction across the beam element.

A number of definitions illustrated in figure 4.1 and relating to the following integral expressions are useful. Concrete compression stresses $\sigma_c(y)$ and steel tensile stresses $\sigma_s(y)$ are taken as positive. The breadth of the concrete section is $b_c(y)$ while $b_s(y)$ is the width function of equivalent but continuous strips of steel representing the reinforcement. E_s and E_c are current values of Young's modulus for steel and concrete and E_o is some reference Young's modulus which is used to define an equivalent section. The section parameters of interest are expressed as follows:

(a) Axial force P is computed by integrating concrete and steel stress distributions across the section.

$$P = \int_o^D b_s(y) \cdot \sigma_s(y) dy - \int_o^D b_c(y) \cdot \sigma_c(y) dy \tag{4.1}$$

(b) Moment on the reference axis M is defined by

$$M = - \int_o^D b_s(y) \cdot \sigma_s(y) \cdot y \, dy + \int_o^D b_c(y) \cdot \sigma_c(y) \cdot y \, dy - P \cdot Y_G \tag{4.2}$$

where Y_G is the distance from the section origin to the reference axis as shown in figure 4.1b.

(c) Axial area A, related to the reference Young's modulus E_o, is computed by integrating current values of Young's moduli across the section.

$$A = \frac{1}{E_o} \int_o^D (b_s(y) \cdot E_s(y) + b_c(y) \cdot E_c(y)) dy \tag{4.3}$$

(d) The 1st moment of area Z is computed in a similar manner to A.

$$Z = \frac{1}{E_o} \int_o^D (b_s(y) \cdot E_s(y) + b_c(y) \cdot E_c(y)) y \, dy \tag{4.4}$$

(e) The eccentricity of the stiffness centroid e_x from the reference axis (figure 4.1) is obtained as in equation 4.5 and it defines the neutral axis of the incremental structure.

$$e_x = \frac{Z}{A} - Y_G \tag{4.5}$$

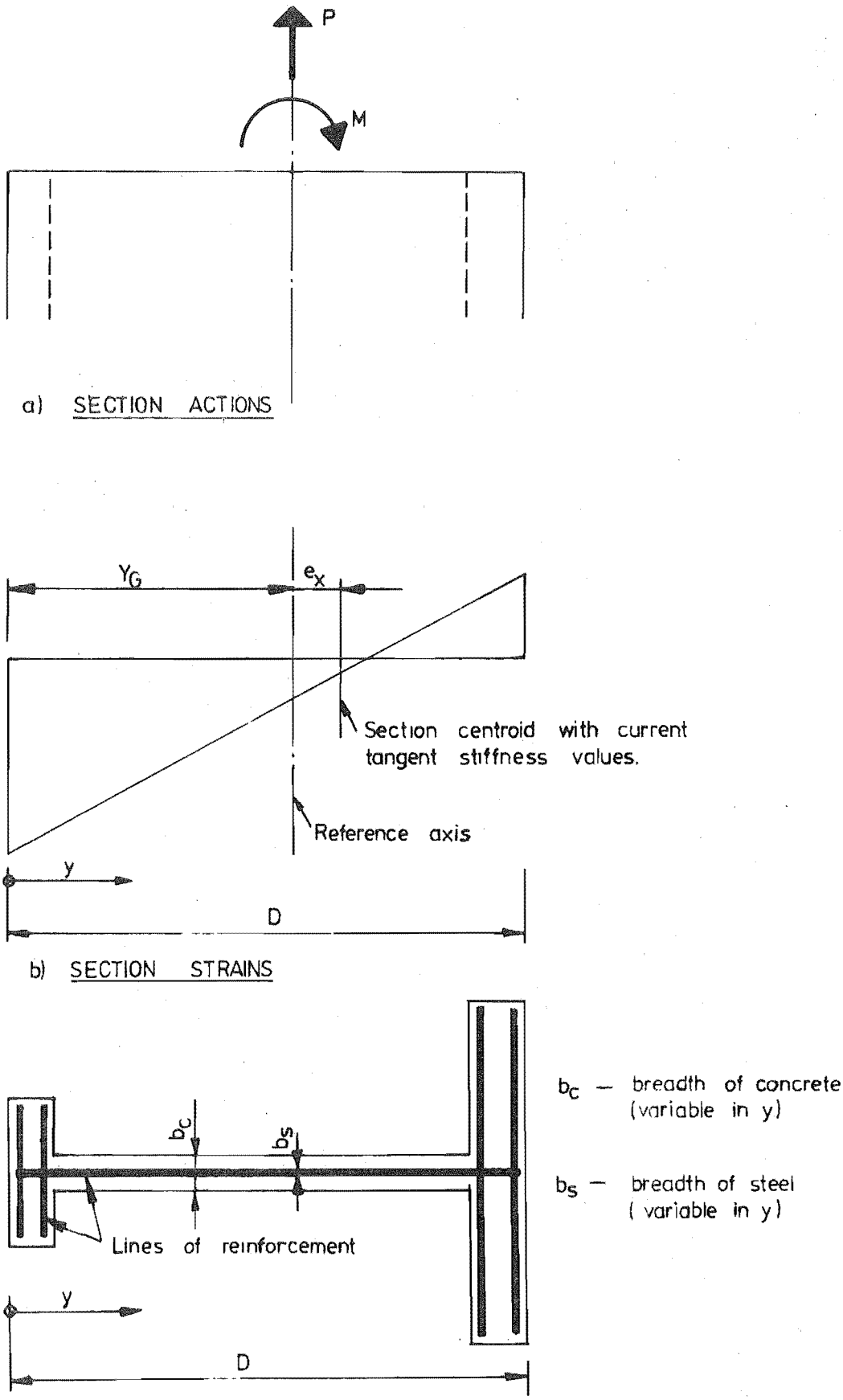

FIGURE 4.1 : DESCRIPTION OF THE SECTION.

(f) The 2nd moment of area I about the neutral axis of the incremental structure is defined as follows:

$$I = \frac{1}{E_o}\left[\int_o^D (b_s(y).E_s(y).y^2 + b_c(y).E_c(y).y^2)dy\right] - A.(e_x + Y_G)^2 \qquad (4.6)$$

Thus, with an appropriate choice of representative sections, current values of the above section parameters may be computed to allow equilibrium checking and tangent stiffness (see figure 3.2) determination for the next step of the analysis. The element tangent stiffness here is defined, as in Chapter 3, as the stiffness based on tangent Young's modulus of the component materials, computed at the beginning of the time step under consideration.

4.4 COMPONENT CONSTITUTIVE RELATIONSHIPS

4.4.1 General Considerations

A prerequisite for the use of equations 4.1 - 4.6 is the definition of constitutive (stress-strain) relationships for concrete and steel. The simplifying assumption of a uniaxial stress state allows direct application of any of a wide range of possibilities, ranging from simple bilinear rules to extremely complex relationships. Again, a reasonable compromise between reality and simplicity must be reached to ensure a practical computer program. More importantly, however, it is probable that more refined stress-strain relationships, which are dependent on precise strain histories, will be limited by the accuracy with which a flexural model can depict nonlinear strain distributions in reinforced concrete.

4.4.2 Selection of Constitutive Relations

Because of model simplification, exemplified by assumption iv) (section 4.2), strains at a particular section may not necessarily be very representative of prototype steel strains. This is seen to be particularly true of the nonlinear strains supposedly depicting plastic hinging of the type measured by Santhakumar [8] and Spurr [9]. Inelastic steel strains in the main longitudinal steel in hinge regions, influenced by diagonal cracking, bond, strain hardening and sliding shear, are not, nor can they be, closely represented by this level of modelling. While the introduction of more representative constitutive relationships has appealed to many writers

as an obvious improvement, this is not necessarily the case because of the inherent model limitations. For example, a factor of two error in nonlinear steel strains computed with a flexural model (and this is considered to be possible) would significantly influence the performance of the typical refined steel constitutive relationship of Kent [42] (figure 4.2b). A simple elasto-plastic steel model is on the other hand quite insensitive to substantial errors in nonlinear strains which may, at their worst, lead to an erroneous estimate of ductility. Furthermore, it seems likely that strains in the cracked state of the member will be accurately represented, leading to good predictions of yielding, when the bilinear relations of figure 4.2a are used.

For the above reasons the constitutive relations illustrated in figure 4.2a were used in this study. A 0.01 strain hardening factor, defined as the ratio of the Young's modulus of the steel after yield to the original Young's modulus, was used in all cases. A variety of slopes for the crushing concrete branch may be selected to make some allowance for confinement although a simple elasto-plastic relationship was retained in this study. These failure criteria were considered most reasonable in the context of the problem and with the present state of knowledge. In confirmation of this choice, the dependence of strains upon sizes and spacing of lower wall elements is demonstrated in Chapter 8.

4.4.3 Branch Points in the Constitutive Relationship

The hysteretic functions of figure 4.2 are non-conservative ones since energy is dissipated. Of particular importance is the fact that a different branch of the curve may be selected for different directions of loading, i.e. when yielding of materials is occurring, then depending on the sign of the subsequent increment, one of two different branches is selected. When a normal incremental procedure is in progress the solution path is closely linked to the physical path and artificial fluctuation of sign does not occur. If, however, iteration is attempted a sign reversal is almost certainly encountered during the convergence process. Unless special provision is made in the nonlinear stiffness determination, a sign reversal will be detected; changes to the unloading curve may be made when the stiffness and force determination should, in fact, remain related to the yield plateau while iterating.

The basic problem is illustrated in figure 4.3 with a simple bilinear hysteretic relationship, which could apply equally to moments or stresses, operating in a multi-degree-of-freedom problem. Supposing that displacement

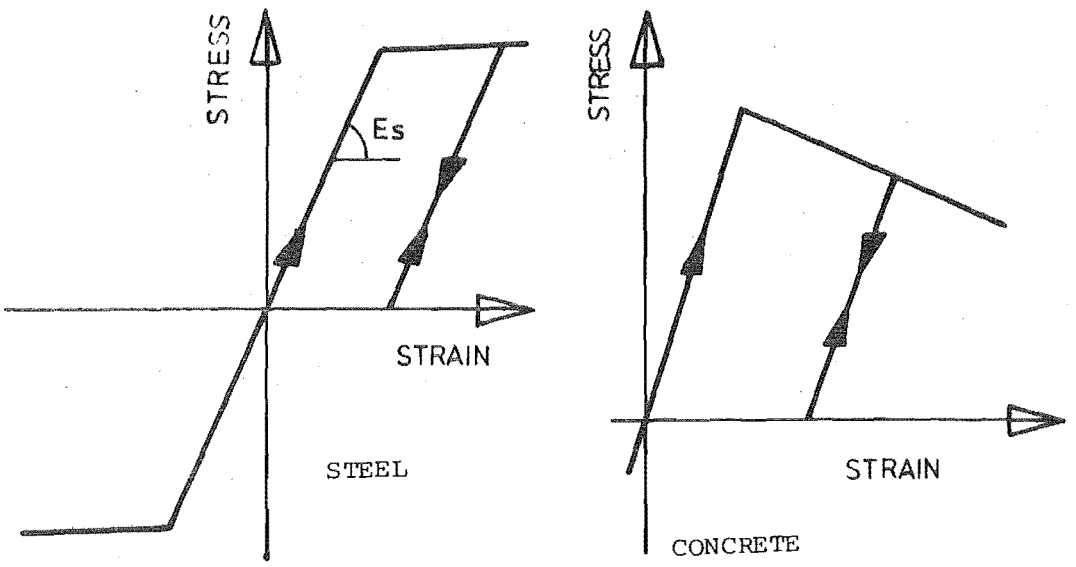

a) Bilinear constitutive relationships

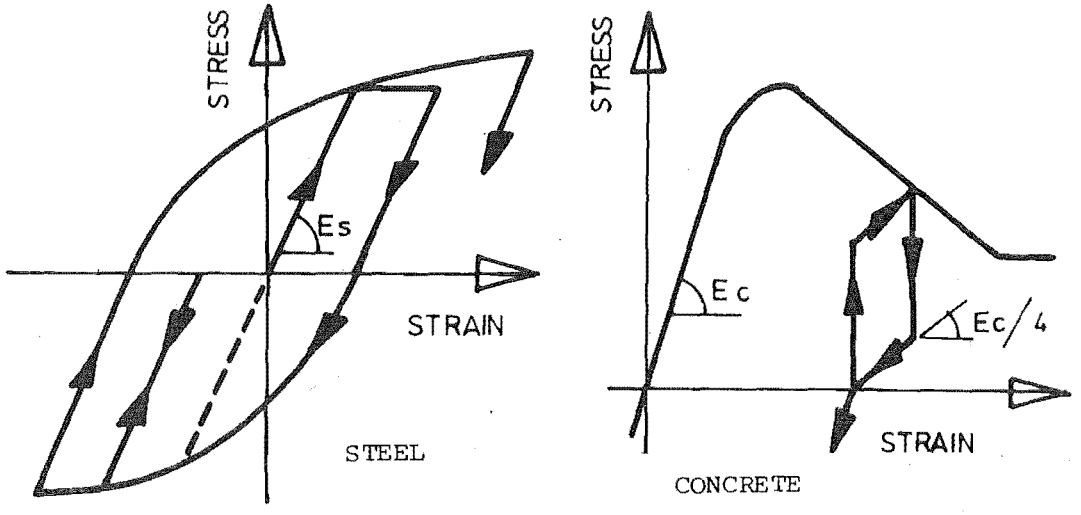

b) Kent's constitutive relationships

FIGURE 4.2 : CONSTITUTIVE RELATIONSHIPS

solution a (figure 4.3) has been computed, the first iterative correction may give increment a - b . If the normal nonlinear stiffness determination remains active, detecting reversal in the usual manner, the subsequent iterative correction obtained will be b - d instead of b - c . The error introduced is progressive and this was the reason for Sharpe's [12] puzzling phenomena of progressive hinge disappearance on iteration.

The remedial approach taken, because of its generality and consistency, was to define material properties in the section analyses on each complete improved estimate of displacement for a time step. For example increment a - c would be used to define stresses, not b - c . With the simpler bilinear moment curvature options, the branch of the curve selected at the end of the first increment was retained for the duration of the iteration. By these means, sensible continuity of the stiffness is maintained and the numerical process remains compatible with the physical situation.

4.4.4 Possibilities in Future Refinements of Constitutive Relationships

Although a simple material property idealisation has been selected for this developmental work, it seemed probable that some future experimentally verified refinement could justify improved representation. Consideration was given to the work of Kent [43] and Thompson [44] which led to the development of computer programs for section analysis. However, large amounts of computational effort are required in that Kent required an estimated 1 hour of Burroughs 6700 processor time to perform a static analysis with 9 sections for 6 postelastic cycles. Thompson stored 47 numbers to characterise each steel integration point and an analysis of a single simple section performed with his program required 0.86 seconds per increment. Clearly, material property determination, utilising subroutines which require excessive computational effort, is not compatible with a dynamic analysis of the type proposed here.

While this study, concentrating on the dynamic aspects of the analysis, was in progress, complementary work by Spurr [9] developing a section analysis for his static analysis program was being undertaken. His refined idealisation requires the storage of 5 parameters for each concrete integration point and 19 parameters for each steel integration point, or approximately 350 parameters to define the three sections in element A (figure 3.1). Despite the storage requirements and the additional computation necessary, Spurr appears to have developed a particularly efficient section analysis procedure which should be suitable for use in the dynamic analysis program of this study.

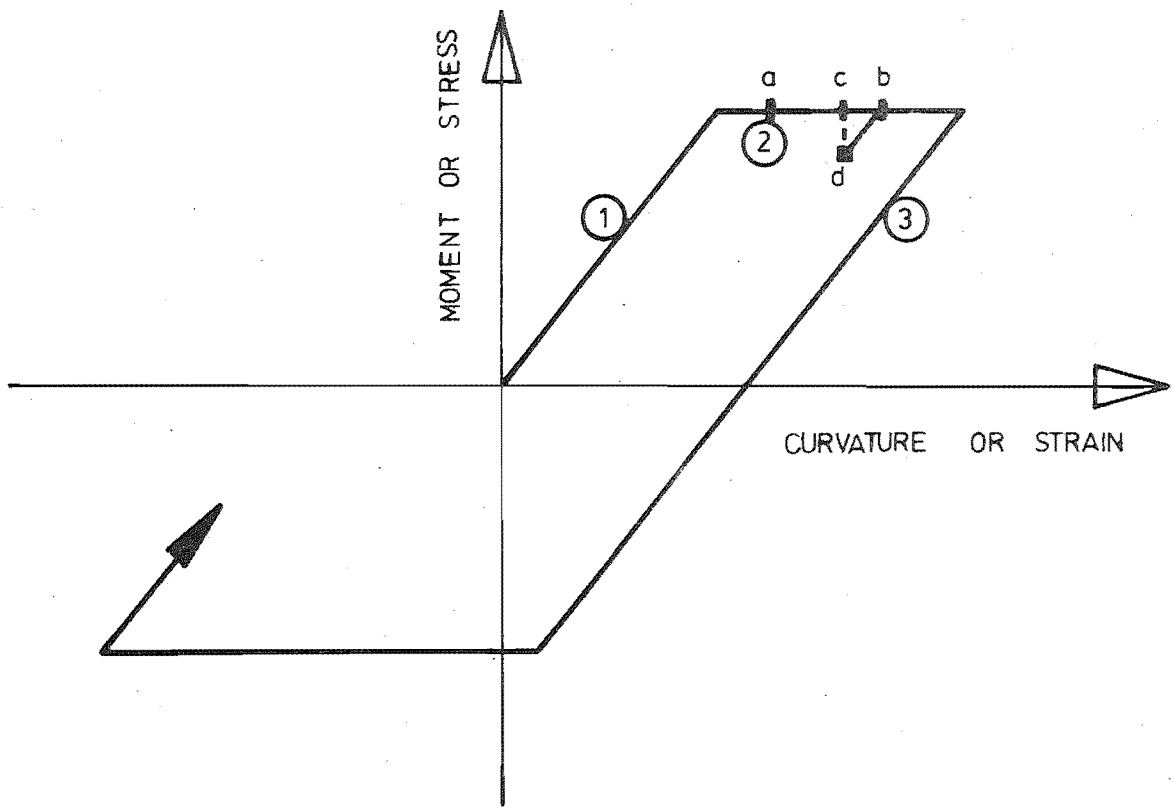

FIGURE 4.3 : TANGENT STIFFNESS DETERMINATION DURING ITERATION.

4.5 DISCUSSION OF THE IMPLEMENTED ANALYSIS

It is recognised that many of the complex phenomena occurring in reinforced concrete, some of which have been listed, are not considered specifically in the selected model. In particular, shear deformation has not been considered in detail and modelled in its own right. However, this development stems from a desire to improve upon the traditional interaction curve approach and recognise some of the fundamental behavioural patterns of shear walls, rather than representing an effort to model continua in minute detail. That the new composite model should closely resemble the actual reinforced concrete construction is a desirable feature, but not an essential one. Similarly, there is no necessity for the idealised mechanical concrete and steel properties to be directly based on real material behaviour - only that realistic overall performance is achieved. This development may be viewed as an extension of the work by Zienkiewicz [45] who successfully used a number of hypothetical bilinear yield criteria to match the more complex hysteretic behaviour of steel. However, experimental basis, as described in section 3.3.3b, was essential.

It is felt that the immediate future of this analysis lies in suitably defining simple section properties, rather than embarking on the development of elaborate material property capabilities that are more complex but possibly less representative than those used in the present approach.

CHAPTER FIVE

INVESTIGATION OF NUMERICAL INTEGRATION TECHNIQUES

5.1 INTRODUCTION

The analysis of elastic structures, to obtain the forced vibration response, is commonly achieved by performing a separate step-by-step integration for each of the first few normal modes of vibration of the structure. The complete response is obtained by superimposing the modal responses. In a nonlinear dynamic analysis this superposition of individual model responses is not applicable. Instead, the response must be obtained by simultaneous direct integration of all of the equations of motion. In this case, each of the natural modes affects the integration procedure, and the presence of natural modes of periods of the order of the integration time step may affect the stability of the numerical scheme.

The integration schemes available divide themselves into two classes: the conditionally stable explicit schemes and the unconditionally or conditionally stable implicit schemes.

Implicit schemes, which entail a simultaneous solution of the equation of motion at each time step, have been selected for most previous structural response studies. Some of these schemes, such as Newmark's $\beta = \frac{1}{4}$ technique involving the assumption of a constant average acceleration over the duration of a time step, are unconditionally stable, i.e. natural periods shorter than the integration time step do not result in a divergent solution ("blowing up"). However, the selected integration time step of unconditionally stable schemes must be sufficiently small to reduce error propagation, due to phase shift and/or amplitude modification,to an acceptable level.

Explicit [46] integration schemes may be single or multistep methods, involving the solutions obtained at the previous one or more time steps. Because they are essentially forward integration procedures they are stable only under favourable conditions (conditionally stable). Although explicit schemes necessarily require a shorter time step than unconditionally stable implicit schemes, no total stiffness matrix formations or decompositions are required and the computational effort at each time step is reduced. It has been suggested [12] that explicit schemes may be suited to solving large systems in which frequent plasticity changes occur.

The purpose of the investigation reported in this chapter was to ascertain whether or not an explicit integration scheme could provide a

viable alternative to the accepted implicit schemes, when a refined dynamic analysis is contemplated. Before a decision on the type of mathematical model to be adopted was reached (discussed in Chapter 3), the following exploratory investigation, assessing the capabilities and limitations of two selected integration schemes, was conducted to determine the most suitable technique for this study. It is essential, of course, that any selected method remains stable with the use of an economically viable time step and a ground motion of realistic magnitude and duration. The technique chosen is a compromise which has been reached in conjunction with a practical mathematical model, consideration of computing resources and satisfactory accuracy of the solution.

5.2 IMPLICIT INTEGRATION OF THE EQUATIONS OF DYNAMIC EQUILIBRIUM USING NEWMARK'S CONSTANT AVERAGE ACCELERATION ($\beta = \frac{1}{4}$) SCHEME

Previous investigations [12,56] suggest that, of the implicit integration schemes, Newmark's constant average acceleration scheme ($\beta = \frac{1}{4}$) is most suitable for computing structural reponses and this method was selected for the preliminary investigation. It is described in the following sections.

(a) Incremental dynamic equilibrium equation.

For a discrete nonlinear structural system dynamic equilibrium at any time t may be written as follows:

$$[M]\{\ddot{u}\} + [C]\{\dot{u}\} + [K_s]\{u\} = \{R\} \qquad (5.1)$$

where $[M]$ is the mass matrix,
$[C]$ is the damping matrix,
$[K_s]$ is the secant stiffness matrix,
$\{R\}$ is the total external load vector,
and $\{\ddot{u}\},\{\dot{u}\},\{u\}$ denote vectors of acceleration, velocity and displacement respectively.

All terms in equation 5.1, except masses, are functions of time.
A linearised incremental form of equation 5.1 is used to solve time step n (between times $(n-1)\Delta t$ and $n\Delta t$). This is described in equation 5.2a where Δ denotes an increment in the variable it precedes and the superscript n denotes values at time $n\Delta t$ or during step n for total and incremental values respectively.

$$[M]\{\Delta\ddot{u}^n\} + [C^{n-1}]\{\Delta\dot{u}^n\} + [K^{n-1}]\{\Delta u^n\} = \{\Delta R^n\} \qquad (5.2a)$$

The approximate acceleration - velocity - displacement relationships,

based on the assumption of a constant average acceleration during an increment (1 time step), were used to rearrange equation 5.2a with the incremental displacement $\{\Delta u^n\}$ as the only unknown term.

$$\left(\frac{4}{(\Delta t)^2} [M] + \frac{2}{\Delta t} [C^{n-1}] + [K^{n-1}] \right) \{\Delta u^n\} = \{\Delta Q^n\} \qquad (5.2b)$$

where $\{\Delta Q\}$ is the incremental dynamic force vector.

Although damping and stiffness terms vary during an increment, they are approximated by values computed at the beginning of an increment, resulting in a set of linear simultaneous equations. These equations are normally solved each time step using an elimination technique and incremental velocities and accelerations are found by substituting in their assumed relationship to displacement. The complete solution at time $n\Delta t$ comprises the sum of all previous incremental solutions. Typically, in a direct application:

(i) Member forces $\{Fe^n\}$ are computed.

$$\{Fe^n\} = \sum_{i=1}^{n} [K^{i-1}] \{\Delta u^i\} \qquad (5.3)$$

(ii) Total displacements $\{u^n\}$ are computed.

$$\{u^n\} = \sum_{i=1}^{n} \{\Delta u^i\} \qquad (5.4)$$

(b) Dynamic load vector

For the structures analysed in this study, the dynamic excitation results from time dependent base motions. In formulating the problem, kinematic parameters (acceleration, velocity, displacement) may be expressed relative to the ground on which the structure rests or alternatively, absolute values may be used. The already coded [12] relative formulation was retained and was satisfactory for this study.

The external load vector $\{R\}$ was defined:

$$\{R\} = - \ddot{u}_g [M] + \{P\} \qquad (5.5a)$$

where $\{P\}$ is the initial load vector which remains constant

and $\ddot{u}_g$ is the absolute base acceleration.

When the equation of dynamic equilibrium is expressed in incremental form

and the constant average acceleration assumption is incorporated, the incremental dynamic load vector, which is compatible with equation 5.2b, is derived.

$$\{\Delta Q^n\} = -\Delta\ddot{u}_g [M] + [M]\left(\frac{4}{\Delta t}\{\dot{u}^{n-1}\} + 2\{\ddot{u}^{n-1}\}\right) + 2[C]\{\dot{u}^{n-1}\} \quad (5.5b)$$

Since $\{\dot{u}^{n-1}\}$ and $\{\ddot{u}^{n-1}\}$ are known, $\{\Delta Q^n\}$ may be evaluated and the incremental dynamic equilibrium equation 5.2b may now be solved for incremental displacements.

Initial conditions were specified as follows:

$$\{\Delta Q^o\} = \{P\} \quad (5.5c)$$

5.3 EXPLICIT INTEGRATION OF THE EQUATION OF MOTION

5.3.1 Selection of an Explicit Scheme for Implementation

Various types of explicit formulation could be considered, ranging from Newmark's original formulation and simple Newton forward difference schemesto Runge-Kutta methods. Although the Runge-Kutta methods were described by Gupta [47] and were considered to be among the better methods, Fu [46] suggests that the amount of repetitive calculation can become disproportionately large. Krieg et al [48] comment on well balanced analyses and state that explicit integration with lumped masses is a practical combination. They concluded that for their shell response work, a 4th order explicit scheme can be more efficient than an implicit one.

All explicit techniques are conditionally stable and Fu [46] has derived a variety of stability criteria. These are related to element dimensions, the dilational wave speed in the material and are thus influenced, to some extent, by the representation of masses.

The 4th order explicit technique used by Hartzman and Hutchinson [49] was selected for implementation so that its performance could be examined. In comparison with a Newton forward difference scheme, this technique offers considerably higher accuracy for a small increase in computational effort and the storage of two additional displacement solutions. Details of the scheme are outlined in the following section.

5.3.2 Mathematical Description

The original implementation of the 4th order scheme by Hartzman and Hutchinson assumed lumped masses and this is retained for the following

derivation. From a rearrangement of equation 5.1

$$\{\ddot{u}^n\} = [M]^{-1}\left(\{R^n\} - [C]\{\dot{u}^n\} - [K_s^n]\{u^n\}\right) \qquad (5.6)$$

where $[K_s^n]$ is the secant stiffness, referenced to the origin, at time $n\Delta t$.

This simplification permits a row by row treatment of the problem since quantities on the right hand side of the expression are known and may be evaluated.

i) The external forces $\{R\}$ are determined from the base motion.

ii) The damping matrix is defined and the current velocity estimated.

iii) Evaluation of actually resisted forces, represented by $[K_s^n]\{u^n\}$, was achieved by stress integration across element boundaries.

Further kinematic quantities may be computed using the following 4th order approximation:

$$\{\dot{u}^n\} = \{\dot{u}^{n-1}\} + \frac{\Delta t}{12}\left[5\{\ddot{u}^n\} + 8\{\ddot{u}^{n-1}\} - \{\ddot{u}^{n-2}\}\right] \qquad (5.7)$$

$$\{u^{n+1}\} = \{u^n\} + \Delta t\{\dot{u}^n\} + \frac{\Delta t^2}{6}\left[4\{\ddot{u}^n\} - \{\ddot{u}^{n-1}\}\right] \qquad (5.8)$$

and $$\{\Delta u^n\} = \{u^n\} - \{u^{n-1}\} \qquad (5.9)$$

To allow velocity dependent damping, an approximate end-of-step velocity was computed using the following equation:

$$\{\dot{u}^{n+1}\} = \{\dot{u}^n\} + \Delta t\{\ddot{u}^n\} \qquad (5.10)$$

Because this 4th order method is a multistep method, a special starting procedure is required. It is assumed for the first increment that

$$\{\ddot{u}^0\} = \{\ddot{u}^{-1}\} = \{\ddot{u}^1\} \qquad (5.11)$$

Thus equation 5.8 reduces to

$$\{u^2\} = \{u^1\} + \Delta t\{\dot{u}^1\} + \frac{\Delta t^2}{2}\{\ddot{u}^1\} \qquad (5.12)$$

Quantities $\{u^1\}$, $\{\dot{u}^1\}$ are given as starting conditions and $\{\ddot{u}^1\}$ is obtained from the equation of motion (equation 5.6).

At the second increment, velocity and displacement vectors are computed as follows:

$$\{\dot{u}^2\} = \{\dot{u}^1\} + \Delta t\{\ddot{u}^2\} \qquad (5.13)$$

$$\{u^3\} = \{u^2\} + \Delta t\{\dot{u}^2\} + \frac{\Delta t^2}{2}\{\ddot{u}^2\} \qquad (5.14)$$

The regular equations are used for the third and subsequent increments.

5.4 METHODOLOGY OF INTEGRATION SCHEME EVALUATION

The 4th order explicit scheme described in section 5.3.2 was implemented using a standard two-dimensional elastic static analysis as a base program. A selection of analyses were performed, first to ensure reliable implementation and secondly, to establish the capabilities of the scheme. Only elastic structures were considered because of limitations of the base program.

To investigate stability of the explicit scheme adequately with a simple model, it was found necessary to define another structure, in addition to those described in Chapter 2. This was because substantial axial forces are induced in the beams in a frame by the explicit numerical technique since nodal deformations are computed independently. The modified portal frame (figure 5.1) exhibited, essentially, a single degree of freedom response and was therefore amenable to analytic solution.

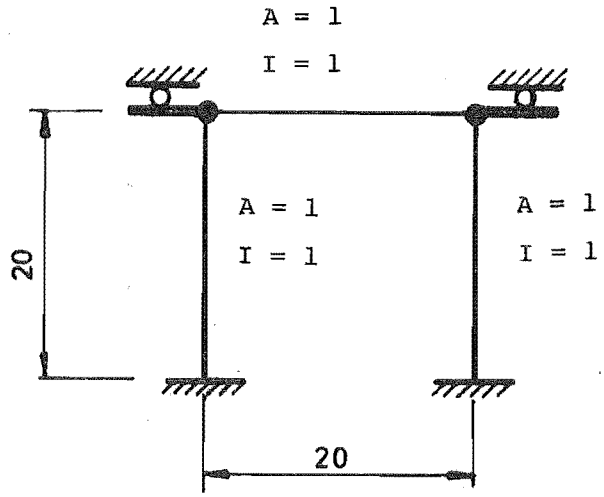

FIGURE 5.1 : SIMPLE MODEL INCORPORATING BEAM ELONGATION MODES.

Beam elongation was observed, affecting solution stability, when the explicit integration was investigated. The response of this simple

structure was compared with that computed using Sharpe's [12] program with the Newmark $\beta = \frac{1}{4}$ scheme. In each case, the forcing function was a continuously applied 0.3 g acceleration.

5.5 RESPONSE RESULTS

The following three analyses are compared in figure 5.2 : (a) An analytic solution computed for the damped response, (b) a solution using implicit integration with $\Delta t = {}^{1}/100$ sec. which, considering the natural periods of the structure, should be (and is) of high accuracy, and (c) an explicitly integrated response with $\Delta t = {}^{1}/100$ sec. showing reduced, but still adequate, accuracy of integration. Some verification of the respective programs (see Chapter 2) is provided. Figure 5.3, showing an elastic response integrated with the explicit scheme of section 5.3.2, illustrates convergence of the scheme with time step refinement and reveals a stability limit in that stable results were obtained with $\Delta t = {}^{1}/50$ sec. but not with $\Delta t = {}^{1}/40$ sec.

For a more representative illustration, Sharpe's [12] 6-storey reinforced concrete frame was integrated, using the explicit scheme, for 4 seconds of the El Centro N.S. 1940 record. Zero damping was assumed and a time step $\Delta t = {}^{1}/600$ was selected. Satisfactory results were obtained although closer comparison with implicit integration results, obtained using Newmark's $\beta = \frac{1}{4}$ scheme and $\Delta t = {}^{1}/100$ sec., would normally be aimed for. Significantly, the respective computer times were almost identical. Two major problems, limiting the application of explicit integration in this study, were encountered:

i) When Caughey damping [50] was applied to the 6-storey frame, a stable solution could not be obtained, even when the time step was refined to ${}^{1}/2000$ seconds. This was because the damping specified was applied to the first two modes and high damping is implied on the higher modes. Because the higher modes are involved with the explicit numerical technique, the high damping severely retards the restoration of equilibrium. In the 6-storey example, unrealistically high damping on the beam dilation modes prevents sufficiently rapid axial elongation of the beams to obtain an accurate stable solution with $\Delta t = {}^{1}/2000$ sec. Orthogonal damping matrices outlined by Wilson et al [51] could overcome this problem because damping may be specified at realistic levels in all modes (or only those modes deemed significant).

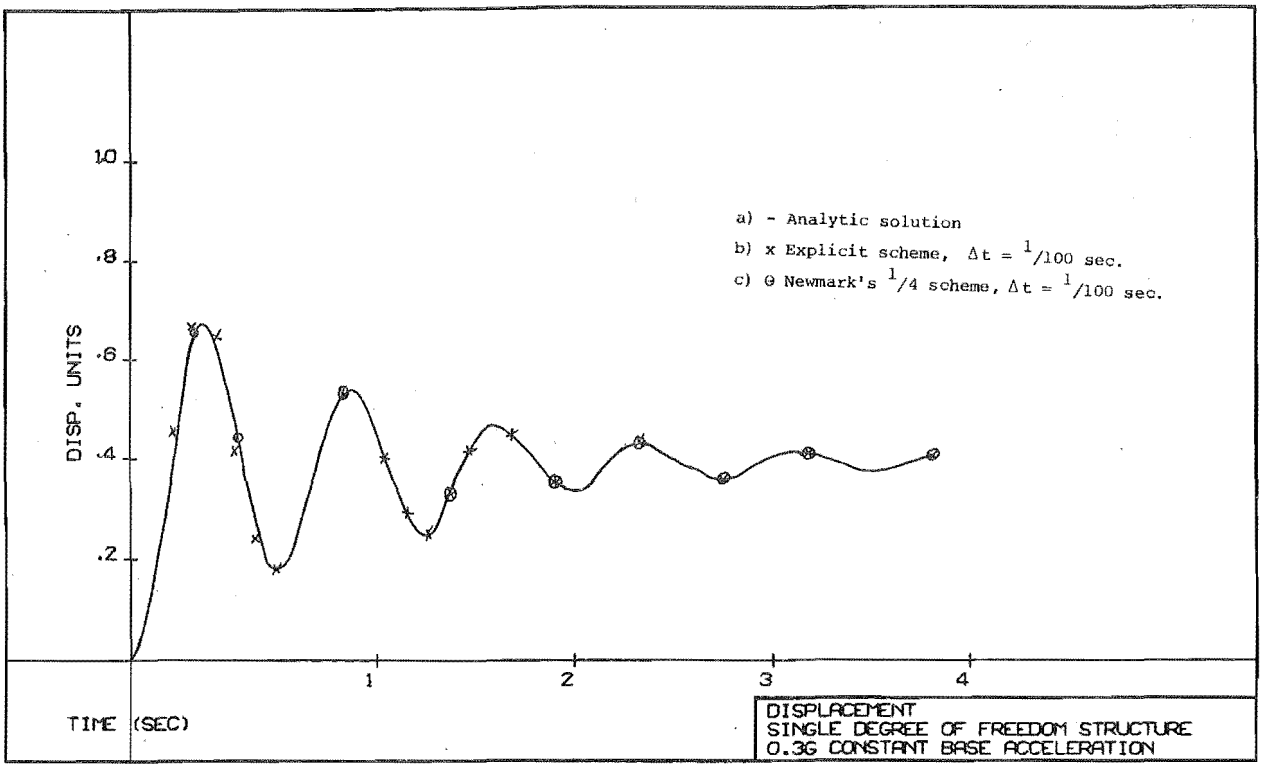

FIGURE 5.2 : COMPARISON OF EXPLICIT AND IMPLICIT INTEGRATION SCHEMES WITH AN ANALYTIC SOLUTION.

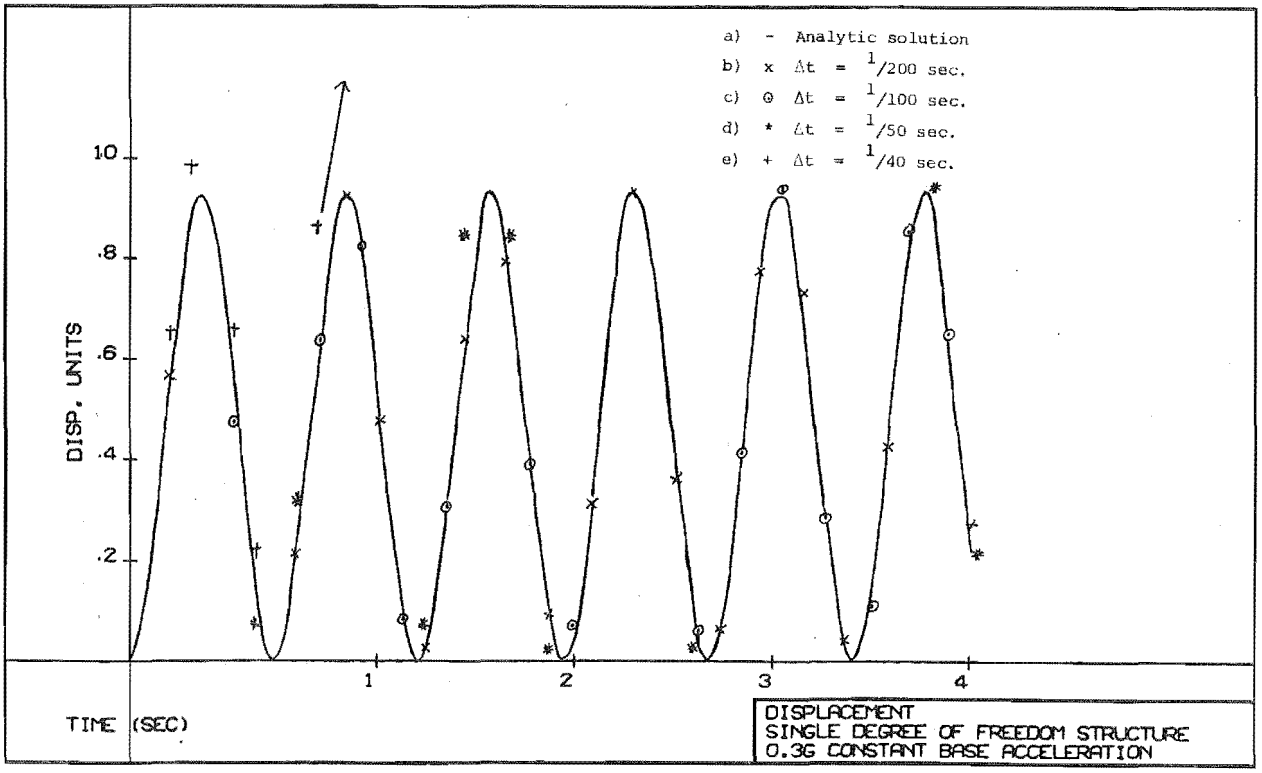

FIGURE 5.3 : UNDAMPED ELASTIC RESPONSE OF SIMPLE STRUCTURE COMPUTED USING THE EXPLICIT SCHEME WITH DIFFERENT TIME STEPS.

(ii) The shortest natural periods of frame structures are usually associated with the axial elongation of beams or columns and typically have natural periods of the order of 0.005 seconds. However, in shear wall structures such as those considered in this study, the most critical modes are those related to the relative vertical movement of interstorey wall nodes at which the only mass (if any) may be a portion of the wall mass. The natural periods of these modes, when compared to those of lateral modes of vibration, are high because they depend on the internodal distance and are related, by a choice of masses, to the compressional wave velocity in the material. Structure C of Chapter 2 has a shortest natural period of 0.0001 seconds when it is idealised with three elements each storey. A time step smaller than this would be required for explicit integration.

5.6 CHOICE OF AN INTEGRATION SCHEME

From the considerations above it is evident that there is no benefit to be gained, in the case of shear walls idealised by two-dimensional beams, by selecting explicit integration in preference to unconditionally stable implicit integration for this study. Newmark's constant acceleration method was selected because of its proven suitability for such analyses. Further confirmation of this choice came by noting that the structural stiffness band width is small for a coupled shear wall, idealised as outlined in Chapter 3. Thus, unless large frame-wall systems are considered, the simultaneous equation solution is unlikely to become a limiting factor.

However, it appears that explicit schemes are well suited to impulse loading analyses where a rapid response for a short duration is of interest or when the number of equations becomes very large. Systems with reasonably large natural periods and simple element properties are likely to represent the most favourable situation.

CHAPTER SIX

IMPLICIT NUMERICAL INTEGRATION OF THE EQUATIONS OF MOTION

6.1 INTRODUCTION

As shown in Chapter 5, Newmark's constant average acceleration ($\beta = \frac{1}{4}$) method was considered the most suitable for this shear wall study. The method has been widely used in dynamic analyses to the point where it may be considered a standard technique. However, some fundamental problems, which required recognition and which are lightly covered in the literature, were encountered. In particular, peculiarities in stability and accuracy criteria associated with a variable structural stiffness were considered. Interest was concentrated on the capabilities and limitations of Newmark's ($\beta = \frac{1}{4}$) scheme to ensure that reliable results were obtained in the later analyses of this study.

6.2 INTEGRATION ACCURACY

6.2.1 Integration Accuracy Considerations in Elastic and Inelastic Analyses

Elastic dynamic time history analyses are not essentially incremental procedures. It is, however, often both convenient and practical to treat them as such, in which case equations 5.1 to 5.5 are satisfactory. In this application the accuracy of integration approximation operators has been well documented [52,53,54,55,56]. Extensive accuracy studies have been performed in the analyses of small elastic, and usually one degree-of-freedom, structures. Various investigators have studied the unconditionally stable Newmark [11], Wilson [57] and Houbolt [56] schemes. Artificial damping [58] and periodicity errors [52] in elastic examples have occupied considerable attention. One general conclusion, relating to the forced response of a multi-degree-of-freedom system and an unconditionally stable scheme, has emerged: Accurate response results will be obtained provided that those modes in which significant response occurs are integrated accurately and large percentage errors in the response of higher modes will make a minimal contribution to the total response of the structure. Sharpe [12] has presented useful comparisons to establish the accuracy of Newmark's constant acceleration ($\beta = \frac{1}{4}$) method in analysing elastic and inelastic frame structures of realistic size and complexity. His elastic studies are consistent with the above general conclusions while

his inelastic studies point, in particular, to the problem of equilibrium imbalance. Since the accuracy of nonlinear analyses is of prime interest, elastic analyses were performed here for comparative purposes only, to assess the magnitude of additional errors incurred in nonlinear analyses.

Nonlinear dynamic time history analyses are, however, because of their path dependence, essentially incremental procedures. Since some approximate constant value of stiffness is used during a time step, equilibrium is not necessarily satisfied, and cumulative drifting from the correct solution is observed. In a recent study [12] "moment overshoot" with a simple bilinear moment-curvature relationship was shown to be a significant problem. In this study, where a realistic section idealisation was attempted, additional and substantially greater departures from equilibrium were encountered. If an excessively small time step is impractical - as is usually the case in nontrivial problems - attention must be given, preferably in a selective manner, to those time steps during which significant errors are introduced. An attempt must be made to remove the effects of an unrepresentative stiffness used during a time step. A short summary of recent work relating to the accuracy of nonlinear integration has been presented by Nickell [56], where he refers to a possible "degeneration" of the constant acceleration Newmark method in certain non-linear problems. He concludes from the evidence available that the Newmark operator is the most attractive direct integration operator for both linear and nonlinear problems.

6.2.2 An Illustrative Example

Depending on the yield conditions, structure A (Chapter 2) may exist so far as incremental solutions are concerned as two distinct different structures. For at least part of the response the original elastic structure is considered, i.e. until yield occurs when portions of the response are computed assuming a pin base structure. Each of these incremental structures possess different natural periods and mode shapes (see figure 6.1) and of these, because stiffness deterioration is present (as for all inelasticity in this study), the original elastic structure should limit the integration because it contains the shorter natural periods. It would seem reasonable that inelastic solutions of comparable accuracy to elastic solutions could be obtained, provided that satisfactory measures are taken to ensure equilibrium preservation and if additional stability problems are not encountered. It remains to establish which (if any) of the equilibrium correction techniques, derived or referred to herein, are

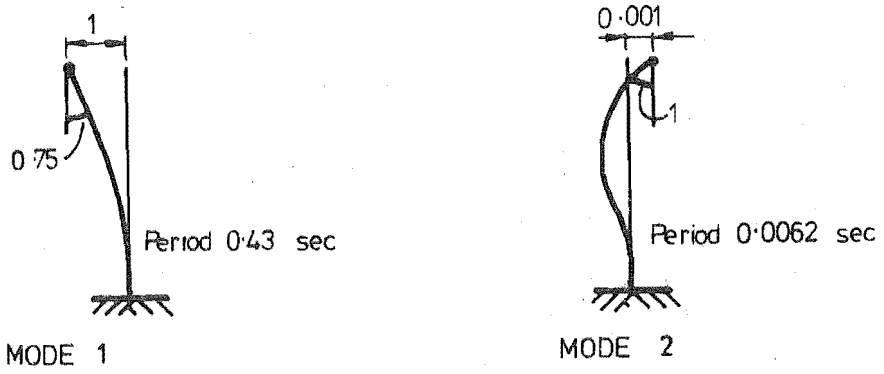

a) First two modes of original elastic structure A

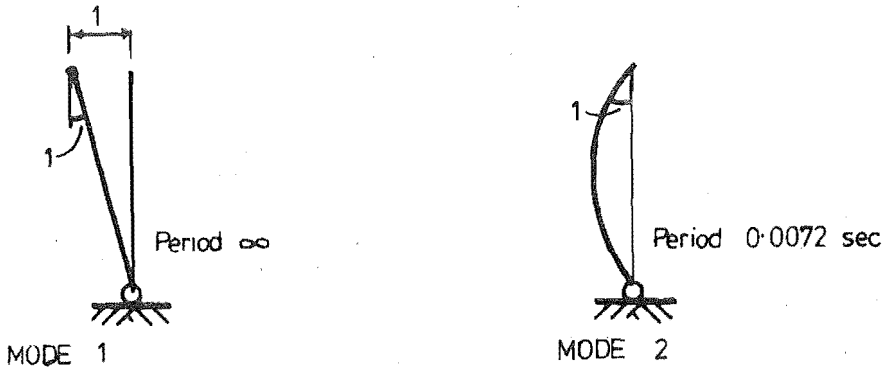

b) First two modes of structure A with a pin at the base

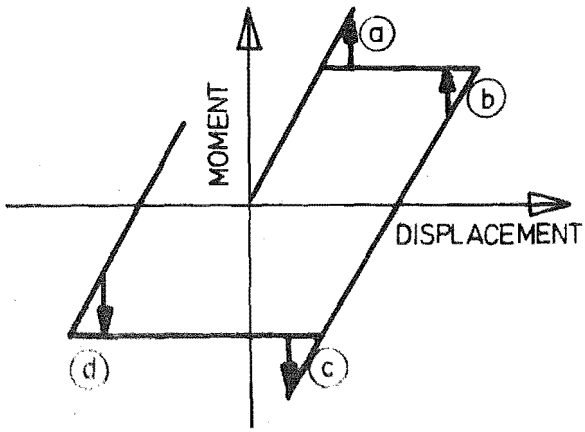

Sense of local force imbalance	ⓐ	ⓑ	ⓒ	ⓓ
Sharpe's correction	+	−	−	+
Modified correction	+	+	−	−

SENSE OF FORCE APPLICATION

c) Excess force magnitudes and signs

FIGURE 6.1 : MODE SHAPES AND EQUILIBRIUM CORRECTION FORCES FOR STRUCTURE A

capable of achieving this goal.

6.2.3 Equilibrium Correction Techniques

The basic equilibrium correction techniques considered, among which combinations are permissible, are:

i) No equilibrium correction by nodal load application, but the total force vector is derived from internally resisted stresses.

ii) Subdivision of timesteps during which changes in stiffness occur.

iii) Internal stresses used to compute out-of-balance forces for application of corrective nodal forces during the subsequent time step (out-of-phase correction).

iv) Newton-Raphson iteration (N.R.) or Modified Newton-Raphson iteration (M.N.R.) performed with the current out-of-balance forces.

v) Iteration on the total equations of dynamic equilibrium.

Suggestion i) was used with a very small time step as a reference against which the effectiveness and accuracy of the other techniques were assessed. Technique ii) was not implemented because of storage problems and the large increase in dynamic stiffness and dynamic load vector formation times when continuously variable member properties are allowed. In the following sections the remaining three suggestions are developed from basic principles, compared with other reported analyses, checked against "benchmark" analyses and assessed for their suitability in the problem type considered.

6.2.4 Out-of-Phase Equilibrium Correction

Two previous research reports [12,59], each describing in detail a programmatic implementation of an out-of-phase equilibrium correction technique and its subsequent use in nonlinear problems, have been reviewed. Both refer to their respective techniques as being approximate, even (presumably) for simple one degree-of-freedom structures, and both are significantly different. In each case the full excess force is applied to the following time step although Sharpe [12] inserted a factor of -1.0 for unloading cases (see figure 6.1c). Powell [59], as interpreted by the author, subtracts whatever force correction was applied during the previous time step. This implies that the "temporary corrective" force must be allowed to act for one time step and in an incremental procedure it must be first applied, then removed. Neither of these approaches were found to

give optimum results for a one degree-of-freedom system. Certainly for simple structures there exists a unique correction which will give the correct result.

a) Details of an out-of-phase equilibrium technique

In equation 5.2 it is assumed that a displacement solution $\{\Delta u^n\}$ based on the linearised stiffness $[K^{n-1}]$, i.e. the stiffness at the beginning of the nth time step, has been found. Thus, values for all the incremental kinematic variables in equation 6.1 have been determined:

$$[M]\{\Delta\ddot{u}^n\} + [C]\{\Delta\dot{u}^n\} + [K^{n-1}]\{\Delta u^n\} = \{\Delta R^n\} \tag{6.1}$$

An equilibrium check is made considering overall equilibrium at the end of the nth increment.

$$[M]\{\ddot{u}^n\} + [C]\{\dot{u}^n\} + \{Fr^n\} = \{R^n\} \tag{6.2}$$

Equation 6.2 is the relationship which must be satisfied, where actually resisted forces $\{Fr^n\}$ are present, and not the predicted forces $\{Fe^n\}$ which are consistent with the increment linearisation. Actually resisted forces $\{Sr^{n-1}\}$ will have been computed at this stage, as described in Chapter 4. Hence the corresponding nodal forces $\{Fr^{n-1}\}$ may be computed using the transformation $[T_g]$ which was described in section 3.9.

$$\{Fr^{n-1}\} = [T_g]^T \{Sr^{n-1}\} \tag{6.3}$$

where $\{Fr^{n-1}\}$ are actually resisted nodal forces present at the end of the previous time step.

Since each increment is linearised, predicted nodal forces $\{Fe^n\}$ may be easily computed.

$$\{Fe^n\} = [T_g]^T [K^{n-1}]\{\Delta u^n\} + \{Fr^{n-1}\} \tag{6.4}$$

The actually resisted internal forces $\{Sr^n\}$ present at the increment end may be derived from element stresses and the corresponding nodal forces computed.

$$\{Fr^n\} = [T_g]^T \{Sr^n\} \tag{6.5}$$

Out-of-balance forces $\{F_{xs}^n\}$ are defined:

$$\{F_{xs}^n\} = \{F_e^n\} - \{F_r^n\} \tag{6.6}$$

On checking equation 6.2, equilibrium satisfaction will only be present if the stiffness remains equal to $[K^{n-1}]$ for the duration of the nth increment. Otherwise some correction, based on the imbalance, is required. An appropriate correction using the out-of-balance force is presented for a single degree-of-freedom system in Appendix A.1.

From this derivation the corresponding incremental equation of motion for a multi-degree-of-freedom system may be deduced and expressed in more general terminology for the nth increment.

$$[M]\{\Delta\ddot{u}^n\} + [C^{n-1}]\{\Delta\dot{u}^n\} + [K^{n-1}]\{\Delta u^n\} = -\Delta\ddot{u}_g[M] + \{F_{xs}^{n-1}\} \tag{6.7}$$

This is precisely the full excess force vector with algebraically consistent signs, without removal at the end of a time step, added to the incremental external force vector. The correction is now seen to be simply the application of the external loading, not already resisted by damping, inertial and internal forces, to a dynamic stiffness based upon the current incremental structural stiffness. It is later confirmed that irrespective of whether this correction was lumped with the next increment or applied separately, convergence in one cycle is obtained when a bilinear stiffness is used with structure A.

b) Use of out-of-phase equilibrium correction

In order to verify the above derivations and to illustrate characteristics which are superior to other techniques, a series of runs were made with structure A and, in each case, comparison was made to a "benchmark" (reference) analysis. The response comparisons are presented in figures 6.2 and 6.3 where both the benchmark and the scheme described above are represented on each graph. The obvious effect of an incorrect sign in Sharpe's force correction (lines b and c on figure 6.2) is still present even at $^1/200$ sec. time step. The modified out-of-phase force application used here proved very efficient for this structure. The absence of any correction is shown (curve c in figure 6.3) to result in significant errors, although not so large as those with a correction of incorrect sign. The final near correct plastic drift is considered to be a coincidence. That the out-of-balance force application with removal (section 6.2.4)

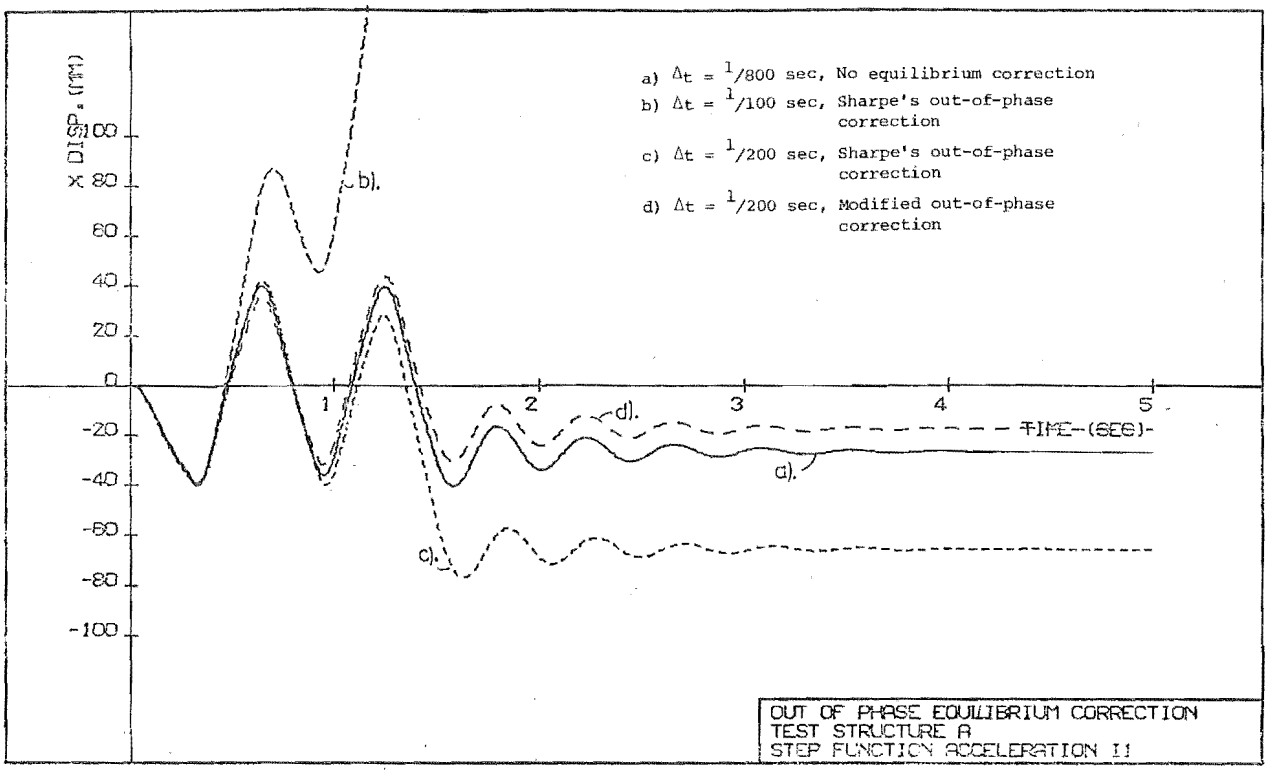

FIGURE 6.2 : OUT-OF-PHASE EQUILIBRIUM CORRECTION (1).

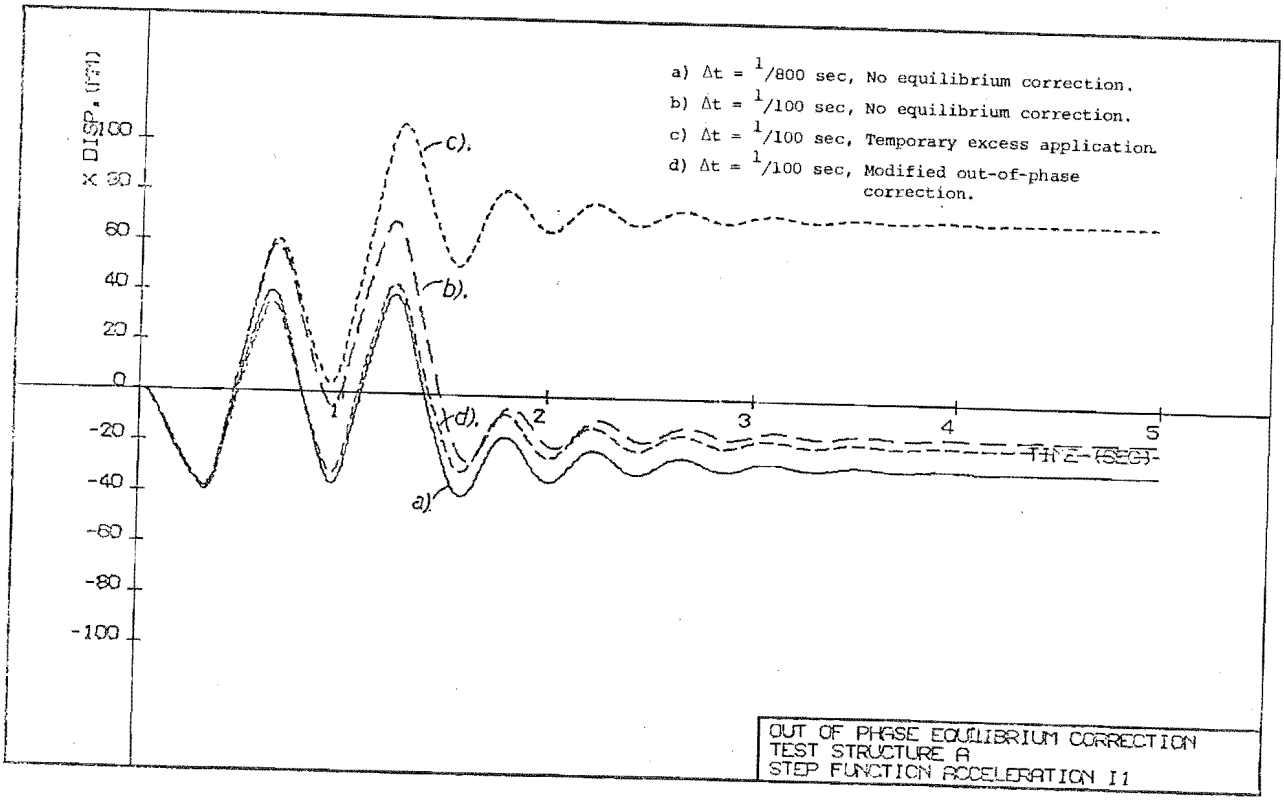

FIGURE 6.3 : OUT-OF-PHASE EQUILIBRIUM CORRECTION (2).

represents a small effort in the right direction is reflected by its similarity to the no correction case - at least until 1 second. Cumulative displacement errors obscure further comparison.

6.2.5 Iteration on the Excess Force Vector

Iteration on a selected time step has also been considered previously. Sharpe [12] attempted iteration on the excess force vector but failed to maintain sensible continuity (discussed in Chapter 4) of incremental curvatures and consequently the scheme "did not portray the physical situation". It is evident (see Chapter 4) that additional constraints incorporated in member stiffness subroutines to ensure sensible continuity of strains during iteration are necessary. It was considered prudent at this stage to examine iterative procedures applied to small problems in a more detailed manner before proceeding to large structures.

a) Description of the excess force iteration

The following relationship was deduced from the single step out-of-phase correction in Appendix A.2 and applies after the initial incremental solution has been obtained with equation 5.2b.

$$\left(\frac{4}{\Delta t^2}[M] + \frac{2}{\Delta t}[C] + [K^n_{i-1}]\right)\{\Delta u^n_i\} = \{F^n_{xs_{i-1}}\} \qquad (6.8)$$

In the notation, the superscript n refers to time, denoting values at time $n\Delta t$ or incremental values for the nth increment, as in preceding sections. The subscript i relates to iteration and denotes values at the end of the ith iteration or incremental values for the ith iteration. A value of $i = o$ indicates values at the end of the initial increment computation and before iteration commences. The formulation may be used for m iterations $i = 1, \ m$ where corrections are accumulated in the following standard manner:

$$\{u^n\} = \sum_{i=1}^{m} \{\Delta u^n_i\} + \{u^n_o\} \qquad (6.9)$$

where $\{u^n_o\}$ is the displacement solution at the end of the nth increment obtained with equation 5.2b.

Various alternative forms using different approximations for $[K^n_i]$ were examined. The following formulation operated particularly well:

$$\left(\frac{4}{\Delta t^2}[M] + \frac{2}{\Delta t}[C] + [K_o^n]\right)\{\Delta u_i^n\} = \{Fxs_{i-1}^n\} \qquad (6.10)$$

where $[K_o^n]$ is the stiffness computed at the end of the nth increment.

A modified Newton-Raphson iteration where $[K^{n-1}]$ was substituted for $[K_o^n]$ in equation 6.10 did not operate satisfactorily when a section idealisation was considered.

In all cases iteration was initiated when any force imbalance was not within a specified tolerance related to respective yield levels. Termination is allowed when force imbalances are sufficiently small, or alternatively, when the displacement correction is detected to be small by examination of displacement vector elements as follows:

$$\frac{|\Delta u_i^n|}{\left|\sum_{i=1}^{m} \Delta u_i^n\right|} < \text{tolerance} \qquad (6.11)$$

In either case, all degrees of freedom were examined individually and checked against the specified tolerance.

b) Use of excess force iteration

A demonstration of the technique in operation was undertaken and figure 6.4 shows runs using excess force iteration (1 cycle to converge) with $t = {}^1/800$, ${}^1/100$ seconds. Results for this simple example are identical in every respect to those for out-of-phase correction. Use in analysing structure C, which is considered to be a more realistic example, is shown in figure 8.11. In the program the damping matrix embodies a portion of the current stiffness matrix which is subject to variation. Figure 6.4 shows comparisons where the equilibrium correction did not include any out-of-balance force due to damping changes and this allows appreciation of the expected error magnitude.

6.2.6 Total Equilibrium Iteration

a) Description

If, when satisfactory iterative equilibrium correction has been achieved for certain increments only, a significant accumulation of small errors occurs, appeal to the total equilibrium equation is the most reliable manner in which to regain overall equilibrium. Such a technique was outlined by Bathe et al [60], and essentially the same scheme is described in Appendix A.

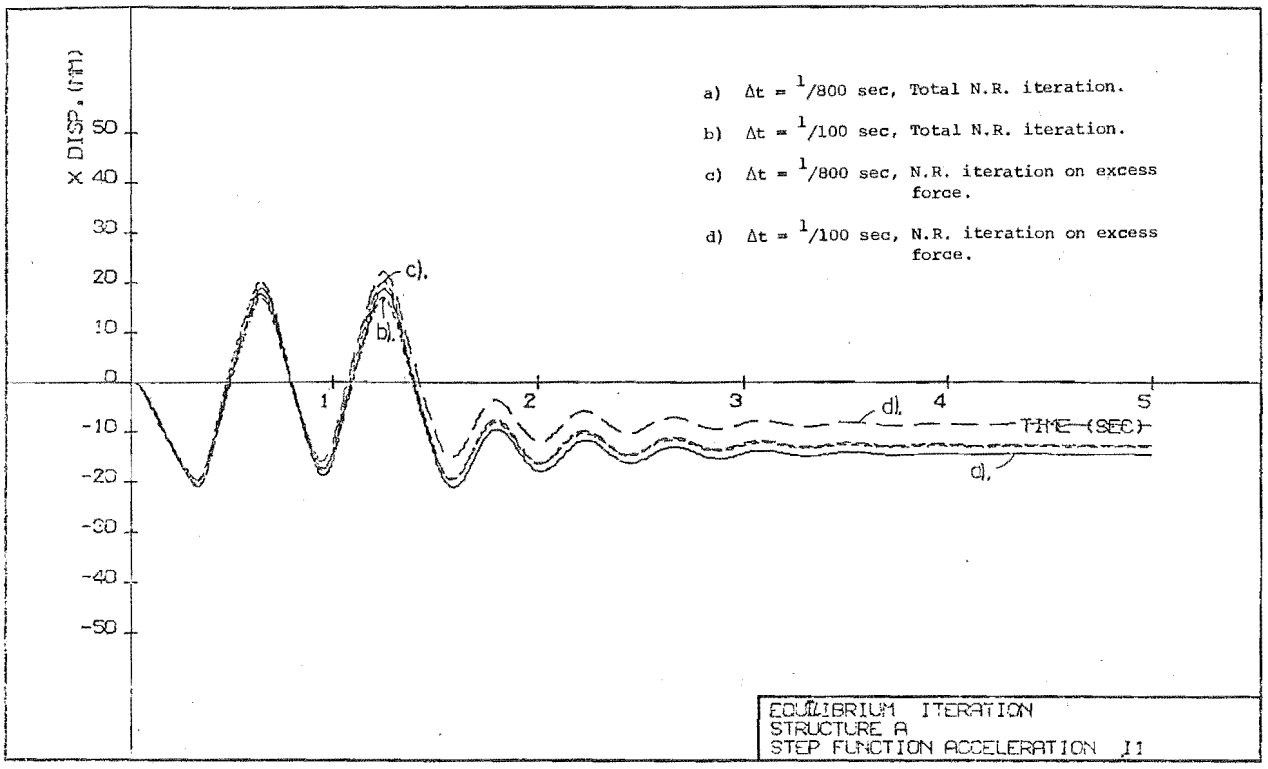

FIGURE 6.4 : COMPARISON BETWEEN ITERATIVE EQUILIBRIUM TECHNIQUES.

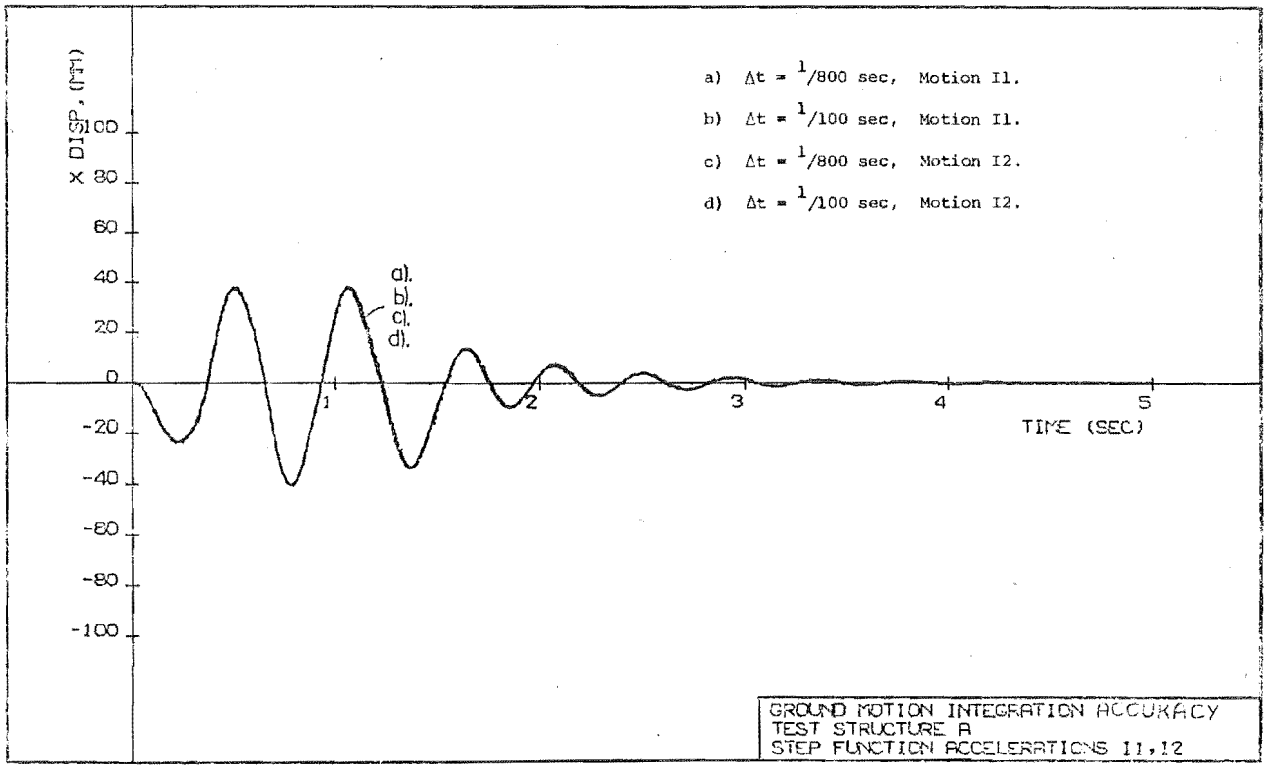

FIGURE 6.5 : INTEGRATION ACCURACY FOR ELASTIC RESPONSE TO IMPULSE FUNCTIONS.

The following recursive relationship refers to the corresponding equation A.12 in Appendix A and applies after the initial incremental solution $\{\Delta u^n\}$ has been obtained.

$$\left(\frac{4}{\Delta t^2}[M] + \frac{2}{\Delta t}[C^n] + [K^n_{i-1}]\right)\{\Delta u^n_i\}$$

$$= -\ddot{u}_g[M] + \{P\} - [M]\{\ddot{u}^n_{i-1}\} - [C^n]\{\dot{u}^n_{i-1}\}$$

$$- \{Fr^n_{i-1}\} \qquad (6.12)$$

As in the previous iteration, the stiffness may be restricted for economy to $[K^n_o]$, the stiffness at time $n\Delta t$ prior to iteration.
To continue the iteration, consecutive corrections are summed and added to the initially estimated incremental displacement $\{\Delta u^n_o\}$:

$$\{\Delta u^n_m\} = \{\Delta u^n_o\} + \sum_{i=1}^{m}\{\Delta u^n_i\} \qquad (6.13)$$

and the total displacements are computed.

$$\{u^n_m\} = \{u^{n-1}\} + \{\Delta u^n_m\} \qquad (6.14)$$

where m iterations have been performed.
Incremental velocity and displacement values for the increment are calculated by re-using Newmark's constant average acceleration assumption as follows:

$$\{\Delta\ddot{u}^n_m\} = \frac{4}{\Delta t^2}\{\Delta u^n_m\} - \frac{4}{\Delta t}\{\dot{u}^{n-1}\} - 2\{\ddot{u}^{n-1}\} \qquad (6.15)$$

$$\{\Delta\dot{u}^n_m\} = \frac{2}{\Delta t}\{\Delta u^n_m\} + 2\{\dot{u}^{n-1}\} \qquad (6.16)$$

Total velocity and displacement values may be accumulated as in equation 6.14.
Total iteration initiation relies, as for excess force iteration, on checking out-of-balance forces and termination may result from the convergence of displacements or forces.

b) Use of total equilibrium iteration

Comparative analyses are presented in figure 6.4, establishing the accuracy of total equilibrium correction. When structure A was analysed with zero damping, identical results were obtained with all three techniques -

confirming the reliability of intensive debugging procedures. Complete Newton-Raphson iteration was used successfully on structure C but modified Newton-Raphson iteration (stiffness restricted to $[K^{n-1}]$) appeared unsatisfactory with the section idealisation. When large changes in the location of the stiffness centroid arose, instabilities occurred in the axial direction. However, restriction of the stiffness to $[K_o^n]$ gave satisfactory convergence for structure C.

6.2.7 Conclusions on Equilibrium Correction Techniques

Out-of-phase equilibrium correction has been shown to be a highly efficient procedure (see section 6.2.4) - at virtually no extra cost the equivalent of one iteration each time step is incorporated. Therefore, all nonlinear analyses performed in this study, excluding those for test purposes, used this facility. It is conceivable that, while this technique may be capable of correcting the majority of errors, there could exist short periods of rapid stiffness change which are solved inaccurately, thus invalidating the entire analysis. Variations on Newton-Raphson iteration were incorporated and should be capable of dealing with these situations as they arise. Although the total equilibrium iteration treats damping more correctly, only minor errors were introduced when excess force iteration was used and both methods provided very satisfactory solutions for structure A.

6.2.8 Accuracy of the Representation of the Ground Motion Record

Another possible source of error, and indeed often a limiting one, results from approximations inherent in digitising the ground acceleration. It has not, as yet, been established what proportion of the errors shown earlier arise from this source, whether or not nonlinear analyses are more susceptible to digitisation errors than elastic ones, or whether function I1 (figure 2.5) is significantly more difficult to integrate than a typical earthquake accelerogram. Analyses were made using structure A but considering a small change at the beginning of function I1 giving function I2 (figure 2.5) in order to show the effects of small errors in base accelerations. Function I2 is more difficult to integrate than I1 since the time step preceding the start of the record has an increment in acceleration of 0.3 g starting at $t = -1/800$ or $-1/100$ sec. depending on the time step. With function I1, the 0.3 g impulse is applied over the interval starting at t = 0 in all cases.

The four elastic runs (figure 6.5) using $\Delta t = 1/100, 1/800$ sec. and I1, I2 acceleration combinations are indistinguishable. The four corresponding nonlinear runs (figure 6.6) show greater variation between

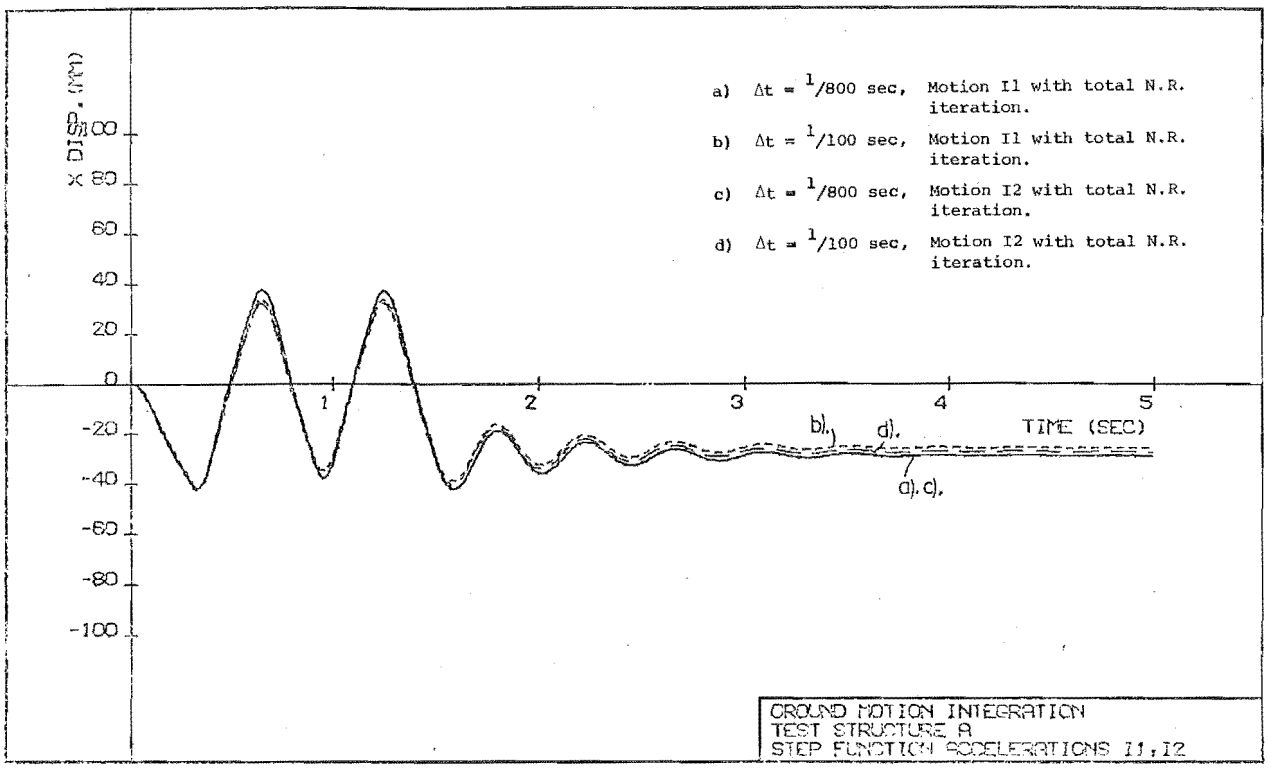

FIGURE 6.6 : INTEGRATION ACCURACY FOR INELASTIC RESPONSE TO IMPULSE FUNCTIONS.

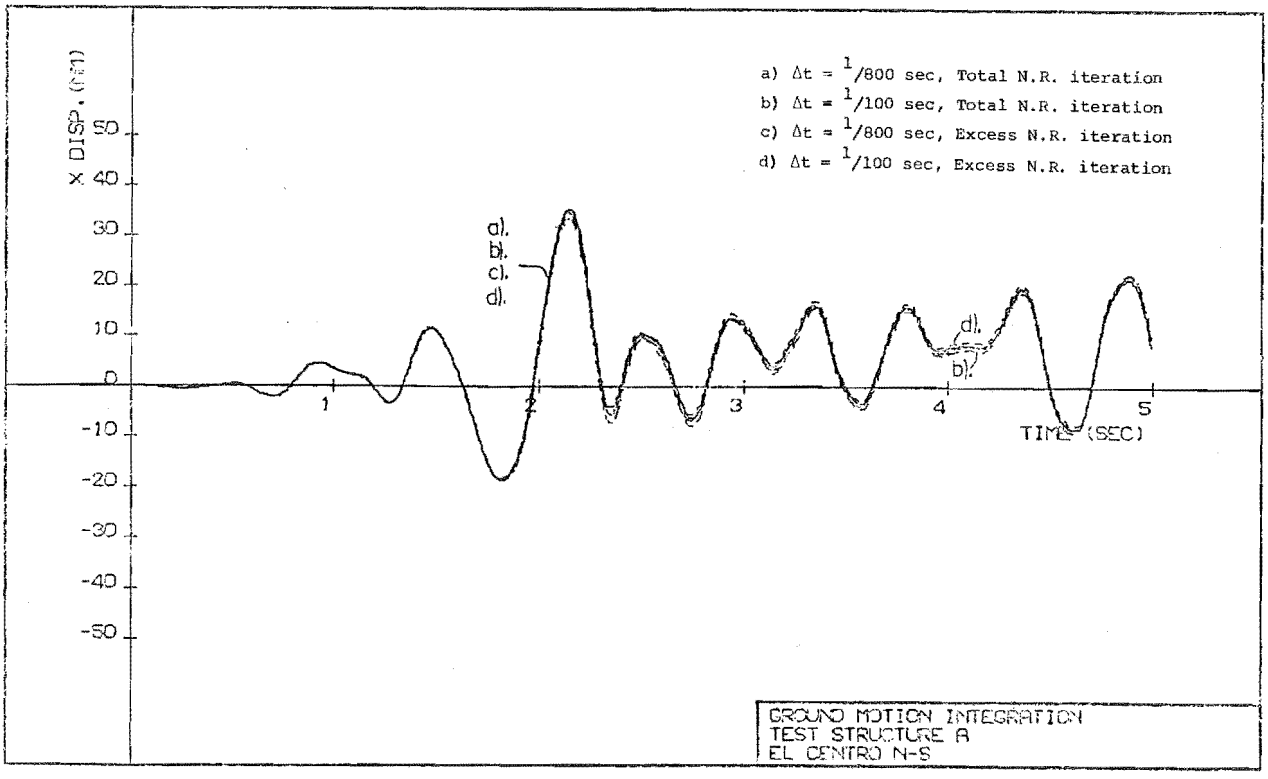

FIGURE 6.7 : INTEGRATION ACCURACY FOR INELASTIC RESPONSE TO EL CENTRO N.S. 1940 GROUND MOTION.

displacements although moment histories were also indistinguishable. It is concluded that nonlinear responses are more difficult to integrate because the entire solution history directly affects the displacement solution, while elastic responses tend to "lose" small historical errors (figure 6.5), particularly if resonance occurs. The acceleration applied $^{1}/_{100}$ second in advance of the commencement of the record results in a noticeable plastic drift (line d in figure 6.6).

In order to assess how significant these discrepancies are, runs using an actual earthquake record were made with the inelastic structure A and are described and plotted in figure 6.7. Comparison with figure 6.6 confirms that discrepancies are generally smaller than in the case of the impulse functions.

It is concluded that errors associated with earthquake accelerogram digitisation are likely to be more important in nonlinear analyses than elastic ones. Therefore elastic analyses cannot provide conservative estimates in this respect. In the case of realistic structures analysed in this study, ground motion integration errors were only examined in the overall accuracy context as the time step was refined because of the computational effort involved.

6.3 INTEGRATION STABILITY

6.3.1 Stability of Numerical Integration in Elastic and Inelastic Analyses

It is possible to consider similar structural problems which lead to almost identical responses but which have different stability criteria restricting the time step because of small differences in the idealisation. The problem of the stability of the numerical technique is one which should be considered if reliable results are to be obtained. Lack of stability gives no warning but introduces spurious increasing oscillation which could be significant but remain undetected even by an experienced user. Distinction is made between two types of a stability problem. First, there is the classical instability where unstable oscillation occurs although overall equilibrium is maintained. This is typified in the elastic analyses performed using Newmark's linear acceleration ($\beta = \frac{1}{6}$) method. Secondly, there is the apparent instability, which may be non-oscillatory, associated with a change of real force resisting capability due to a variation of the structural stiffness. In such cases, the apparent lack of stability may also be a function of the type of equilibrium correction and, as outlined later, is perhaps better considered as a convergence problem.

Newmark [11], in his classical work, has shown the constant acceleration ($\beta = \frac{1}{4}$) method to be unconditionally stable for undamped elastic one degree-of-freedom structures. Unconditional stability of this method in multi-degree-of-freedom structures is generally accepted. In nonlinear analyses using Newmark's $\beta = \frac{1}{4}$ method, stability problems which may be presumed to be of the second type above, have been reported by other authors [56] and have been encountered in this study. A limited numerical study with particular emphasis on the effects of changes in structural stiffness, was undertaken.

6.3.2 An Illustrative Example

Structure A, as described previously, may assume a number of incremental configurations consecutively (two transverse ones) and, of these, the original elastic structure possesses the shortest natural periods. If equilibrium is not violated during transitional increments, then, effectively, a structure possessing properties between the previous two is considered. Presumably, the stability criteria should be based on the most critical of these incremental structures, i.e. the original elastic structure. The principal omission in this hypothesis is the effect of changes in the incremental structure. After each transition between the two phases of structure A, the respective short period modes are forced to participate because of the different shapes of the respective modes as described below.

The following three analyses were performed to illustrate the effects of a changing structural stiffness:

i) Structure A was constrained to remain elastic and when this structure was subjected to any horizontal base motion an entirely first mode response was observed.

ii) When a pin was inserted at the base of structure A for an entire response, again a pure first mode response was observed. In this case different modes from those in i) are present (see figure 6.1b).

iii) Finally, when the two configurations were allowed to follow one another consecutively, as in a normal elastoplastic analysis, a response in both translational modes of each incremental structure was observed.

Thus, higher mode response may be initiated by a variable stiffness alone. It is inevitable, for most practical nonlinear analyses of multi-degree-of-freedom systems, that the modes so excited will possess small natural periods when compared with the integration time step.

It remains to establish what deleterious effects (if any) this phenomena will have on nonlinear analyses performed with Newmark's $\beta = \frac{1}{4}$ "unconditionally stable" integration scheme. Although equilibrium correction was applied, the corrective force was simply another horizontally applied load at the top node and was therefore indistinguishable from inertial loads in this simple problem. Oscillation in the higher mode occurred irrespective of equilibrium correction. The separate problem of the effect of externally applied equilibrium correction forces in more general problems is discussed in section 6.4.

6.3.3 Numerical Investigation

Speculation regarding the nature of the vibration in the second translational mode of structure A (figure 6.1a) arises, particularly when its response is inadequately integrated. Basic comparisons were made between analyses using different time steps. As a control, structure A1 (figure 2.2), which has essentially identical properties to structure A excepting the removal of the high frequency mode of vibration, was also analysed with different time step sizes. The runs were performed with zero damping and a modification of the ground motion I1 which contained a uniformly decreasing acceleration from 1.5 to 5 seconds to expose the higher mode vibration. This higher mode vibration is evident in figure 6.8 and is inaccurately integrated in the analysis with $\Delta t = {}^{1}/_{100}$ sec. Structure A1 (figure 6.8), with the higher mode removed, exhibits no such oscillation. Higher mode vibration is also seen in figure 6.9 where the integration is performed more accurately and these reduced vibrations are an actual physical phenomena. Even when it is inaccurately integrated ($\Delta t = {}^{1}/_{100}$ sec.) the higher mode response does not appear to significantly affect the accuracy of the overall response (figures 6.8 and 6.9), nor does the magnitude of the spurious oscillation appear to grow over a longer period of time (figure 6.10). In figures 6.2 and 6.3 this higher mode oscillation was eliminated by supercritical damping applied to the higher mode. The figure 6.11 comparisons show that structure A, with the higher mode present, may be integrated just as accurately as structure A1 which has no higher mode.

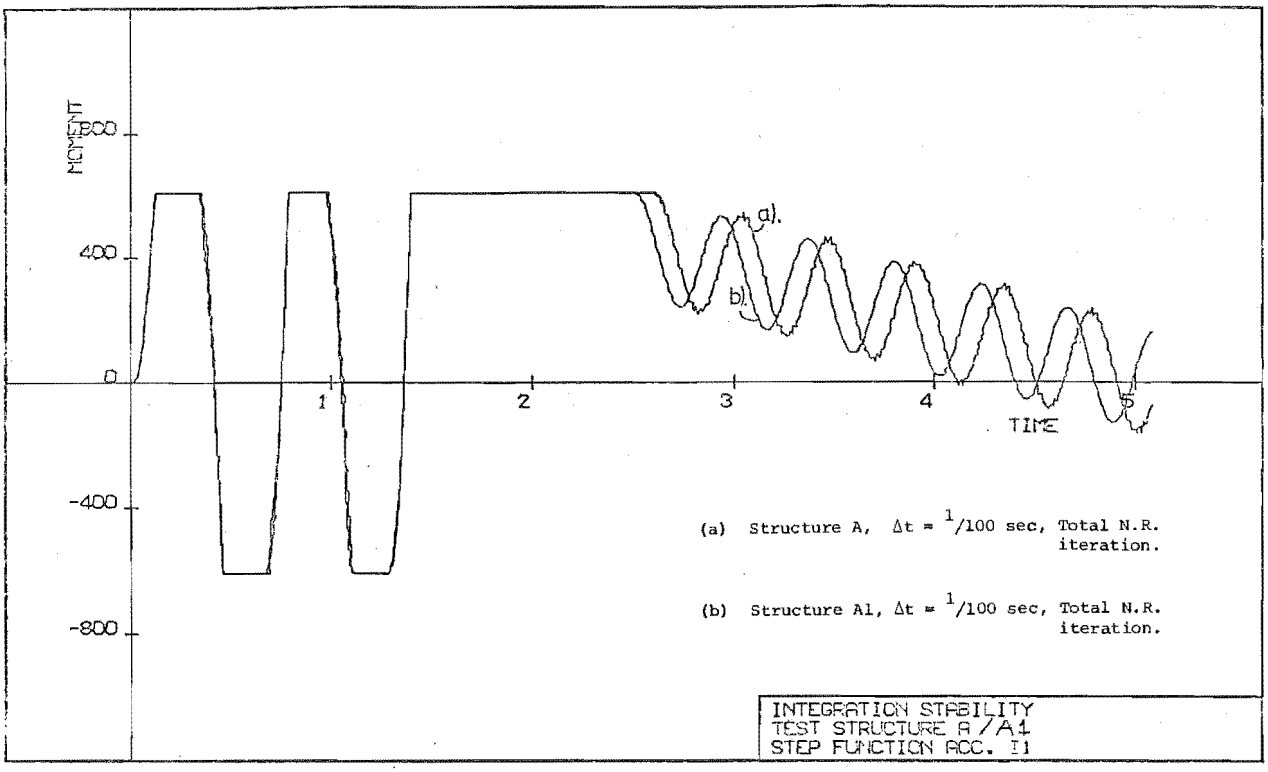

FIGURE 6.8 : SPURIOUS HIGHER MODE VIBRATION IN STRUCTURE A.

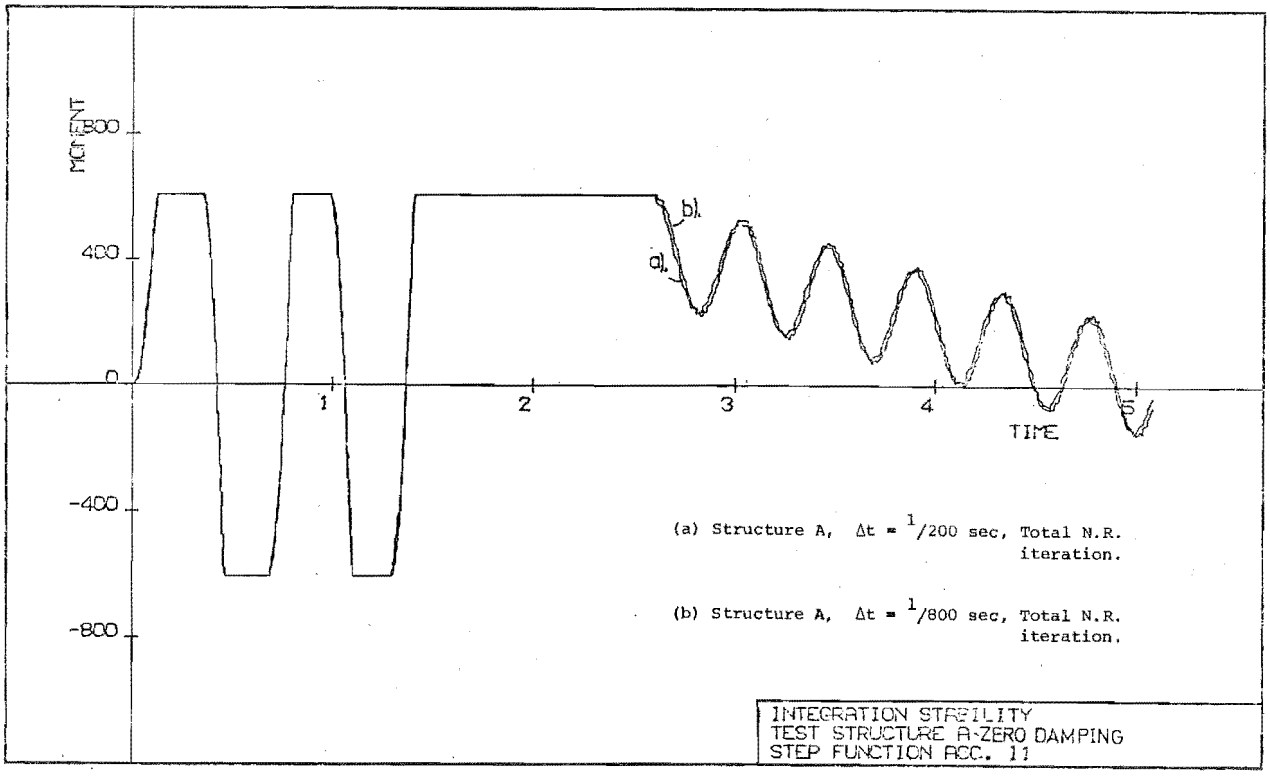

FIGURE 6.9 : ACCURATE NUMERICAL INTEGRATION WHERE HIGHER MODE RESPONSE IS EVIDENT IN STRUCTURE A.

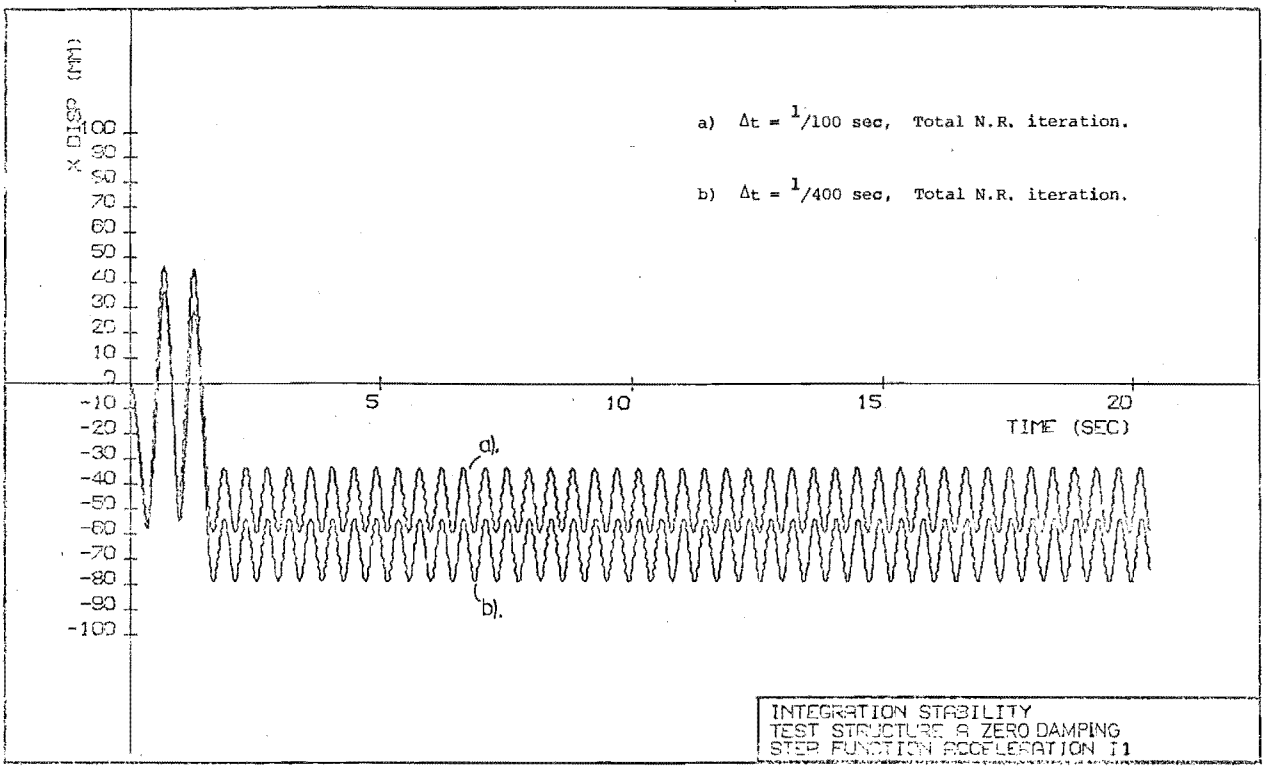

FIGURE 6.10 : LONGER DURATION ANALYSES WITH SPURIOUS VIBRATION PRESENT.

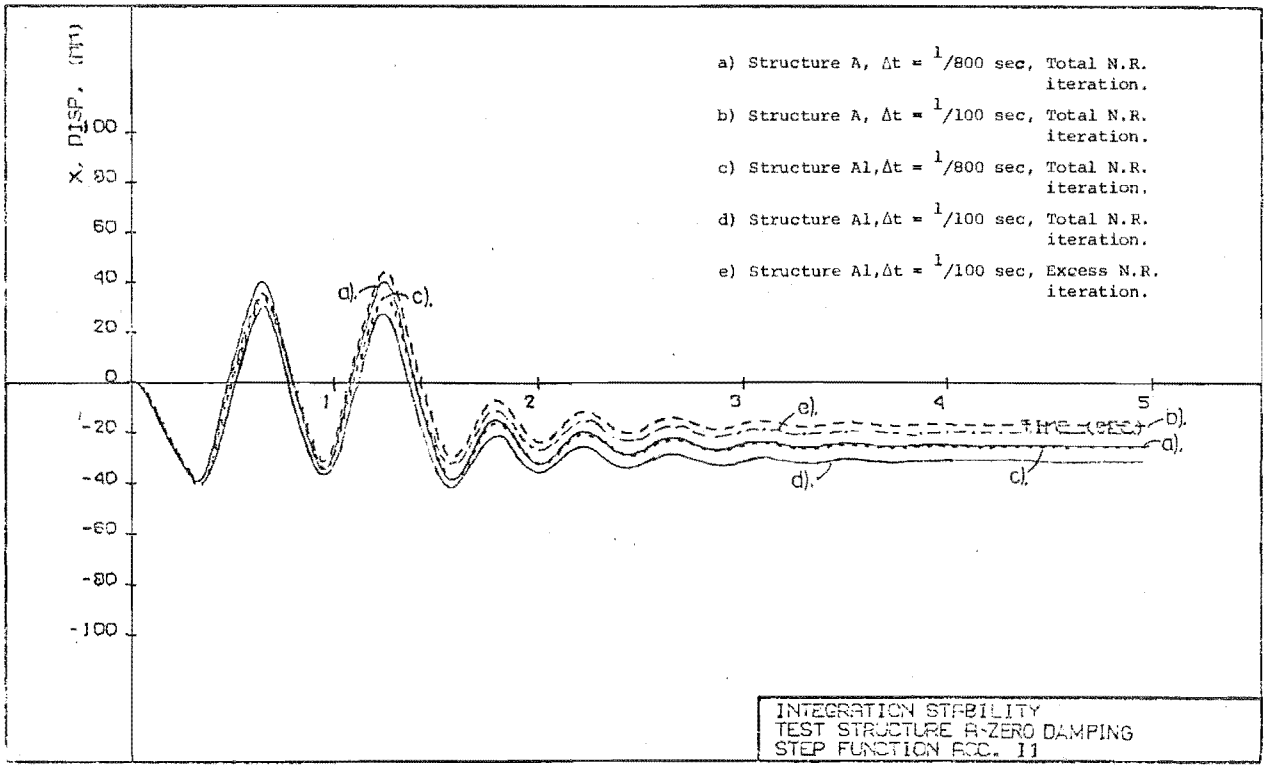

FIGURE 6.11 : EFFECT OF REMOVING THE HIGHER NATURAL MODE ON THE ACCURACY OF INTEGRATION.

6.4 CONVERGENCE OF THE NUMERICAL INTEGRATION

6.4.1 A Definition

In Newmark's [11] original formulation of his numerical integration techniques, which involve some iteration each time step, the dual criteria of stability and convergence arose. When using an implicit formulation to analyse elastic structures, the convergence limit based on the shortest natural period is no longer significant because no iteration is necessary. However, when an inelastic response is computed, even an implicit formulation frequently requires some form of iteration during the course of an analysis. In some of the analyses performed in this study, a divergent solution was obtained when iteration was allowed, even after sensible continuity of the tangent modulus (during iteration) had been assured (Chapter 4). It was considered that this problem was one of convergence.

6.4.2 An Illustrative Example

A useful illustration is provided by structure B which allows bilinear hinging in the lower member. Its essential distinctive feature with respect to structure A is the inclusion of an additional node, having small lumped masses, near the base. Newton-Raphson iteration may still converge in one iteration but equilibrium corrections associated with nonlinearity in the lower member must be made by means of forces at the lower node. Inevitably, a higher mode response is initiated. Structure B was unstable when analysed with $\Delta t = {}^{1}/100$ sec. only if equilibrium correction was made. Convergence was obtained in all cases if $\Delta t = {}^{1}/200$ sec. was used. When the height of the lower member was halved (to 0.1 m) the response computed with $\Delta t = {}^{1}/200$ sec. was divergent but only when equilibrium correction with external nodal forces was attempted at this time step. It is believed that these counter-examples show that a convergence limit exists when nonlinear analyses requiring equilibrium correction are undertaken with Newmark's constant acceleration ($\beta = \frac{1}{4}$) method.

6.4.3 Bounding of the Convergence Limit

Unlike Newmark's original convergence limit, this limit on the time step is not easily defined. As a result of a preliminary investigation the following factors are believed to influence the convergence limit associated with Newmark's constant acceleration method in nonlinear examples:

i) Displacement function of the element.

ii) State and type of nonlinearity.

iii) Severity of the forcing function.

iv) Period of nodes excited directly by equilibrium correction forces.

In all structures analysed, the limit encountered in this study was related to a substantially larger time step than Newmark's classical convergence criteria [11]. Structure A, considered earlier in this chapter, confirms that Newmark's limits are not the criteria when an implicit formulation is used. The convergence limit encountered here was often somewhat smaller than the maximum size time step with which sufficiently accurate results could be obtained with an unconditionally stable integration scheme. The analyses of structure B suggest that the periods of the higher natural modes, based on the current tangent stiffness, which actively participate during the iteration process, are important. However, some difficulty exists in identifying which modes are likely to be important. Alternatively, it may be preferable to base approximate convergence criteria on the stiffness matrix diagonal term and the lumped mass associated with degrees of freedom of interest. If degrees of freedom were chosen which were likely to be excited with equilibrium correction forces, this simple calculation could provide indications of the high frequency response affecting the convergence. A comprehensive numerical study would be required to confirm the usefulness of this suggestion.

In the absence of further research, it seems that the best approach is to actually monitor any iteration and check convergence. In the remainder of this study, where the original objective of shear wall response prediction was pursued, iteration was generally limited to one cycle and a sufficiently small time step designed to provide adequate accuracy was used.

CHAPTER SEVEN

THE COMPUTER PROGRAM STRUCTURE AND ITS APPLICATION

7.1 INTRODUCTION

The computer program was developed from the two-dimensional inelastic analysis of Sharpe [12]. All original capabilities have been retained and a number of new features have been incorporated, resulting in greater capacity and complexity of the program. To conduct research using the new idealisations greater understanding of the program than is necessary to use bilinear hinge elements is required: the quantity of coding is approximately doubled and the input information is considerably more detailed. This chapter provides a brief outline of some of the more significant, different details of implementation, not referred to elsewhere, together with general advice and instruction on the use of the program. Suggestions and general guidance for future research, which relate to aspects of program implementation, are also included in this chapter.

7.2 ORGANISATION OF THE PROGRAM

7.2.1 Summary

The following additional features have been incorporated in the program:

i) A variety of elements capable of general section idealisation.

ii) Systems for the magnetic tape storage of data and interfacing with a separate plotting program.

iii) An efficient alternative equation solving routine.

iv) Newton-Raphson iteration procedures for use within a time step and a modification to the out-of-phase equilibrium correction technique.

v) Two restart capabilities - one is a user-developed routine and the other is a system capability.

The structure of the program (see Sharpe [12] Appendix D) remains unchanged and all modifications, except the equilibrium correction techniques, are included in the form alternative subroutines and subroutine strings.

A number of important aspects which have required attention during the development of the program are discussed in the remainder of this section.

7.2.2 Reference Axis Locality

Gross section properties are computed initially, using input material properties. The program assumes at this stage that the reference axis is aligned with concrete section centroids and actual agreement may be checked later by reviewing the internally computed properties printout. The reference axis locality could, in principle, be arbitrarily selected but efforts have been made here to ensure coincidence with the mass centroid since no eccentricity transformations are performed on the mass matrix.

7.2.3 Section Numbering

Simple point section integration was adopted, allowing complete freedom of the order of numbering across sections. The automatic subdivision of typical sections actually numbers concrete flanges, or outer elements, first so that if cracking is to be considered it may be related to the first two integration points. It is important to ensure that a particular section is not operated on twice because of a data error in the schedule which allocates sections to members.

7.2.4 Organisation of Element Property Computation

Elements A and B curvature and section properties computations were coded in separate subroutines called directly from the main routine for performing the dynamic analysis. Transfer of section data from main storage arrays to local working arrays was effected by arithmatic assignment statement loops. Initial communication from the University of Canterbury Computer Centre analysts recommended this program construction in preference to disk operations on the Burroughs 6700 computer. Somewhat later, the Computer Centre programmers suggested the matching of portions of large arrays with small working arrays by using appropriate array elements (instead of usual array names) as arguments in subroutine call statements. Elements C1 and C2 branch to section routines from the original curvature subroutine and are based on this concept. The gains in computational efficiency proved disappointing.

7.2.5 Stiffness Matrix Changes

Present coding modifies the total stiffness matrix by addition and subtraction of individual stiffness matrices to be interchanged. Economy is to be gained by the alternative total reformation of the total stiffness matrix when, on an average, more than half the member stiffnesses change each increment. A test to change, or not to change, stiffnesses is at

present used for elements C1 and C2, based on any detectable numerical change in stiffness. Further work could establish what percentage of current (or cumulative) change in member stiffness warrants a change in the global stiffness matrix. This technique could allow significant savings in the effort required to form incremental stiffness matrices. However, an additional unessential variability in results was considered highly undesirable at this stage.

7.3 MEMBER DUCTILITY AND DAMAGE ASSESSMENT

7.3.1 Survival of the Structure

Assessing the damage extent is of principal importance, especially relating response results to element performance data which has been (and can be) obtained from experiment. Usually, the extent of the nonlinear rotation is of interest and this property is considered with the two types of element adopted in the structural idealisations.

a) Spring hinge element

A usual definition of ductility, the total member end rotation divided by the elastic rotation, was adopted for these elements. So far as the needs of this study are concerned, the experimental work on coupling systems by Paulay [3] and Binney [4] and the slab coupling study reported in this thesis may be related directly through this definition.

b) Section defined elements

The capability is available to specify a yield curvature and to compute a history of nonlinear curvatures for ductility computations. In practice it was found preferable to plot moment curvature diagrams and to estimate section ductilities by geometrical construction. The reliability of ductilities determined in this manner is limited by the accuracy of strains computed in the program (see Chapter 4).

7.3.2 Secondary Damage

The above considerations relate, primarily, to major structural damage. The extent of secondary, nonstructural damage is also of interest, but it is not well described in shear wall structures by interstorey displacements. However, all displacement histories may be stored for plotting, including interstorey displacements which should be useful for investigating attached frames. Wall rotations which relate to the area of distortion between walls are also available.

7.4 DAMPING AND MASS REPRESENTATION

7.4.1 Damping

Caughey [50] damping relates the mass matrix [M] and the current stiffness matrix [K] to the damping matrix [C] as follows:

$$[C] = \alpha[M] + \beta[K] \tag{7.1}$$

Terms α and β are defined:

$$\alpha = \frac{2\omega_1\omega_2(\omega_2\lambda_1 - \omega_1\lambda_2)}{\omega_1^2 - \omega_2^2} \tag{7.2}$$

$$\beta = \frac{2(\omega_1\lambda_1 - \omega_2\lambda_2)}{\omega_1^2 - \omega_2^2} \tag{7.3}$$

where ω_1 , ω_2 are the smallest two natural circular frequencies and λ_1 , λ_2 are the respective fractions of critical damping applied to the first two natural modes.

7.4.2 Mass Representation

In the majority of analyses performed, lumped masses at nodes were used, although the capability of consistent mass representation [61] is present. Preliminary runs and other work [15,16] have indicated that mass representation errors are likely to be less significant than most of the idealisation and integration problems considered here. It is thought however, that rotation of section terms of the consistent mass matrix could be significant in some structures.

7.5 DATA FILES AND PLOTTED PRESENTATIONS

Inevitably, dynamic time history analyses produce enormous quantities of data from which particular structural performances must be gauged or different structural responses compared. A comprehensive printout at execution time is not the answer; rather, magnetic tape storage of histories of a wide, but selected, variety of parameters which may be assessed for printing or plotting at any later time has proved very satisfactory. Most results presented here have been plotted using the Computer Centre Calcomp plotter which has a $^1/_{100}$ inch resolution. Tape handling systems developed allow the production of time history sequences

to plot any two of the following variables against one another: time, displacements, forces, out-of-balance forces, total curvatures, nonlinear curvatures, axial strains, nonlinear axial strains, section stiffnesses and eccentricities of section stiffness centroids.

It is only study and evaluation of suitably plotted presentations of basic parameters which can lead to an understanding of structural performance. Extensive use of the plotting routine is considered mandatory, to provide satisfactory verification, when large structures and inexperienced users are involved.

7.6 EQUATION SOLVERS

When an implicit integration scheme is used the solution of a set of simultaneous equations becomes a vital part of the solution process, and often a particularly time consuming portion. Consideration was given to making this process more efficient, now that previously used assembler language equation solvers [12] have become redundant with the installation of the Burroughs 6700 computer.

In technical terms, the Burroughs 6700 is a stack orientated machine on which the Algol language, with its block structure, has considerable advantage in operational efficiency over Fortran. Although the entire program has been written in Fortran, the possibility of binding in efficient Algol subroutines, displacing original Fortran versions, to economise some of the time consuming operations, appears attractive. Attention here was concentrated on the equation solver for which an Algol version was developed. A listing together with the complementary Fortran version is presented in Appendix B. Examination of Table 7.1 shows a substantial gain in computational efficiency, indicative of savings possible in other portions of the program if similar modifications were made. However, the subroutine incorporates a number of machine dependent features, including vector mode processing and nonsegmentation of arrays, which would complicate transfer to other machines. For this reason emphasis has not been placed on applying the same degree of specialisation to other portions of the program. Instead a high degree of machine independence has been aimed for.

TABLE 7.1 : COMPARISON OF COMPUTER TIMES

Description of equation solver	2-storey 2-bay frame Semi band 12 x 18		6-storey 8-bay frame Semi band 54 x 63	
	Relative decomposition times	Relative backsubstitution times	Relative decomposition times	Relative back-substitution times
Original Fortran version processing across rows of the stiffness matrix	1.00	1.00	1.00	1.00
Original Fortran version with no array segmentation	0.77	0.87	0.74	0.68
Fortran with processing down columns of the stiffness matrix for efficiency	1.03	1.00	1.02	1.02
Fortran with processing down columns and no array segmentation	0.82	0.92	0.74	0.88
Algol subroutine	0.46	0.39	0.25	0.22

7.7 ITERATION AND EQUILIBRIUM CORRECTION

The three basic forms of equilibrium correction, derived in Chapter 6, were implemented with variations being available. Out-of-phase equilibrium correction remains, because of the negligible extra effort involved, operational at all times. Depending on the relative magnitude of out-of-balance forces, a level one type of iteration or a level two type of iteration may be activated and, ultimately, a condition where errors are so large as to invalidate the analysis may be detected. Types of iteration which are available and which have been used in this research include original Newton-Raphson, alternatively with modifications to retain the initial tangent stiffness or the stiffness of the first iteration. Each of these three may operate on the out-of-balance force vector or overall equilibrium. In practice only one level of iteration was used - usually Newton-Raphson operating on the out-of-balance forces which was modified to use the stiffness computed after the first iteration. The omission of additional storage arrays so that initially applied loads (dead loads) could be considered with total equilibrium iteration is one shortcoming of the program. However, excess force iteration, which deals only with force increments, appeared quite adequate to accommodate most practical situations.

7.8 RESTART CAPABILITIES

7.8.1 System Restart Capability

In concept, system based Algol routines for a fully automatic restart, simply initiated by a single command

RERUN (Previous job number in system)/
(Number of starting point),

and starting from any previous checkpoint, appeared ideal. The use of this procedure was attempted. In practice, machine operational procedures which resulted in the indiscriminate removal of disk files and difficulties with the machines internal security controls made restarting a hazardous and involved operation.

7.8.2 User Developed Restart Capability

A restart capability developed by the author and included in the program proved more easily manageable within system operational limitations. Simply, all arrays and most variables were written to magnetic tape at selected time intervals. On restarting the basic analysis information is re-read as input data (first 5 cards) allowing changes in time step size,

iteration types, iteration limits and the base acceleration. The main structural parameters - geometry, connectivity,member properties and material properties - are recovered from the tape file for all subsequent runs. The complete base acceleration is read again from the beginning but until the restart point is reached the program runs in a "pending restart mode". In this state the main computational cycle is swept through but all the work is omitted except reading the base motion, positioning output files and printing times for the user. The main plotting data file is read and so repositioned or, alternatively, a new data file may be defined and the original is copied until the restart point. Any combination of runs may be performed and used to create continuous data files for plotting. A further capability (at present a single patch card is required) is that of computing natural mode shapes and frequencies of the structure in its deteriorated condition at the instant of restarting. A study using this facility to investigate the variation of mode shapes during a nonlinear response could lead to further understanding of structural behaviour.

CHAPTER EIGHT

ELEMENT PERFORMANCE

8.1 INTRODUCTION

Most of the elements described in Chapter 3 have been used previously to model flexural behaviour in reinforced concrete structures. Spring hinge elements have been used previously in the dynamic analysis of shear walls to study seismic responses [15,16]. However, published work describing the capabilities and limitations of these elements, particularly in dynamic analyses, is almost non-existent. It would seem that simple examination of typical problem solutions is unlikely to provide reliable indications of element performance. An attempt is made in this chapter to confirm that the postulated analysis is operating satisfactorily in simple problems and is capable of providing satisfactory solutions for typical structures.

First, to examine flexibilities, element deformations with a simple force distribution were considered. By computing eigenvalues and eigenvectors of the stiffness matrices and establishing the strain energy associated with different mode shapes, further insight into element behaviour was gained. The different elements were used in a simple test environment, provided by structure B, and interelement comparisons were made. Structure C was used to make projections to a structure more realistic in size.

Indications, at least, of reliability and accuracy of the various elements have been obtained and, in particular, inherent problems in idealising continua with spring hinges have been identified.

8.2 EXAMINATION OF STIFFNESS MATRICES DEPICTING NONLINEAR BEHAVIOUR

8.2.1 Illustrative Example

For the purpose of demonstration, a simple but important example was selected. The model is that of a prismatic beam of length 10 units, an arbitrary Young's modulus value of 30×10^6, and having an original stiffness 100 units which due to nonlinearity deteriorated to 10 units. Three elements were considered: element A, element C1 which in this case is identical to the element used in the P.C.A. study [15], and an element with spring hinges at both ends as used in the study by Blakeley et al for the New Zealand Ministry of Works and Development (MWD) [16].

8.2.2 Deformations Under a Uniformly Distributed Moment

Examination of element deformations with a constant moment distribution, a condition which is approached on idealisation refinement, reveals an incompatibility in element C1 when a prismatic beam of stiffness 10 units is taken as a reference. The element C1 spring stiffness was defined, as in [15], such that rotations θ and θ' in figure 8.1 were equal. Clearly, in this case, the nonlinear transverse deformation (i.e. associated with the hinge rotation) of element C1 is double that of the other two elements. This implies an imaginary shear deformation equal to the nonlinear transverse deformation. The problem is one of an internal incompatibility in the nonlinear curvature displacement relationship. Hence response solutions will not necessarily converge to the correct solution with the use of more closely spaced elements (mesh refinement). In fact, if mesh refinement is performed using element C1 in a region of constant moment (and curvature), then from the deformations in figure 8.1 it is apparent that the overall incompatible displacement will remain undiminished.

8.2.3 Examination of Eigenvalues and Eigenvectors of the Stiffness Matrices

A technique which has proved useful [62],when new finite elements are being developed or studied in greater detail,is the examination of eigenvalues and eigenvectors of the element stiffness matrices. The eigenvectors give a set of uncoupled deformation patterns while the eigenvalues can be shown to represent twice the strain energy associated with these modes. Any deformation pattern can be represented by a linear combination of eigenvectors and thus their various contributions to the total strain energy may be identified.

The element C1 results are not particularly useful in that direct comparison of modes is not possible and the constant moment example is more instructive. It may be reasonably concluded, however, that deformation will tend to occur in the lower energy mode (figure 8.2). Investigation of the two hinge element (used in the MWD investigation)reveals a more subtle problem. Although the springs have been proportioned such that the symmetric flexural mode stiffness is correct, the antisymmetric (or shear) mode stiffness (figure 8.2) is in error by a factor of 3. This implies that, under a given load pattern, the nonlinear translational deformation of the two hinge element will be enhanced by a factor of 3. In general it is impossible to achieve, simultaneously, the correct symmetric and antisymmetric stiffness with this type of model.

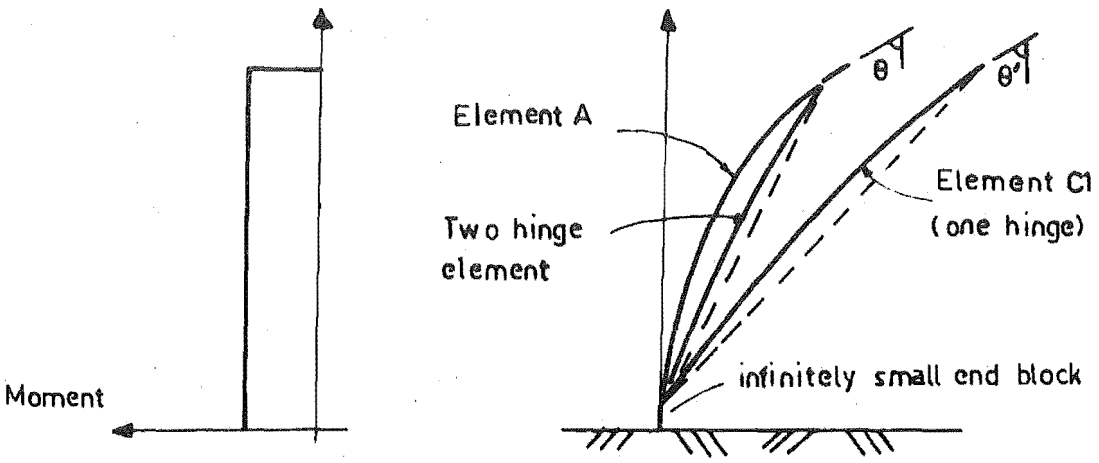

a) Moment pattern

b) Element deformations under constant moment

FIGURE 8.1 : DEFORMED SHAPES OF ELEMENTS.

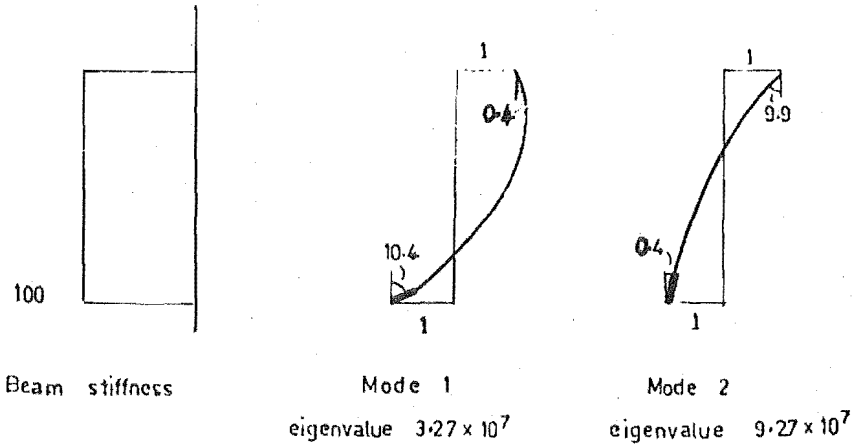

Beam stiffness — Mode 1 eigenvalue $3{\cdot}27 \times 10^7$ — Mode 2 eigenvalue $9{\cdot}27 \times 10^7$

a) Spring hinge at lower end (C1)

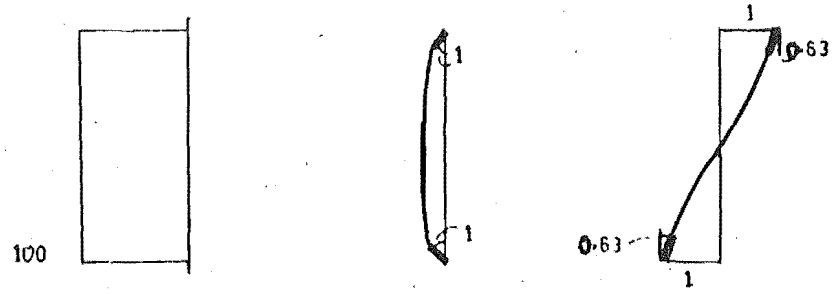

Beam stiffness — Mode 1 eigenvalue $6{\cdot}00 \times 10^7$ — Mode 2 eigenvalue $6{\cdot}68 \times 10^7$

b) Two spring hinge element

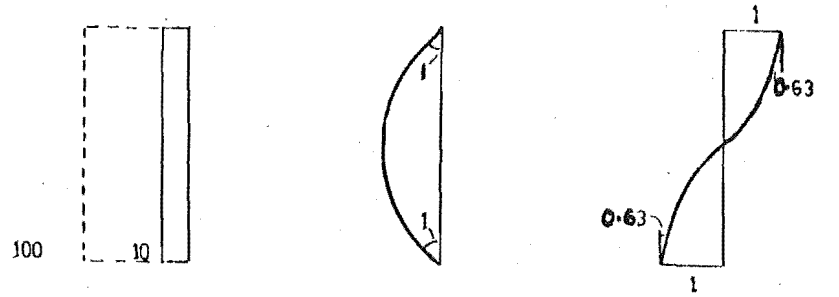

Beam stiffness — Mode 1 eigenvalue $6{\cdot}00 \times 10^7$ — Mode 2 eigenvalue $18{\cdot}72 \times 10^7$

c) Finite element model A

FIGURE 8.2 : STIFFNESS MATRIX EIGENVALUES AND MODE SHAPES.

8.3 DYNAMIC ANALYSES USING THESE ELEMENTS

8.3.1 Introduction

Possibly one of the most powerful tools in assessing any Finite Element is that of comparative analyses. It is particularly useful here where a controlled element environment has been provided and attempts have been made to isolate the investigation from time integration effects. The main aspects of interest in this study are the stability and accuracy of elements when significant nonlinearity is present. For the following analyses of the three different elements, either the member sections are arranged to give an elastoplastic moment curvature response or the corresponding yield moment is specified when a bilinear spring hinge element is used.

8.3.2 Element A

In figures 8.3 to 8.5 a variation in the accuracy of integration along the length of the element,with the use of 3, 5 and 7 point Simpson's rule integration schemes,is illustrated. A time step $\Delta t = {}^{1}/200$ sec. was used in most cases and was seen to provide response integration of adequate accuracy except when element instabilities arose. For 5 and 7 point integration schemes the responses were particularly close with 3 point integration showing greater differences. The final drift appears to be the result of an accumulation of smaller errors and any particular peak to peak distances, especially for the lower node, are comparable. Structure B, however, is considered to be more difficult to integrate than is typical of shear wall structures because of steeper curvature gradients in the lower element. A surprising result, that higher order integration imposed more demanding convergence requirements, was seen when 3 and 5 point integration analyses were stable with $\Delta t = {}^{1}/200$ sec. while the 7 point integration was not (figure 8.5). The convergence limit was only encountered when iteration was attempted and its characteristics were discussed in section 6.4.

Only three section integration is considered to be a practical and balanced procedure for use in large structures. It does, however, appear sufficiently accurate, and later runs with typical structures provide further confirmation, for the element and analysis proposed.

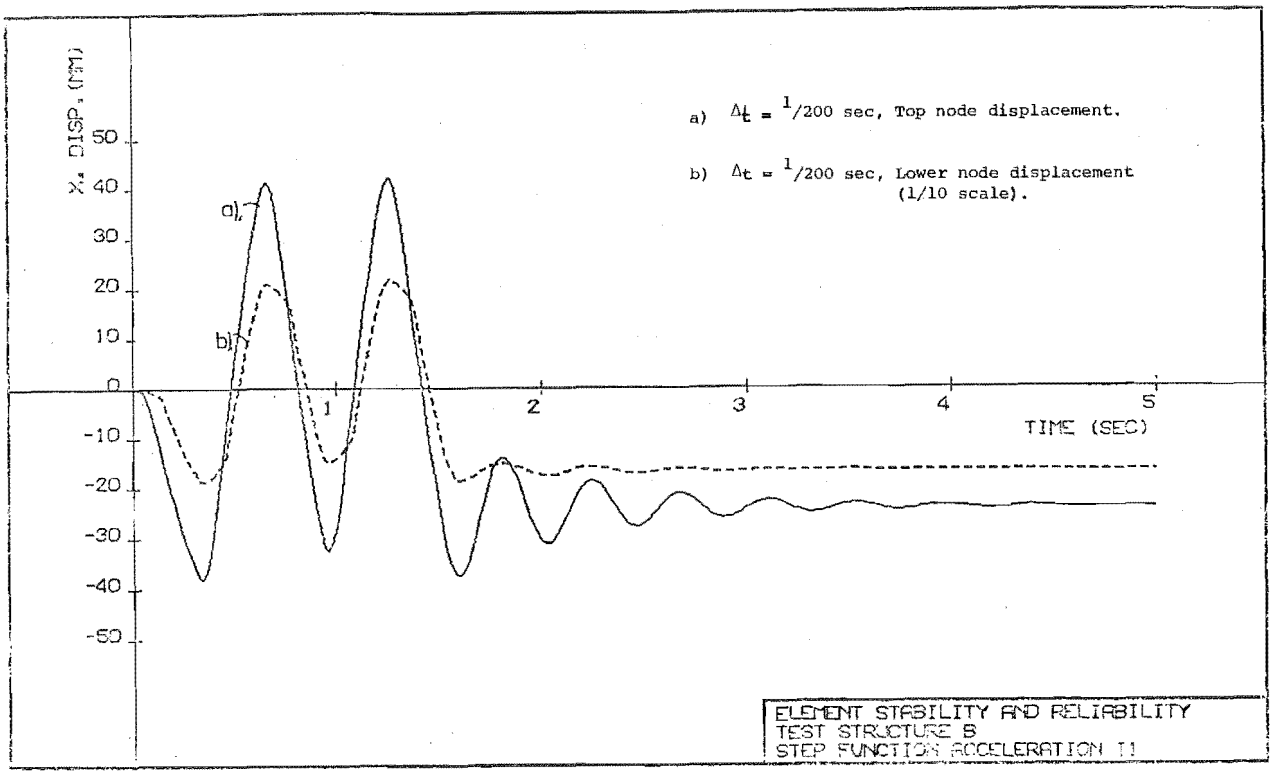

FIGURE 8.3 : DISPLACEMENT SOLUTION OBTAINED USING ELEMENT A WITH 3 INTEGRATION SECTIONS.

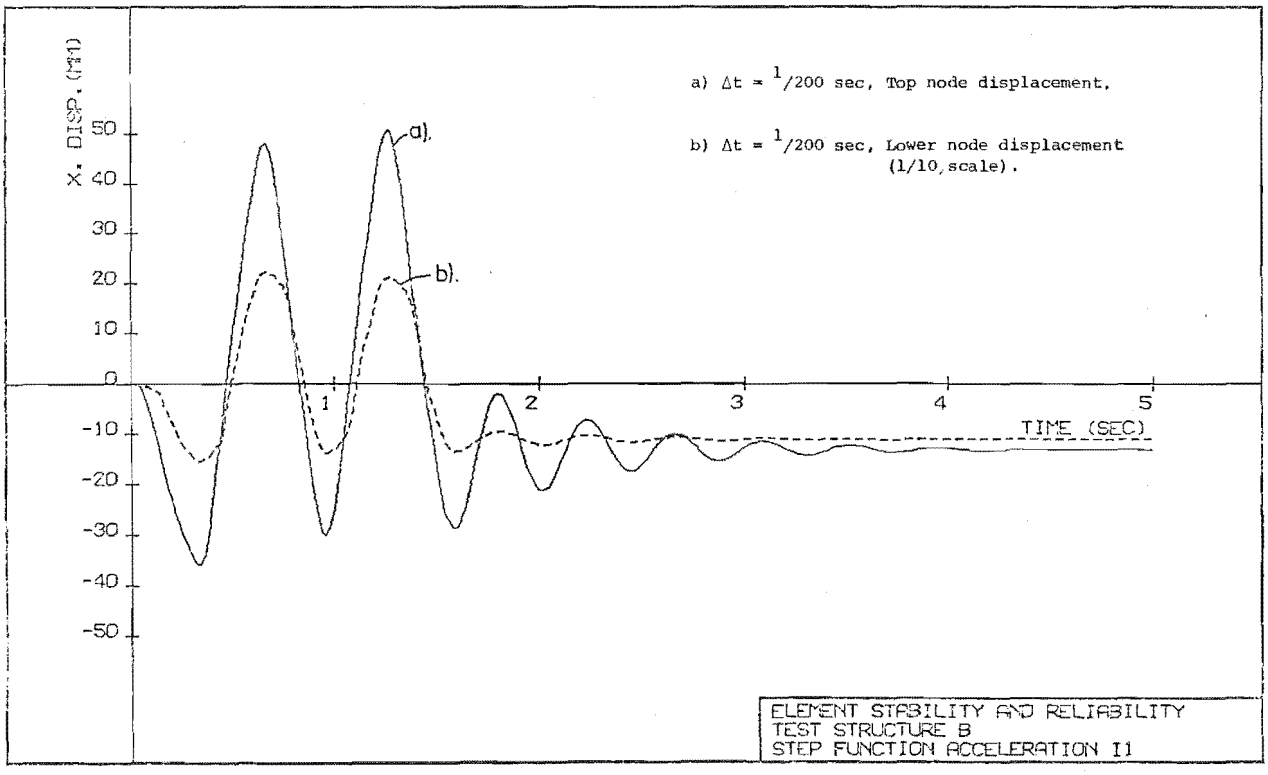

FIGURE 8.4 : DISPLACEMENT SOLUTION OBTAINED USING ELEMENT A WITH 5 INTEGRATION SECTIONS.

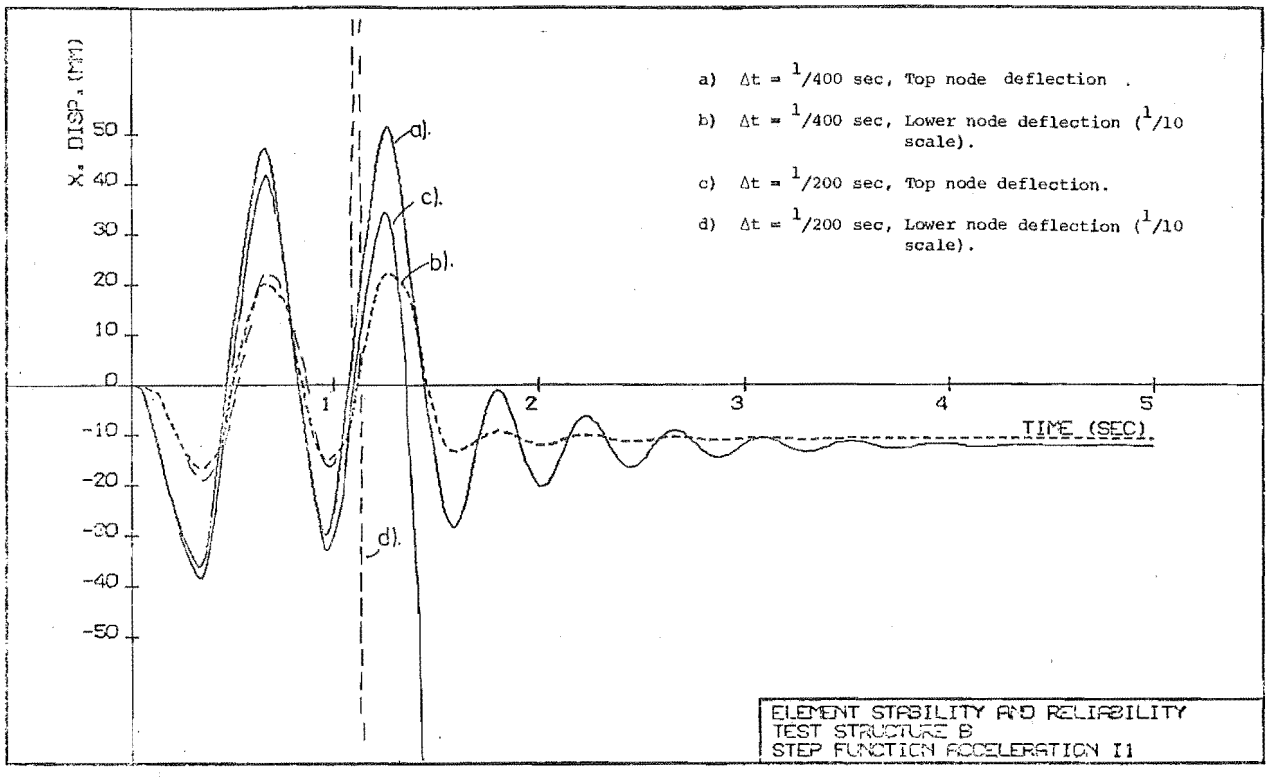

FIGURE 8.5 : DISPLACEMENT SOLUTIONS OBTAINED USING ELEMENT A WITH 7 INTEGRATION SECTIONS.

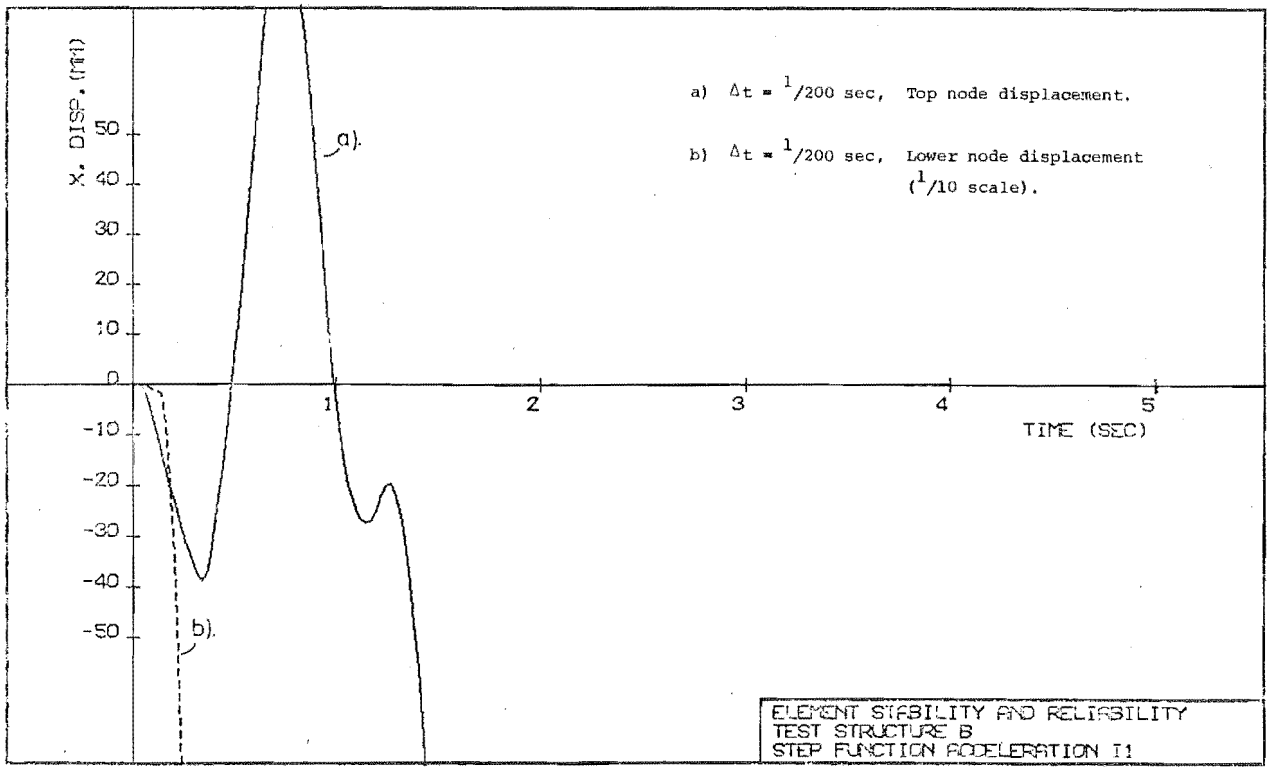

FIGURE 8.6 : DISPLACEMENT SOLUTION OBTAINED USING ELEMENT B.

8.3.3 Element B

A test of element B modelling structure B, with the critical section located at the lower end of the element, revealed a severe sidesway instability of the lower node (figure 8.6). In this example no iteration, which usually tends to increase stability problems, was used. Similar behaviour was observed when the critical section was located at positions other than the base. These findings confirm the discussion on the problems of reduced order integration in Chapter 3.

8.3.4 Elements C1 and C2

Extensive dynamic testing has shown the two elements, C1 and C2, to be completely stable, i.e. although divergence of the solution due to the numerical technique is still possible, no premature instability which could be attributed to the elements themselves was detected.

One of the main functions of element C1 in this study was to aid in the debugging process. It was ideally suited since exact agreement was achieved between different runs using element C1 and a one hinge version of Giberson's [35] bilinear spring hinge element (figure 8.7). The lower node displacements were significantly higher with the single hinge elements (e.g. C1) reflecting the internal incompatibility. That the incompatibility was not more significant could point to one untypical aspect of structure B. Some similar structures of different natural periods showed more substantial errors when element C1 was used.

Following the discussion in Chapter 3, element C2 should allow complete convergence on refinement of the idealisation. The basic element C2 response is seen in figure 8.8 and the close agreement with the three section integration of element A is considered to be significant. It is suggested that errors associated with the reduced order of integration of element A affect the higher antisymmetric mode first. This is consistent with previous findings on the use of reduced order integration [34]. Differences between elements C1 and C2 are shown in figures 8.7 and 8.8. In particular, the transverse nonlinear deformations of the lower node differ by a factor of 2 at 5 seconds, showing the incompatibility in element C1.

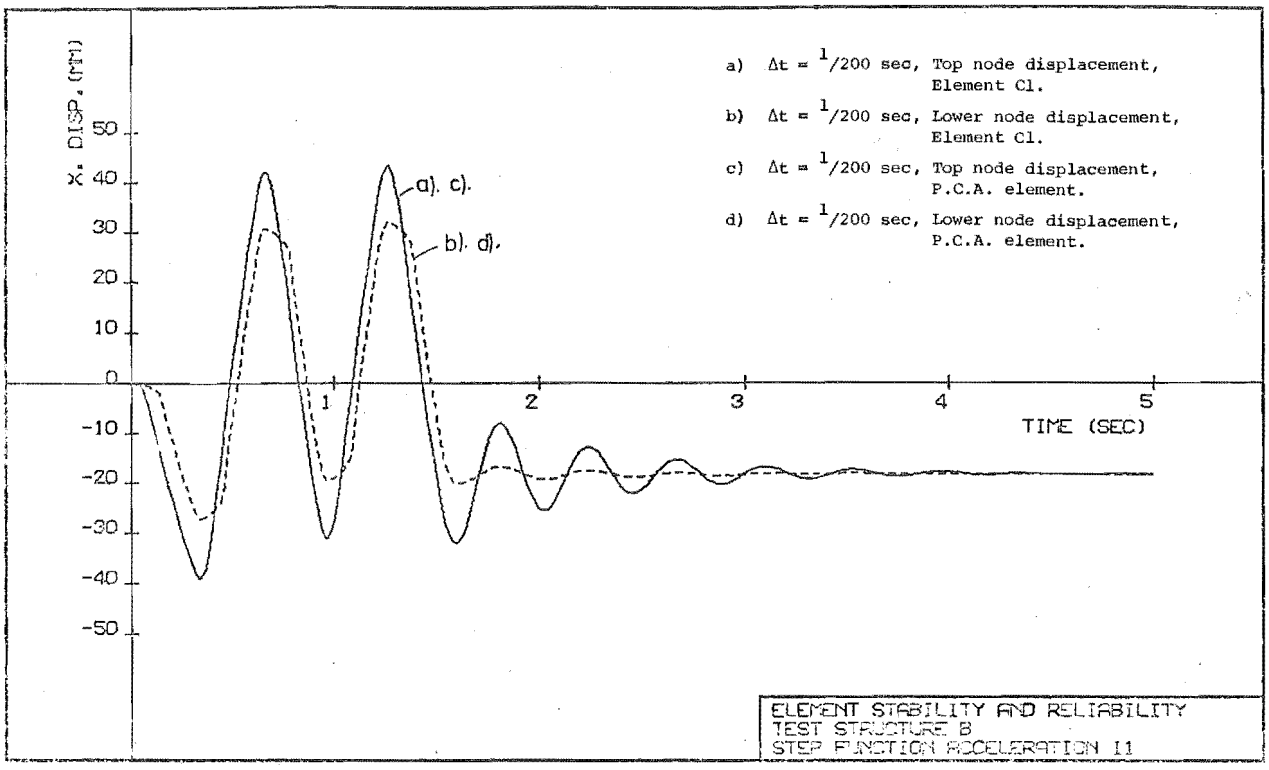

FIGURE 8.7 : IDENTICAL DISPLACEMENT SOLUTIONS OBTAINED USING ELEMENT C1 AND THE P.C.A. SINGLE SPRING HINGE BILINEAR ELEMENT.

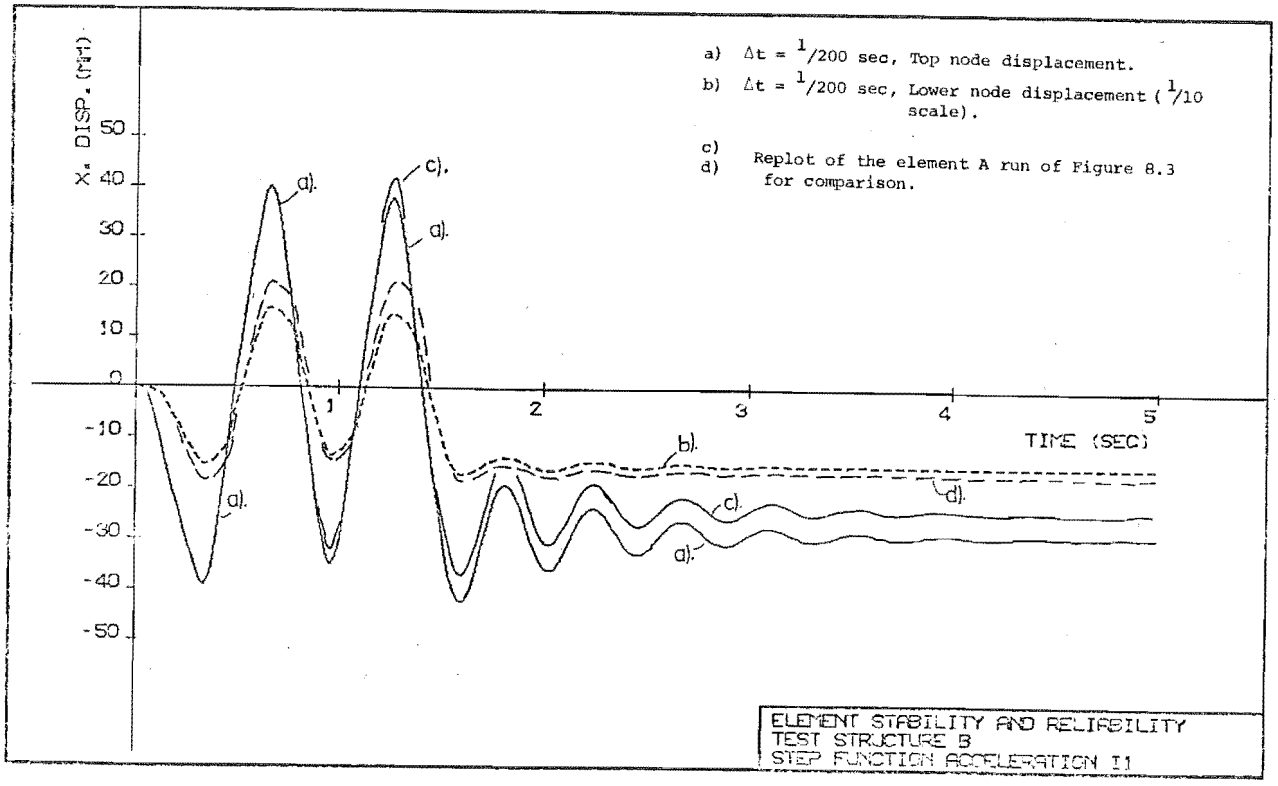

FIGURE 8.8 : DISPLACEMENT SOLUTION OBTAINED USING ELEMENT C2.

8.3.5 Two Hinge Element

The two hinge bilinear element, as used by Blakeley et al [16], was also investigated. A case of marginal element stability was encountered with $\Delta t = {}^{1}/200$ sec. and drifting of the solution, not related to excessive sidesway deformation of the lower node, is seen in figure 8.9. The probable cause is the fact that yield at top and bottom hinges of the lower element may be detected within a single increment, especially when larger time steps are used. Apart from the fact that the resulting mechanism will normally possess an inappropriately low antisymmetric mode stiffness (section 8.2.3) the application of equilibrium correction forces is likely to result in spurious vibration of the lower node. If a time step $\Delta t = {}^{1}/400$ sec. was used, a solution (figure 8.10) close to the solutions obtained with elements A and C2 was achieved. It is difficult to isolate the increased shear deformations (antisymmetric flexure in the lower element), but it is noted that the proportional deformation of the lower node with respect to the top node (figure 8.10) is less than in the case of element C1 (figure 8.7).

8.3.6 Element A in a Realistic Environment

Before the study of a typical structure, which is presented in Chapter 9, was undertaken, the selected element A was examined for stability and accuracy in the more realistic structure C. The following three aspects were considered:

a) Convergence of solution with time step changes

From a number of time step convergence studies which were performed one is presented which indicates that $\Delta t = {}^{1}/100$ sec. with out-of-phase equilibrium correction can provide solutions of adequate accuracy. This result should not be taken as proof of convergence. Instead, each problem should be (and was) treated in its own right with 1 - 2 second exploratory runs providing confirmation of convergence. Figures 8.11 and 8.12 do, however, provide guidance in the accuracy of displacements and moments to be expected for the class of problem considered.

b) Section integration accuracy

Various orders of accuracy of transverse section integration were considered with $\Delta t = {}^{1}/350$ sec., out-of-phase equilibrium correction and with a single element A containing 3 integration sections to model the lower floor. The 5 point section integration gives good results in this example (figures 8.13 and 8.14) and may well be adequate in cases when flanges dominate the response of the section. At this stage

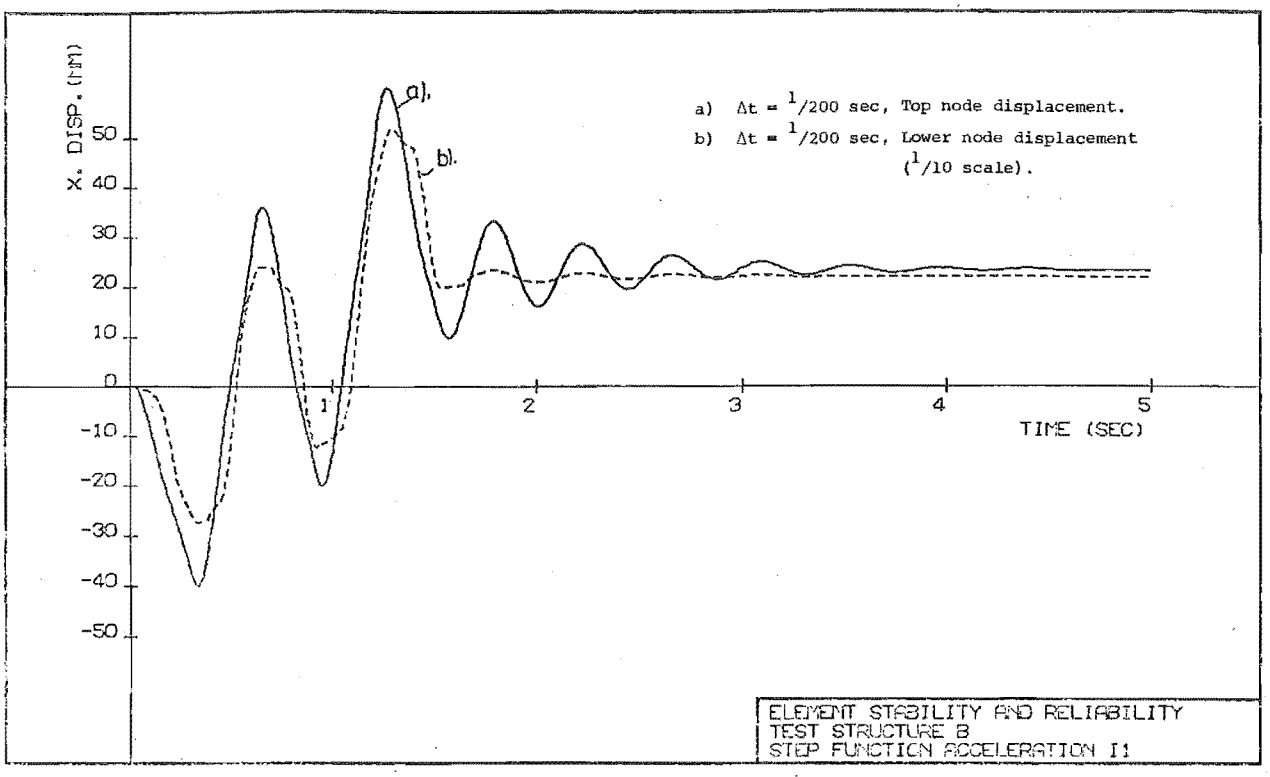

FIGURE 8.9 : MARGINAL STABILITY WHEN BILINEAR HINGING IS ALLOWED AT EACH END OF THE LOWER ELEMENT.

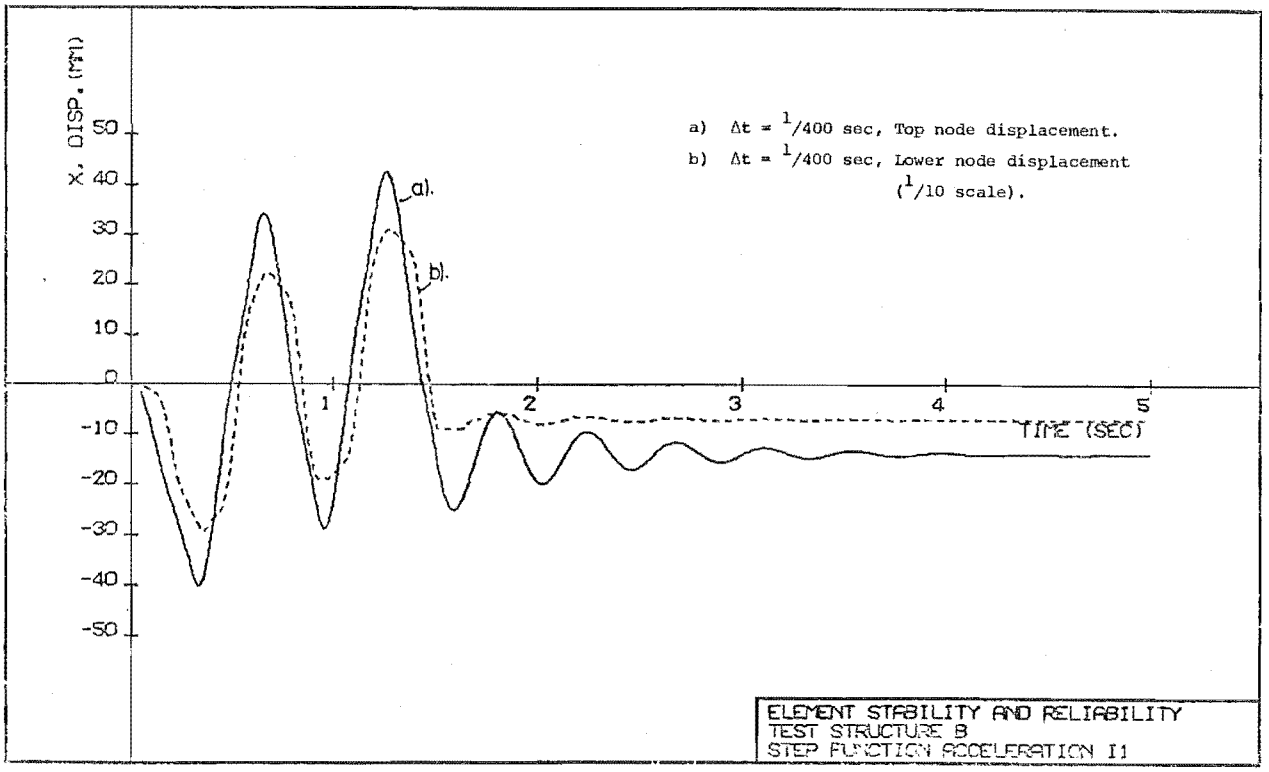

FIGURE 8.10 : SATISFACTORY STABILITY WHEN HINGING IS ALLOWED AT EACH END OF THE LOWER ELEMENT.

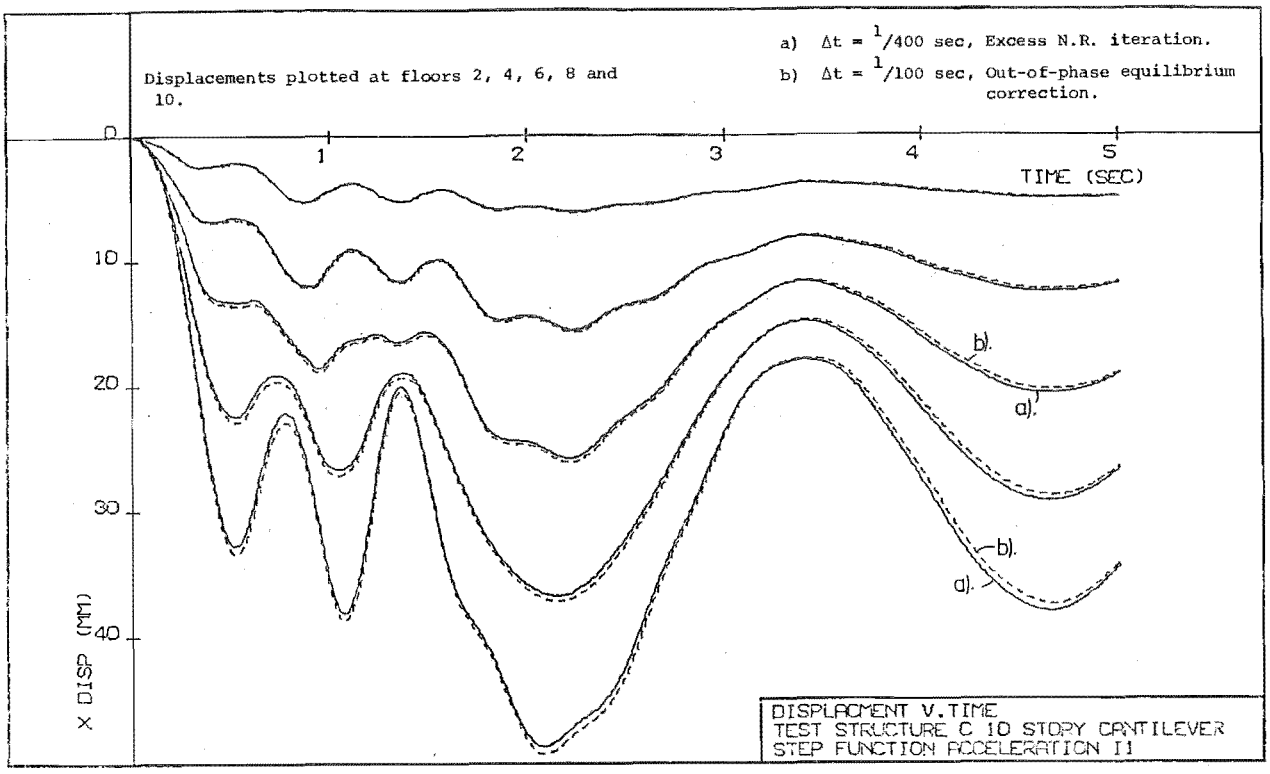

FIGURE 8.11 : INTEGRATION SCHEME ACCURACY FOR STRUCTURE C: DISPLACEMENT SOLUTION COMPARISON.

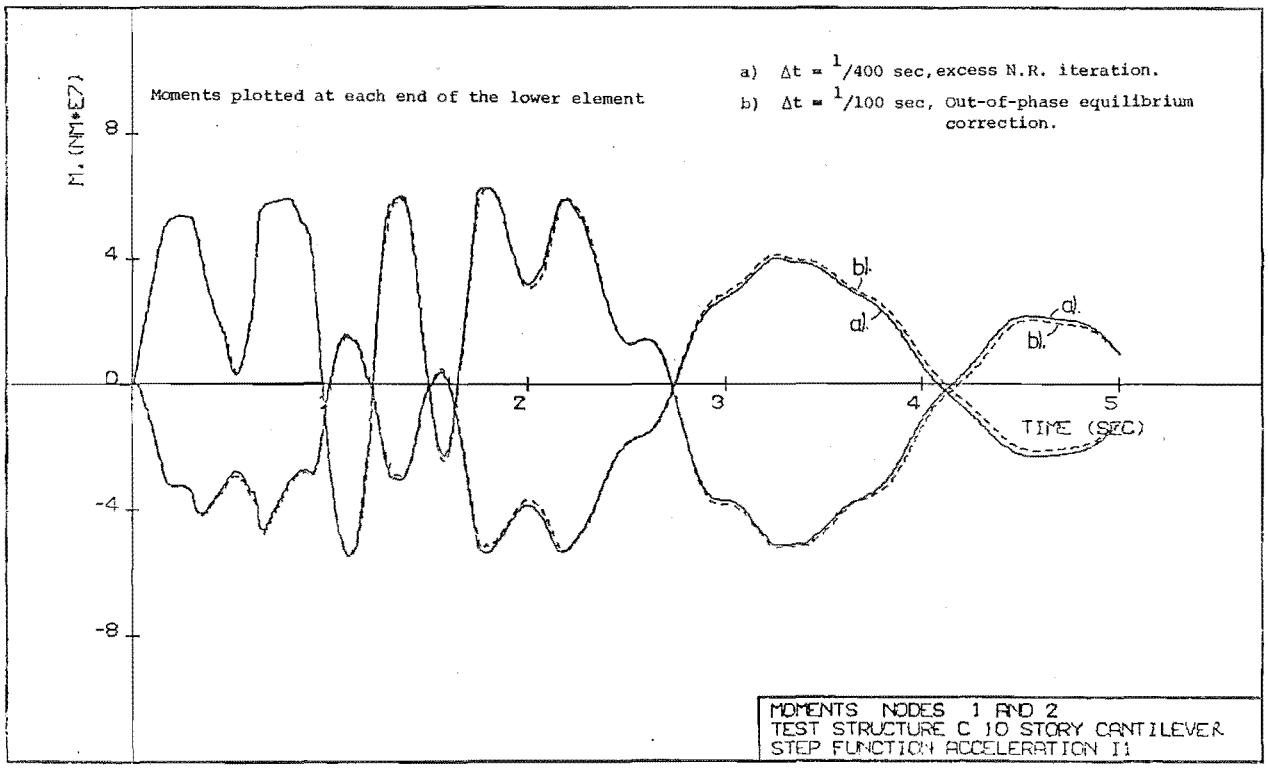

FIGURE 8.12 : INTEGRATION SCHEME ACCURACY FOR STRUCTURE C: MOMENT SOLUTION COMPARISON.

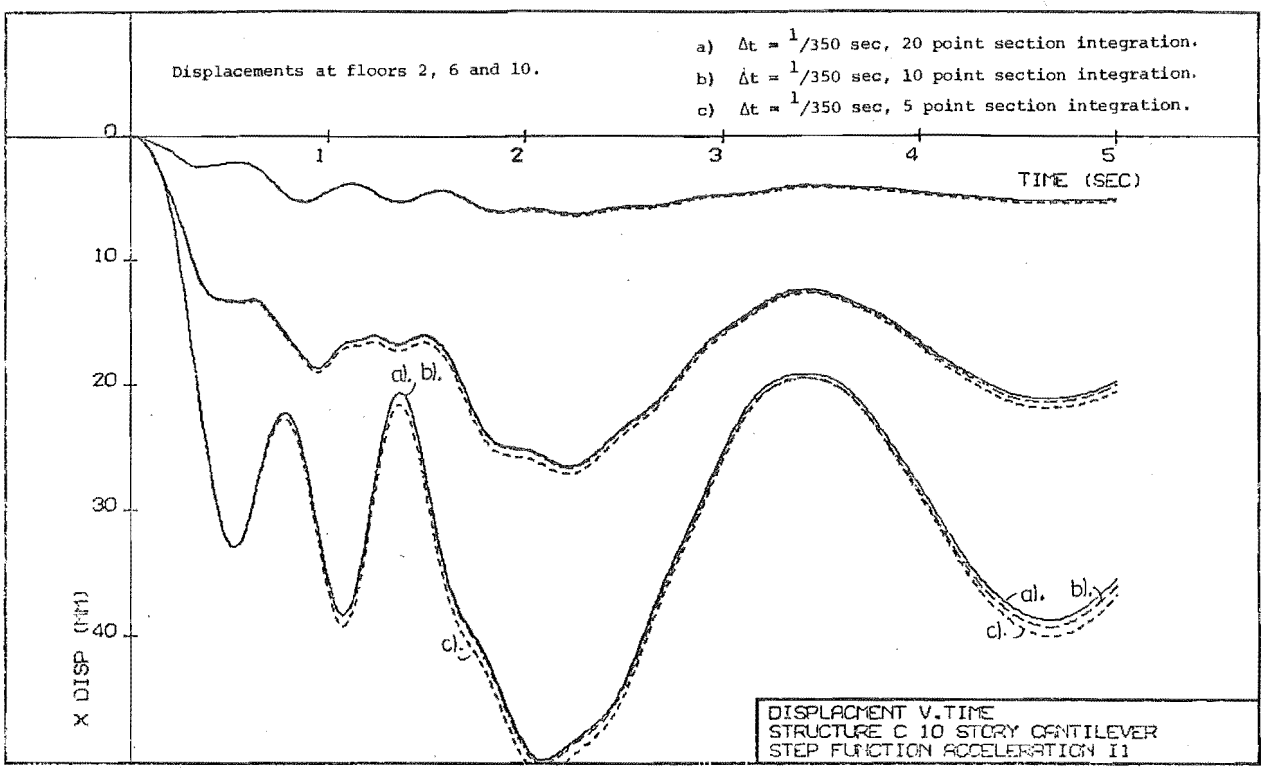

FIGURE 8.13 : VARIATION OF SECTION INTEGRATION:
DISPLACEMENT SOLUTION COMPARISON.

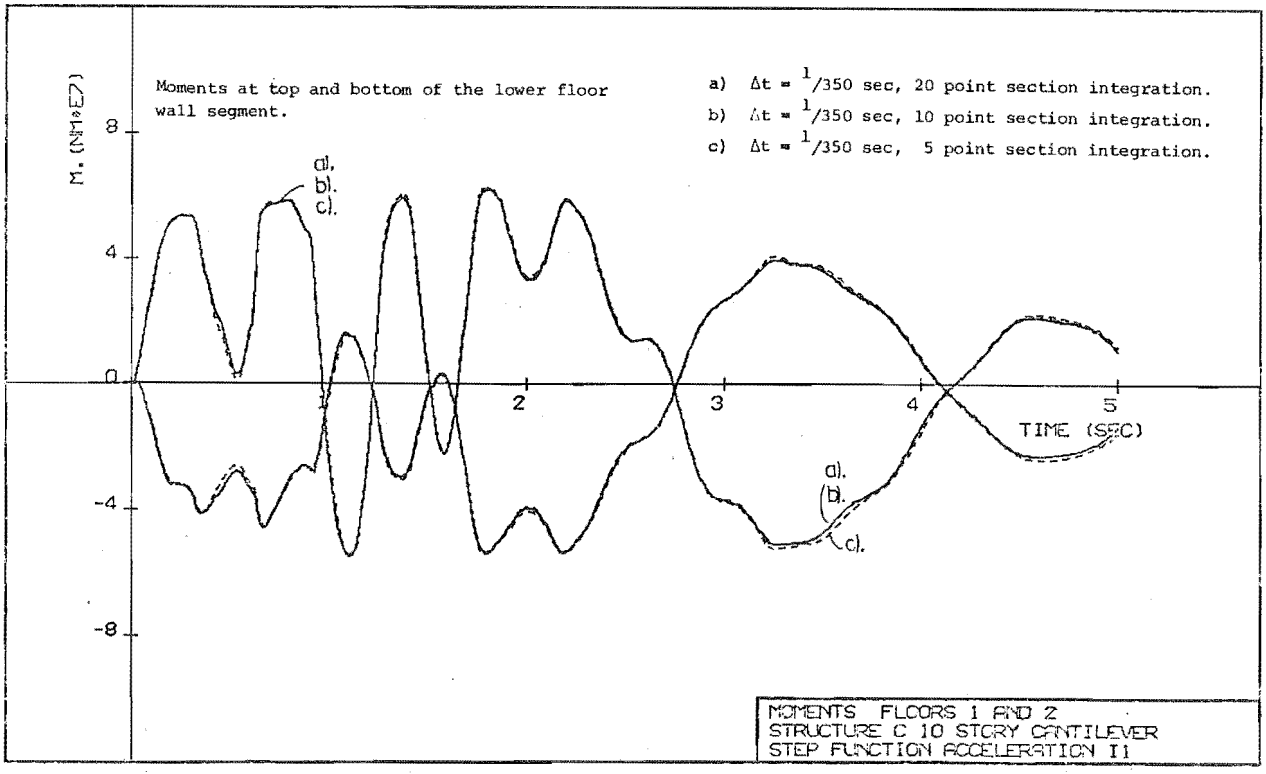

FIGURE 8.14 : VARIATION OF SECTION INTEGRATION:
MOMENT SOLUTION COMPARISON.

10 integration points were selected to ensure reliable section integration and this is in agreement with the conclusions of Kent [43].

c) Refinement of structural idealisation

Finally, comparisons were made between runs where different numbers of elements were used to idealise the lower floor of structure C. Three integration sections with 10 points per section were used in each case with $\Delta t = {}^{1}/_{350}$ sec. and out-of-phase equilibrium correction. Large differences in displacements (figure 8.15) were observed and even the comparison between 3 member and 5 member representations of the lower floor is poor. The problem observed is one of the major difficulties encountered in representing reinforced concrete behaviour with a simple flexural element - that of achieving realistic strain distributions. In this example, where a 0.01 steel strain hardening factor was used, the majority of nonlinear rotation was restricted to the lower element, irrespective of the number of elements used. When fewer elements were used, a greater transverse deflection was observed, and this affects the entire response (figures 8.15 and 8.16). A substantial strain hardening factor, while ensuring a spread of nonlinear curvatures to other elements, was found to significantly distort the sectional hysteretic response before ensuring a realistic distribution of curvatures.

This problem, which led to the selection of bilinear steel and concrete properties, has been discussed in section 4.4.2. The approach adopted was to select the lower element size to match the physical plastic hinge length.

8.4 SUMMARY

All elements, except B, performed satisfactorily and could provide quite reliable estimates of structural response. Although absolute proof is difficult, it was considered that element A was most representative of the physical situation when discrepancies between various elements arose. This was confimed to some extent by agreement of element A results with element C2 (figure 8.8) which also satisfies the Finite Element convergence criteria.

Some of the experience gained with the use of different models representing a simple structure, which was considered to be representative and free from peculiarities, is presented and intended for use as a guide in the choice of modelling. In view of the difficulty of defining rules for the use of elements it was concluded that the most practical means of

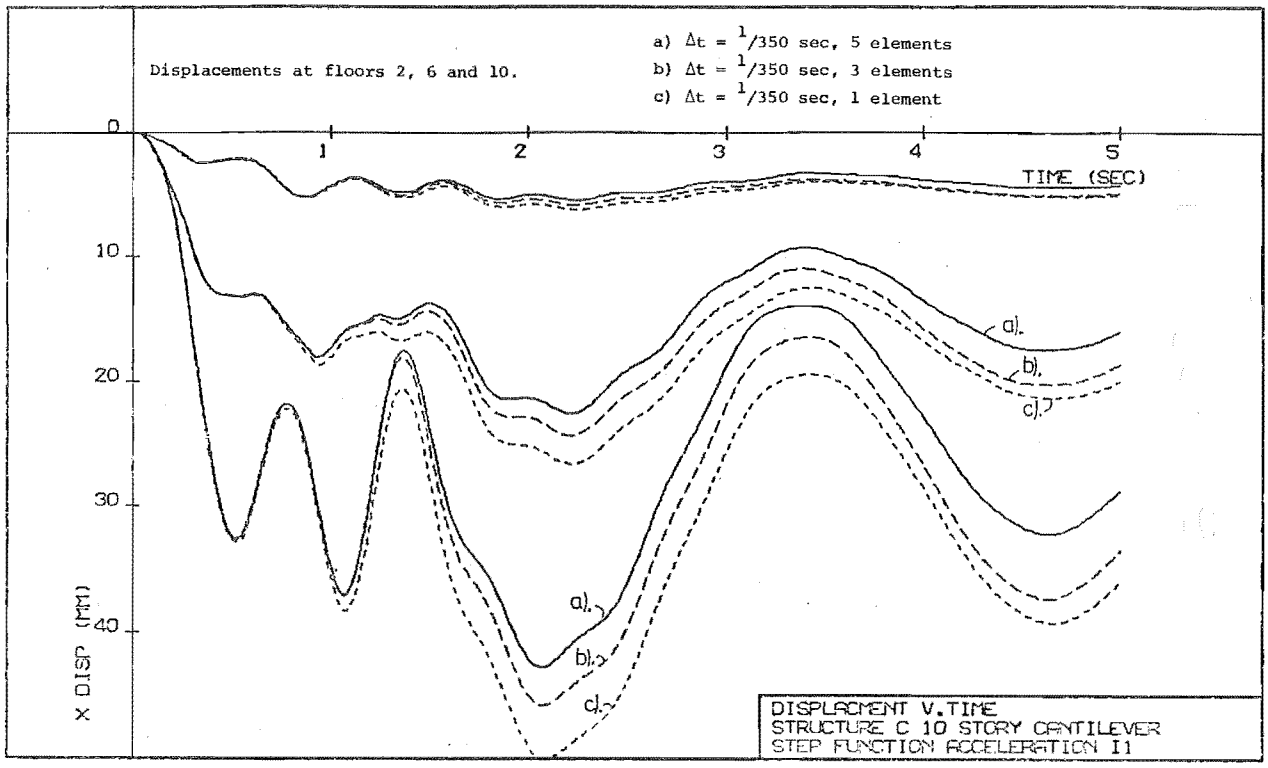

FIGURE 8.15 : REFINEMENT OF LOWER FLOOR IDEALISATION: DISPLACEMENT SOLUTION COMPARISON.

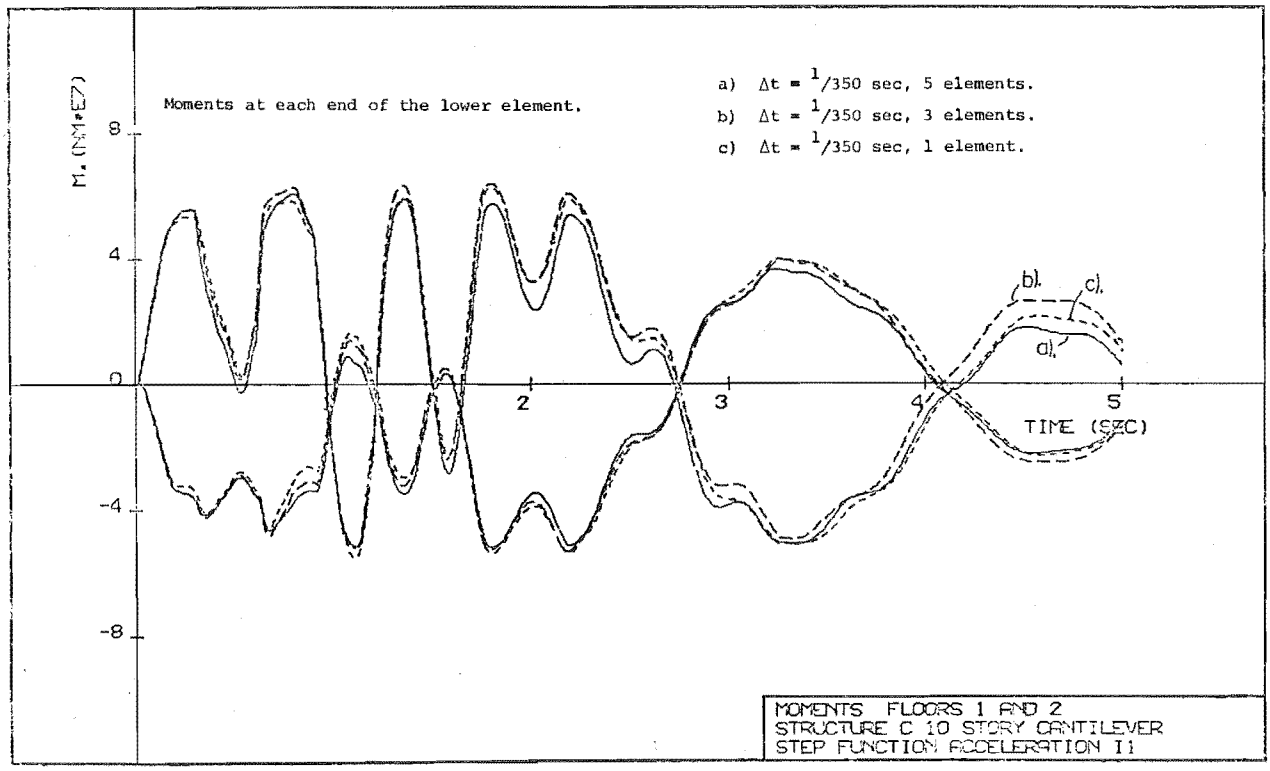

FIGURE 8.16 : REFINEMENT OF LOWER FLOOR IDEALISATION: MOMENT SOLUTION COMPARISON.

presenting operational information, related to the interaction of a complex assemblage of nonlinear phenomena, is by example. Specific reference has been made to some of the more outstanding features of model behaviour but a full comparison relates to a vast quantity of information which is relevant to element response.

CHAPTER NINE

STRUCTURAL RESPONSE STUDY

9.1 INTRODUCTION

This chapter outlines the successful application of the dynamic response computer program to an actual structure. In each case the structures analysed utilise special features of the analysis and the computational effort required was considered to be well within the range of economic viability for this study.

Shear wall structures have been seen to require a higher order of physical modelling because of their outstanding features (see section 3.2) which make them different from frame structures. Applying the newly developed model and reviewing the computed results shows the importance of some of its features. This allows improved assessment of the response and leads to a better understanding of structural behaviour. Because of the higher resolution (accuracy) of the refined model, moderate variations on a basic structure were examined for changes in the response. This illustrates the potential of the model. The alternative study of a wide range of structures could probably be adequately performed, at least to the determination of overall effects, by a more approximate model of lower resolution, eg. the extensive study of cantilever shear walls by the Portland Cement Association [15].

9.2 SCOPE OF THE STRUCTURAL RESPONSE STUDY

The selected structure has been examined previously by Santhakumar [8] who carried out a monotonic nonlinear static analysis, based on bilinear stress-strain relationships similar to those illustrated in figure 4.2. He provided a history of its response including the sequence of hinge formation. Correlation with the dynamic response results obtained in this study was attempted in section 9.6.

Because the basic structure was designed using capacity design methods, in which a cumulative series of conservative assumptions were used to ensure a desirable sequence of plastification (yielding in the structure), the total overturning moment is excessive. Question arises as to the justifiability of these conservative assumptions, i.e. whether or not benefits in improved seismic behaviour outweigh additional structure costs.

By varying the structure in a controlled manner and taking advantage of the higher resolution (better idealisation) of the model, a variation of base shear, related to natural period and factors on the design of important components, was considered. Features of particular interest include the distribution with height of wall bending moments and shears induced during the dynamic excitation and the sequence of failure throughout the structure.

A final aspect considered in this study was that of light coupling in shear walls when slabs, possibly incorporating a shallow coupling beam, provide the only connection between two walls. This structure, which relates to the experimental work of the following chapters, was achieved by modification of the basic structure.

9.3 THE STRUCTURE AND ITS DESIGN

The selected structure comprised two coupled shear walls constructed upon a massive three-storey basement, which is supported on a pile foundation. The two coupled shear walls (figure 9.1), one at each end of the building, were designed to carry the entire lateral load in their planar direction. Because of the small tributary floor area they carried a relatively small axial load.

The structure was first designed in 1972 and proposed for construction in Wellington, New Zealand. The original design considered the deformation of the foundation walls and the piles and a 1.15 second natural period was computed which, in the terms of the New Zealand loading code [64], led to a design base acceleration of 0.09 g. It is to be noted that design loadings are referred to in this chapter in terms of base accelerations. Although this quantity has limited physical significance in the dynamic analysis, it allows direct appreciation of code design force levels. The base acceleration relates directly to the base shear throughout this chapter because the same masses were used for each analysis.

During the design process 23% excess dependable capacity of the coupling beams resulted from the final practicable arrangement of the reinforcement. Minimum specified yield strengths and a capacity reduction factor (ϕ factor) of 0.9 were used. Hence the coupling beams have been designed for static loads in an inverted triangular distribution which correspond to a 0.111 g base acceleration. During the subsequent wall design, the coupling beams were presumed to yield at their reliable strengths when computing the axial loads in the wall. The original design philosophy required that beam hinges form before wall hinging occurs and the suggested

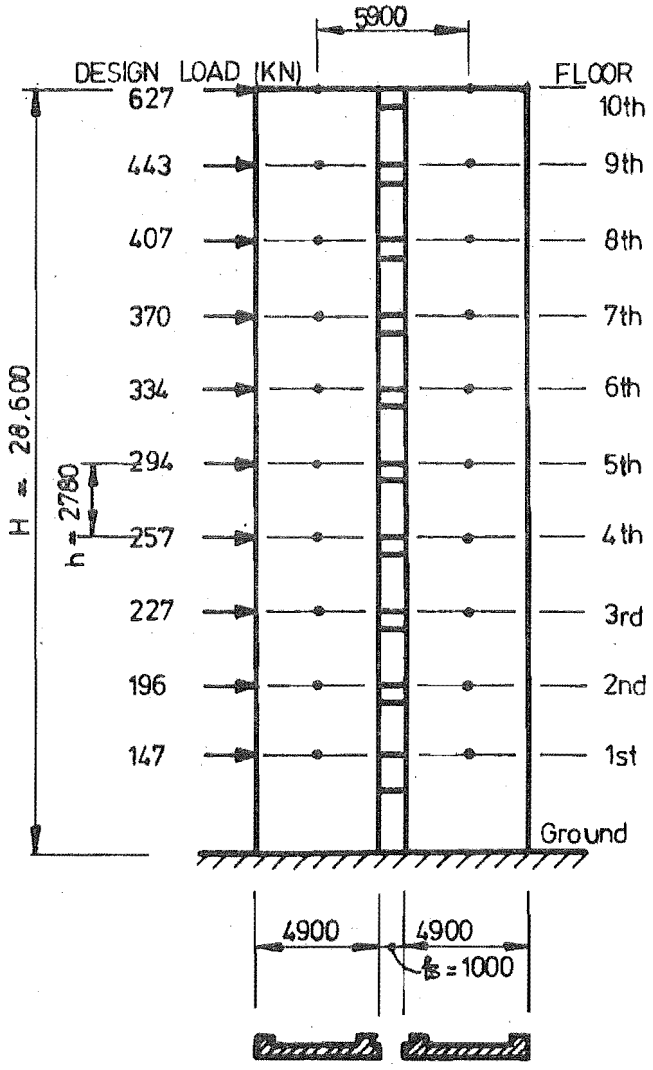

(a) Dimensions of shear wall and loading

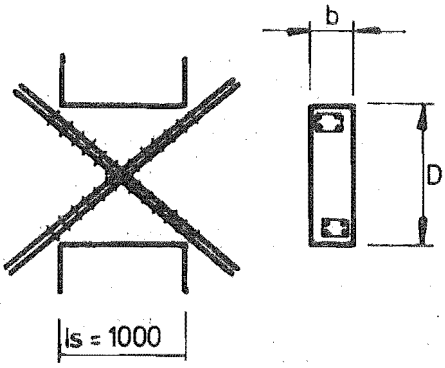

(b) Typical coupling beam

FLOOR	WIDTH b	DEPTH D	BEAM STEEL
9th & 10th	250	830	4 D25
7th & 8th	300	830	4 D28
2nd to 6th	350	830	4 D32
1st	350	1500	4 D25

(d) Beam dimensions and reinforcement

FLOOR	THICKNESS t	MASSES (Mg)	
		HORIZ	VERT
9th & 10th	200	3540	467
7th & 8th	250	3580	431
2nd to 6th	300	3580	431
1st	300	3600	450

(e) Wall thickness and inertial masses

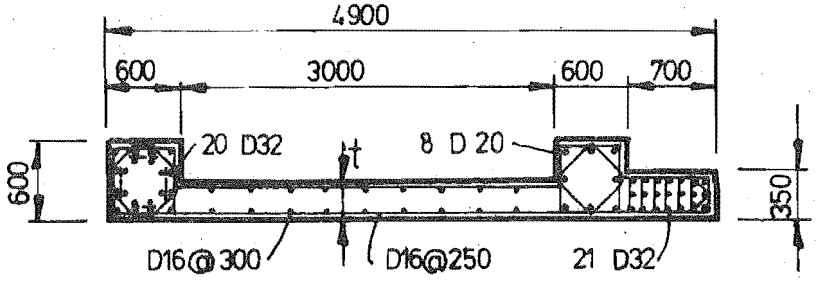

(c) Base cross section of the left wall

FIGURE 9.1 : THE BASIC STRUCTURE

means of ensuring this was to magnify wall design moments. Therefore, the wall design moments, initially arising from the elastic lateral analysis for the code loading, were amplified by 23% to allow for the additional beam steel and a further 10% to enhance the desired hierarchy of failure. This resulted in wall moments corresponding to a base acceleration of 0.122 g. In addition, a ϕ factor of 0.7 was used for compression wall design while a ϕ factor of .9 was retained when designing the tension wall.

Eliminating the effects of the differential ϕ factors, the proportions of the total overturning moment at the ground floor level, associated with different resistance mechanisms and assessed from the dependable strengths, are listed below. Corresponding values obtained in the original elastic laminar analysis are included in brackets.

i) 40% (42%) resisted by the coupling system and the resulting base couple.

ii) 23% (18%) resisted by the tension wall moment.

iii) 37% (40%) resisted by the compression wall moment.

The resulting effective design base acceleration was 0.139 g if the ultimate overturning moment is computed using dependable strengths of the members. An ultimate overturning moment which is based on dependable strengths and which corresponds more closely to the code specified 0.09 g base acceleration should have been possible if overly conservative assumptions had not been used.

As mentioned previously, the initial design for lateral loads was based on a period of 1.15 seconds. The original computations were based on gross concrete wall properties and allowed for base flexibility. When the base of the coupled shear wall was assumed to be fixed (figure 9.1), as in the majority of the computer analyses, a higher design base shear was appropriate. The first natural period computed assuming the gross concrete and steel section of the walls was 0.89 seconds, for which a base acceleration of 0.105 g is the appropriate code value. Thus if the original structure is considered with fixed base conditions, then the dependable strengths of the coupling beams in the basic structure are only 6% above the 0.105 g base acceleration design level. The actual design moments of the tension and compression walls were 16% and 49% respectively above this design level (ϕ = 0.9 for both walls). However, the compression wall was originally designed with ϕ = 0.7 applied to the axial load (as well as the moment) and because the section does not approach a balanced failure this additional factor on the axial load leads to a reduction in the area of reinforcing steel.

When specifying reinforcement areas in the program, curtailment of the vertical wall reinforcement more nearly approximated a linear distribution over the height than the elastic analysis bending moment diagram indicates. Longitudinal wall flexural steel areas at wall edges were reduced to 66% and 33% of that at the base (figure 9.1) at floors 3 and 6 respectively. In the program the transition was considered effective at these levels. The vertical web reinforcement at the base (figure 9.1) was provided over the height up to floor 8 above which it was reduced to 66% of that at the base.

9.4 DETAILS OF STRUCTURAL IDEALISATION

9.4.1 Flexural Idealisation

All coupling elements were defined by Giberson's [35] nonlinear spring hinge model with a bilinear hysteretic relationship. Because of the antisymmetric deformations of the coupling beams, both flexural and shear deformations can be uniquely allowed for with this nonlinear element. Rigid end blocks were used to allow the idealisation of large wall widths.

The walls were idealised, in general, by element A (see Chapter 3) although element C1 was used to allow an assessment of the importance of shear deformation (see section 9.4.2). The reference axis was located on the wall centroids (figure 9.1).

No allowance was made for the higher strain rates encountered in dynamic responses as the problem has been shown to be important for initial cycles only [65].

9.4.2 Shear Modelling

No specific allowance for shear is possible with element A as the model is intended to represent reinforced concrete flexural members in which shear deformations are not significant. Nayar et al [67] performed nonlinear static analyses of an 18-storey shear wall and found that the inclusion of shear deformations had only minor effects on the computed displacements. It seems unlikely that shear deformations, large enough to significantly disturb the response, would arise in the 10-storey structure of this study.

9.4.3 Representation of Mass and Damping

Lumped floor masses were used while an allowance for the distributed wall mass was made as in Chapter 7. Damping on the first two modes of 3% of critical damping was assumed in all cases [63].

9.5 SELECTION OF EARTHQUAKE RECORDS

Because of the significant computer time involved it was decided, from the outset, to use a 10 second duration of base acceleration for each computer run. Previous investigators [12,15] have accepted, with good justification, the 10 second duration as being adequate for assessing the response. Further guidance from these investigators resulted in a choice of the following acceleration records:

i) The El Centro 1940 (N.S. component) accelerogram was selected because of its widespread use and a high level of acceptance within the engineering profession, engendered by this frequent use.

ii) Jennings' artificial earthquake accelerogram A1 [66] was used to represent a very severe excitation so as to examine extreme conditions. The first analysis investigating the basic structure used the first 10 seconds of the record and was useful in showing some initial elastic behaviour as well as a period of severe excitation.

iii) Jennings' artificial earthquake record B1 [66] was used as a second base motion of approximately the same magnitude but having different characteristics to the El Centro 1940 N.S. record. The 10 seconds used started at a point 3 seconds from the beginning of the original record to include most of the major excitation.

9.6 SUMMARY OF SANTHAKUMAR'S ANALYSIS

Santhakumar's analytic model [8] predicts a top floor displacement of 25 mm at first yield, which occurred at the 4th floor coupling beam. A structural displacement ductility of 4 was estimated to occur at 150 mm top floor displacement, if effective yield at the intersection of tangents to the initial elastic and the yield plateau portions of the response is assumed to represent equivalent bilinear behaviour. When the response to the El Centro N.S. 1940 ground motion was computed in this study, a maximum displacement of 125 mm occurred. At this maximum displacement, some wall yielding occurred but significantly less than predicted by Santhakumar. The difference between the two analyses is attributed to differences in the modelling and material assumptions. For example, Santhakumar considered all plasticity to occur at the wall bases and did not consider the possibility of the translation of the stiffness centroid. Furthermore, Santhakumar computed ultimate wall yield moments which were substantially smaller than those used in the present analysis.

The sequence of plastic hinge formation under monotonic static load is of interest and is seen to bear a resemblance to that in the dynamic analysis (e.g. figure 9.18). However, a tendency for early hinging of beams near the base, probably associated with higher mode response, is not predicted in a static analysis.

9.7 DETAILED DESCRIPTION OF THE PERFORMANCE OF THE BASIC STRUCTURE

9.7.1 General

Artificial earthquake A1 was selected to illustrate the performance of the basic structure. A selection of time-history plots is included in the following sections to allow detailed examination of the structural characteristics and of the finite element model capabilities.

9.7.2 Displacements

Horizontal displacements (figure 9.2) plotted at alternate floors, starting at floor 2, show the displacement histories. As the transverse displacements are plotted at equally spaced points over the height of the structure, the displaced shapes may be derived directly. It is evident that these are predominantly first mode shapes and that the majority of the nonlinear rotation occurs near the base. Good estimates of inter-storey deflection may be made and the top floor displacement provides a basis for comparing with Santhakumar's results. The yield displacement drawn on figure 9.2 was computed by Santhakumar and is shown to be reasonable by examining stiffnesses at 3.9 seconds where the top floor displacement first exceeded the yield level (figure 9.2). Short duration yielding may be seen at time 3.9 seconds in figure 9.9. For compactness of presentation, later displacement comparisons are made with the use of displacement envelopes.

Vertical displacement of points on the wall reference axis, associated with the translation of the centre of stiffness, appear significant (figure 9.3). Initial compressive strain due to the presence of gravitational loads may be observed at zero time. Temporary increases in the compressive strain above the gravity load strains is attributed to the additional axial loads associated with coupling beam actions. The large axial elongations, which concentrate in the lower elements, are related to cracking, yielding of the tension steel and the consequent translation of the stiffness centroid. Although a vertical earthquake component was not considered in this case, vertical motion, associated

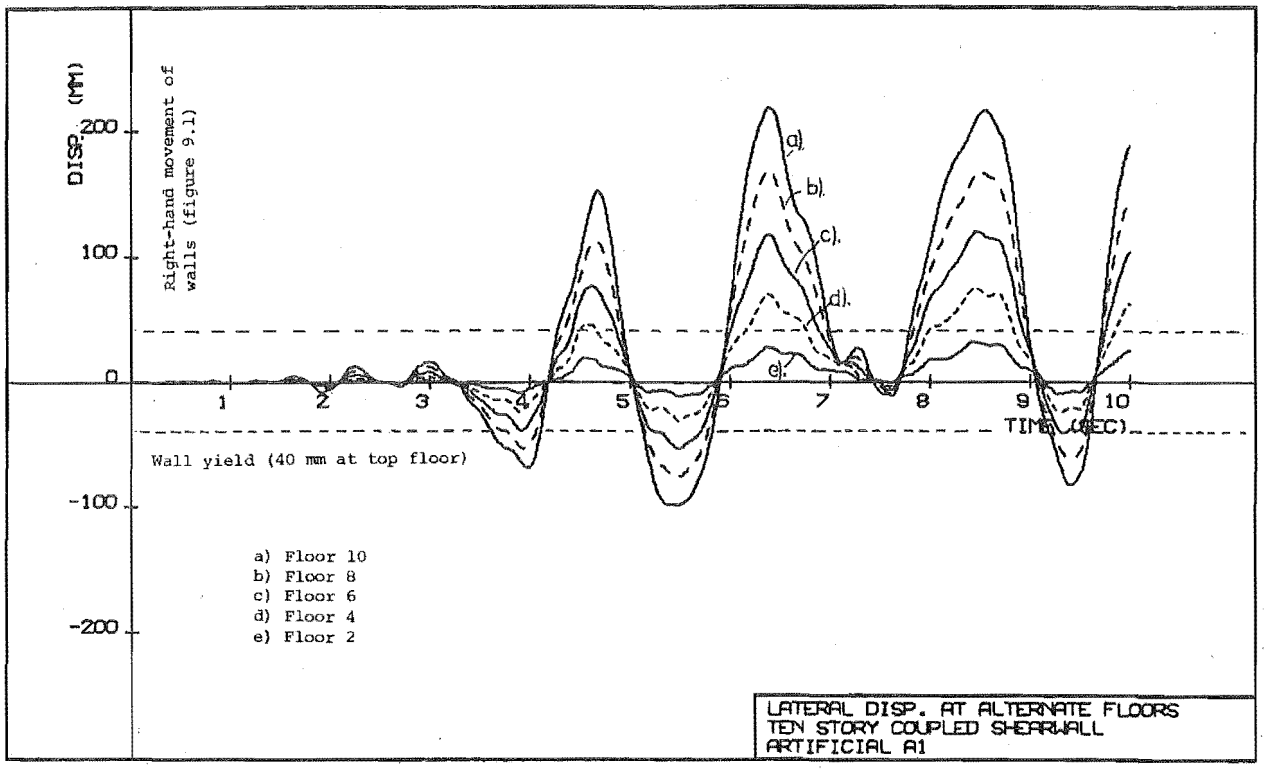

FIGURE 9.2 : HORIZONTAL DISPLACEMENT HISTORY

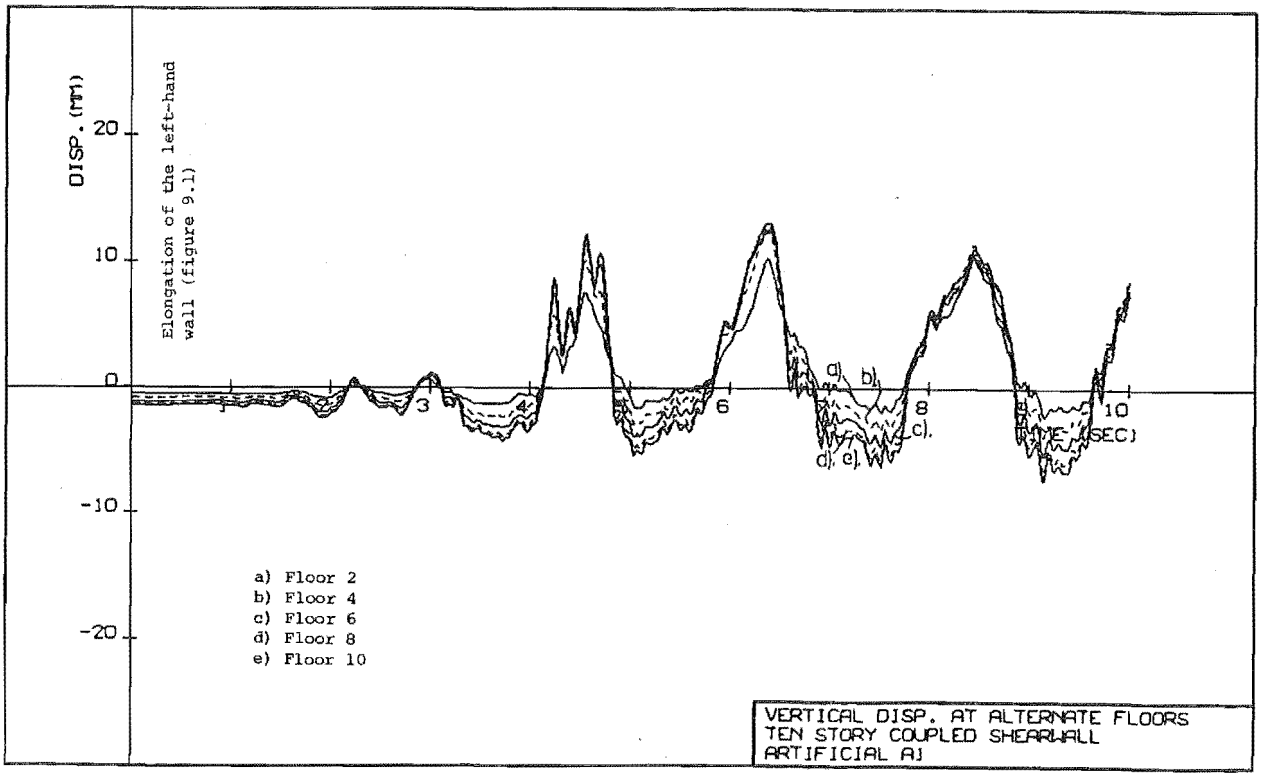

FIGURE 9.3 : VERTICAL DISPLACEMENT HISTORY

with these effective changes in geometry, was seen to initiate response of the vertical component of the masses.

9.7.3 Behaviour of Coupling Beams

Histories of coupling beam moments at floors 1,2,4,6,8 and 10 show in figure 9.19 the yield status at these locations. If comparison is made with wall 2nd moment of area plots, examination of the relative order of yielding of walls and particular coupling beams is possible. To facilitate direct assessment, a yield histogram for the respective walls is plotted on the time axis of the coupling beam moment diagram (e.g. figure 9.19). The shaded regions indicate a wall 2nd moment of area less than 5% of the gross concrete section value and these regions, which were taken to define wall yielding, were determined directly from graphs such as figure 9.9. Because of the value of this information with regard to the sequence of plastification, such graphs are presented in sections 9.8 and 9.9 for a variety of analyses. Also presented are maximum coupling beam rotations throughout the structure to allow an assessment of ductility demand in these analyses.

The coupling beam information for the response of the basic structure to the "A1" record is presented in figures 9.19 and 9.23. A maximum coupling beam rotational ductility of 13 is predicted (figure 9.23) when the yield rotation was computed by examining the yield deformations of a diagonal coupling beam. Maximum coupling beam end rotations are nearly constant with height, particularly in the upper part of the wall. First coupling beam yielding for the yield excursion considered is seen to occur in the lowermost coupling beam (figure 9.19) at 3.95 seconds. The floor 2 beam follows soon after and the beams at floors 4 - 10 yield simultaneously approximately 0.2 seconds after the lower coupling beam yields. This was followed by a long and largely uninterrupted period of yield lasting until 4.7 seconds during which the first large horizontal translation (figure 9.2) and significant axial elongation of the lower storey centreline (figure 9.3) occurred. The small drop in moment in beams of the upper floors below the yield level at approximately 4.4 seconds represents a reversal of curvature of coupling beams above floor 4. This reversal is associated with a change in the centreline length of the lower element at 4.4 seconds (figure 9.3) and is not related to a change in direction of horizontal displacement as figure 9.2 shows no corresponding discontinuity at 4.4 seconds. This is the time at which the tension steel in both the compression (right-hand) wall and in the tension (left-hand) wall yielded

as shown in figure 9.9. It is to be noted that there is more frequent reversal of curvature of the first floor coupling beam during a single yield excursion (e.g. 4.0 to 4.5 seconds in figure 9.2) than in the upper floors. It is unlikely, however, that yielding at the base and the consequent centreline elongation will cause yielding (or a reversal) at the lower coupling beam only as all floors tend to be elevated by the same amount (figure 9.3) since the majority of nonlinear behaviour occurs in the lower storey. Rather, the large lower beam reversals are due to the high frequency components of the base motion exciting a higher mode response in the lower part of the structure.

9.7.4 Wall Actions

a) Axial forces in walls

The effects of coupling beam behaviour are seen in the substantial change in wall axial forces, reaching definite plateau when coupling beams yield and fluctuating because of complex stiffness deterioration and higher mode response in the structure. The axial forces at the bottom of the structure are plotted at each wall base in figure 9.4. The distribution of axial force over the height of the left-hand wall (figure 9.1) is shown in figure 9.5 where the initial gravity load forces at 0.0 seconds should be noted. The effects of axial forces induced by the coupling beams may be seen at 3.5 seconds (figure 9.5) where they are additive to the gravity loads in the left-hand wall. During the 4.4 - 4.6 second interval, fluctuation of axial force occurred at all levels after the tension steel at the wall base in the compression wall yielded.

It is noted that there is a tendency for axial load in the left-hand wall (figure 9.5) to increase (i.e. drift) gradually with time. This is compensated by a corresponding tension in the right-hand wall (figure 9.4) to maintain vertical equilibrium.

b) Wall moments

Wall base moments (figure 9.6) fluctuate both directly and as a result of coupling beam induced axial load fluctuation and contain significant higher mode components because of the structure's response to the high frequency base motion components. Nevertheless, distinct yield plateau can be detected such as in the left-hand wall between 6 and 7 seconds (figure 9.6). Wall moments plotted over the height of the left-hand wall (figure 9.7) allow some appreciation of moment distribution in walls. Yielding at the base is seen to limit the

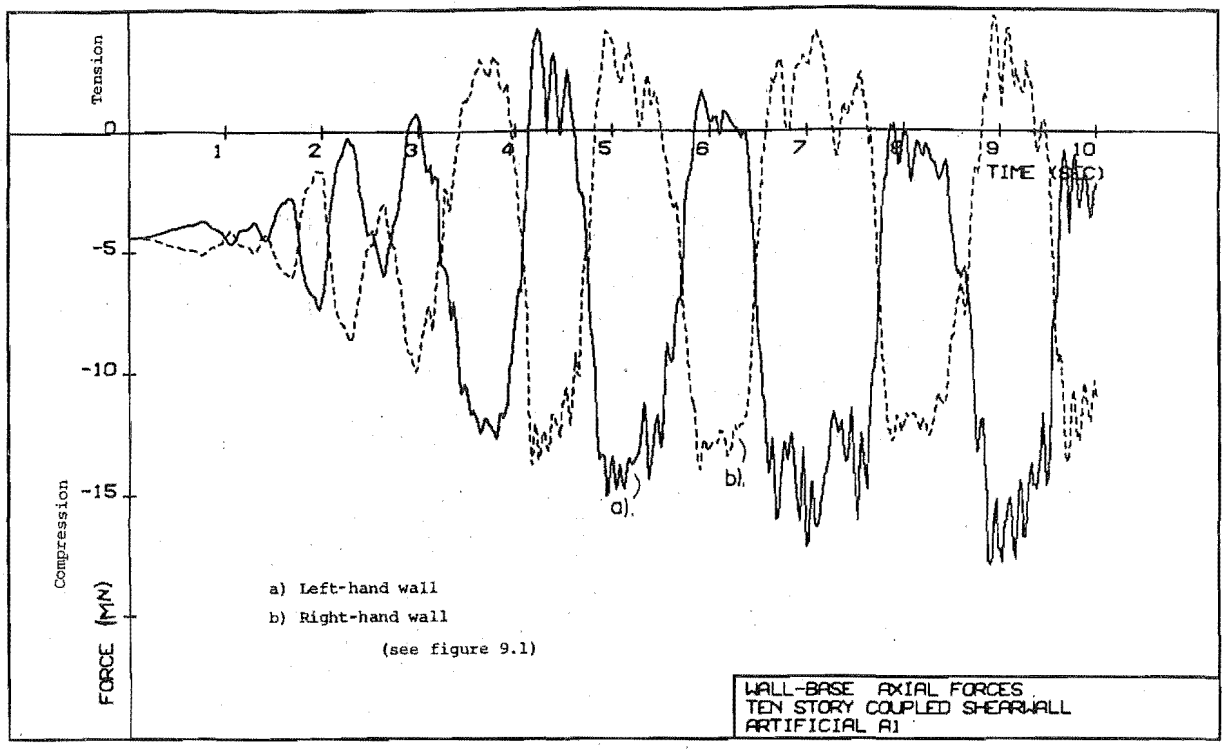

FIGURE 9.4 : AXIAL FORCE HISTORIES AT EACH WALL BASE

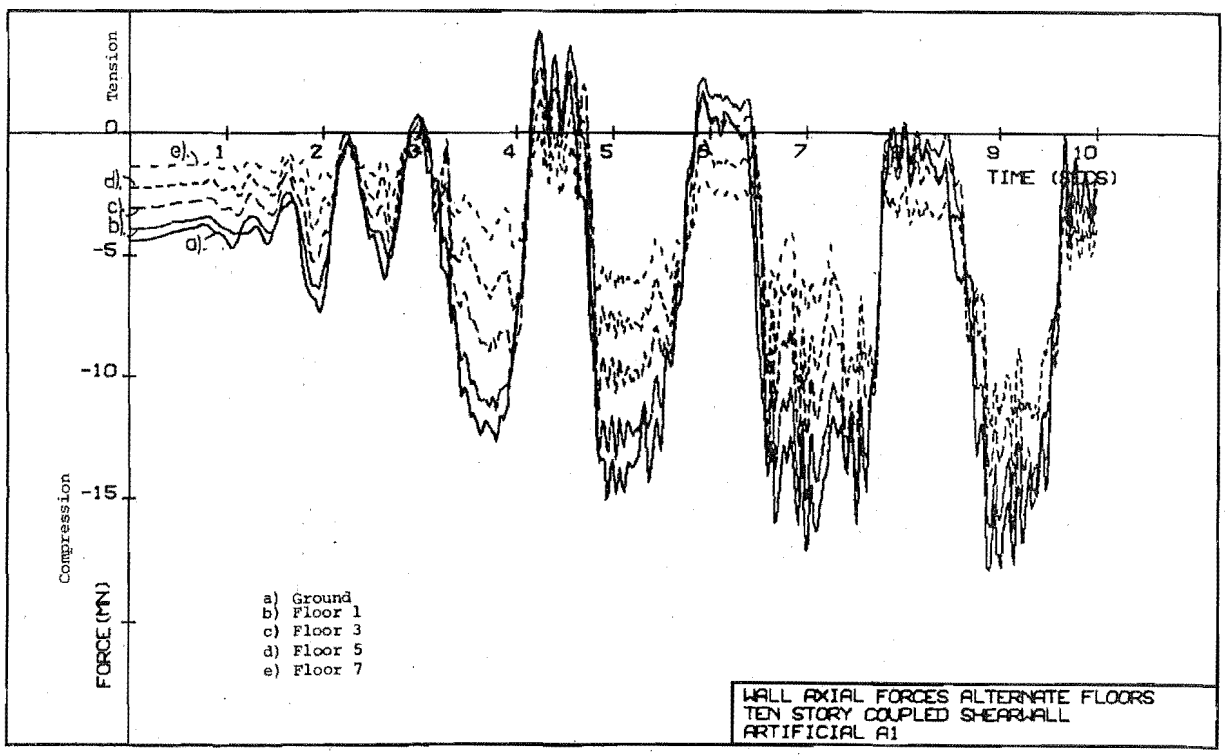

FIGURE 9.5 : AXIAL FORCES IN THE LEFT-HAND WALL

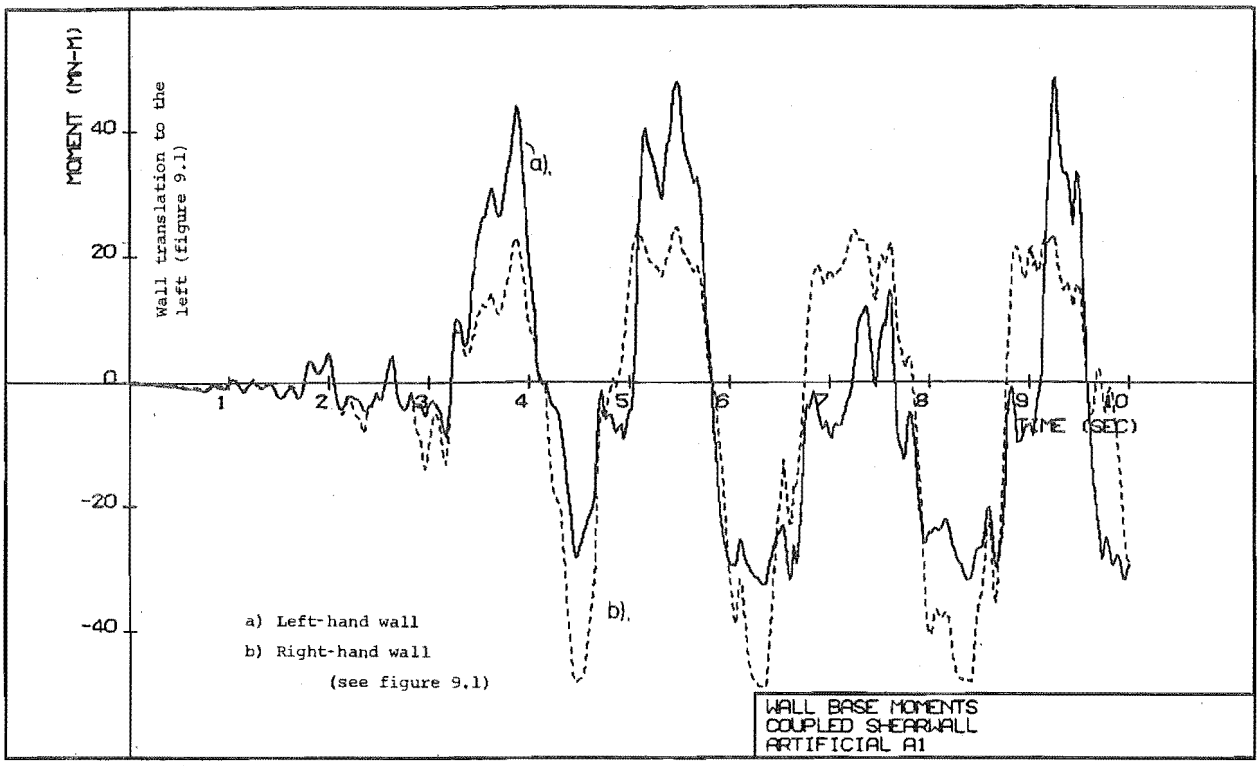

FIGURE 9.6 : WALL MOMENTS ON WALL CENTRELINE AT EACH WALL BASE

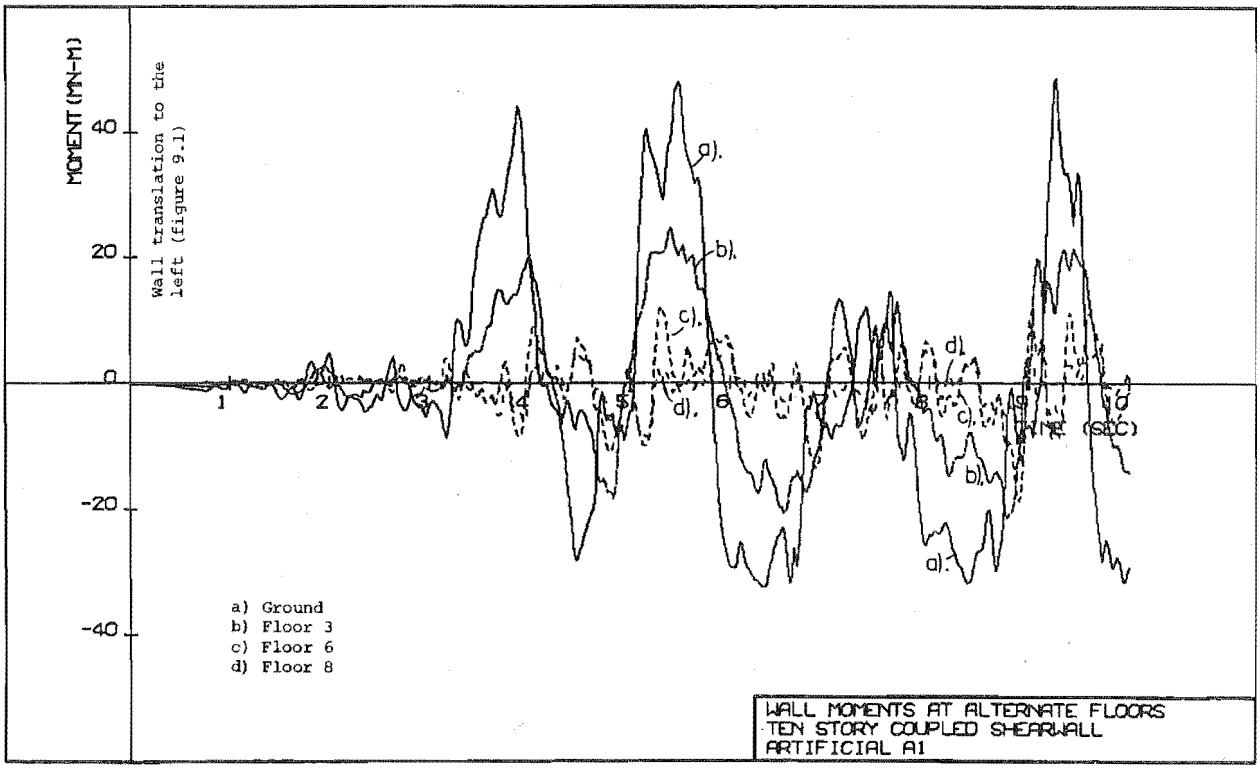

FIGURE 9.7 : MOMENTS ON THE LEFT-HAND WALL CENTRELINE

moment buildup in other parts of the structure.

A sequence of wall moment patterns is shown in figure 9.8, starting at 4.4 seconds when yielding of the walls was first seen to occur. At 4.4 seconds the bending moment distribution conforms closely to the elastic bending moment pattern for a static code loading. However, when reversal occurred a shape which more nearly approximates a 2nd mode response was seen at 5.2 seconds. At 5.4 seconds a typical first mode shape bending moment pattern occurs again. High frequency vibration present results in significant inertial moments at the first floor level, causing variations from equilibrium of static forces.

9.7.5 Wall Stiffness Parameters

a) 2nd moment of area at wall bases

Figure 9.9 shows the history of the wall base stiffness where the base 2nd moment of area, computed from a section analysis and used to determine the stiffness for each following time step of the dynamic response, is plotted as a proportion of the gross concrete 2nd moment of area. It is interesting that the section stiffness in the cracked elastic state during the "A1" response ranges between 40% and 60% of the stiffness computed assuming an uncracked section and considering concrete only. For the "El Centro" response, during which the walls barely yield, a higher average stiffness in the cracked state exists (figure 9.10). Finally, in the "A1" response (figure 9.9) the stiffness in the left-hand wall has a tendency to remain larger than the right-hand wall stiffness because of a higher axial load (see section 9.7.4).

b) Section areas at wall bases

Effective areas, as defined in Chapter 4, are shown in figure 9.11 for the duration of the analysis where the structure is a) uncracked, b) cracked but all components remain elastic and c) some components behaviour is nonlinear. The near zero areas in the right-hand wall occur at times when there is a significant axial elongation of that wall and most of the reinforcement yields because of a changing curvature. This is confirmed by noting that extreme compression strains in the left-hand wall, and hence tensile strains in the right-hand wall, occur during the 5 - 6, 7 - 8 and 9 - 10 second intervals (figure 9.3). These intervals correspond to the periods when small effective areas were computed (figure 9.11).

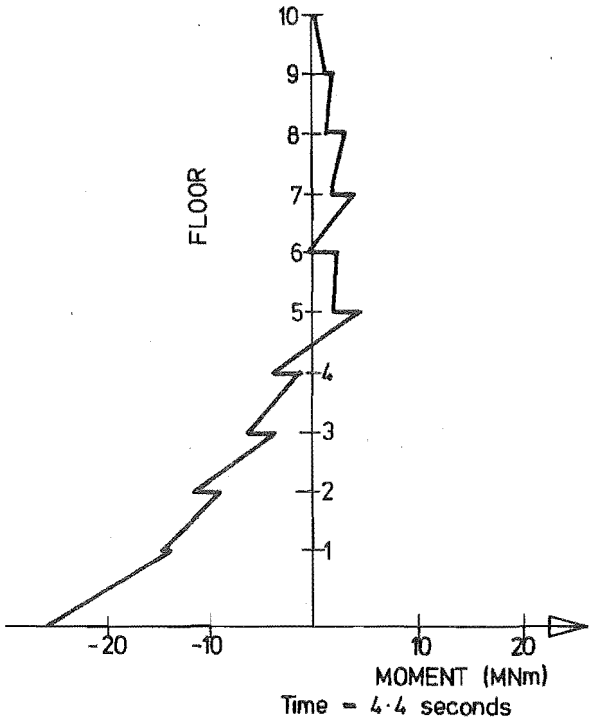

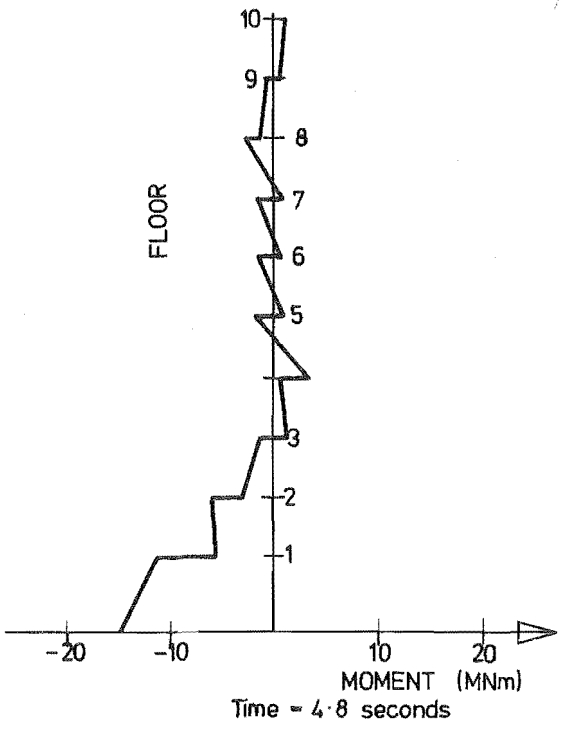

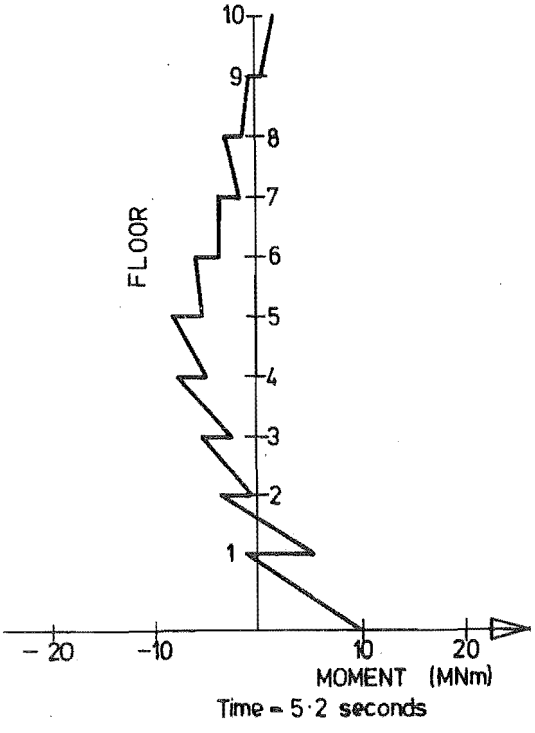

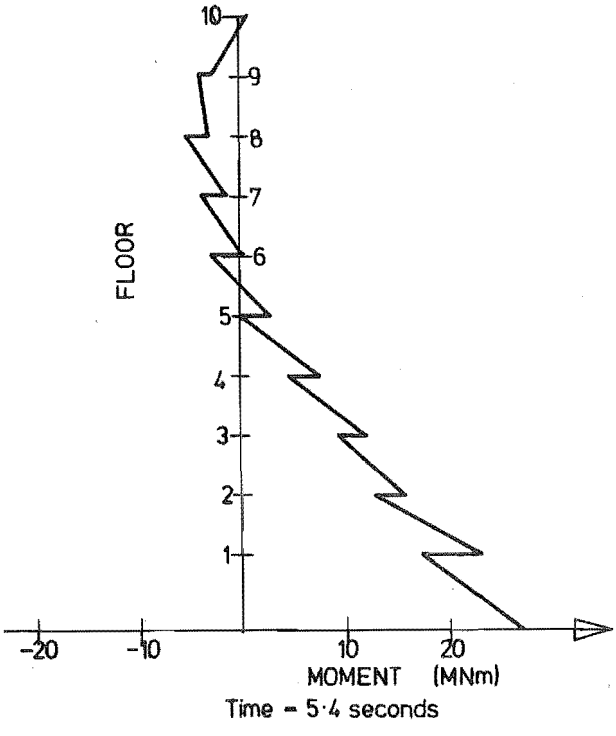

FIGURE 9.8 : INSTANTANEOUS WALL MOMENT DISTRIBUTIONS

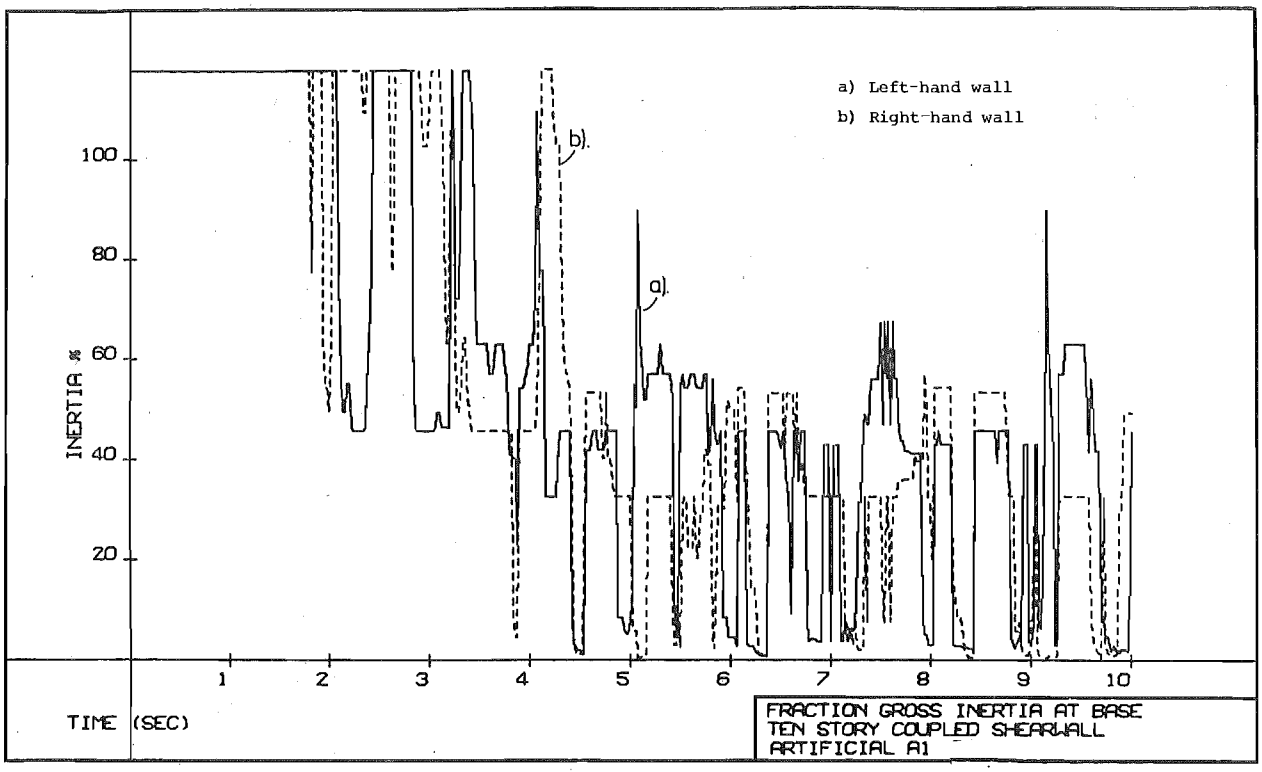

FIGURE 9.9 : 2ND MOMENT OF AREA AT EACH WALL BASE AS A PROPORTION OF THE CONCRETE SECTION VALUE

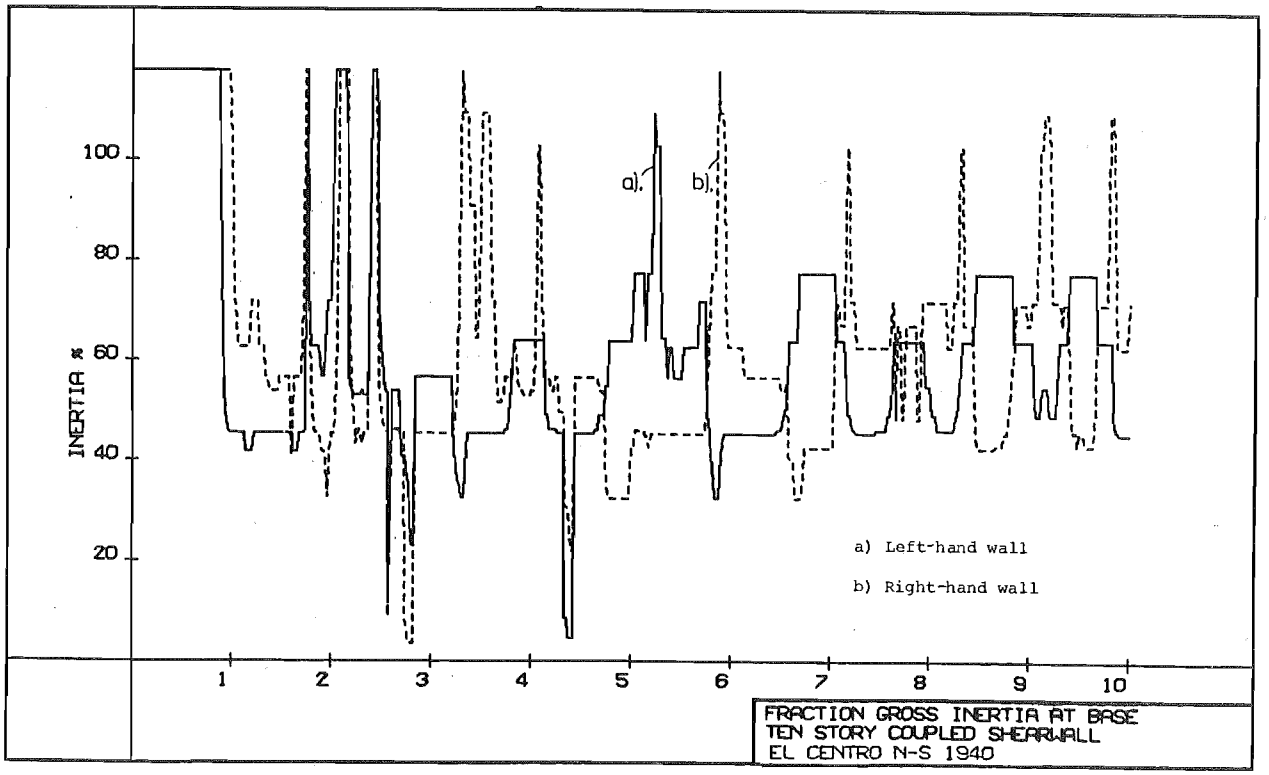

FIGURE 9.10 : HISTORY OF WALL 2ND MOMENT OF AREAS FOR THE EL CENTRO RESPONSE

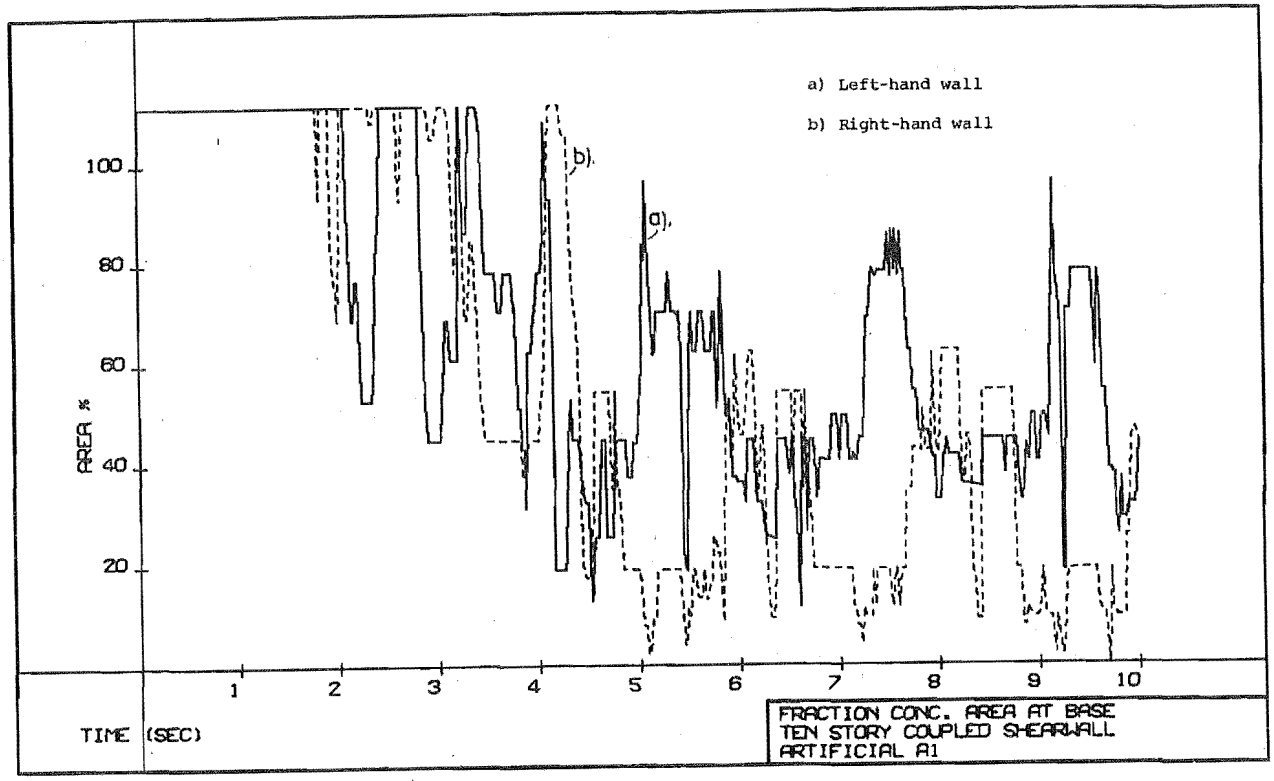

FIGURE 9.11 : EFFECTIVE AREA AT EACH WALL BASE AS A PROPORTION OF THE GROSS CONCRETE SECTION AREA

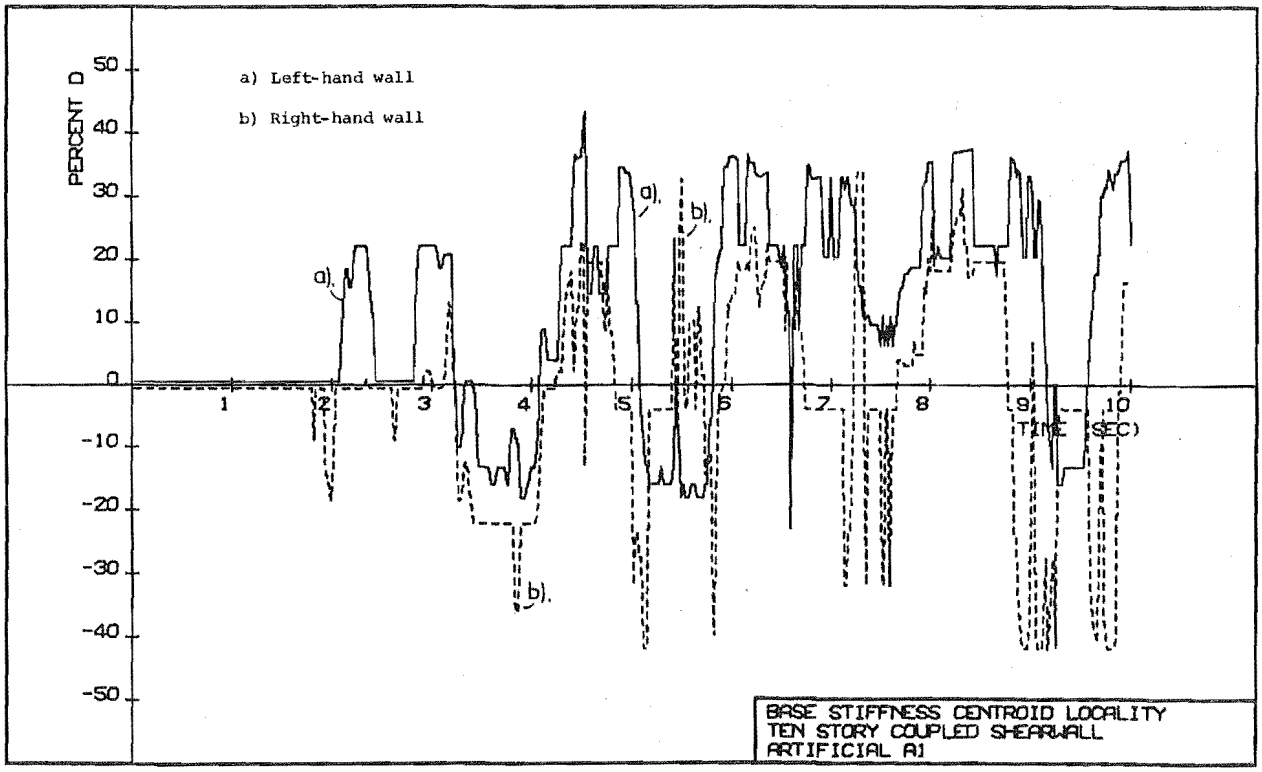

FIGURE 9.12 : INSTANTANEOUS STIFFNESS CENTROID LOCALITY AS A PROPORTION OF WALL WIDTH

c) Wall base stiffness centroid location

Location of the stiffness centroid (see Chapter 4) as a function of wall width D (figure 9.12) shows large variations. Significantly, the variation is not the same for each wall and for relatively long periods of time large differences between respective translations of wall centroids exist. This is because the different strain histories of individual components after yielding occurs (see section 3.4) complicates the subsequent response.

It is evident that the translation of the stiffness centroid can be important in the case of typical shear walls and that, in particular, coupling beam rotations may be disturbed because of an effective change of structural geometry.

9.7.6 Moment Curvature Relationships

Further useful results are the moment curvature histories providing indications of ductility demand at various locations in the walls. Figures 9.13 - 9.15 show such plots and, as expected, the major rotations occur near the base. Except in variation C (section 9.9.3) only minor yielding occurred in the upper parts of the walls. In computing a ductility, the intersection of tangents to the initial slope representing the stiffness in the cracked state and to the yield plateau was taken as a yield point (figure 9.13). It should be noted that moments shown are those with reference to the axes of the walls and therefore graphs may not compare directly with single section analyses because of the presence of the axial force-eccentricity product. In this example no large positive nonlinear curvatures appear because the structure "drifted" to the right (figure 9.2).

9.7.7 Shear Forces in the Walls

Wall shear forces fluctuate considerably and have been found to contain significant contributions from higher mode responses. A history of the shear forces in the lower element of each wall (figure 9.16) shows this fluctuation and also a considerable accumulation of interactive residual shear forces in the lower walls. These are shear forces which tended to accumulate as indicated by the permanent offset between the left-hand and right-hand wall shears in figure 9.16. As a result larger shear forces were present in each wall and a horizontal force was transmitted through the lowermost coupling beam. This observation is seen as a limitation of the mathematical model with respect to shear force prediction because the interactive shear forces

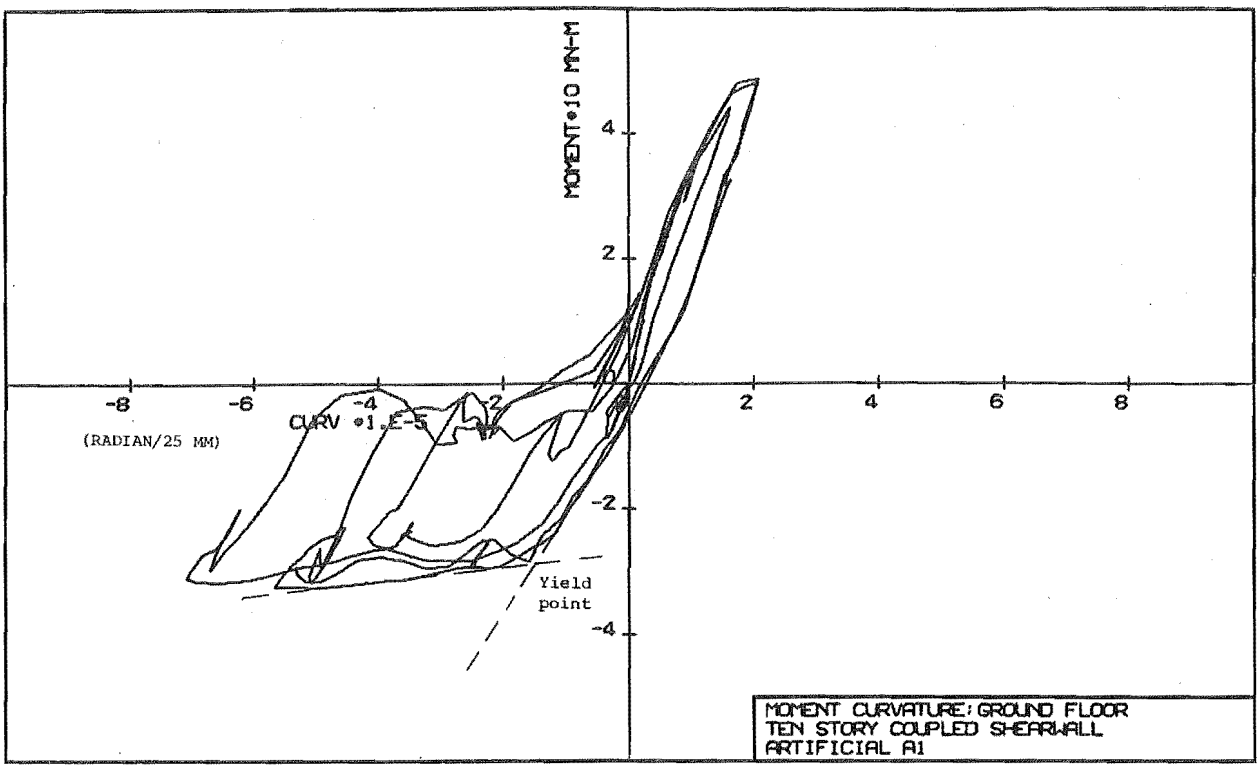

FIGURE 9.13 : MOMENT CURVATURE RELATIONSHIP IN LEFT-HAND WALL

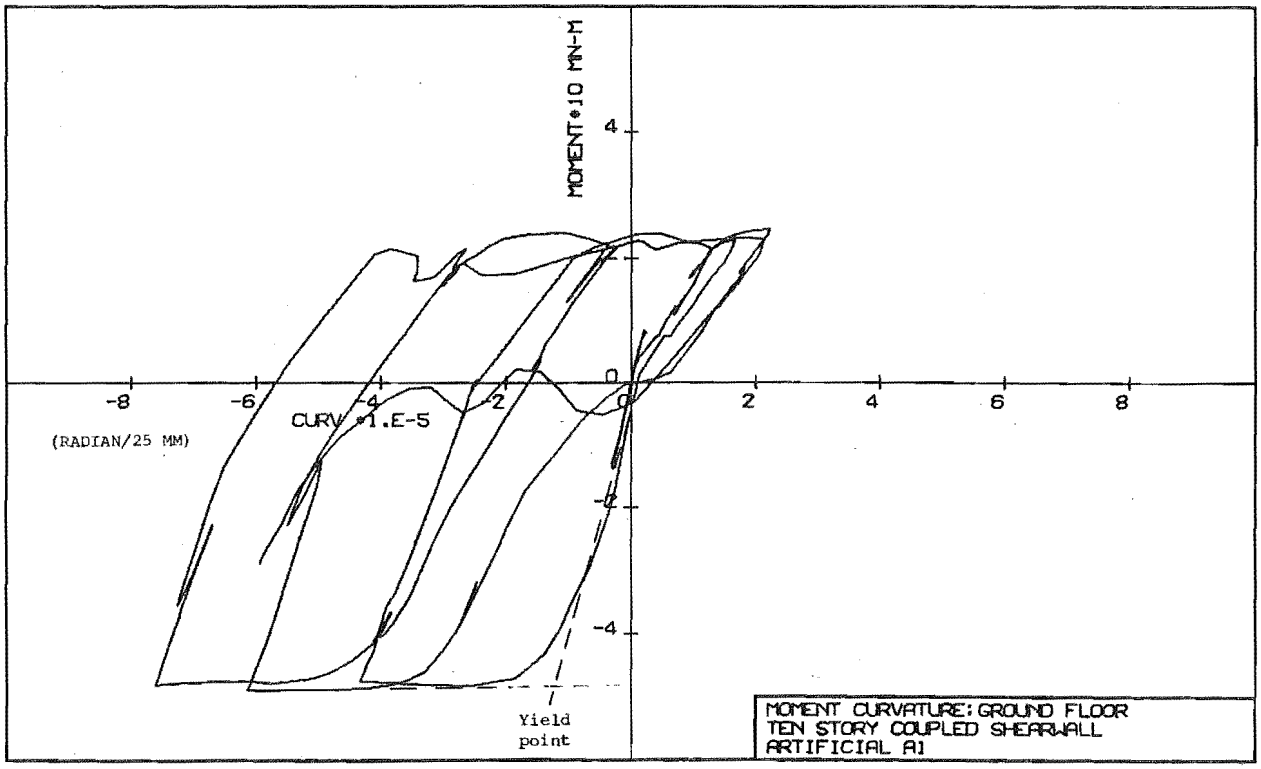

FIGURE 9.14 : MOMENT CURVATURE RELATIONSHIP IN RIGHT-HAND WALL

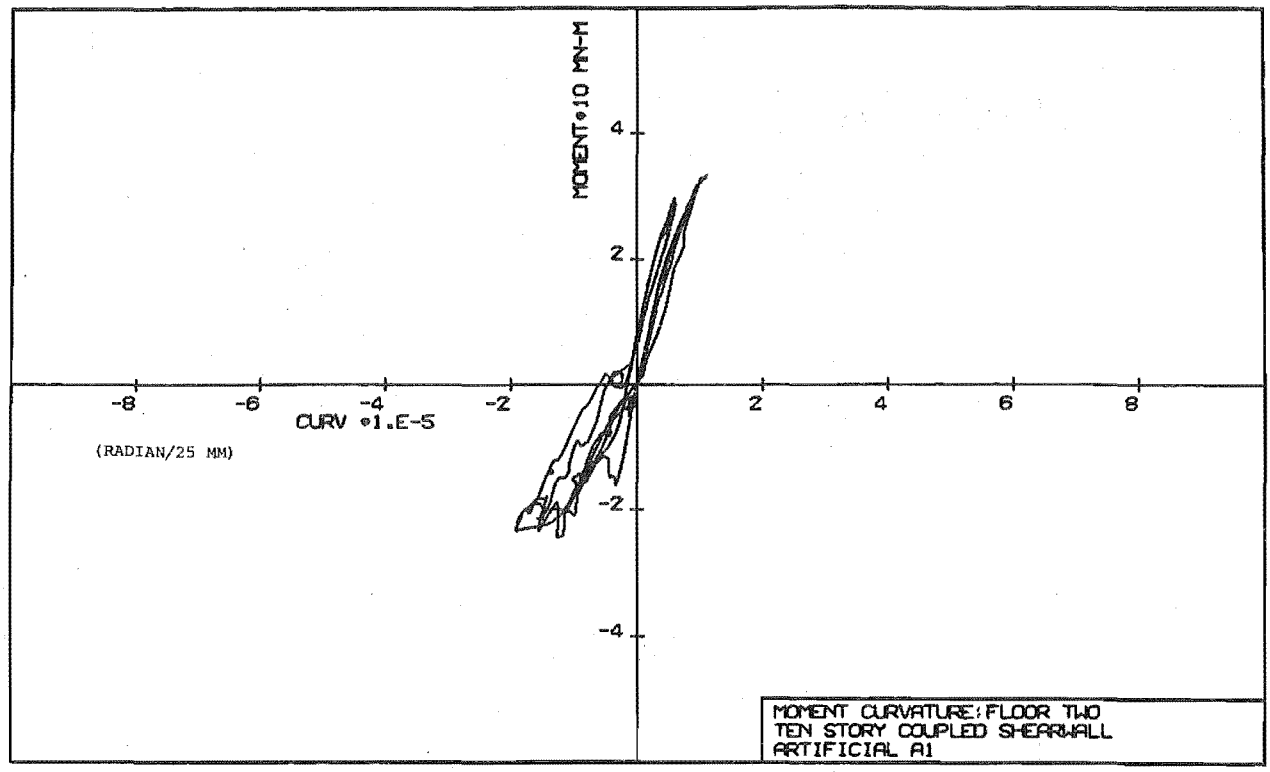

FIGURE 9.15 : MOMENT CURVATURE RELATIONSHIP AT FLOOR TWO IN THE LEFT-HAND WALL

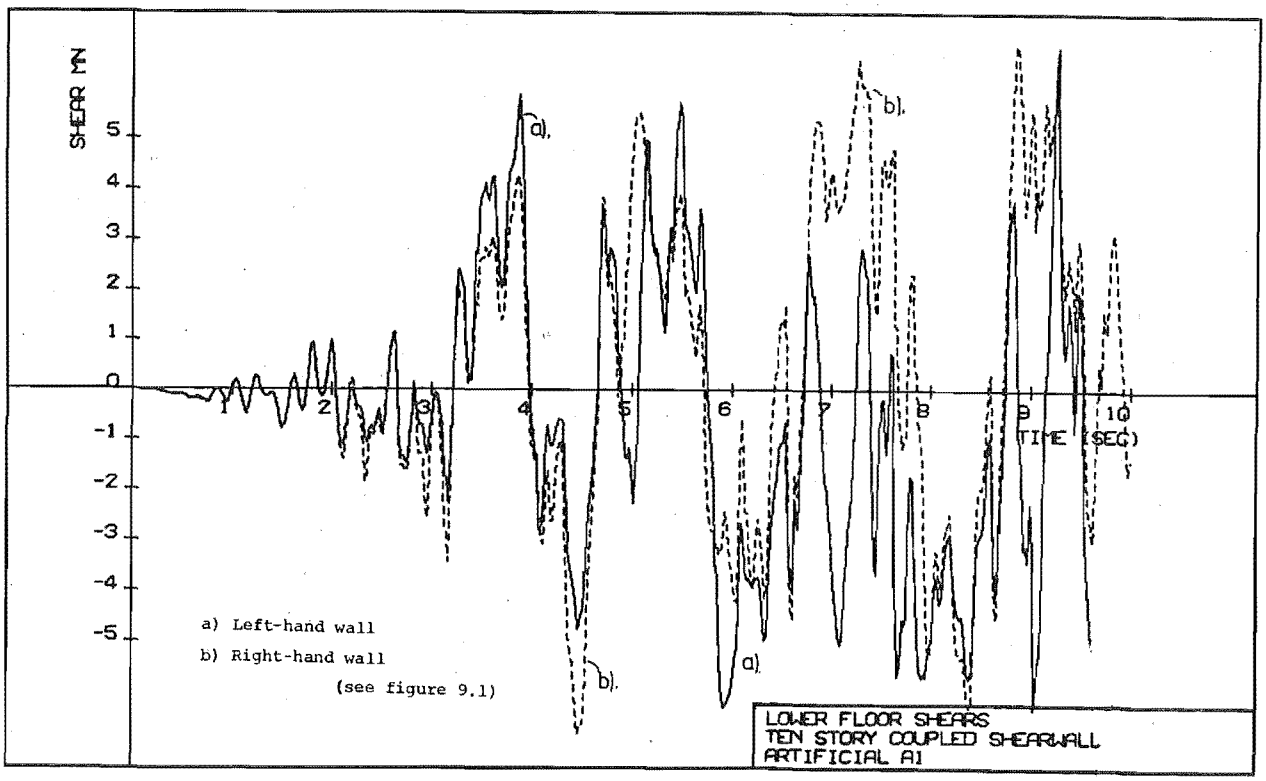

FIGURE 9.16 : SHEAR FORCES AT WALL BASES

are believed to be smaller in the real structure. Significant differences only occurred in the lower storey and averaging results for the two walls, to compute seismic shears, appears the best compromise. These averaged shears have been plotted in figure 9.24 where the actual shear force provided for in the original design and maximum static shears are present for comparison. The maximum static shears were computed assuming the formation of a collapse mechanism with members yielding at probable strengths as in the program. One half of the total shear was plotted (figure 9.24) for comparison with the left-hand wall results. Design shears have not been plotted in figure 9.16 because the comparison should be made with the average of the wall shear forces as discussed above.

It is interesting to note the axial force levels in figure 9.4 in conjunction with shear forces at wall bases in figure 9.16. Useful observations can be made because axial forces reach definite plateau of approximately 1 second duration while the shear forces fluctuate within these time periods. The mathematical model makes no allowance for different shear stiffnesses in the tension and compression walls of a coupled shear wall. Therefore, it was considered that shear force - axial force plots are of limited applicability and could be misleading. Instead it is preferable to gain this information by simultaneous examination of actions in both walls at their bases (figures 9.4 and 9.16).

Decreasing shears are seen at levels 1 - 2 and 3 - 4 (figure 9.1) in figure 9.17 although the high frequency components are still present.

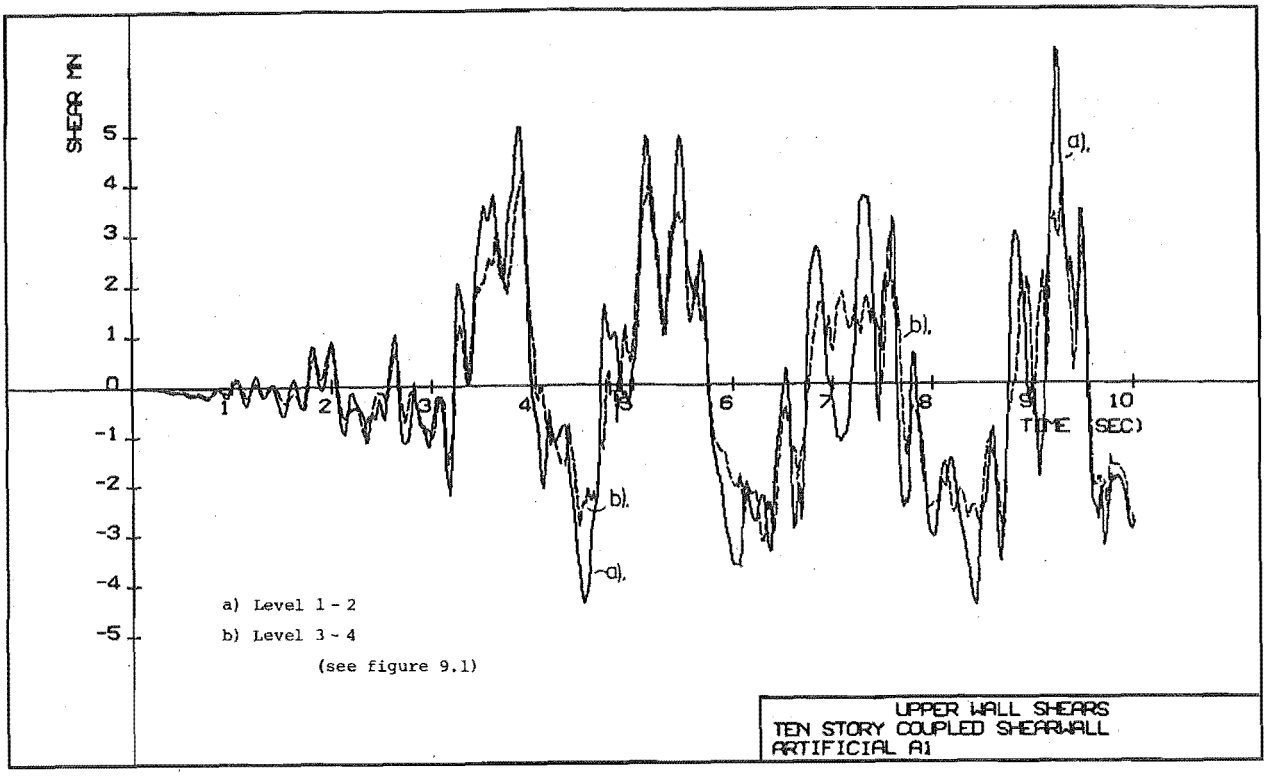

FIGURE 9.17 : WALL SHEARS IN UPPER LEFT-HAND WALL

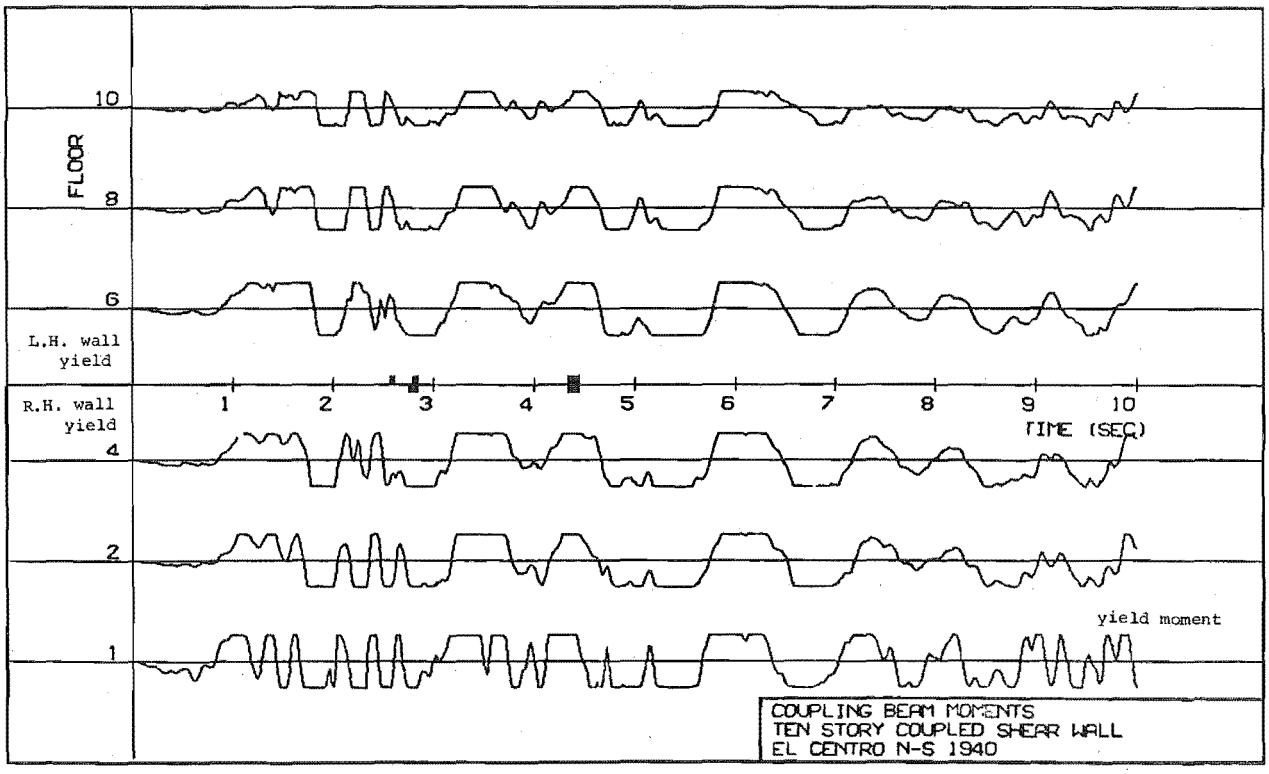

FIGURE 9.18 : COUPLING BEAM MOMENTS AND WALL YIELDING IN THE BASIC STRUCTURE WITH THE EL CENTRO N-S 1940 EXCITATION

9.8 RESPONSE OF THE BASIC STRUCTURE TO A RANGE OF BASE MOTIONS

In addition to the Artificial A1 excitation, El Centro N.S. 1940 and Artificial B1 records were used to allow a number of different responses of the same structure to be examined.

Comparison of the states of yield throughout the structure in figures 9.18 to 9.20 shows similarity in the yield patterns despite differences in the acceleration records. Since wall yielding is indicated by the histogram on the time axis, the relative order of component yielding (see section 9.7.3) may be examined. Coupling beam yield generally occurs before wall yielding and fluctuation of yielding due to higher modes, as discussed previously (section 9.7.3), was observed in all cases.

The similarity of wall bending moment envelopes (figure 9.22) and wall shears (figure 9.24) is noteworthy. It is interesting that wall bending moment envelopes (figure 9.22) show a near linear variation with height, starting from the base moment. Substantial shear forces which significantly exceeded the probable shear strengths (i.e. computed with probable capacities as in the program) in all cases. Higher mode vibration has been seen to increase the shear forces considerably.

A further 5 second run from 3 to 8 seconds in the Artificial B1 record was performed using element C1 (see section 9.4.2) to examine wall shears when shear flexibility is introduced. Unfortunately, the 5 seconds of the Artificial B1 record did not include the peak at 10 seconds, but was adequate to establish that no reduction in wall shear forces occurred.

Large differences in nonlinear deformation were seen between runs using the El Centro N.S. 1940 and the Artificial B1 results, despite the fact that they are considered to be of similar magnitudes. In particular, the Artificial B1 response showed nearly twice the maximum displacement obtained with the El Centro record (figure 9.21) and this resulted in considerably higher coupling beam rotations (figure 9.23). It seems probable that the "broad band" [15] of the Artificial Earthquake B1 response spectrum, providing high excitation irrespective of period changes, is the main cause of the larger inelastic distortions. The Artificial B1 record was used for the remainder of this study because of the broad band of frequencies which it excites.

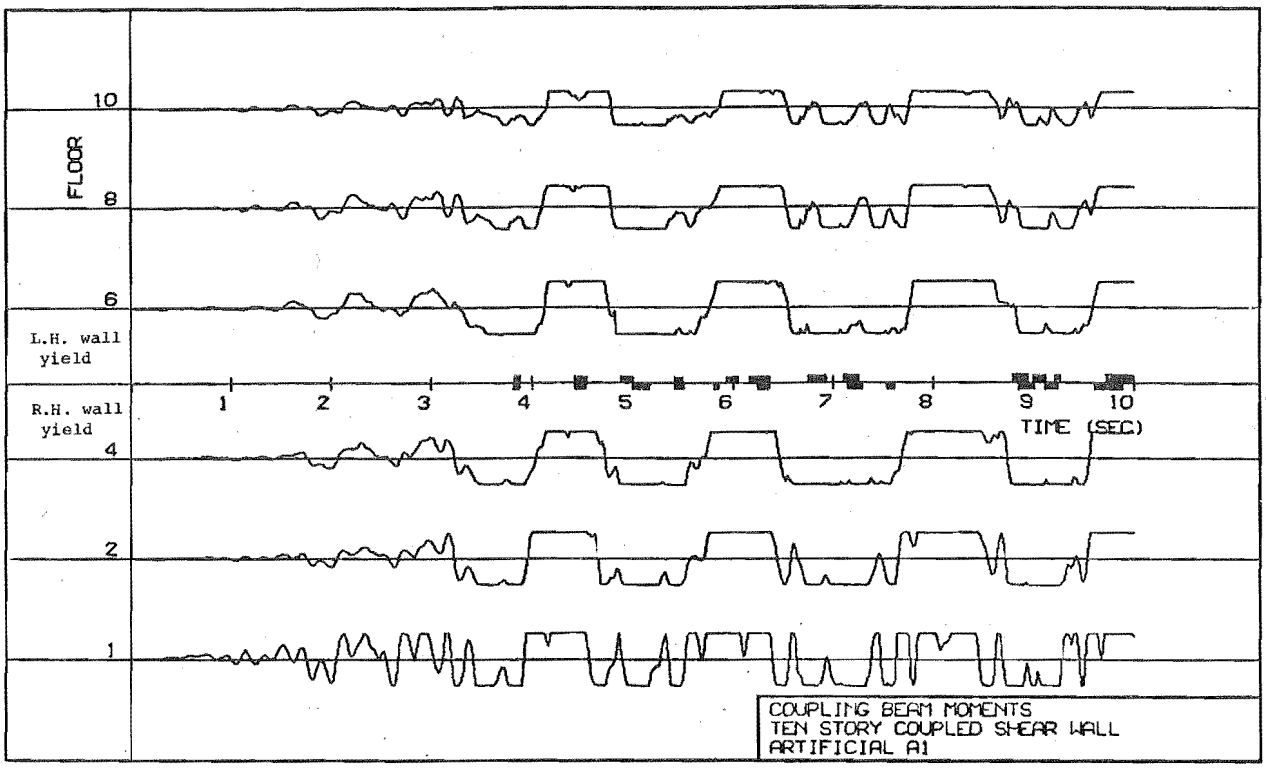

FIGURE 9.19 : COUPLING BEAM MOMENTS AND WALL YIELDING IN THE BASIC STRUCTURE WITH ARTIFICIAL A1 EXCITATION

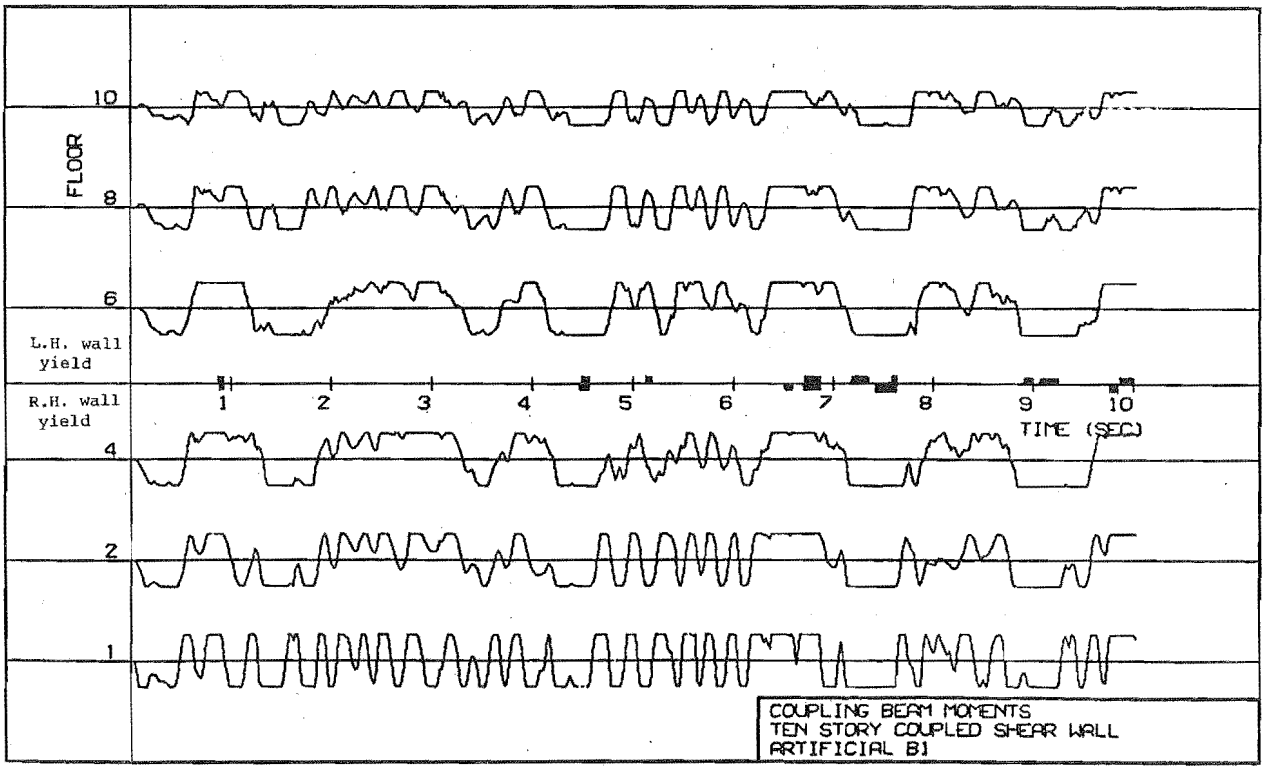

FIGURE 9.20 : COUPLING BEAM MOMENTS AND WALL YIELDING IN THE BASIC STRUCTURE WITH ARTIFICIAL B1 EXCITATION

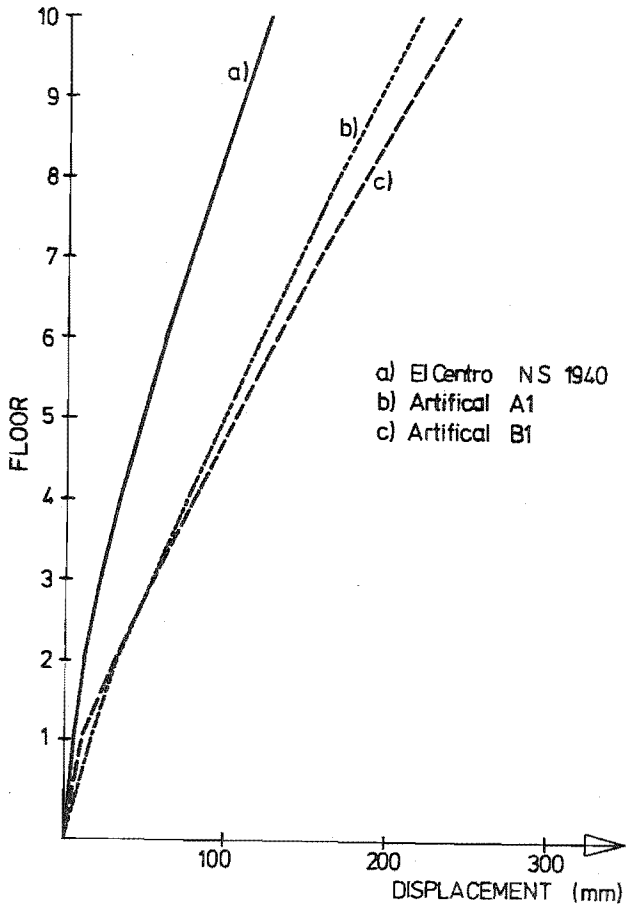

FIGURE 9.21 : MAXIMUM DISPLACEMENTS OF THE BASIC STRUCTURE

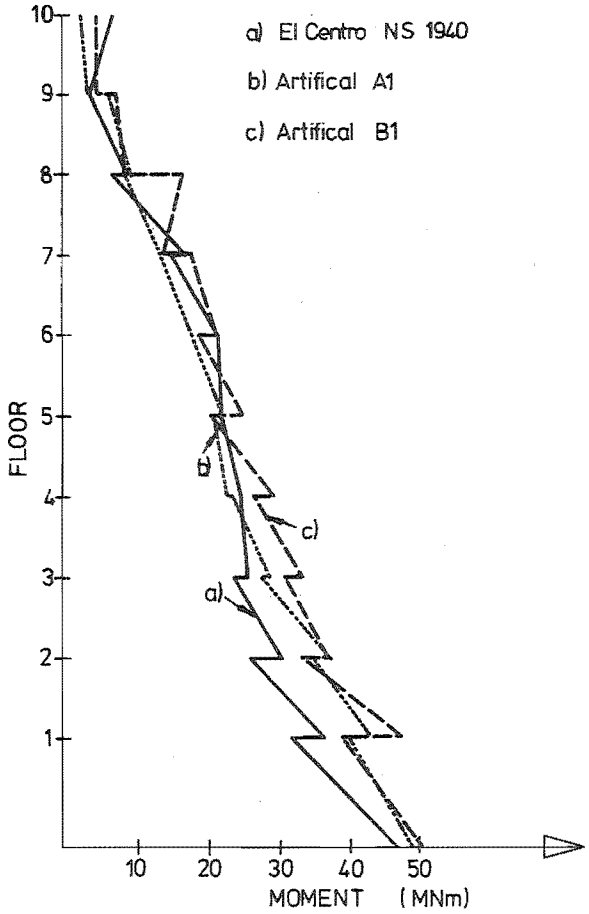

FIGURE 9.22 : WALL BENDING MOMENT ENVELOPES FOR THE BASIC STRUCTURE

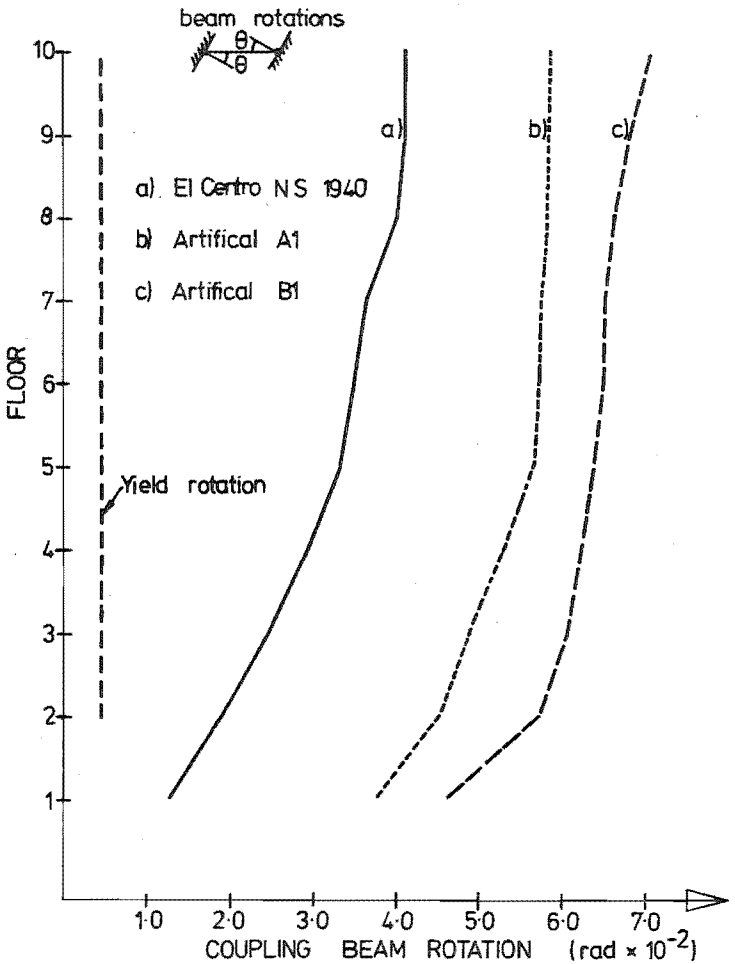

FIGURE 9.23 : BASIC STRUCTURE COUPLING BEAM ROTATIONS

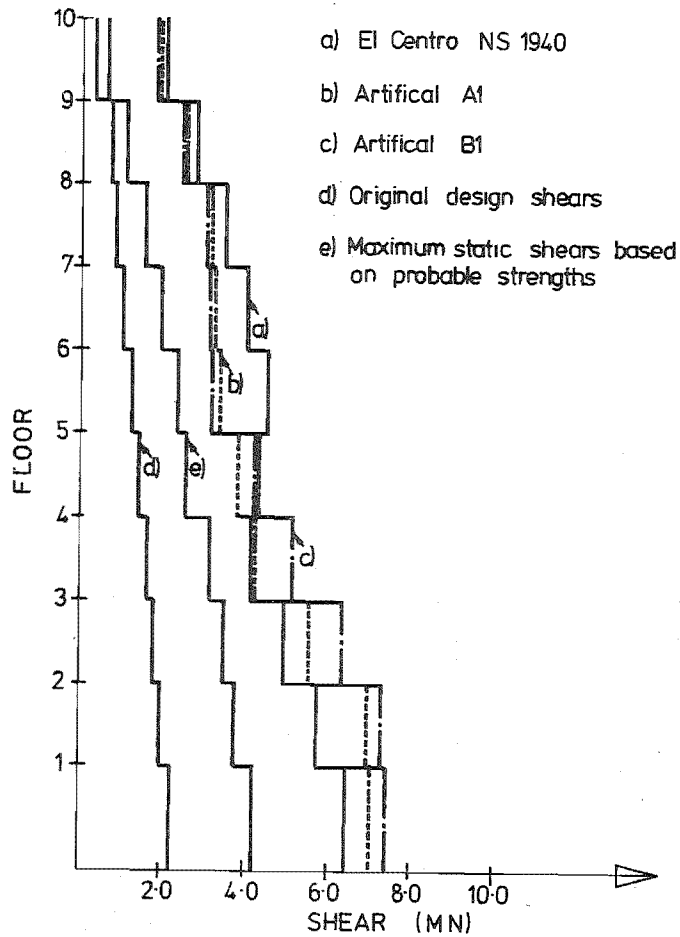

FIGURE 9.24 : WALL SHEAR ENVELOPES FOR THE BASIC STRUCTURE

9.9 PROGRESSIVE MODIFICATION OF THE BASIC STRUCTURE

9.9.1 Variation A

a) Design

The first modification, made for this run only, was the introduction of vertical flexibility under the wall supports to allow for foundation deformations. This variation is approximately equivalent to the proposed original structure and it is even more conservatively designed than the fixed-base basic structure considered earlier in this chapter. Base flexibility, allowing approximately 50% of the original substructure deformation, resulted in an increase of the first natural period from 0.89 to 1.2 seconds.

b) Results

A history of yielding throughout the structure (figure 9.25) shows a reduced frequency and duration of coupling beam yielding in comparison with figure 9.20. Maximum horizontal deflections were almost unchanged (figure 9.29) with an additional 12 mm vertical movement at the wall bases allowing sufficient rigid body rotation to compensate for reduced wall deformations. Substantial reductions in coupling beam ductility demand resulted (figure 9.31). It is interesting to note that lower shear forces occurred in the lower storeys, showing some shear relief with increased flexibility, while higher shear forces occurred in the upper part of the structure (figure 9.30).

9.9.2 Variation B

a) Design

Base fixity of the walls was restored and identical coupling retained, as in the original structure, but the wall steel was redesigned achieving a wall design level corresponding to a 0.105 g base acceleration. A capacity reduction factor of 0.9 was used for the design of both tension and compression walls. The coupling beam yield moments remain, as in the basic structure, 6% above the 0.105 g design level. This variation should provide useful information regarding the effect (if any) of changes in relative wall and coupling beam strengths on the sequence of plastification.

The changes resulted in a 62% reduction in the compression wall tensile steel and a 36% reduction in the tension steel when designing the tension wall. Steel curtailment to 66% and 33% of the base areas was assumed effective at floors 3 and 6 respectively.

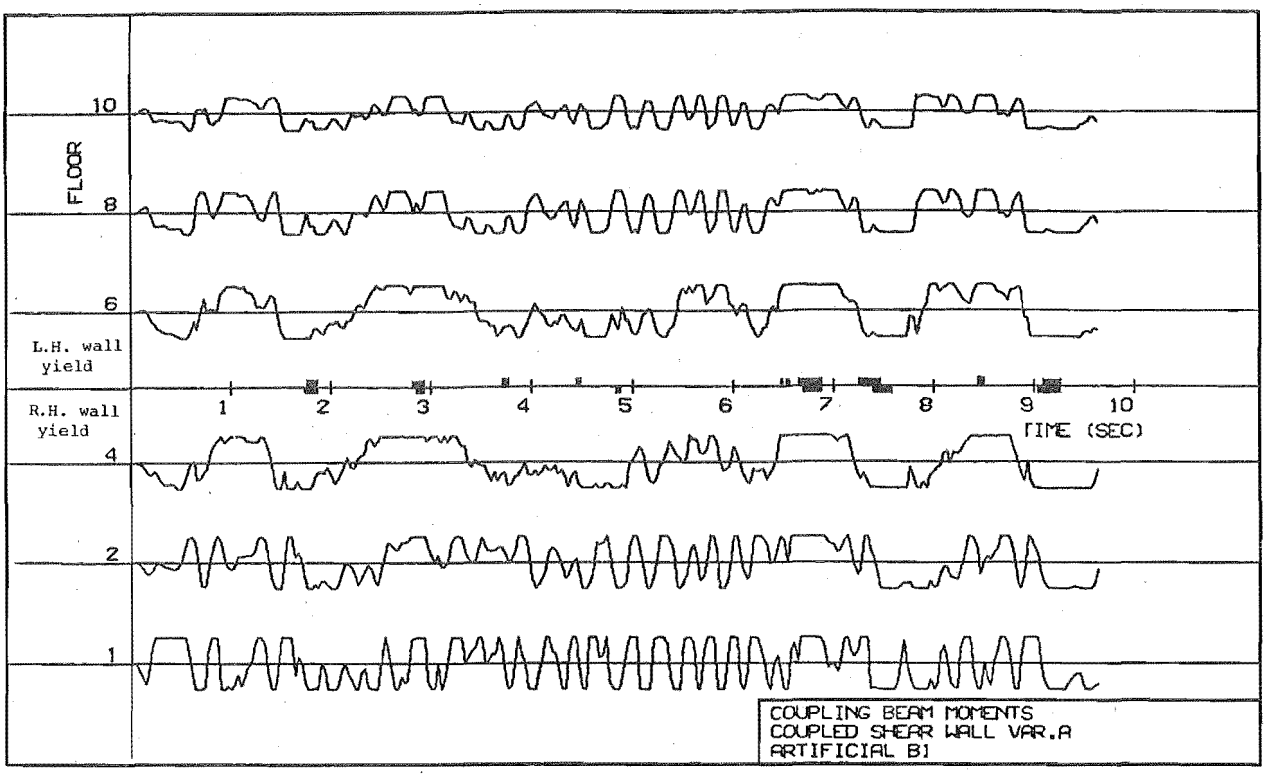

FIGURE 9.25 : COUPLING BEAM MOMENTS AND WALL YIELDING IN THE VARIATION A STRUCTURE WITH ARTIFICIAL B1 RECORD

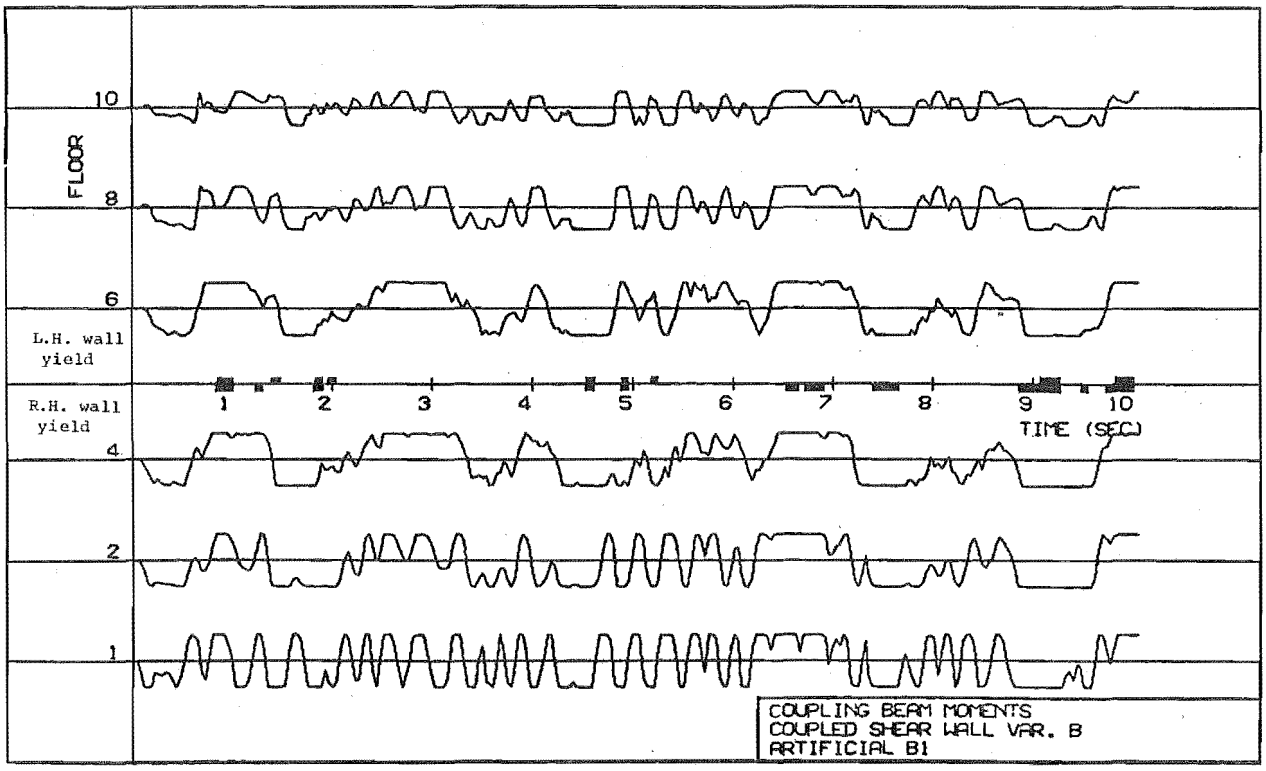

FIGURE 9.26 : COUPLING BEAM MOMENTS AND WALL YIELDING IN THE VARIATION B STRUCTURE WITH ARTIFICIAL B1 RECORD

b) Results

Almost identical maximum displacements resulted (figure 9.29). However, slightly reduced coupling beam rotations were recorded (figure 9.31), probably because of reduced compression steel in the walls and the different translations of the centres of stiffness. It is disappointing that wall shear forces (figure 9.30) do not appear to reduce substantially with a considerable reduction in wall steel and the consequent reduction in flexural strength at the base of the walls. There is, however, relatively little change in the pattern of yielding at the wall bases (figure 9.26). Coupling beams continue to yield more freely than wall bases. The wall moment at floor 3 very nearly reached the capacity provided, which was well in excess of the moment computed in the original laminar elastic static analysis.

9.9.3 Variation C

a) Design

Variation B above was retained, except that the mild steel wall reinforcement was replaced with an equivalent quantity of steel of 50% higher yield strength. This resulted in a slightly lower stiffness but a substantially higher yield curvature than in variation B.

b) Results

The significant single yield of a wall above the third floor level, as seen in the maximum displacement profiles (figure 9.29) and in the coupling beam rotations (figure 9.31), was an unexpected result of this analysis. The wall shear forces (figure 9.30) tended to be slightly reduced and the frequency, although not the extent, of the wall yielding was substantially reduced (figure 9.27).

9.9.4 Variation D

a) Design

The original wall steel reinforcement was used, this being approximately equal in each face (figure 9.1), while the coupling system strength and stiffness levels were reduced by 75% to represent a structure with light coupling. This run was intended to relate to the experimental work of this study but a moderately high level of coupling capacity was retained because of the relatively high lateral load that the structure was expected to support. In addition, because the coupling beams are considered to yield at the same rotation as experienced previously,

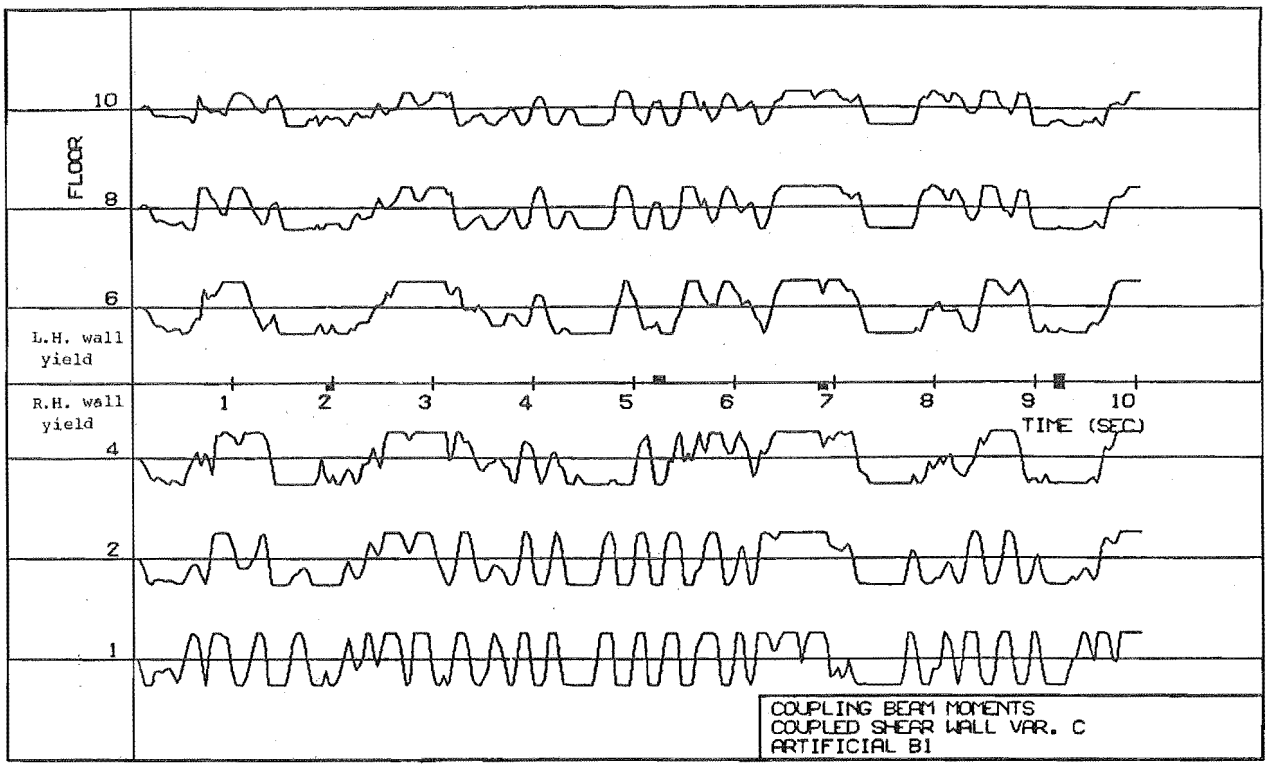

FIGURE 9.27 : COUPLING BEAM MOMENTS AND WALL YIELDING IN THE VARIATION C STRUCTURE WITH ARTIFICIAL B1 RECORD

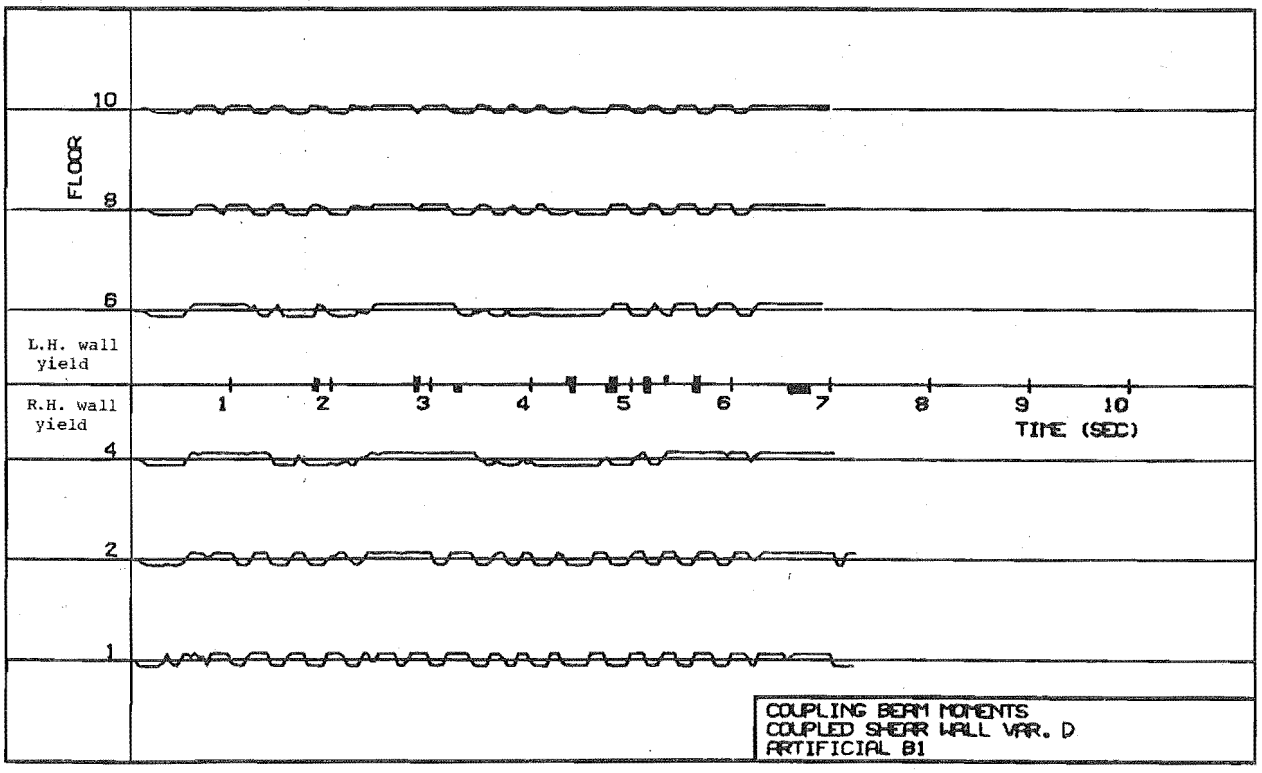

FIGURE 9.28 : COUPLING BEAM MOMENTS AND WALL YIELDING IN THE VARIATION D STRUCTURE WITH ARTIFICIAL B1 RECORD

effects of the reduced coupling strength on the sequence of failure and the maximum deformations may be assessed.

b) Results

Because of Computer Centre operational problems only 7 seconds of the response was computed which, fortunately, included the peak deformation period of all previous Artificial B1 runs. Reduced energy absorption in the coupling system led to larger deformations (figure 9.29) and consequently larger coupling beam rotations (figure 9.31). Shear forces (figure 9.30) lie between extremes for previous runs except at the base where slightly higher shear forces may be seen. It is interesting that a substantial reduction in overturning moment, which was achieved by reducing the coupling beams, does not result in a reduction in wall shear forces. The sequence of failure does not appear to have changed significantly from previous analyses and the coupling beams still yield more freely than the walls (figure 9.28).

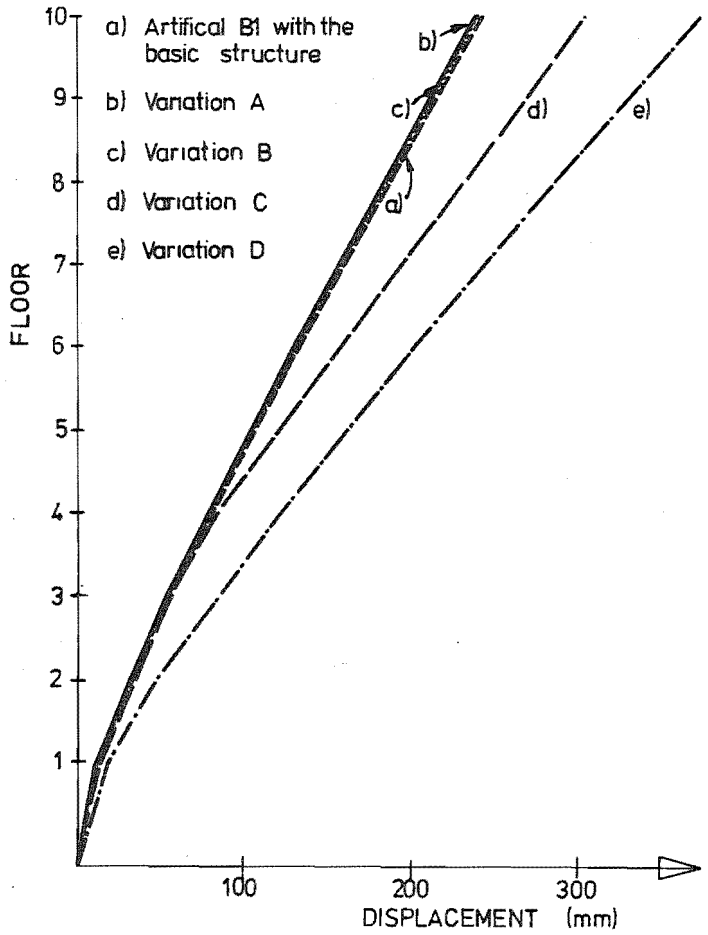

FIGURE 9.29 : DISPLACEMENT ENVELOPES FOR VARIATIONS ON THE BASIC STRUCTURE

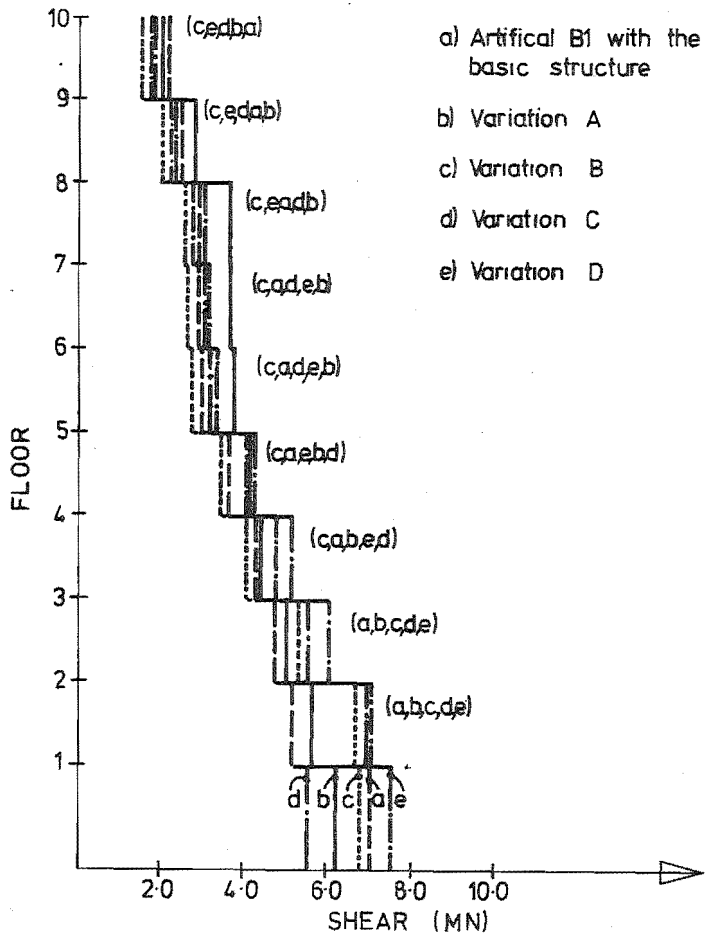

FIGURE 9.30 : WALL SHEAR ENVELOPES FOR THE MODIFIED STRUCTURE

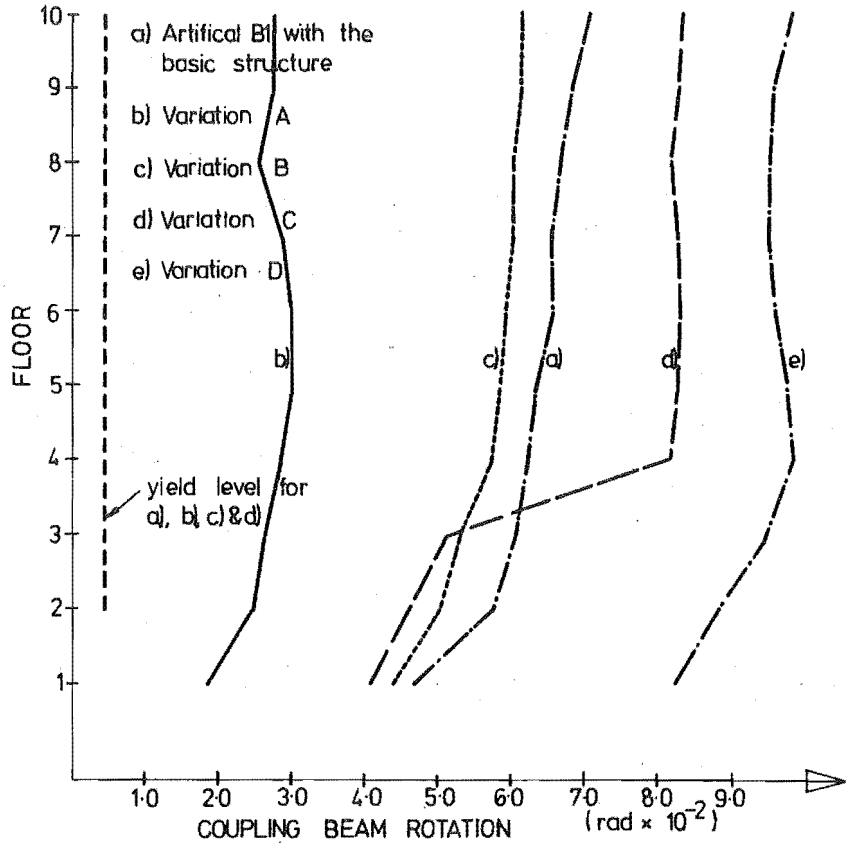

FIGURE 9.31 : COUPLING BEAM ROTATIONS FOR THE MODIFIED STRUCTURE

9.10 OBSERVATIONS OF BEHAVIOUR AND DESIGN RECOMMENDATIONS

i) Coupling beam ductility requirements are large and a coupling system capable of supplying adequate energy absorption together with the necessary ductility is vital if performance is to equal that predicted by the mathematical model. Diagonally reinforced deep coupling beams, as suggested by Paulay [3], should prove adequate although the use of diagonal lead extrusion devices between walls [80] may be preferable if coupling system energy absorption is to be maximised and overall damage minimised. The introduction of base flexibility to the basic structure was beneficial in reducing coupling beam ductility demand although coupling beam energy absorption would be reduced.

ii) It appears that the relative order of coupling beam to wall yield is a function of geometry and stiffness rather than of small differences in design strengths. The reduction of the wall strengths at the base to the values obtained in an elastic analysis for the code loading resulted in no change in the yield sequence in this study. Coupling beams generally yielded before walls and significant energy absorption in beams, prior to wall yield, was confirmed to be highly beneficial in the control of displacements and damage. Because only one basic structure was considered no general recommendations can be made except to suggest that proportioning of the beam and wall base reinforcement in accordance with forces computed in an elastic analysis is satisfactory. If coupling beams are of sufficient stiffness such that significant coupling action is present - a minimum depth to span ratio of 0.33 for coupling beams was suggested by Santhakumar [8] - then it is likely that coupling beams will yield first.

iii) The variation C structure, with a slightly more rapid curtailment of the vertical steel over the height of the wall than is consistent with a linear moment distribution, exhibited yielding of walls above the third floor. This illustrates the possibility of yielding of the wall flexural steel at upper floors when moment capacities are far in excess of the elastic bending moment distribution for the code loading. A linear variation of moments over the height of the walls appears to fit the circumstances well and should provide a sound basis for design.

iv) Although high wall shear forces, not including some observed interaction between walls, have been computed it seems probable that considerable relief could be provided by typical "shear softening".

This "softening" refers to a limited central region on a shear force-displacement diagram which appears similar in shape to that shown in figure 12.2. A considerable portion of the high frequency response may be expected to take place in the "soft" central region, significantly reducing the resulting shear forces. Inclusion of uniform "shear softening" has been seen to result in very little change in shear forces in this study. Thus, while differences in shear modelling should not, in general, significantly affect the overall response it is almost certain that predicted shear forces will be reduced by the inclusion of a realistic "soft - stiff" shear model. In view of the difficulty in assessing shear forces without a realistic shear model it is suggested that the design level for shear be higher than the ultimate static shear level but not so high as the maximum shears computed in this and most other dynamic studies. The suggested design approach is to compute shear forces associated with the formation of a collapse mechanism in the structure to determine a distribution of shear forces. These forces should be magnified by some yet-to-be-determined factor (perhaps in the vicinity of 1.4) to allow for higher mode response. However, the mathematical model of this study was considered unsatisfactory for the determination of this factor.

CHAPTER TEN

EXPERIMENTAL INVESTIGATION OF SLAB COUPLING OF SHEAR WALLS

10.1 INTRODUCTION

Because of their basic structural efficiency and architectural suitability, tall "Shear Wall - Slab Structures" [68] have been widely used in high rise appartment buildings. In the seismic analysis of such structures, realistic assessments of coupling system attributes - stiffness, yield moment and ductility - should be made to ensure reliable design. Yet, of the referenced papers reporting experimental investigations on slab coupling, which are outlined in the following section, all are limited to various degrees by simplifying assumptions. Either elastic perspex or microconcrete models representing reinforced concrete have been used, or the loading has been monotonic and the basic attributes of seismic performance remain inadequately defined.

Over a considerable number of years cast insitu slabs, sometimes cast monolithically with a coupling beam, have been incorporated into a large number of structures. It would appear desirable that a clearer understanding of their structural behaviour be gained.

10.2 SUMMARY OF PREVIOUS WORK

To the writer's knowledge only limited documented information relating to slab coupling is available. As recently as 1966 Barnard et al [68] were unable to find any and in this literature survey no information relevant to a cyclic test of a reasonable scale reinforced concrete model has been found.

A number of papers [68,69,70,71], assessing an effective width of slab, based on elastic models or elastic theory, have appeared over recent years and in some cases design information has been presented. Others [72, 73,74,75] rely upon concrete model tests of various scales. Both types of investigation are discussed briefly below.

Barnard and Schwaighofer [68] constructed $^{1}/_{64}$th scale models of 22-storey structures of glued epoxy sheet, included floor slabs and found that the entire slab width must be taken to ensure correspondence with Rosman's analysis for coupled shear walls [76]. For each of the three tests performed, stresses computed with Rosman's theory compared well with

test results.

Qadeer and Stafford-Smith [69] performed a series of finite difference analyses using an elastic plate idealisation. They have presented non-dimensional graphical results for a variety of geometrical configurations and an effective width may be derived directly from their curves. In addition, small scale tests, comprising two pin-based laterally loaded steel walls with an asbestos slab, provided close comparison with the theoretical work.

Mirza and Jaeger [72], who performed monotonic tests on reinforced microconcrete walls and slabs, present photographically recorded crack patterns and plotted force displacement relationships. In these small scale tests the two two-storey walls were fixed at their bases and were tested together with the two floor slabs. No special slab reinforcement appears to have been included in the wall toe region, nor does any tendency towards a punching shear failure appear to have been encountered. No strains were measured.

Simmonds [73] investigated slabs supported on walls, both with elastic finite difference analyses and a series of one third scale reinforced concrete test structures. He considered only gravity loading.

Schwaighofer and Collins [74] examined monotonic seismic loading in a one third scale reinforced concrete specimen and have presented useful results including force displacement relationships, crack patterns and steel strains. A punching shear failure at one wall toe occurred in the absence of shear reinforcement in this critical region.

A report by Szalwinski [75] describing the test reported by Schwaighofer and Collins in greater detail and presenting elastic finite element studies for comparative purposes, became available during the final drafting of this thesis. Tentative design recommendations, based on the elastic finite element study and partially verified by his monotonic test, are outlined (see Chapter 12).

10.3 OBJECTIVES AND SCOPE OF THIS INVESTIGATION

Experimental investigation of the fundamental behavioural characteristics of reinforced concrete slabs, providing or enhancing coupling between shear walls, is the general objective of this study. Original intentions were to investigate simple slab coupling with a range of wall spacings and, if possible, a range of seismic reinforcement. It was felt that such a study

could lead to a useful analytic model for dynamic and static analyses. Instead, in the absence of satisfactory reinforcement solutions for the wall toe region, this project concentrated, as its first objective, on providing design recommendations for the engineering profession. To this end three slabs, between which the only significant difference was the reinforcement in the wall toe region, were tested.

A fourth specimen, incorporating a shallow coupling beam cast monolithically with the slab, was constructed as a pilot test in an area of proposed future research. In approaching the more general problem, the assessment of isolated slab performance was considered to be a logical first step. The pilot test of a slab and beam coupling system represents the next important step, which involves assessing the strength enhancement afforded by composite action between the beam and the slab. Although pressure for research in this field and the concern expressed by a number of designers were the main reasons for performing this final, incomplete investigation, correlation between all four units has enhanced its value considerably.

The following objectives were of principal interest in this study:

i) The comparison of strength predictions with test results, providing indications on the applicability of the predicted yield lines.

ii) The determination, by trial and error, of suitable combinations of transverse reinforcement at wall toes, first, to control damage and, secondly, to improve stiffness properties.

iii) Approximate calibration and matching of standard hysteretic relationships to experimental data to represent slab coupling for dynamic analyses.

iv) Attempted generalisation of results by using approximate empirical relationships to express design and analysis parameters.

10.4 THE PROTOTYPE STRUCTURE

10.4.1 Proportions of the Prototype

Typical layouts of apartment buildings [68] lead to bay sizes of 6 - 7 m, building widths of 15 - 20 m while retaining a floor height of 2.8 m. Building heights are, depending on location, in the 30 - 60 m range. A 15-storey prototype structure of typical plan (figure 10.1) and floor height, although of greater overall height (figure 10.2) than is

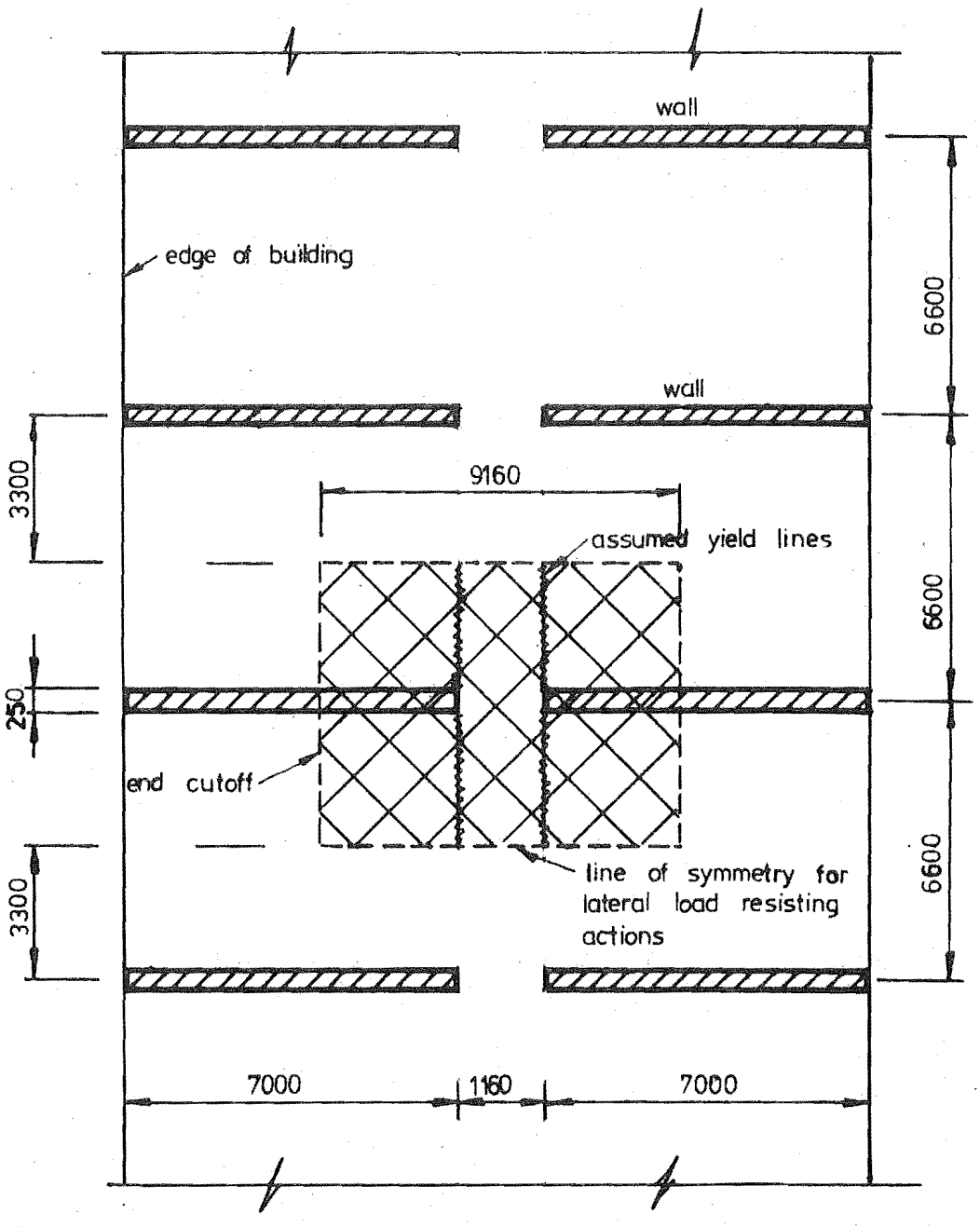

FIGURE 10.1 : PLAN OF THE PROTOTYPE STRUCTURE SHOWING MODEL LOCALITY.

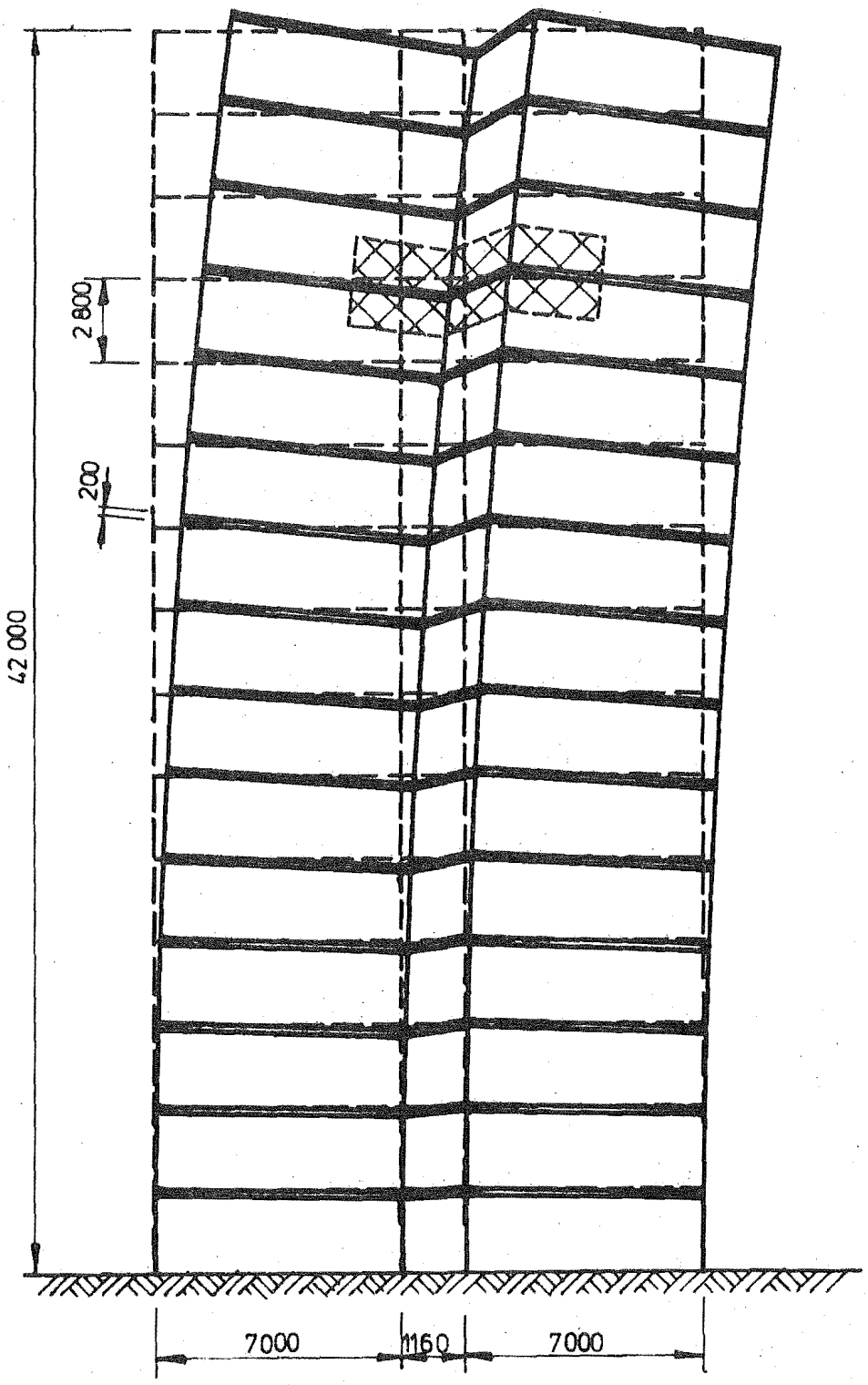

FIGURE 10.2 : ELEVATION OF THE PROTOTYPE SHOWING MODEL LOCALITY AND A TYPICAL DEFORMATION PATTERN.

typical of New Zealand conditions, was selected for this study. If a 10-storey structure had been nominated and an elastic slab design performed, a greatly reduced seismic steel content would have been the consequence. However, this arbitrary choice is unimportant in the assessment of results, rather it is important that a representative slab configuration is chosen for the test.

10.4.2 Design of the Prototype Slab

For the purposes of design and description, reinforcement is referred to as being either longitudinal (primary, seismic) or transverse (secondary and gravity load) with respect to the line of the walls. Reinforcement in these directions was designed, assuming the use of mild steel and medium strength concrete.

(a) Transverse Reinforcement for Gravity Load

Transverse reinforcement, placed in outer layers, was designed for dead load and a prescribed code live load of 1.94 kPa (40 lb/ft^2) for one way action assuming flexural fixity at walls. Moment redistribution reducing the negative support moments by 20% was allowed and 14% excess bottom reinforcement was provided to allow uniformity in placing the transverse bars. This reinforcement was placed in the top and bottommost layers in the slab.

(b) Longitudinal Seismic Action

The recommendations of Qadeer et al [69] were used to assess the stiffness of the slab in its uncracked state and an effective width corresponding to this stiffness was computed. To allow for cracking, the slab stiffness was reduced by 50% when performing the lateral load analysis. Zone A lateral loading from NZSS 1900 Chapter 8 "Basic Design Loads" [64] was used in conjunction with a two-dimensional frame analysis to compute slab moments. This analysis incorporated rigid end blocks to allow for the significant wall widths. The resulting seismic reinforcement was placed in second layers below or above the reinforcement required for gravity load.

10.5 CONSIDERATIONS FOR AN EXPERIMENTAL STUDY

A half scale model, described in detail in the following chapter, was derived from the prototype utilising the following assumptions:

i) Equal wall rotations are representative of prototype deformations.

ii) Unresisted longitudinal in-plane expansion of the model slab, achieved with equal wall jack forces, is considered to be representative of prototype conditions.

iii) The use of precast wall segments, which were moderately stressed during the test, instead of cast-in-place construction is unlikely to affect slab performance significantly.

iv) Failure to accurately model dead and live load actions has only minor effects on the failure mechanism and the ultimate moments due to lateral loading. The use of a longitudinal line of symmetry is therefore reasonable in the model.

v) The model is of sufficient length so that the free end boundary conditions of the model slab are of minimal importance.

vi) Insignificant separation forces in the slab are generated as a consequence of small differences in yield moments at wall faces (see section 11.3).

Although the prototype structure was designed and the model derived in a similar fashion to that of Islam [77], only basic outlines have been presented here because of the subjective nature of structure selection and, to some extent, of its design. Rather, the test structure examined in Chapter 11 is submitted as representative in its own right and suitable in which to examine the seismic behaviour of slab coupling of shear walls. It is considered, however, that the principles with which the test structure has been derived from the prototype are of general applicability. Subsequent inspection of results is claimed to provide some supporting evidence.

CHAPTER ELEVEN

TEST SPECIMEN AND TEST PROCEDURES

11.1 INTRODUCTION

Inevitably, when a model of a portion of a complex structure is simplified to the point of being practical, approximation and errors are introduced. Compromise between keeping these errors to an acceptable level and retaining simplicity in the model is essential in the conception of any experiment. In some cases oversimplification does lead to a suppression of significant features of performance. In comparison with previous work outlined, excepting the one third scale monotonic test first reported by Schwaighofer and Collins [74], a higher order of realism has been achieved in this study by testing actual reinforced concrete components and by minimising scale effects. In particular, more representative shear behaviour and flexural cracking in the slab has been achieved with the use of a half scale model. In addition, cyclic loading was applied and torsional movements at cracks were found to be significant.

11.2 BASIC TEST CONFIGURATION

Based on the assumptions of section 10.5 a test model, which is illustrated schematically in figure 11.1, was constructed. In achieving a model which was practical to construct precast segmental construction was adopted in which four wall pieces were cast first and re-used where possible, while new slabs were cast for each test. Prestress applied with high strength bars in the walls clamped wall and slab units together to simulate gravity loads and to facilitate testing of the slab. The wall bases were pinned at strong floor fixtures while equal horizontal jack forces were applied to each wall top in the longitudinal direction. Lateral restraint was provided with adjustable balls in sockets which were in contact with the wall tops and fixed to a transverse frame.

A more complete picture may be obtained from figure 11.2, a photograph of the actual test set-up, in conjunction with table 11-I which lists definitions.

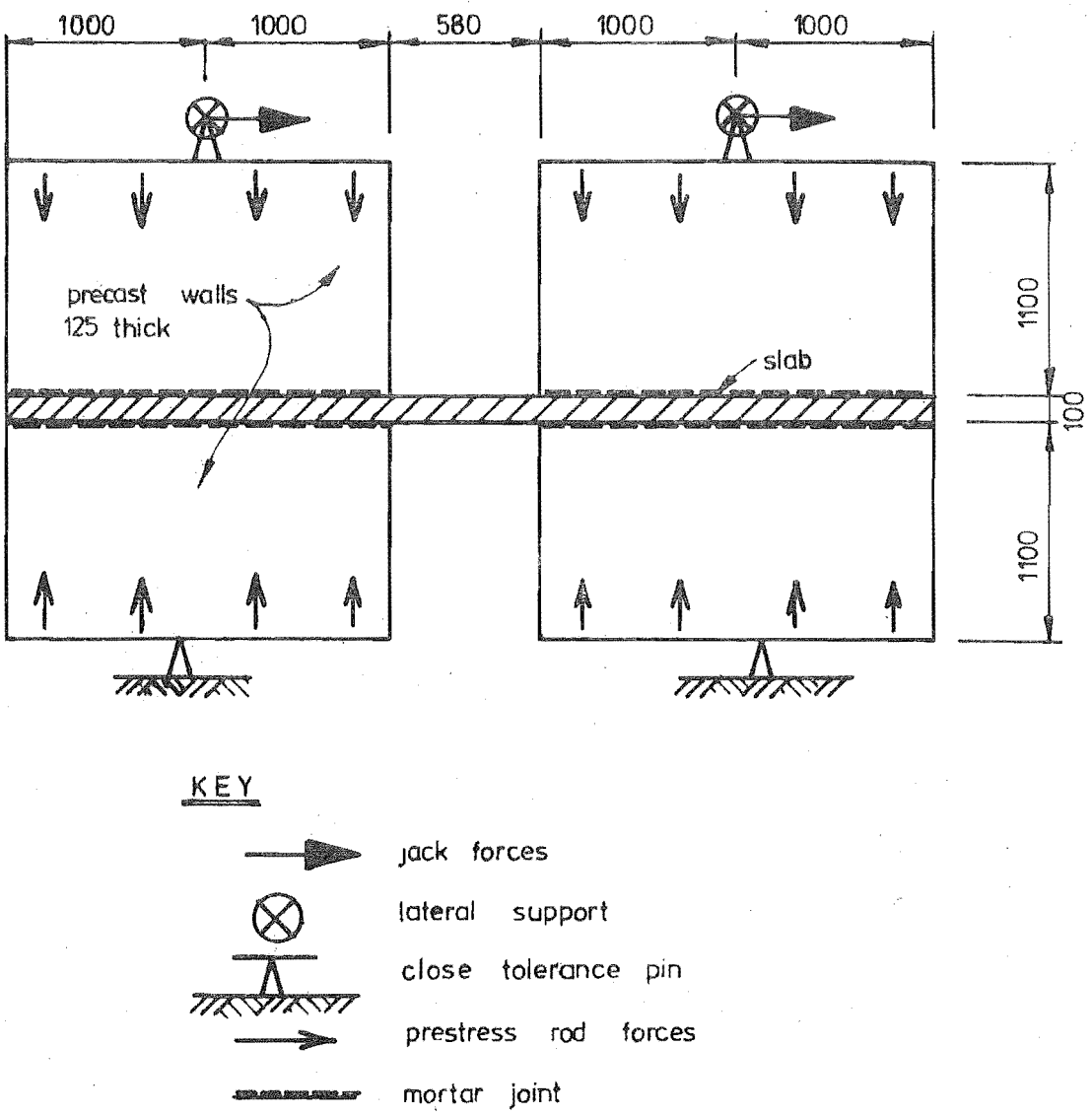

FIGURE 11.1 : SCHEMATIC ILLUSTRATION OF TEST MODEL.

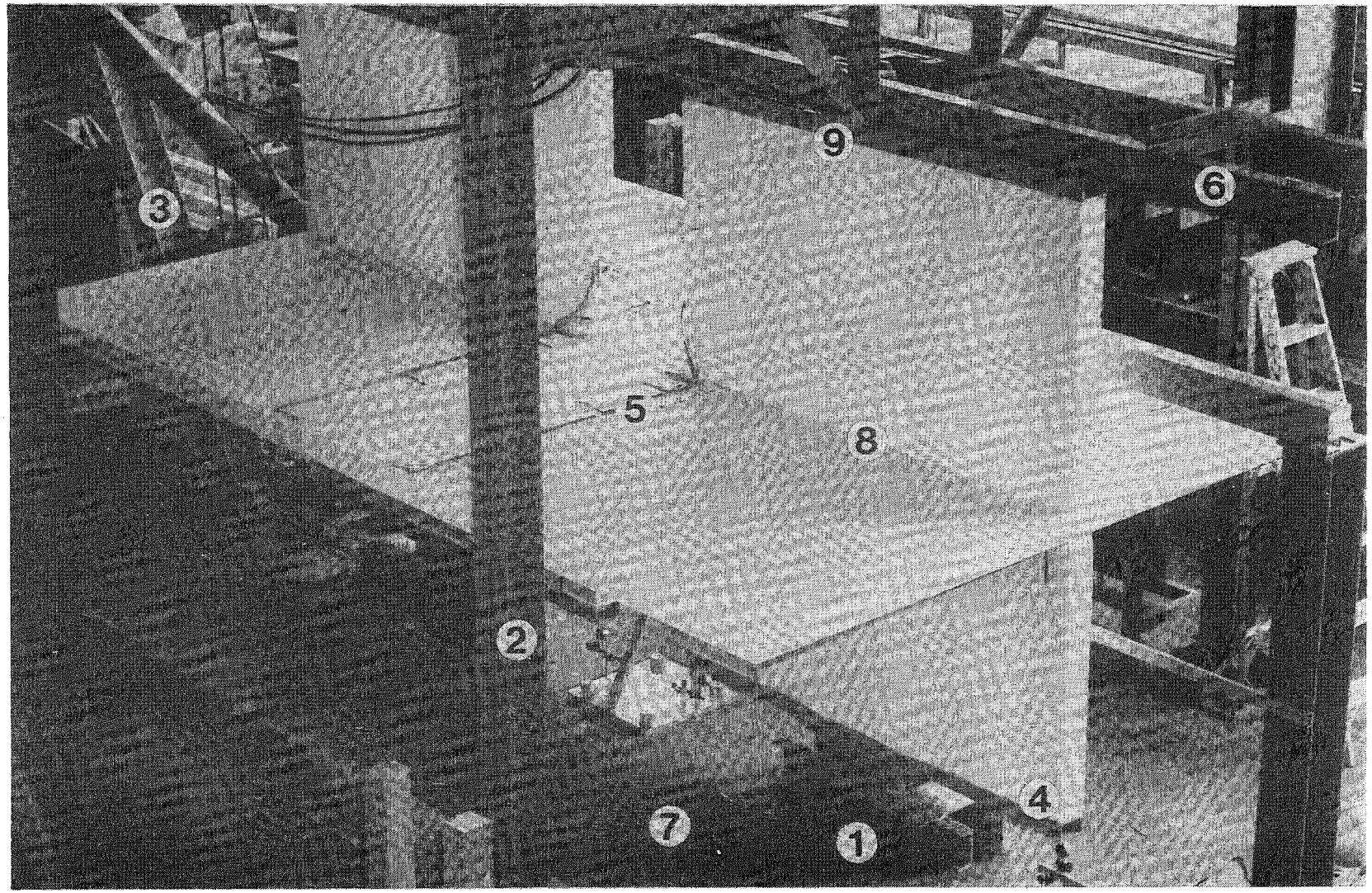

FIGURE 11.2 : THE TEST SET-UP.

TABLE 11-I : TEST SETUP DEFINITIONS FOR USE WITH FIGURE 11.2

1	-	Pin base
2	-	Support frame
3	-	Main loading reaction frame
4	-	Steel attachment pieces fixed to walls by clamping prestress and shear connection
5	-	Strain gauges on seismic steel
6	-	Alternative jack position for load reversal
7	-	Strong floor
8	-	Mortar joint at wall-slab interface
9	-	Lateral support

11.3 MODEL LIMITATIONS

As outlined above, two equal longitudinal jack forces were applied at respective wall tops to conveniently introduce the loading. However, unless equal reactive moments and shears are applied to each wall toe some separation force, i.e. an axial force, transmitted through the coupling system, is introduced and, depending on its relative magnitude, assumption (vi) in section 10.5 may be violated. It is instructive to consider an idealised elastic coupled shear wall structure where identically yielding coupling beams, each transmitting a shear q, have a point of contraflexure at e from the beam centreline. It can be shown by statics alone that in such a symmetrical coupled shear wall a separation force is transmitted as an axial force in the uppermost coupling beam while zero separation force is predicted for all other coupling beams.

Where identical top and bottom longitudinal steel is used in simple slab sections, only small unintended differences in performance will occur at respective hinges, and consequently negligible separation forces are to be expected in the model. Such forces, attracted by the stiffer section components, seem unlikely to be significant because of the large slab area.

More significantly, in unit 4 (see figure 11.7b) where different degrees of composite action and deterioration occur at each beam end, near equal end moments are less probable. Actually, unit 4 was specifically designed to minimise this problem, having equal positive and negative theoretical ultimate moments when the outer slab steel is assumed to yield and operate in conjunction with the beam compression block. At the other extreme, where completely independent action of the beam and slab are assumed, a maximum compressive separation force of 12.5 kN would be generated in unit 4. Additional in-plane forces associated with differences in materials and their deterioration rates, may also occur. Because special efforts were made to design the coupling system for near equal end moments, the in-plane force problem is considered to be moderate in this case, and although the comparison between theoretical and experimental results may be distorted, the type of behaviour certainly will not be greatly disturbed. Horizontal loading, as in this study, is not recommended, however, if a more general beam-slab interaction study were to be performed. Vertical jacking of walls, maintaining centrelines parallel, would be the means best suited to testing a range of beams. The potential problem of separation forces would be eliminated by the introduction of vertical loads perpendicular to the axis of the beam.

The other assumptions (see section 10.5) have been seen to be reasonable, either by observation of the test in progress, or by examination of the results.

It should be noted that the behaviour of the walls was not a subject of this test.

11.4 DESIGN OF TEST STRUCTURE REINFORCEMENT

11.4.1 General

In keeping with the stated first objective, units 1 - 3 incorporated progressively improving transverse secondary reinforcement at the wall toes while retaining the same basic gravity and primary seismic reinforcement. The modifications (including unit 4) together with a brief description of performance, are listed in table 11-II while a more complete description is presented below. The cross-sections are shown in figure 11.7 and material properties are listed in table 11-III.

TABLE 11-II : MAIN FEATURES OF THE SLAB COUPLING EXPERIMENTAL INVESTIGATION.

UNIT	Stirrups across the wall opening	Special transverse reinforcement across wall toes	Transverse structural steel at wall toes	General Observations
1	4 leg 6.5 mm stirrups at 38 mm centres	None	None	Basically satisfactory performance Large but controlled shear deformations in slab near wall toes
2	4 leg 6.5 mm stirrups at 50 mm centres	For full transfer of primary actions	None	No obvious improvement from Unit 1 Small improvement in hysteretic response
3	4 leg 6.5 mm stirrups at 50 mm centres	For full transfer of primary actions	Excess capacity for shears due to full primary action. Instrumented.	Excellent control of slab shear deformations near wall toes Slightly improved hysteresis and energy dissipation
4	No slab stirrups. Stirrups in shallow beam 6.5 mm at 50 mm centres	None	Excess capacity for full primary action shears Heavily instrumented	Excellent control of slab shear deformations near wall toes Inadequate beam stirrups

11.4.2 Unit 1

This basic configuration, illustrated in figure 11.3, is considered to represent a typical floor design as might be arrived at in practice but with two notable exceptions: the inclusion of a strip of stirrups between walls and the use of a considerable quantity of longitudinal seismic steel in the door strip. The stirrups, providing transverse flexural reinforcement as well as shear reinforcement with respect to seismic actions, were introduced to control the following;deformations and damage in the central critical region, punching shear, buckling of the flexural reinforcement and diagonal cracking. The enhanced ductility of slabs containing a band reinforced with closed stirrups was convincingly demonstrated by Islam [77].

Within the central stirrup cage (figure 11.7) 1.04% longitudinal reinforcement was provided in each face. This was reduced to 0.26% in each face outside the central cage area. The total steel content was a direct outcome of the lateral load analysis and the steel was proportioned to avoid extremely wide placing of bars in the model. Averaged over the slab width 0.42% steel is present in each face. The minimum code specified total reinforcement in a slab is 0.25%.

11.4.3 Unit 2

In an attempt to provide a transverse "beam" to engage the outer seismic reinforcement, considerable quantities of deformed bar reinforcement were provided in the wall toe regions of unit 2 (figure 11.4). Two full width yield lines, perpendicular to the walls, were assumed to be located one slab depth behind the wall toes. This assumption was supported by the observed yield line locations in unit 1 (figure 12.25). Along these yield lines, which are similar to although offset from those shown in figure 11.8, shear forces associated with yielding of the longitudinal seismic reinforcement must be transferred laterally to the walls. These seismic shear forces were assumed to provide a line load across each yield line. A transverse strip of slab was presumed to act as a cantilever extending either side of each wall toe and flexural reinforcement was designed as in a typical beam. Transverse flexural resistance provided by stirrups was also considered and 8 additional D10 bars at 50 mm centres were placed, top and bottom, in strips across the wall toes (see figure 11.4). The assumption of one-way action was later seen to provide an unsatisfactory representation of the actual transverse action.

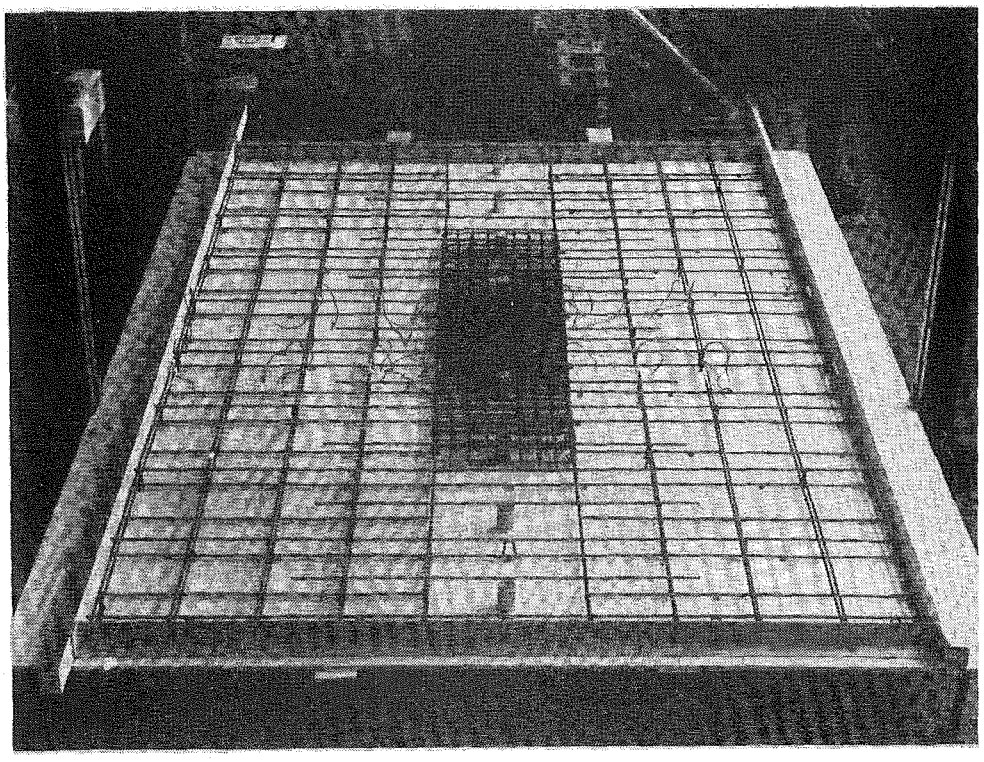

FIGURE 11.3 : REINFORCEMENT IN UNIT 1.

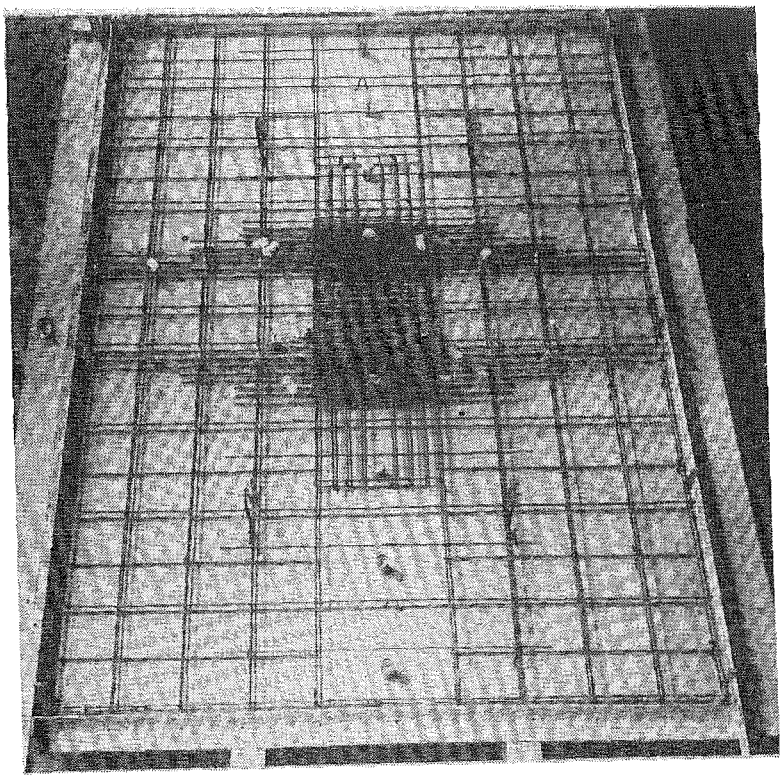

FIGURE 11.4 : REINFORCEMENT IN UNIT 2.

11.4.4 Unit 3

After testing unit 2 and observing the ineffective behaviour of the special secondary reinforcement, the feeling was that shear deformations in the slab near the wall toes reduced the transverse flexural action of the slab substantially. The logical improvement appeared to be to control the local shear deformations with a relatively stiff structural steel section. Such a section was designed, again based on the summation of shears associated with transverse yield lines perpendicular to the walls (see yield lines in figure 11.8). The selected 40 x 25 I section was made up of 6.5 mm thick flats, as shown in figure 12.19, and it provides excess capacity if shear resistance was the section's only strength requirement. The special transverse secondary flexural reinforcement used in unit 2 was retained, hoping that it would now become effective in ensuring the full and non-diminishing participation of the primary reinforcement. Figure 11.5 shows the central cage with the structural steel in place before the basic reinforcement configuration in the slab, shown in figure 11.4, was completed.

11.4.5 Unit 4

Unit 4, shown in figure 11.6, included a shallow beam cast together with the slab. This unit had different stiffness and strength properties from those present in the previous specimens but the slab thickness and overall dimensions were the same. The main benefit of this similarity was that reasonable correlation with previous tests was possible. In fact, the only changes were that the primary (longitudinal) reinforcement in the central strip was replaced by reinforcement in the beam, and that slab stirrups were replaced with beam stirrups which were designed to resist the full shear associated with an effective T-beam action. In accordance with ACI recommendations [78] an effective slab width of 145 mm on either side of the beam was considered, which excluded all longitudinal slab reinforcement, when computing shear forces. As mentioned in section 11.3, the design was adjusted to ensure near equal ultimate moments at the beam ends when composite action of the beam and slab at ultimate load is assumed. These moments were used as reference moments in the unit 4 response presentation.

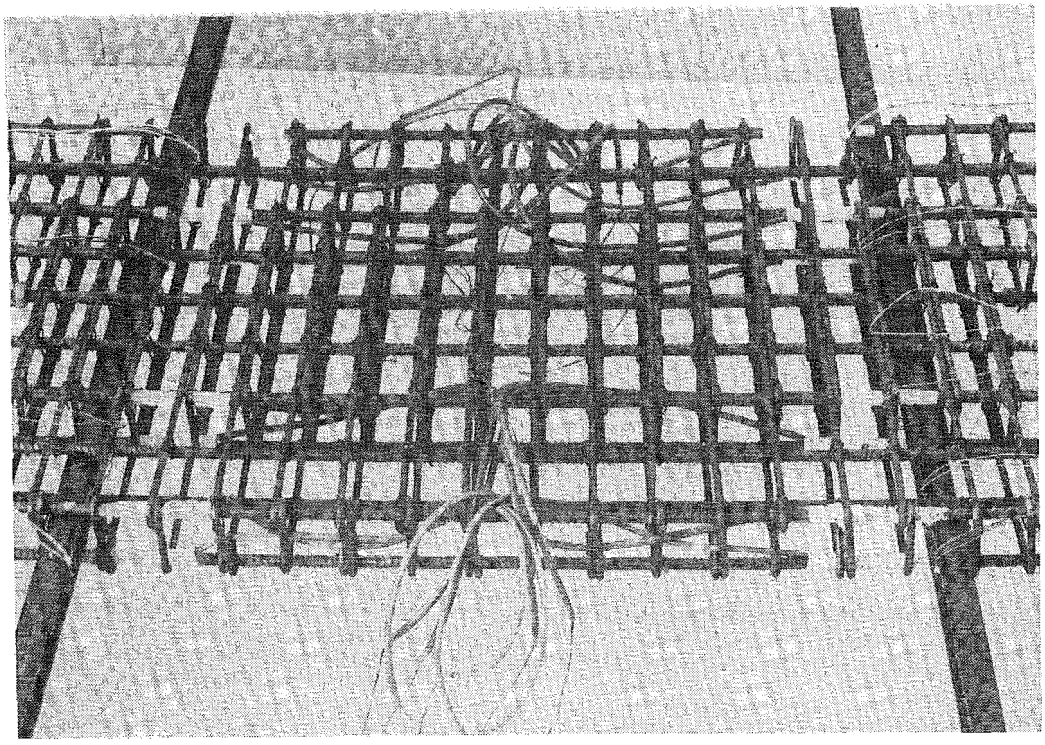

FIGURE 11.5 : CAGE AND STRUCTURAL STEEL FOR UNIT 3.

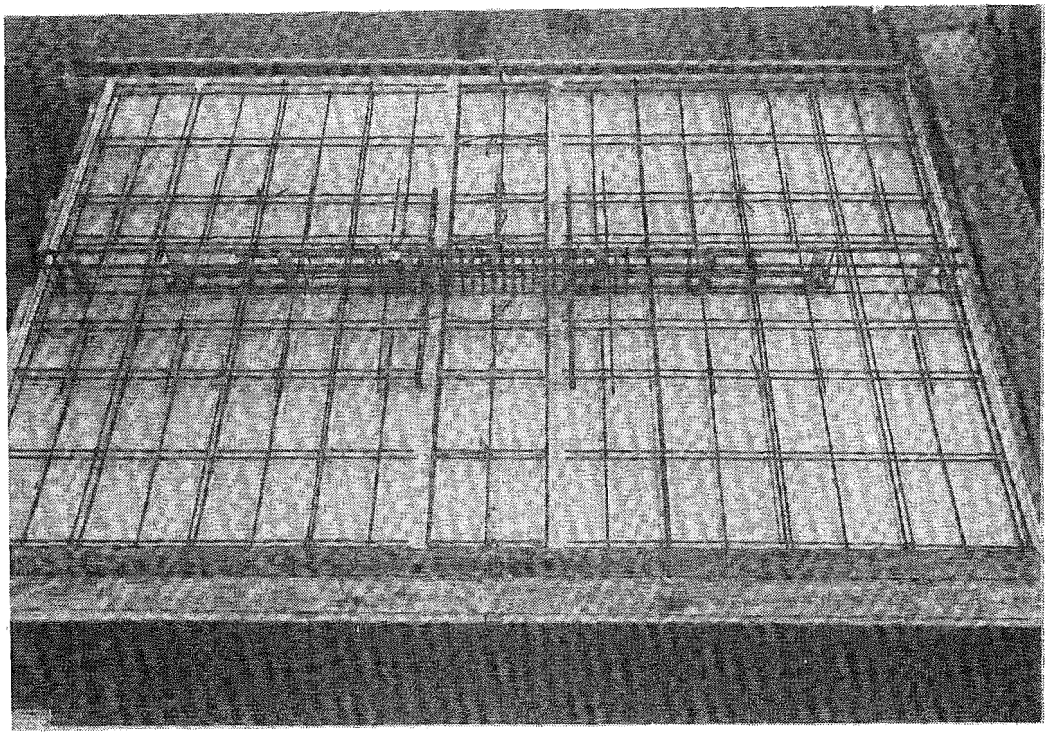

FIGURE 11.6 : REINFORCEMENT FOR UNIT 4.

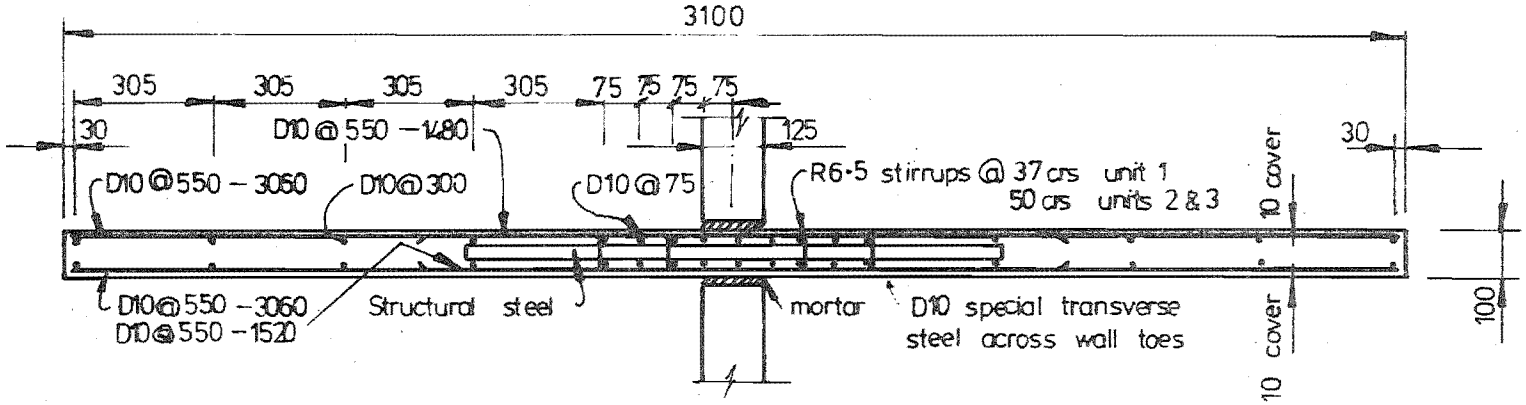

(a) Units 1 - 3 cross-sections at wall edge.

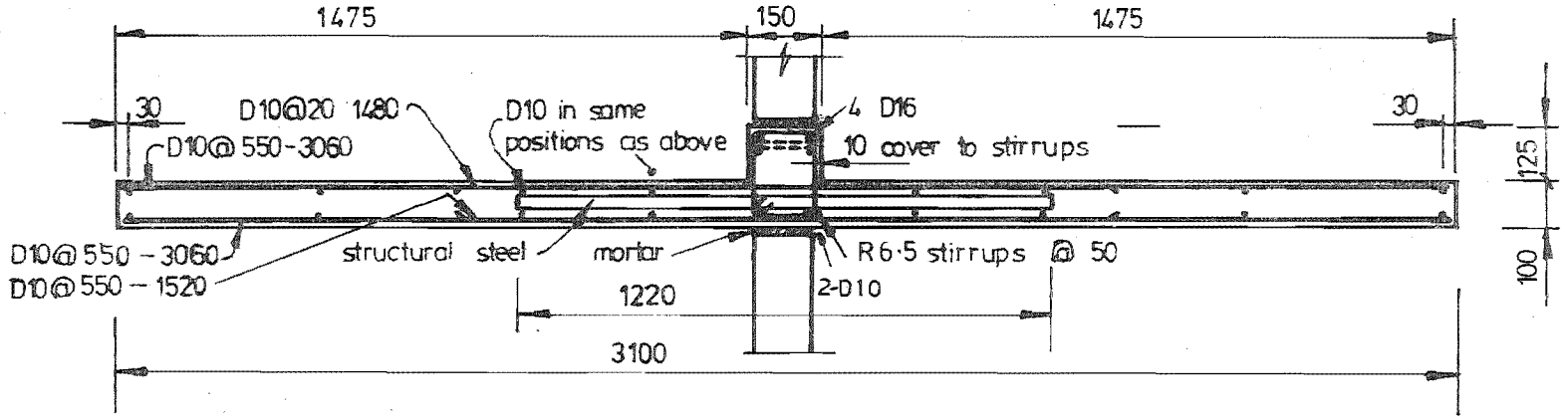

(b) Unit 4 cross-section at wall edge.

FIGURE 11.7 : CROSS-SECTIONS OF UNITS 1 - 4.

11.5 INSTRUMENTATION

11.5.1 General

In each case the following measurements were made as the test progressed:

i) Jack loads using load cells.

ii) Wall deformations using dial gauges.

iii) Slab deflection profiles using an automatic level instrument and optical targets.

iv) Strains of primary (longitudinal) steel at yield line localities using electrical strain gauges.

v) Strains of the transverse reinforcement using a mechanical Pfender gauge.

vi) Strains in the embedded structural steel beam using electrical strain gauges.

viii) Some stirrup strains using electrical strain gauges.

All instrumentation was in keeping with standard practice at the University of Canterbury [29] and as a general rule, unless otherwise stated, it may be assumed that recorded results were of higher accuracy than is commensurate with plotted presentations. A general view of the test setup with complete instrumentation may be seen in figure 11.12. A brief discussion on the various measurements made is presented in the following sections.

11.5.2 Force - Displacement Results

These plots are based on data from 16 dial gauges, 2 linear voltage transducers and three load cells where averages of measurements of the two wall rotations are plotted. Graphic presentations are, as measured, plotted to ± 1 mm (1.0% of the maximum deflection) although changes in the rates of loading could influence the response by at least twice this amount. Creep effects were suppressed, as far as possible, by loading at a moderate and approximately constant rate.

11.5.3 Displacement Profiles

Vertical displacement measurements are of high accuracy and a tolerance of ± 0.1 mm is thought to be typical and the accuracy is well in excess of plot resolution. Profiles of average deflections from each side of wall units are plotted along lines A to D, shown in figure 11.8.

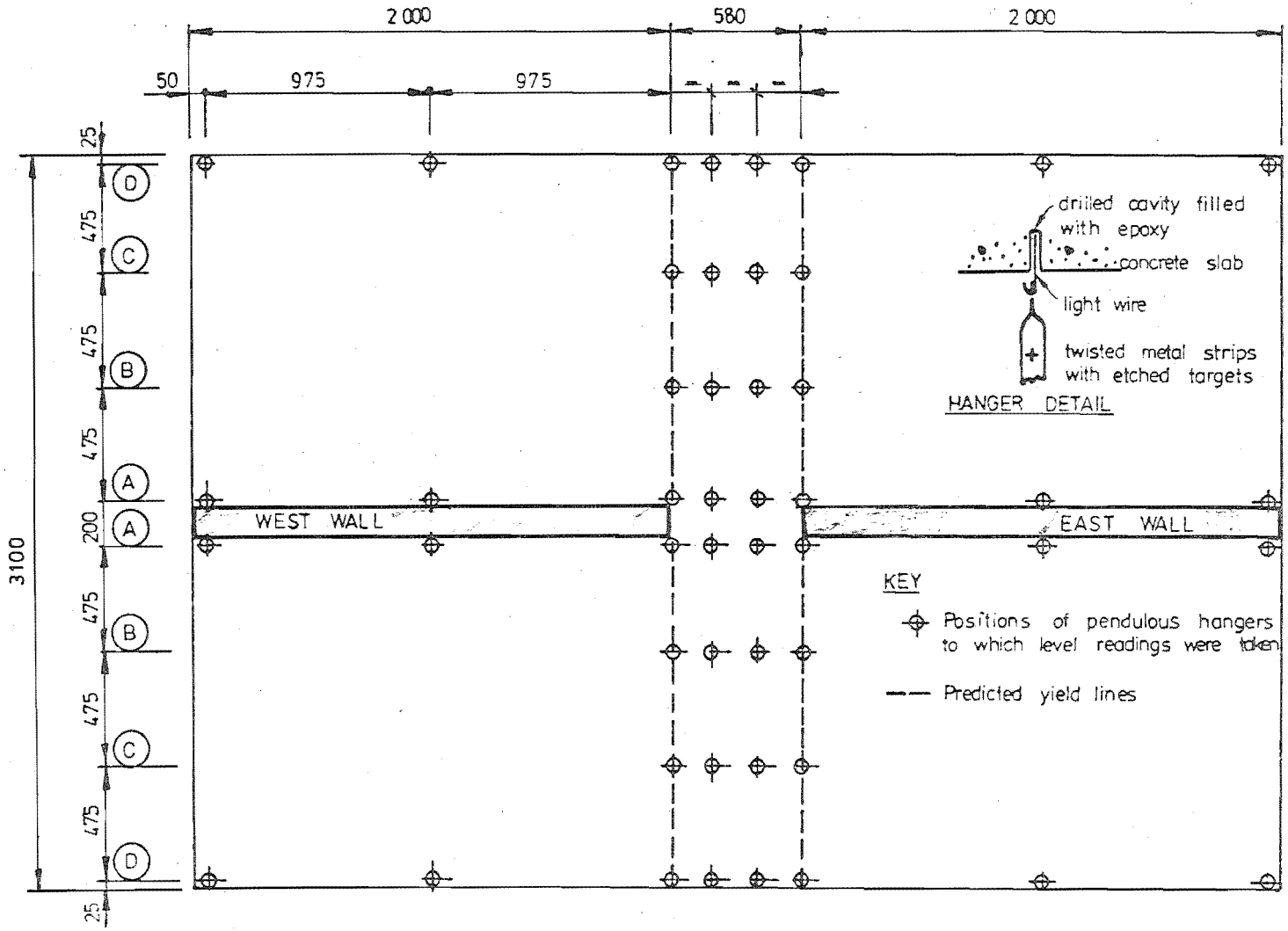

FIGURE 11.8 : POSITIONS OF DEFLECTION MEASUREMENTS AND ASSUMED YIELD LINES.

11.5.4 Strains in the Primary Seismic Slab Reinforcement

The usual means of strain measurement at the University of Canterbury, the use of Demec gauges, was not considered practical in the slab because there was no access to the flexural steel centrelines. Strains were measured with 40 electrical strain gauges, 10 across each layer of longitudinal steel, situated close to each predicted yield line. Gauges were thoroughly protected with flexible waterproof materials to enable them to sustain deformations without damage. In practice, however, they were only satisfactory in the elastic range and for detection of initial yield because large widely spaced cracks markedly affected strain distributions. Although full length longitudinal reinforcement was incorporated in the models, primarily for lifting purposes, it is envisaged that curtailment of this reinforcement some distance behind the yield lines (figure 10.1) would allow economy in the prototype, while retaining the full yield strength. Unfortunately, the use of sufficiently extensive instrumentation to determine a satisfactory curtailment pattern was not possible with the available data acquisition equipment. Reliable indications are provided by observation of cracks (or absence of them) and deflection profiles.

Temperature compensation was made by means of a 100 mm thick concrete block with 20 mm cover to the steel which was in fact a replica of the slab. Figure 11.9 shows the locality of the slab gauges with respect to the postulated yield lines.

11.5.5 Strains in the Special Transverse Reinforcement

Strains were measured with a Pfender mechanical gauge for which balls were punched directly into deformed bars and gauge extension legs were inserted through 10 mm of cover to the bars. Figure 11.10 shows the locality of gauge points on top and bottom of the special transverse reinforcement across the wall toes.

11.5.6 Beam Steel Strains in Unit 4

With free horizontal access to the beam steel, Pfender measurement of strains was adopted in preference to electrical strain gauges, providing average strain results from the two top bars. Positions of these gauge points are illustrated on the diagram of figure 11.11.

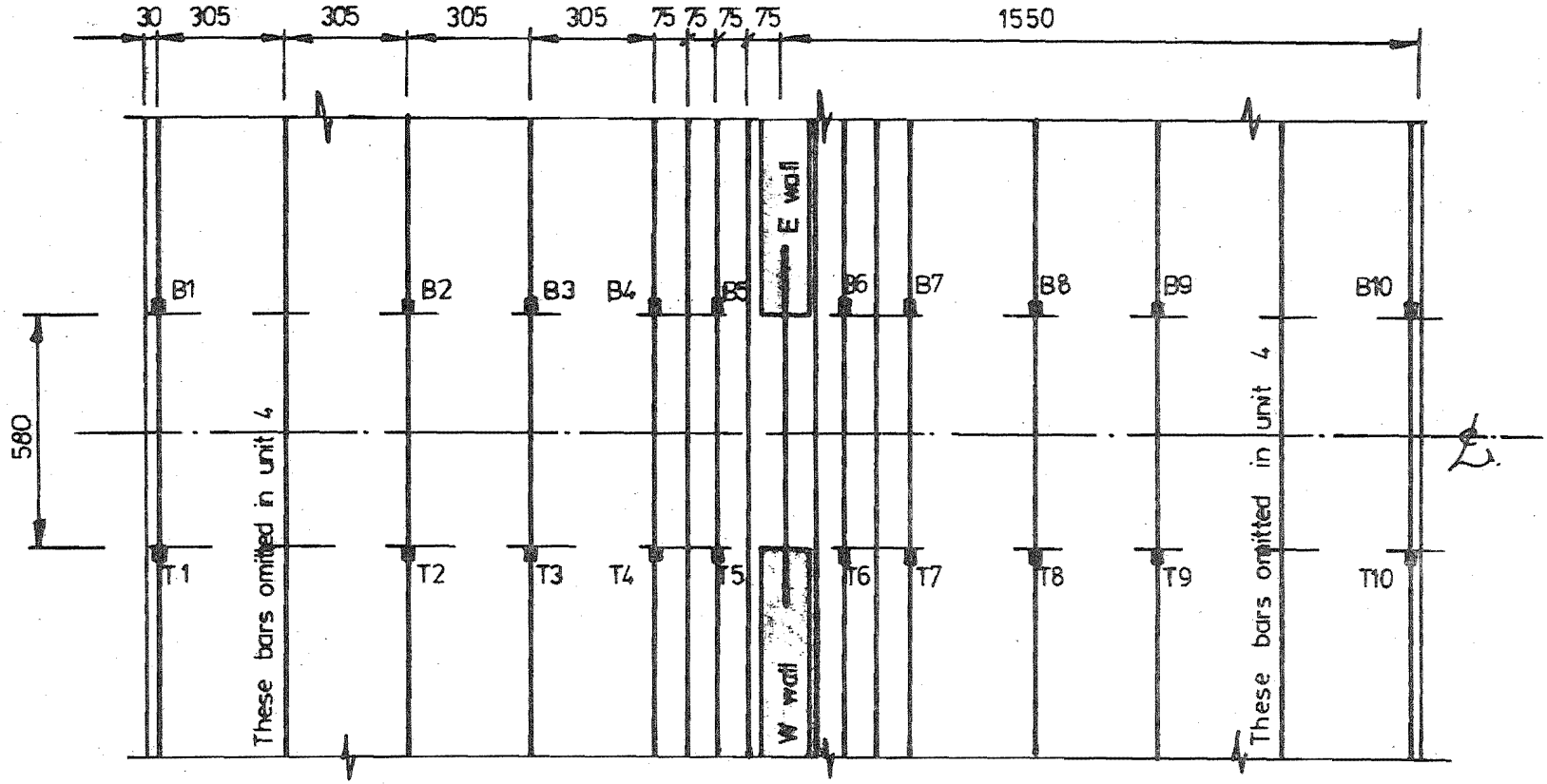

FIGURE 11.9 : POSITIONS OF STRAIN GAUGES ON LONGITUDINAL SEISMIC REINFORCEMENT.

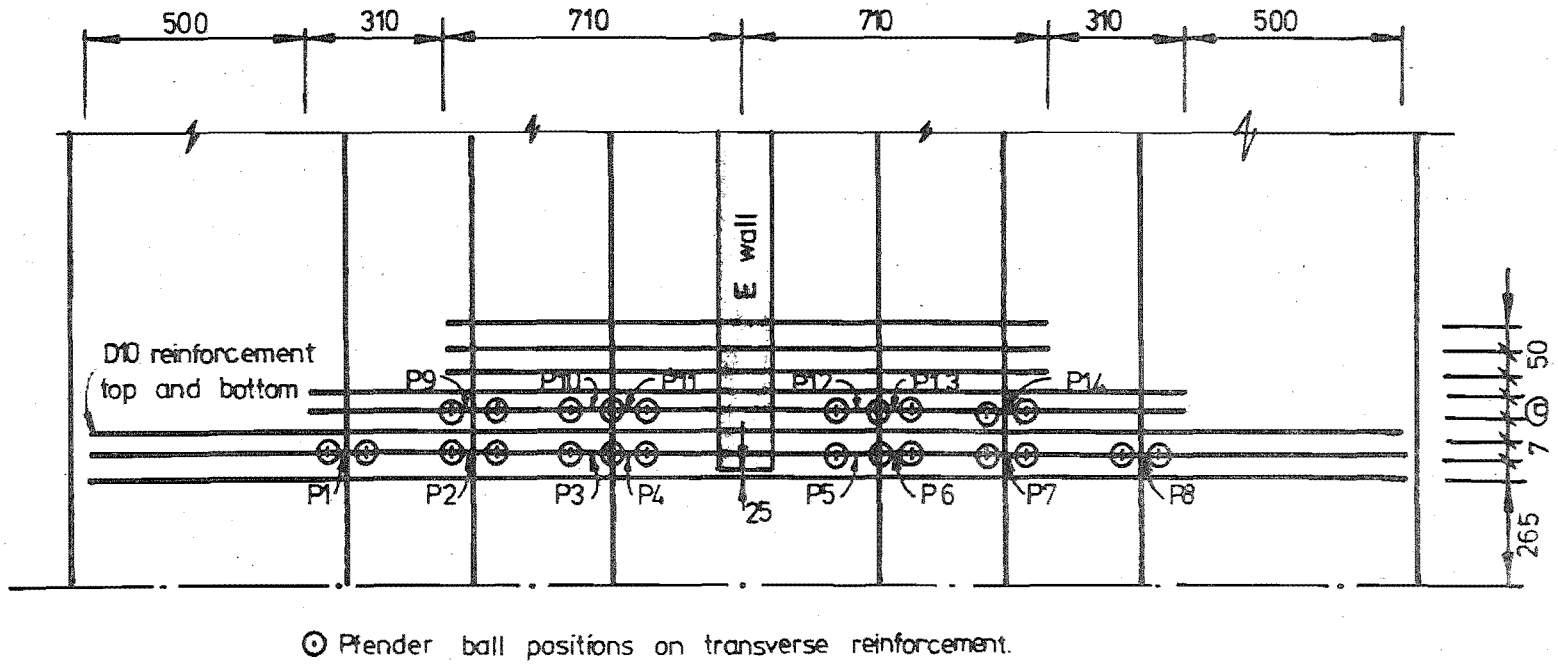

⊙ Pfender ball positions on transverse reinforcement.

FIGURE 11.10 : PFENDER GAUGE POSITIONS ON TOP AND BOTTOM REINFORCEMENT PLACED TRANSVERSELY ACROSS WALL TOES.

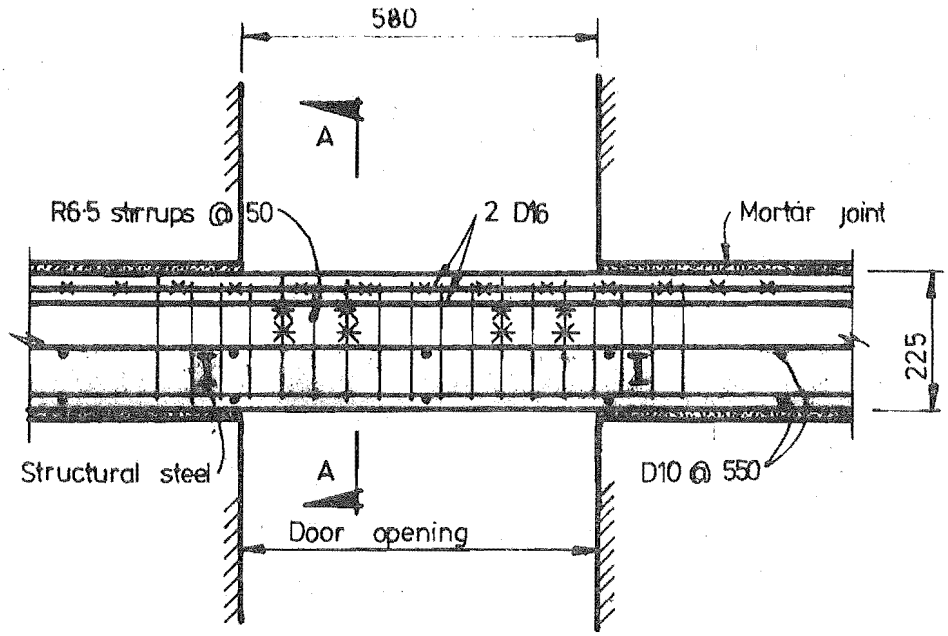

(a) Longitudinal section

KEY

× Pfender studs on longitudinal reinforcement

✳ Demec studs on beam stirrups

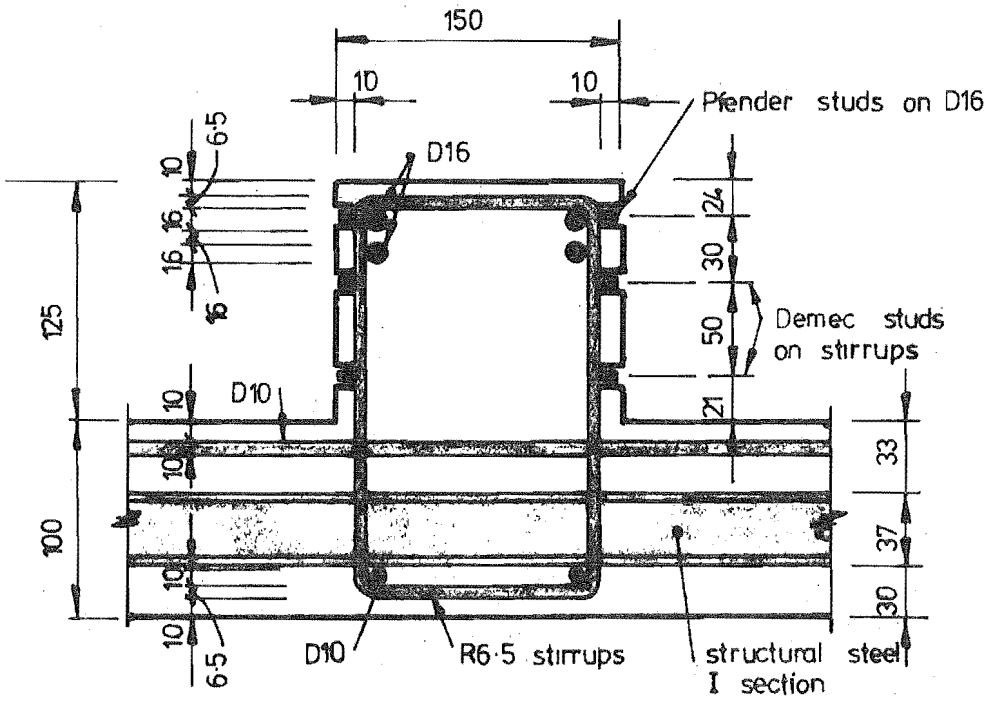

(b) Section A – A

FIGURE 11.11 : UNIT 4 BEAM REINFORCEMENT AND INSTRUMENTATION.

11.5.7 Utilisation of a Structural Steel Beam

A structural steel I section was used in units 3 and 4 and it was instrumented with strain gauges to determine the extent of its utilisation. The instrumentation positions are shown together with results in section 12.6.

11.5.8 Axial Elongation of the Coupling System

Coupling system elongation was deduced from dial gauge measurements of relative wall deformations. The dial gauge positions may be seen in figure 11.12.

11.5.9 Stirrup Strains

Attempts were made to measure strains on vertical legs of slab stirrups using electrical strain gauges while horizontal strains were deduced from Pfender strain readings on the special transverse steel. Demec readings on unit 4 beam stirrups provided the results in the last specimen.

11.6 LOADING CYCLES

A uniform loading procedure for all tests, illustrated in figure 11.13 and based on the theoretical ultimate load and initial observed stiffness, was adopted. The same displacements were used for units 1 to 3 and the procedure was reapplied to unit 4. The pattern of progressively increasing ductilities, all referenced to the response origin, provides a useful loading sequence for attempting to assess hysteretic degradation. Regular small cycles to 60% of the theoretical ultimate load indicated the extent of the deterioration. A displacement ductility of 11 was ascertained to be an extreme value which could be attained in the prototype structure.

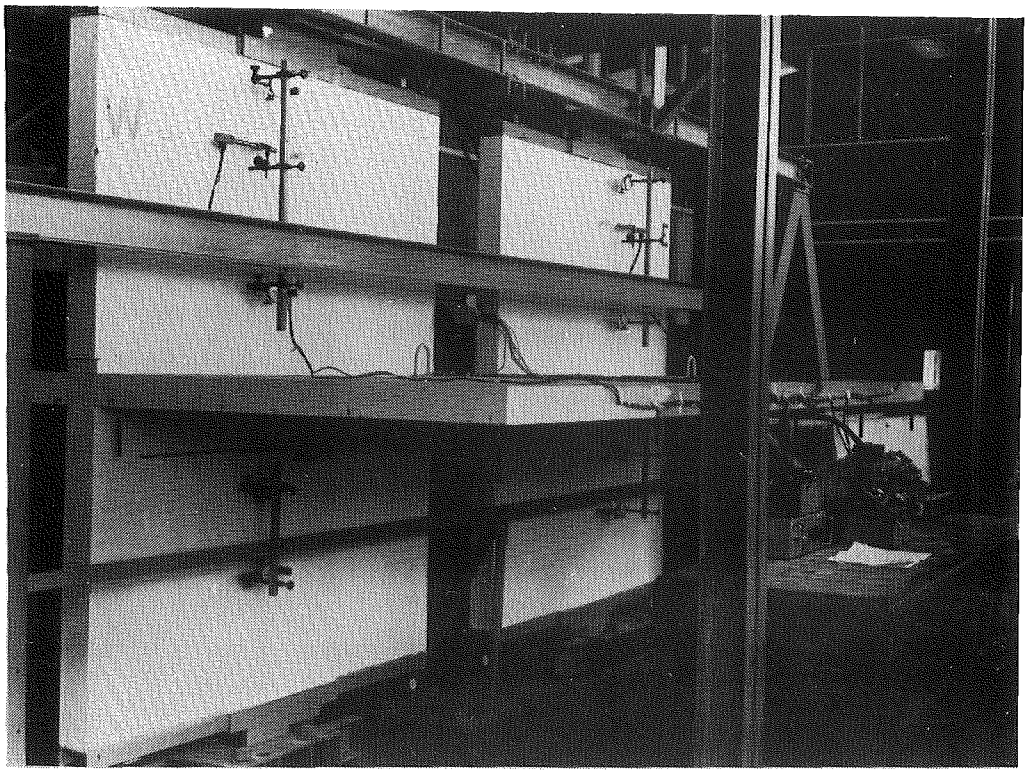

FIGURE 11.12 : GENERAL VIEW OF THE INSTRUMENTATION.

TABLE 11-III - MATERIAL PROPERTIES

Steel Yield Strengths (MPa)

Unit	D16	D10	R6.5	Structural Steel
1	-	345	352	-
2	-	345	352	-
3	-	315	352	341
4	326	314	352	350

Concrete Compression Strengths (MPa)

Unit	300 x 50 cylinders	200 x 100 cylinders
1	25	-
2	23	-
3	21	23
4	25	24

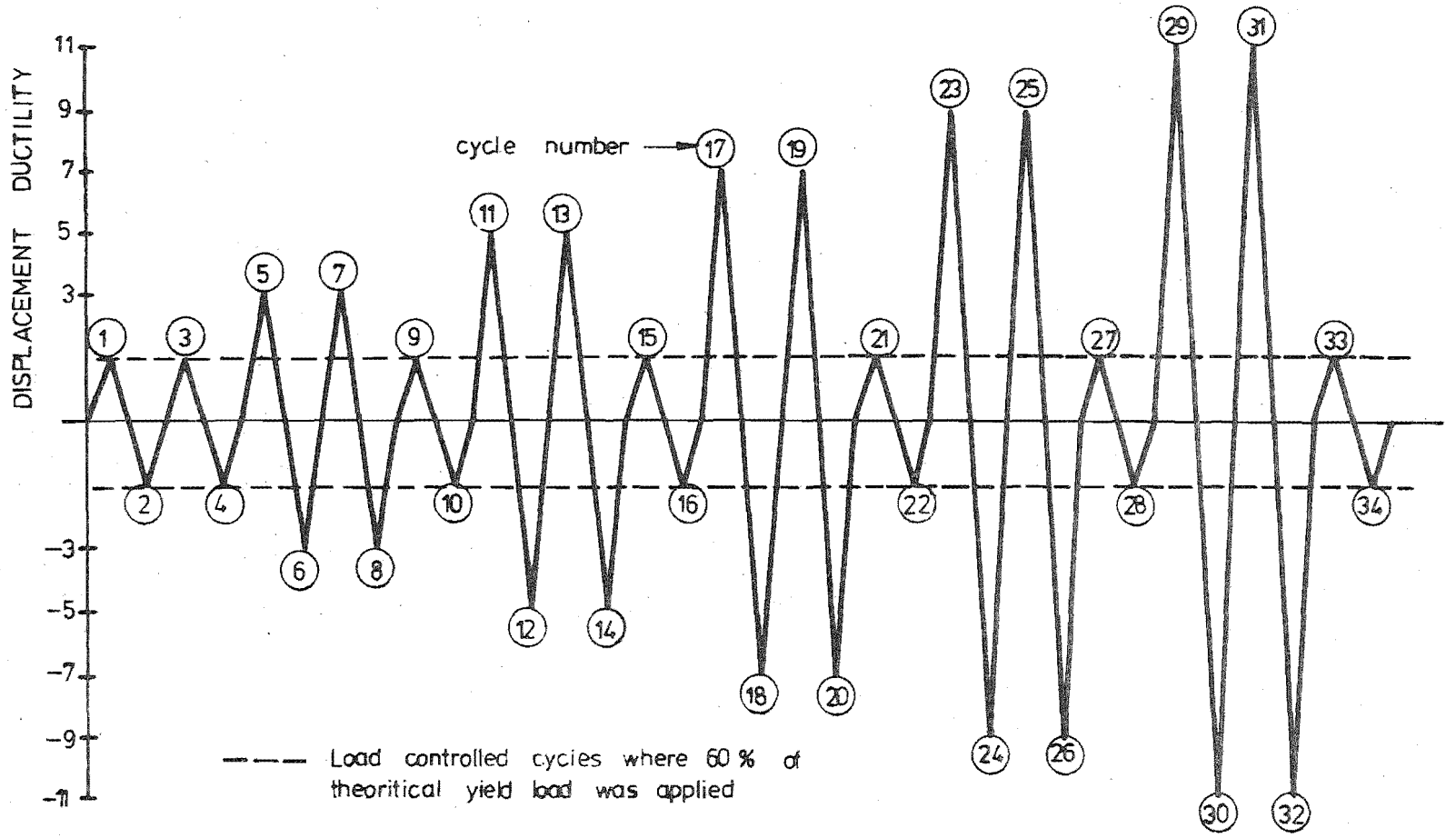

FIGURE 11.13 : LOADING SEQUENCE.

CHAPTER TWELVE

EXPERIMENTAL RESULTS

12.1 INTRODUCTION

A representative selection of the data, collected on a relatively large scale to be reasonably sure of measuring unexpected events, reduced and plotted by computer to aid in understanding structural behaviour, is presented. Concentration is on the more important original features, and some of the fundamental behavioural characteristics,not investigated in previous known work, have been presented for evaluation. In particular, stiffness degradation associated with cyclic loading was found to be very significant.

12.2 STRENGTH AND STIFFNESS DEGRADATION

12.2.1 Slab Tests

The following observations, relating to the response diagrams of figures 12.1 - 12.3, where wall jack forces are plotted against wall rotation, are of interest:

i) The ultimate load was considerably higher than the theoretical predictions (section 11.4). This is almost certainly because of strain hardening of the longitudinal flexural steel. Observation of all crack patterns showed a few widely spaced cracks (e.g. figure 12.23) at which small diameter bars were subjected to large tensile strains. Early strain hardening may be expected to be a phenomenon of slab coupling.

ii) The stiffness seen in the small intermediate load cycles (figures 12.1 - 12.3) deteriorated severely as load cycling continued. During the slab tests, the stiffness reduced to less than 10% of the value measured during the initial elastic cycles. Stiffness degradation is known to be linked to the mechanisms of reinforced concrete, especially with cyclic loading in the inelastic range. In typical beams, when simple flexural yielding constitutes the failure mechanism, degradation remains reasonably controlled. In the slab coupling case, however, where torsional stresses in the slab are considered to be associated with flexure across the width of the specimen, extremely severe degradation, associated with cyclic actions was encountered. Inclined cracking which was associated with lateral loading was observed and a typical example is indicated by the arrow in figure 12.23. Although these cracks may have been caused by principal moments perpendicular to the direction of the

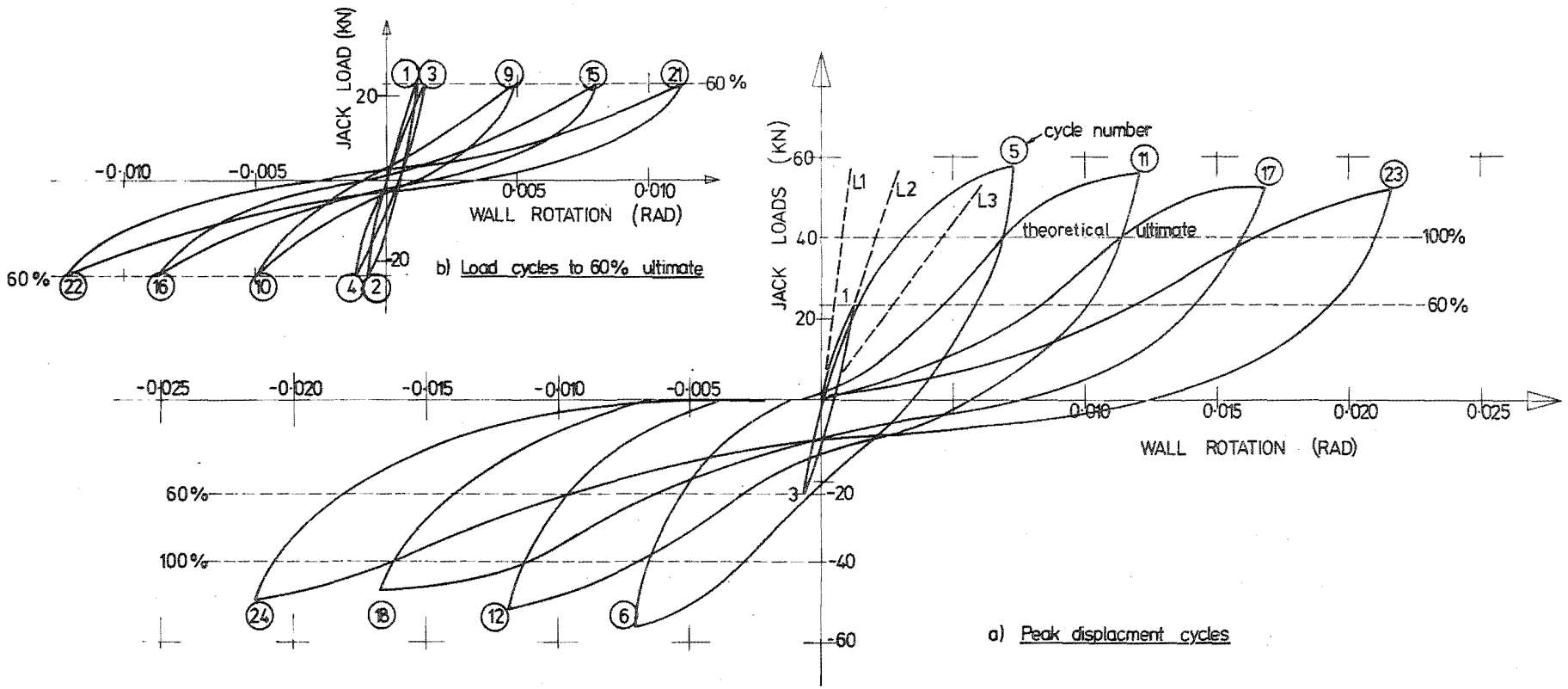

FIGURE 12.1 : UNIT 1 FORCE DISPLACEMENT RESPONSE.

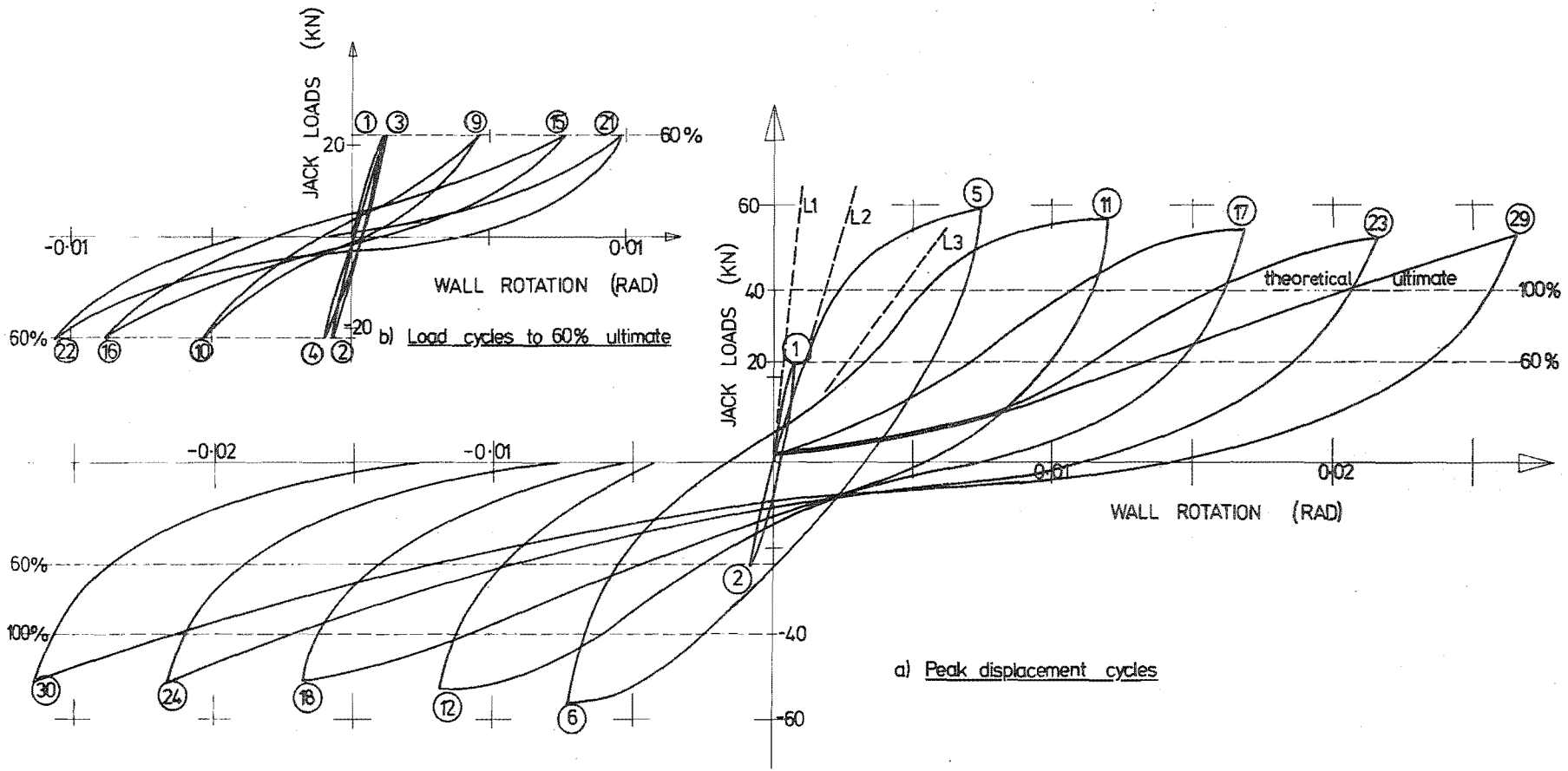

FIGURE 12.2 : UNIT 2 FORCE DISPLACEMENT RESPONSE.

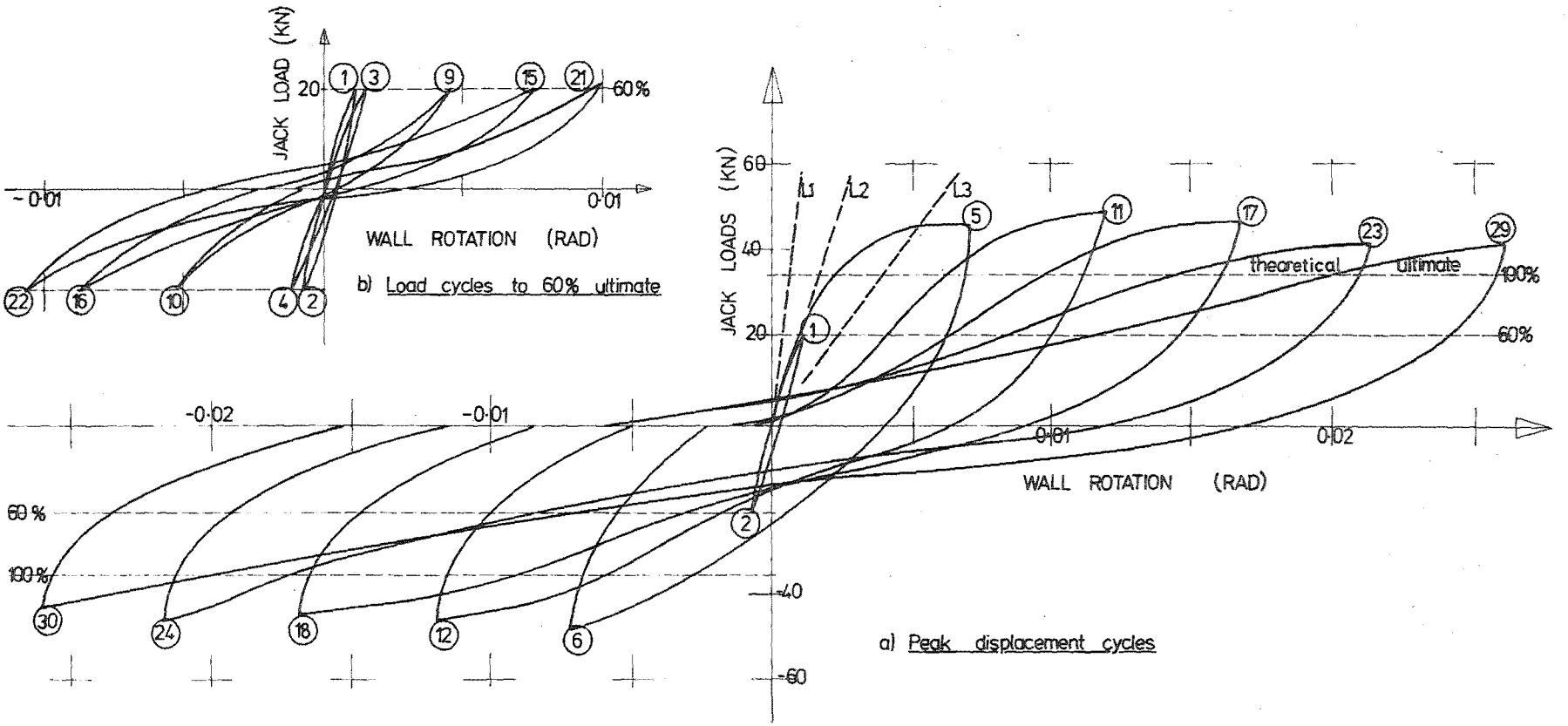

FIGURE 12.3 : UNIT 3 FORCE DISPLACEMENT RESPONSE.

crack, opening of the cracks with subsequent large deformation loading was not observed as with the majority of flexural cracking in all specimens. Instead, spalling of concrete along the line of the crack on the top and bottom surfaces of the slab was observed. This suggests relative deformation of the concrete either side of the crack, associated with torsional deformations.

Initially it was thought that shear deformation in the wall toe region, effectively increasing the clear span of the coupling system, made a significant contribution towards the stiffness loss of the model. However, in unit 3, where shear deformation at the wall toes was almost completely controlled, a similar pattern and magnitude of stiffness loss was observed (figure 12.3).

iii) Energy absorption is relatively low, especially in unit 1 where large central regions of the response show a very small stiffness (figure 12.1).

iv) Because of pin positions at the wall bases, the model wall rotations are approximately 3 times greater than in a corresponding typical structure. The actual magnitudes of wall rotations in the model are unimportant since the only function of the walls during the test was to provide the desired slab deformations.

12.2.2 Unit 4

The response of unit 4, which incorporated a shallow coupling beam and which is presented in figure 12.4, is basically similar in appearance to the three slab responses. Some significant differences are outlined below:

i) During the initial "elastic" cycles to 60% of the estimated ultimate load, a considerable degree of nonlinearity is evident at loads substantially smaller than the peak load reached in cycle 5 (figure 12.4). This is because longitudinal reinforcement close to the walls reached yield while longitudinal reinforcement near the outer edges of the slab was relatively lightly stressed.

ii) In cycle 5 the theoretical ultimate load, which was computed assuming composite action of the beam and slab, was almost reached. Some strain hardening, mainly in the slab, may be expected to be present but it is likely to be less significant than in the slab units. This is because the beam reinforcement makes a substantial contribution to the resisted moment and beam behaviour is characterised by a well distributed average strain pattern (figure 12.21) and relatively closely spaced

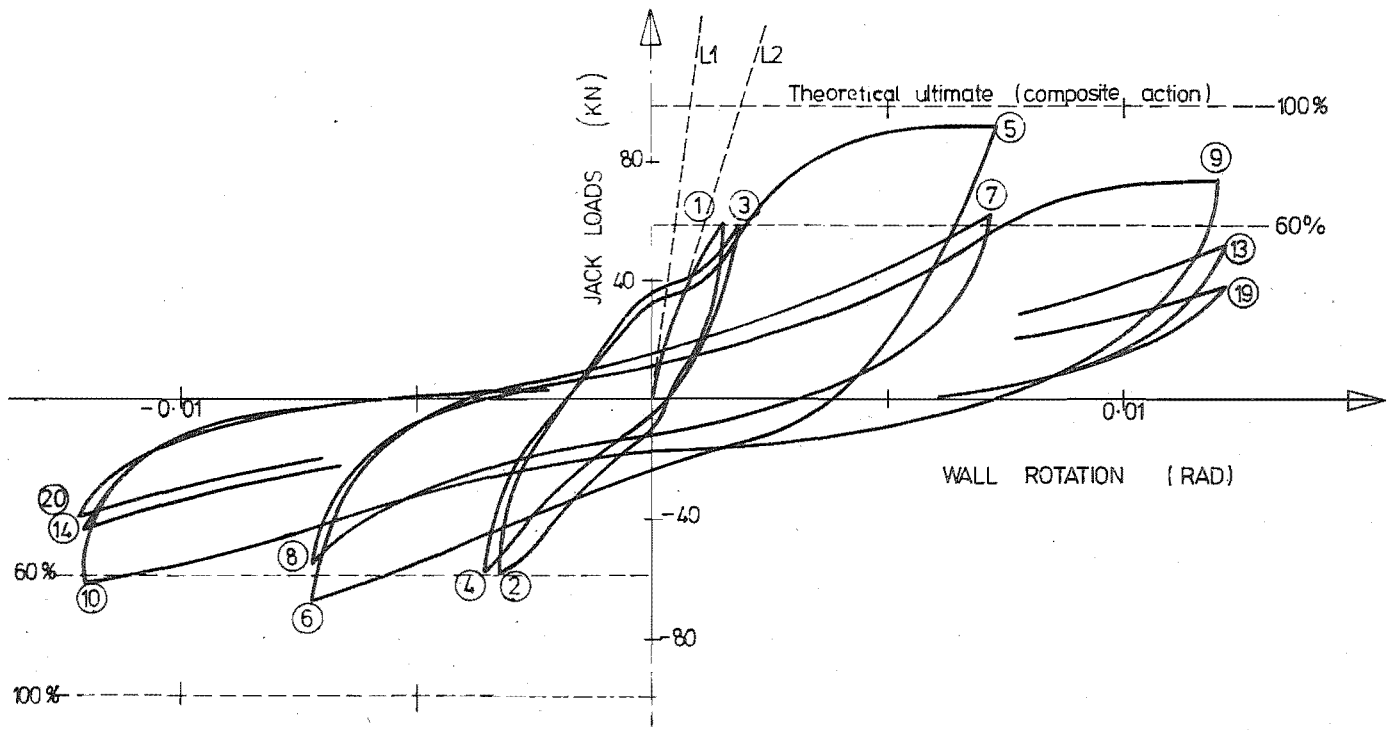

FIGURE 12.4 : UNIT 4 FORCE DISPLACEMENT RESPONSE.

flexural cracks on the beam top (figure 12.33), i.e. the beam shows a larger spread of yielding in its plastic hinge region.

iii) A reduction in the maximum load reached (figure 12.4) was observed in all subsequent cycles and this was associated with a horizontal shear failure in the beam. A number of near horizontal beam cracks may be seen in figure 12.33 and relative horizontal displacements of upper and lower portions of the beam were easily observable while loading the specimen. This shear failure is discussed in section 12.9.2. Further progressive deterioration occurred during the constant displacement cycles to a ductility of 5 as a result of the shear failure in the beam. It should be noted that the ultimate load used to define ductilities, based on full composite action of the beam and slab, was substantially higher than achieved in the test (figure 12.4). The ductility at the maximum displacement, computed with a more realistic estimate of the yield moment, would be approximately 8.

iv) The last four cycles (19 to 22) to a ductility of 5 were performed by jacking with a single jack acting on the leading wall, introducing a substantial tension in the coupling system without noticeably disturbing the force-displacement response. It appears that the beam-slab coupling system is considerably less sensitive to the presence of axial forces than a typical beam, because of the relatively large cross-sectional area of the slab.

12.3 DEFLECTION PROFILES

12.3.1 Slab Tests

Deflection measurements taken at the points shown in figure 11.8 are presented in figures 12.5 to 12.10. These provide evidence of concentrated shear deformation in the wall toe region in that substantial departures from asymmetry of the longitudinal deflection profiles may be observed. Considering shear forces concentrating in the two wall toe regions as loading progresses: at the upward moving wall toe dead load shears, redistributed as cracking and yielding in the slab occurs, are additive to seismic shears; at the downward moving wall toe shear forces are of the opposite sign to seismic shears. The concentration of gravity load shears in the wall toe region is moderate before lateral loads are applied because one way slab action, as confirmed by Simmonds [73], will be the dominant load transfer mechanism. Although difficult to assess the difference in total shears at the two wall toes, caused by combining

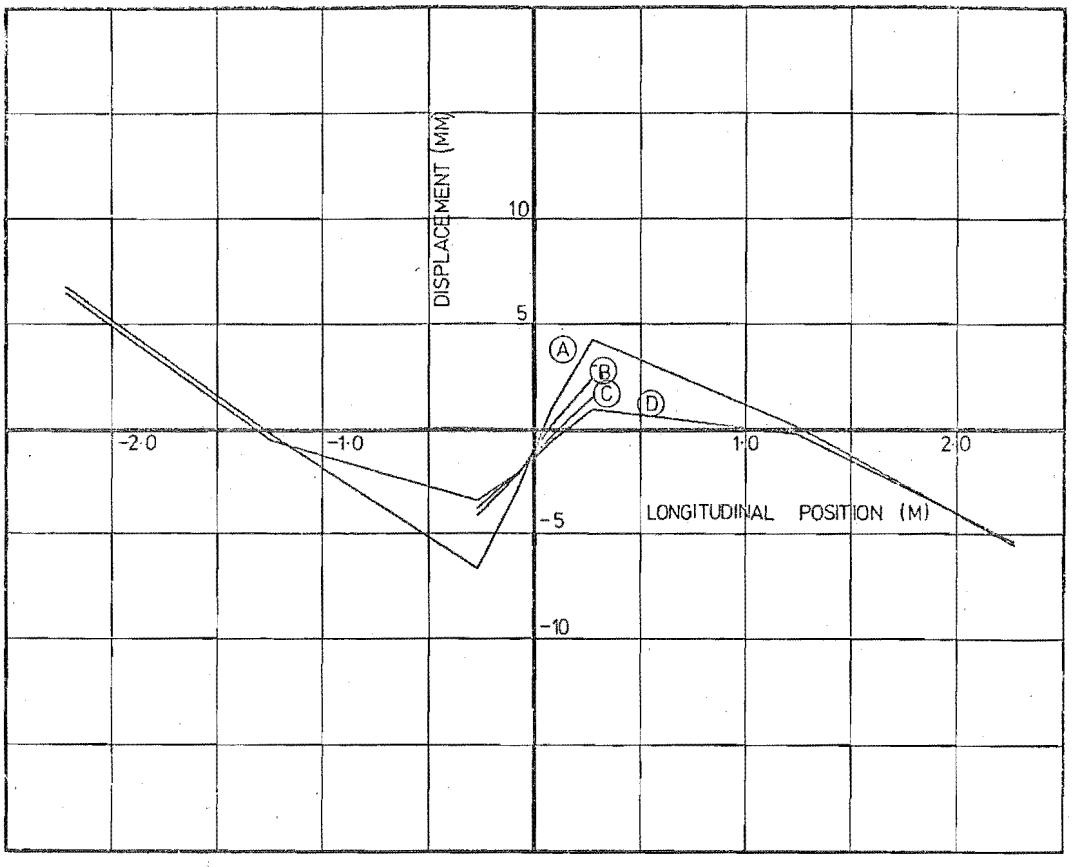

FIGURE 12.5 : DISPLACEMENT PROFILE OF UNIT 1 AT CYCLE 5 (μ = 3)

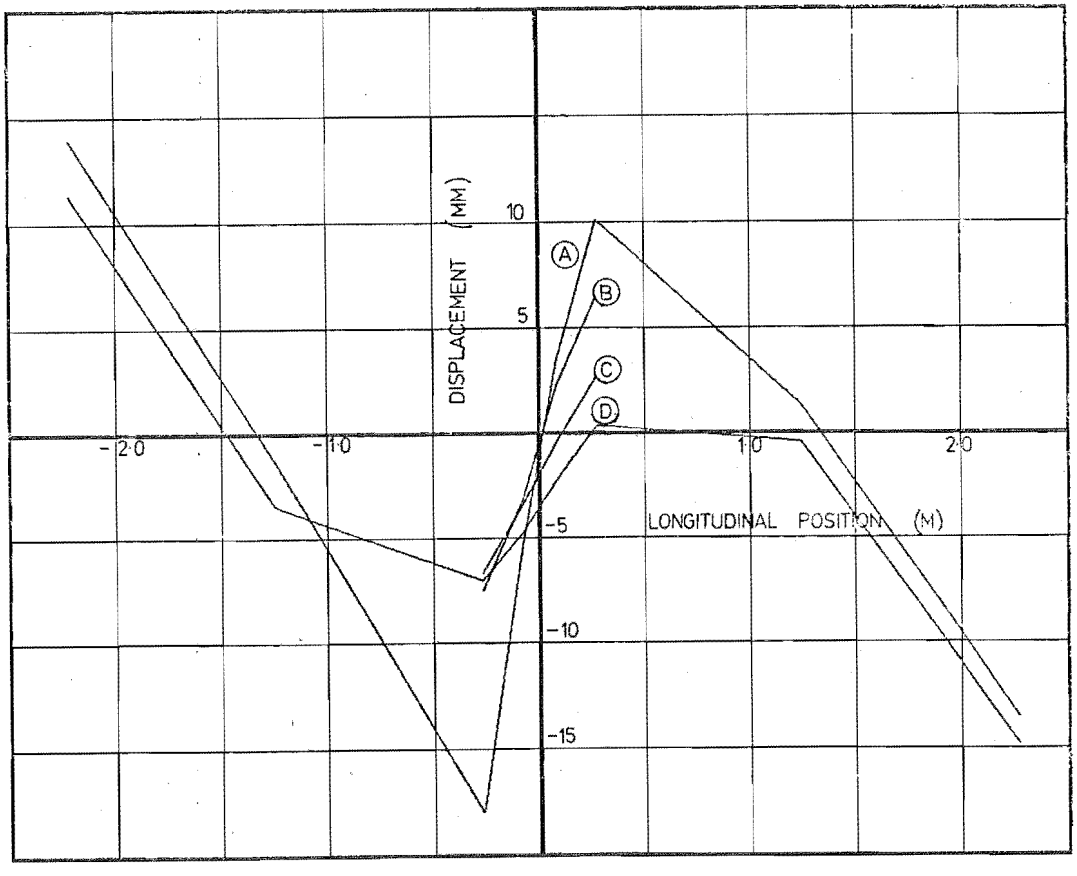

FIGURE 12.6 : DISPLACEMENT PROFILE OF UNIT 1 AT CYCLE 17 (μ = 7)

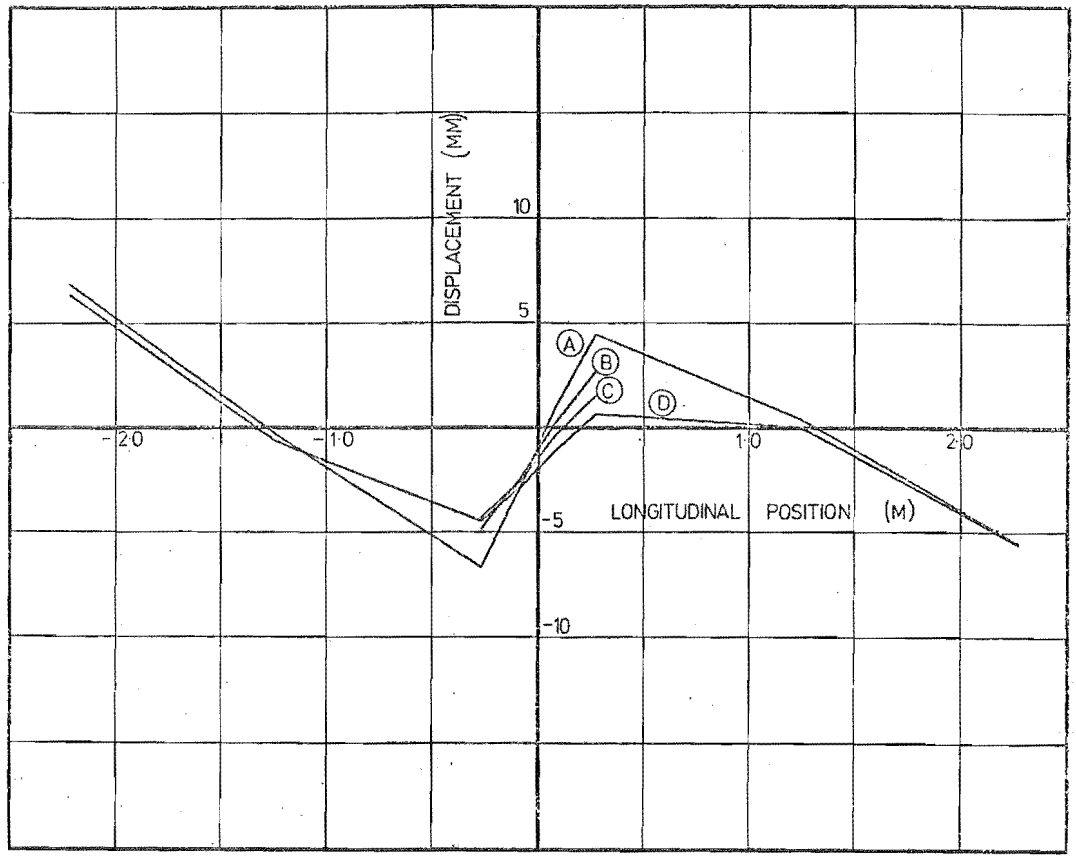

FIGURE 12.7 : DISPLACEMENT PROFILE OF UNIT 2 AT CYCLE 5 (μ = 3)

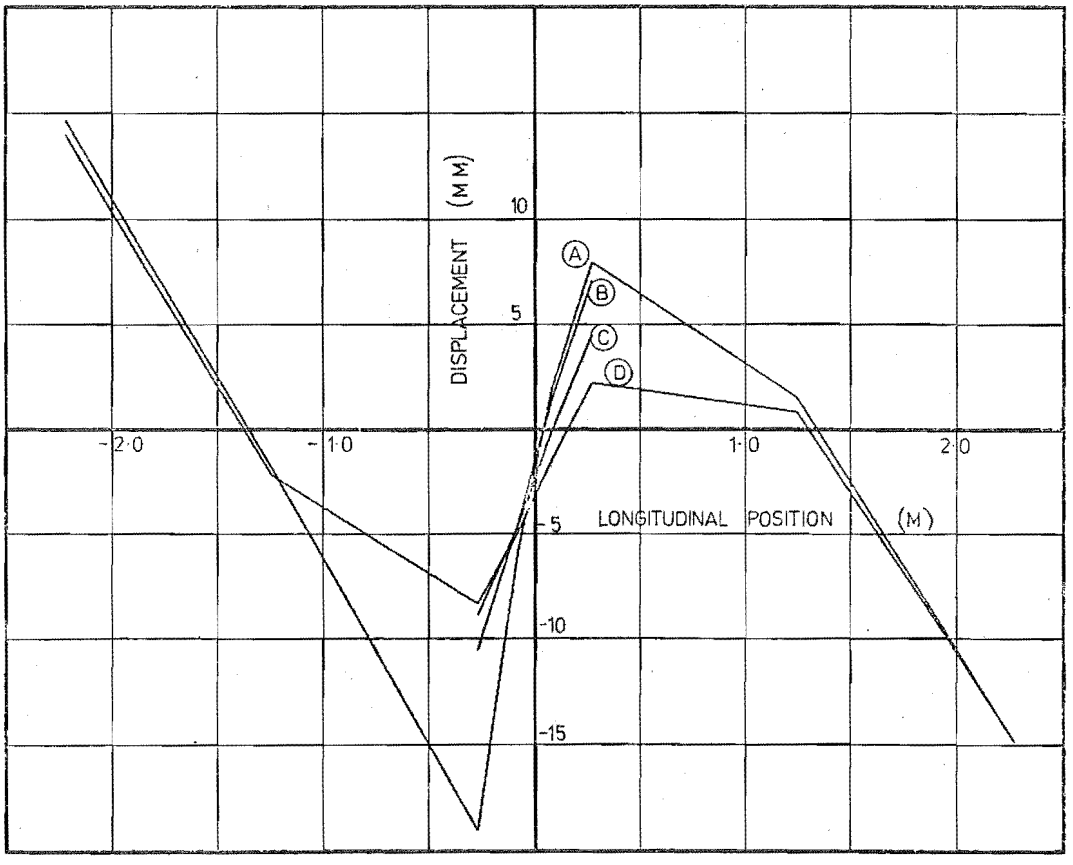

FIGURE 12.8 : DISPLACEMENT PROFILE OF UNIT 2 AT CYCLE 17 (μ = 7)

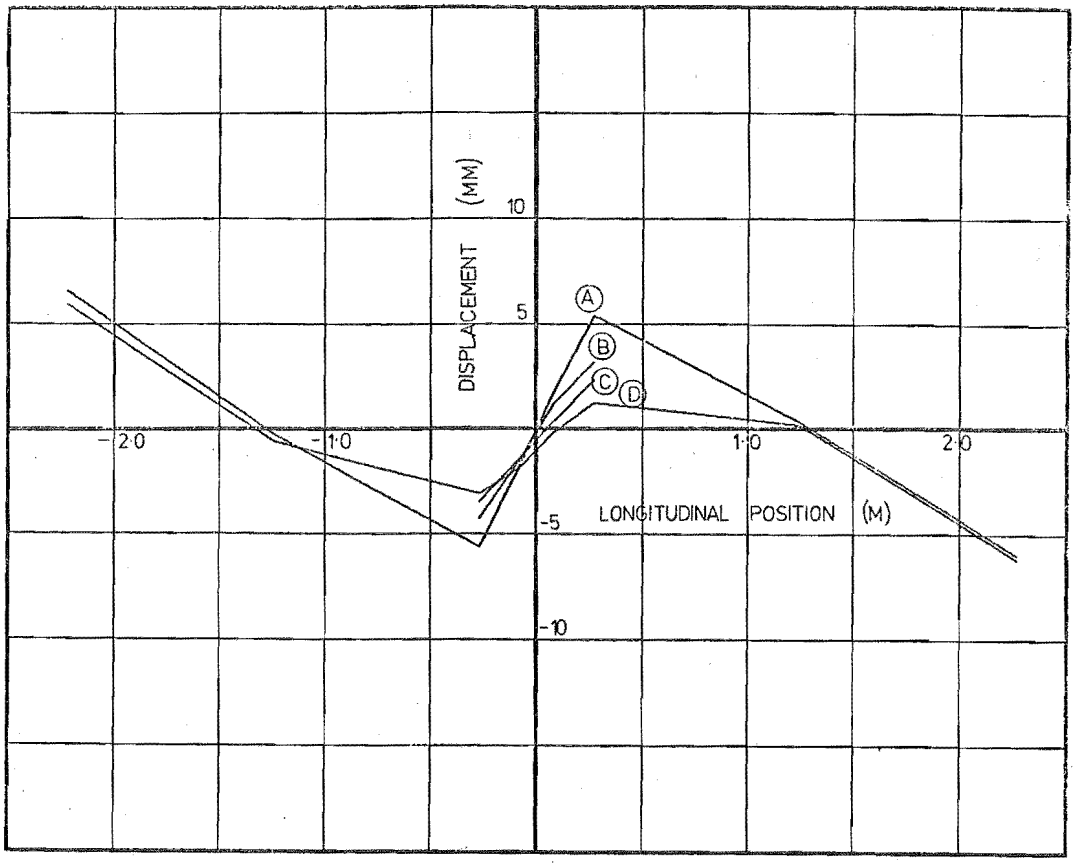

FIGURE 12.9 : DISPLACEMENT PROFILE OF UNIT 3 AT CYCLE 5 (μ = 3)

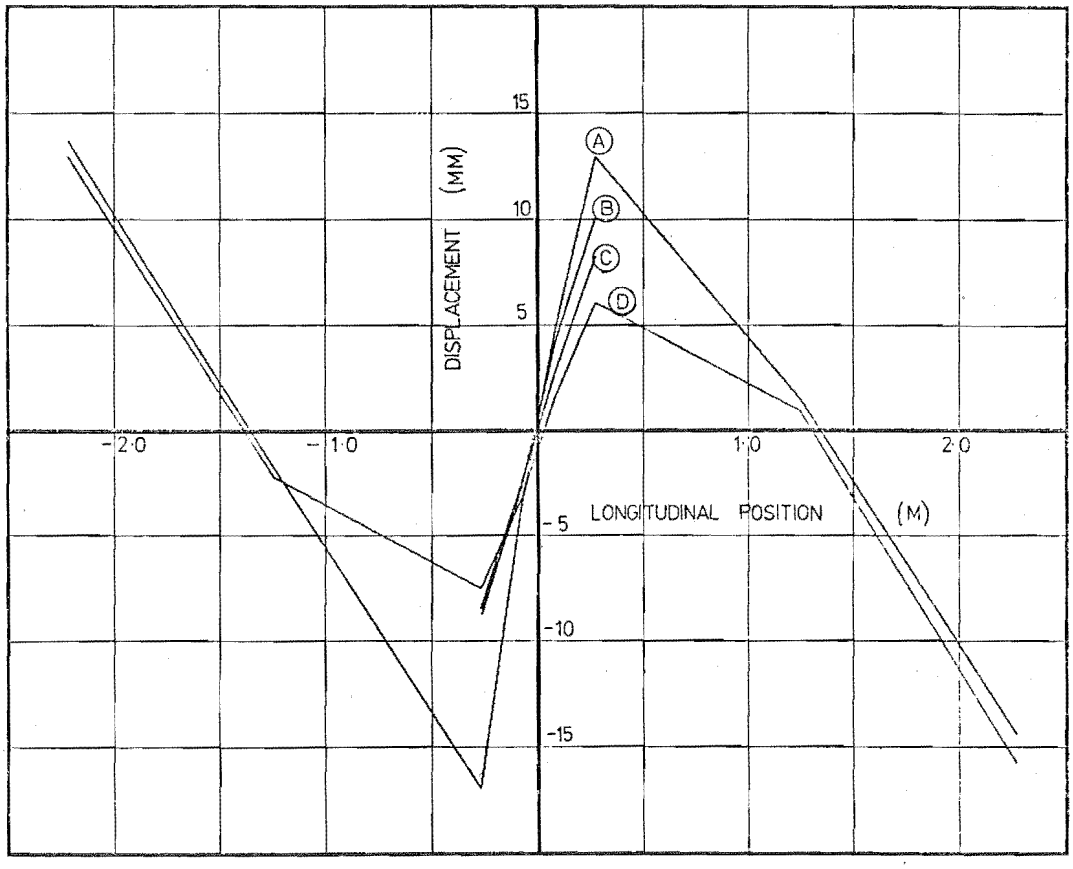

FIGURE 12.10 : DISPLACEMENT PROFILE OF UNIT 3 AT CYCLE 17 (μ = 7)

gravity and lateral load forces, must be sufficient to cause the inelastic downward deformations as described above. Units 1 and 2 (figures 12.5 - 12.8) both showed substantial permanent downward deformations at each wall toe as testing progressed. A high degree of control of shear displacement, however, was achieved with the relatively stiff transverse structural steel beam in unit 3, where departures from antisymmetric profiles were barely detectable in the early stages of the test (figure 12.9).

A permanent downward deformation of the outer edges of the slab was observed in all specimens. This also was attributed to cracking and yielding of portions of the slab (see the arrow in figure 12.23 indicating an inclined crack) and redistribution of the dead load transfer mechanisms as described above. Because transverse cantilever action is present in the model, instead of continuous beam action, these small slab edge deformations were considered to be insignificant.

Transverse slopes and curvatures may be obtained by differentiation of displacement patterns, provided that measurement is not too course. In this study, approximate values were computed. In all specimens the greatest transverse curvature occurred close to the walls and only small cyclic changes in transverse slope were observed at the model slab edges (figures 12.5 - 12.10). This confirms, to some extent, assumption iv) of section 10.5 regarding the use of a longitudinal line of symmetry.

Also in the original model derivation, a cut-off of the longitudinal steel two metres behind the model wall toes was made, assuming the remainder of the prototype structure not to influence the coupling region. This is justified by the near perfectly parallel wall and slab edge profiles at either end of the model.

Level points were concentrated on and between the expected yield line positions (see figure 11.8) but, in some cases, yield lines formed beyond this region, evidenced by a marked change of slope at slab edge level points outside the expected yield line positions. The significance of this discontinuity is that it indicates the amount of longitudinal reinforcement yield occurring outside the assumed yield lines (figures 12.5 to 12.10). In figure 12.5 slab rotations can be seen to be concentrated close to assumed yield lines while in figure 12.8 there is a greater longitudinal spread of curvatures at slab edges. Along the assumed yield lines a noticeable reduction in the displacement at slab edges, evident in all profiles (figures 12.5 - 12.10) and particularly pronounced in cycles inside previous maximum bounds, increasing as damage occurred, reflected the incomplete participation of longitudinal seismic reinforcement (figure 11.3).

12.3.2 Unit 4

Unit 4 slab deflection profiles (figures 12.11 and 12.12) were, in the main, similar to the previous three units. It was noticeable, however, that the beam, although completely split in the horizontal direction, still provided good punching shear control at wall edges. A consequent feature was that the wide cracks in the slab at which hinging occurred coincided almost exactly with the assumed yield lines which pass through the wall toes (figure 12.34).

12.4 STRESSES IN THE LONGITUDINAL SEISMIC REINFORCEMENT

12.4.1 Slab Tests

In the first elastic cycles, higher steel stresses were concentrated in the central region (figures 12.13 - 12.15). The downward yield line referred to in these figures is the yield line which moves downward when the unit deforms towards the right (figure 11.12). With further and increasingly larger displacements, high stresses in the outermost longitudinal steel were observed (figures 12.13 - 12.15). However, the high lateral spread of stresses shown in figure 12.13, relating to unit 1, is somewhat misleading. Throughout this test no longitudinal bars outside the stirrup cage gave measured strains greater than 1.8 times yield. In the main, this was true also of unit 2. In unit 3, even the outer bars consistently gave strain readings greater than 15 times yield. It may be concluded that the steel beam of unit 3 resulted in greater participation across the slab width and this was borne out by crack widths (see figure 12.32) and deflected shapes. Part of the large strain must be attributed to yield line locality because some yield lines in unit 3 almost exactly coincided with strain gauge positions (figure 12.32). Detailed observation of the sequence of photographs in figures 12.29 to 12.32, noting crack localities and relative crack widths, can provide indications of longitudinal steel strain distributions.

12.4.2 Unit 4

Electrical strain gauges attached to the longitudinal slab reinforcement performed well throughout the test because of the very light damage in the slab before the final large deformation occurred. Results are plotted for a downward moving yield line (figure 12.16), showing transverse stress distributions for top and bottom longitudinal reinforcement. It can be seen that, in comparison with slab units, a significant overall tension is present across the width of the slab.

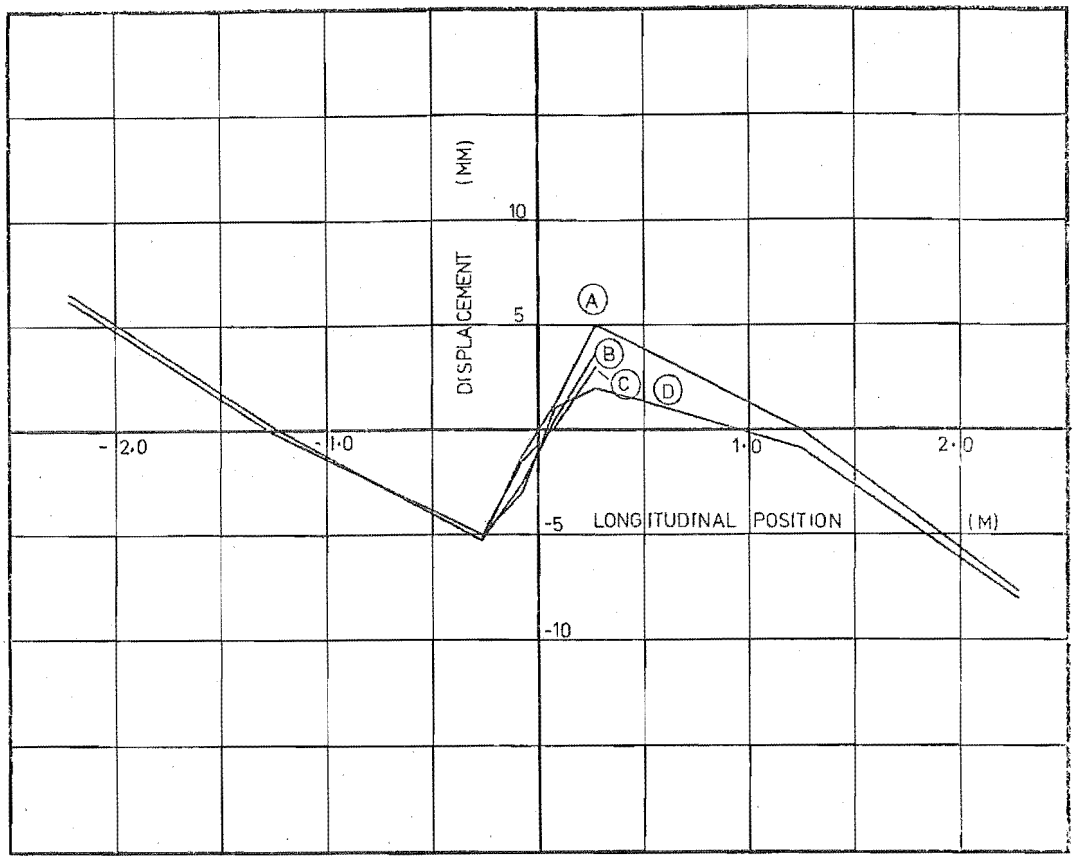

FIGURE 12.11 : DISPLACEMENT PROFILE OF UNIT 4 AT CYCLE 5 (μ = 3)

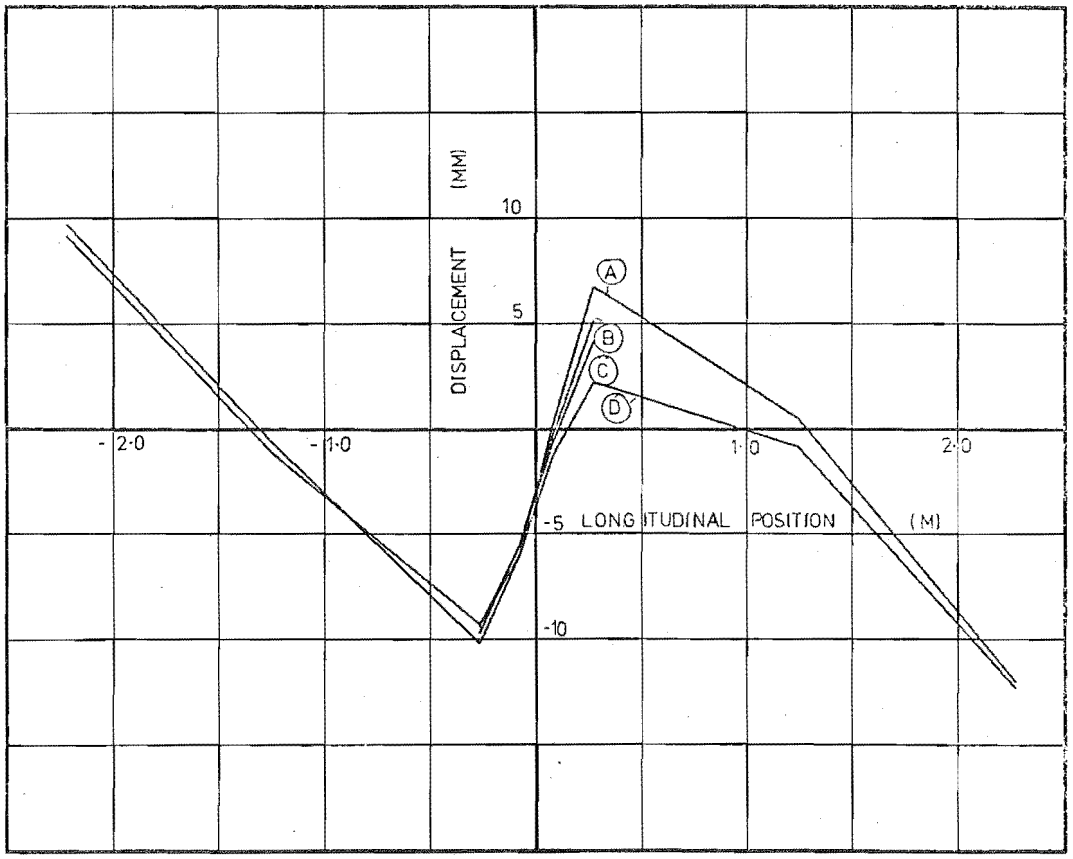

FIGURE 12.12 : DISPLACEMENT PROFILE OF UNIT 4 AT CYCLE 11 (μ = 5)

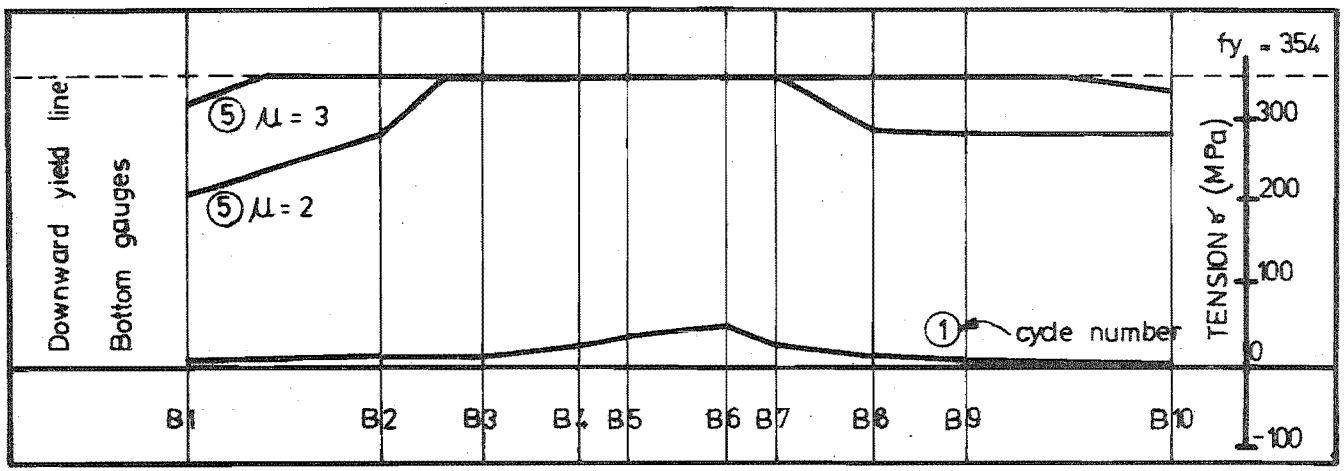

For gauge locations see figure 11·9

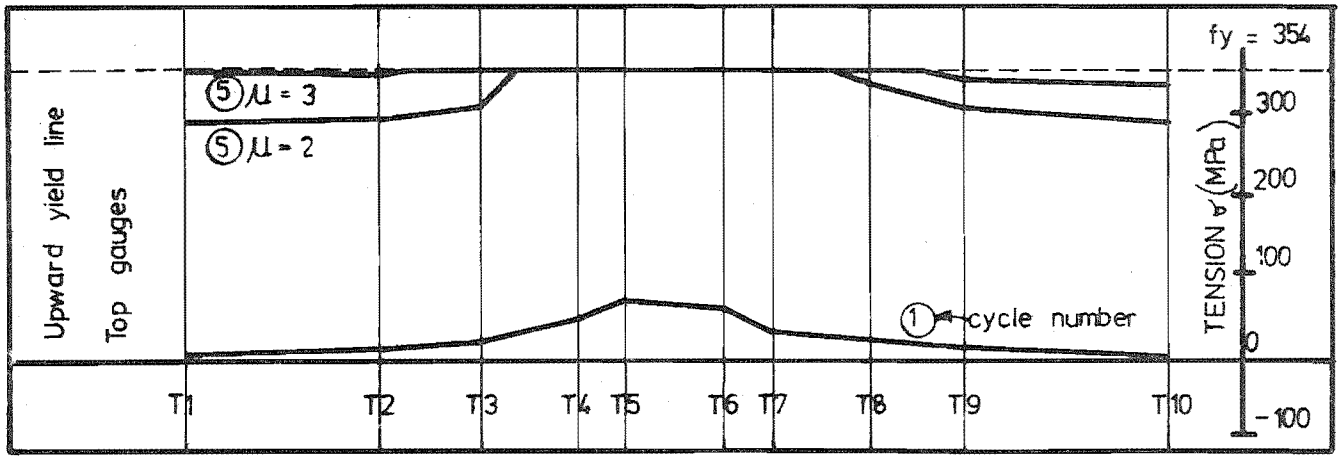

FIGURE 12.13 : LONGITUDINAL SEISMIC REINFORCEMENT STRESSES IN UNIT 1.

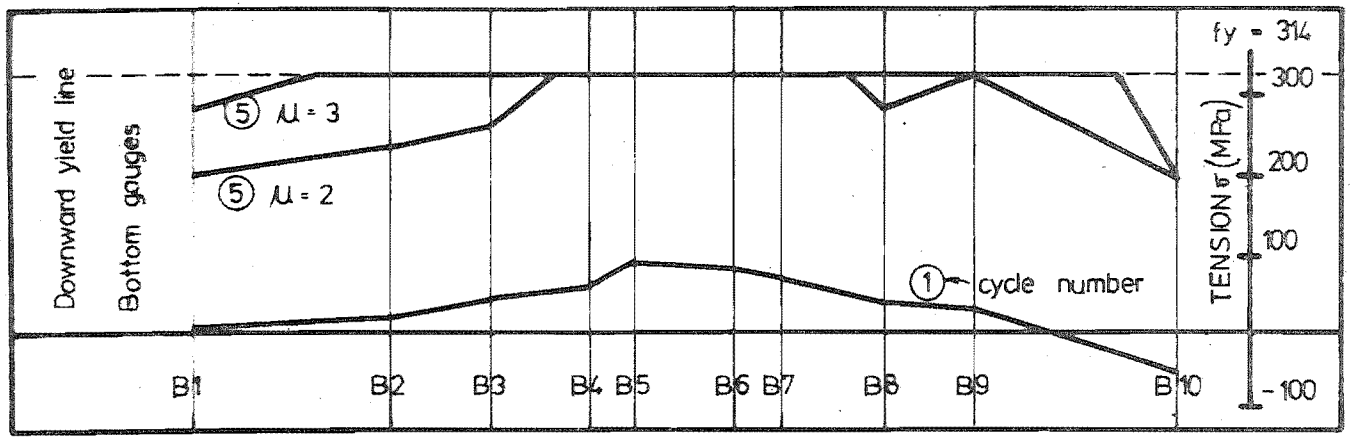

For gauge locations see figure 11·9

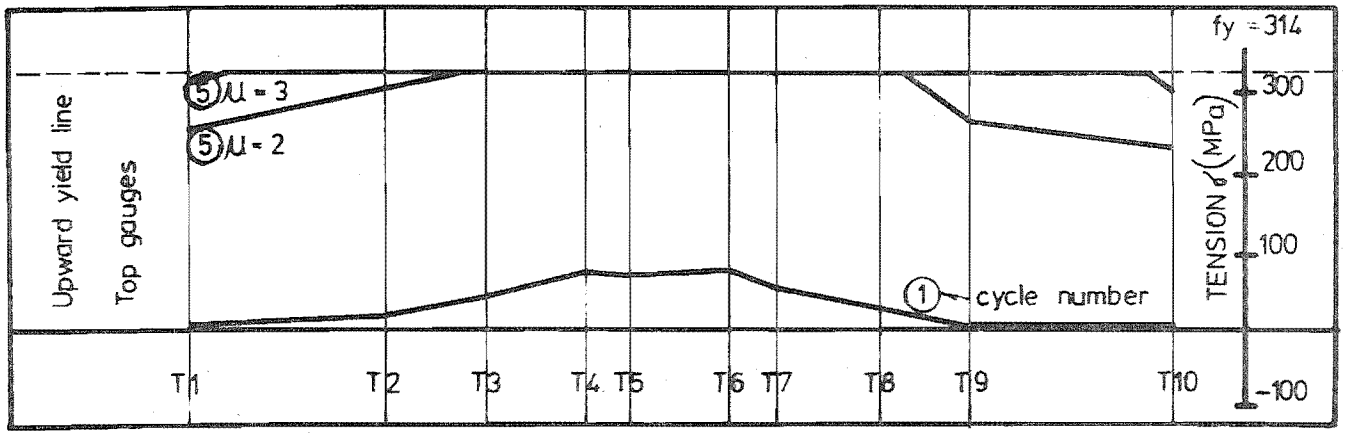

FIGURE 12.15 : LONGITUDINAL SEISMIC REINFORCEMENT STRESSES IN UNIT 3.

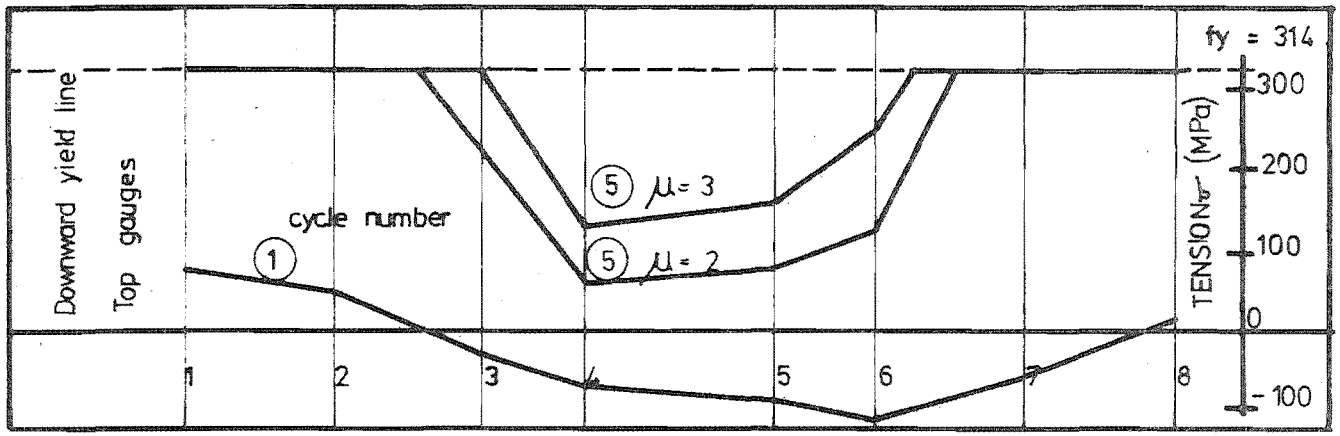

All gauge locations except 2 & 7
correspond to previous positions

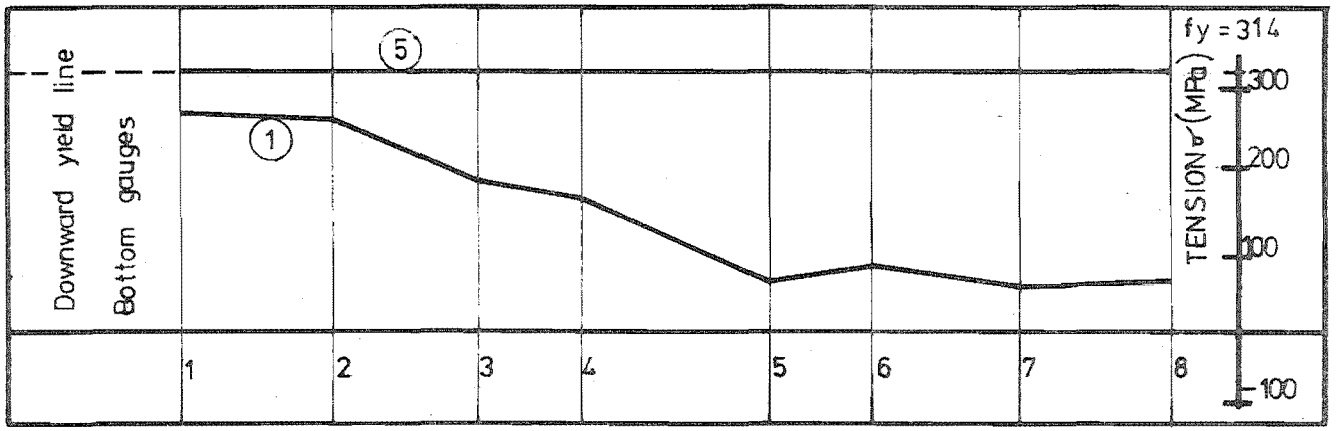

FIGURE 12.16 : LONGITUDINAL SLAB REINFORCEMENT STRESSES IN UNIT 4.

This is because there is a strong tendency for the entire width of the slab to act as a tension flange in conjunction with a compression block in the beam. In the central region near the beam top reinforcement strains in the slab (figure 12.16) decrease as they are influenced by beam strain profiles. Thus full composite action is restricted in its lateral extent and becomes more so as loading progresses. Unfortunately, it was not possible to assess the effect of residual strains in the slab steel because composite action of the beam and slab reduced after the first major inelastic cycle when the horizontal shear failure occurred. At the upward moving yield line stress distributions in the longitudinal slab steel were similar to those observed in the slab specimens.

12.5 STRAINS IN SECONDARY D10 REINFORCEMENT PLACED TRANSVERSELY ACROSS WALL TOES

In the early stages of the tests, before significant shear deformation at the wall toes was observed (cycle 17 for units 1 and 2), extremely low strains were observed in the secondary transverse reinforcement (see figures 12.17 and 12.18). Although yielding of all longitudinal steel occurred in unit 1, requiring lateral load transfer across the slab, simple transverse beam action as assumed for the transverse reinforcement design was not observed. After testing unit 2 the overall inefficiency of the transverse secondary reinforcement was erroneously attributed to large shear deformations reducing effective secondary beam action. In fact, examination of unit 3, in which these shear deformations were controlled with a structural steel beam, revealed smaller strains in the secondary transverse reinforcement (figure 12.18).

A surprising result observed in units 2 and 3 was the sudden increase in strain at Pfender gauge positions 4 and 5 (see figures 12.17 and 12.18). In these regions the slab stirrups, acting also as transverse flexural reinforcement, are present and terminate as effective flexural reinforcement in the transverse direction immediately beyond these gauge lengths. If flexure in accordance with assumed transverse one-way beam action was the principal mode of load transfer (see section 11.4.3), then a sudden increase in strain at Pfender positions 3 and 6 (figure 12.17) was to be expected, i.e. immediately after the reduction in effective flexural reinforcement. This effect was also observed in unit 3 (figure 12.18) but because a steel beam was embedded in the slab it was less significant. Two mechanisms provide explanations of the observed strain patterns:

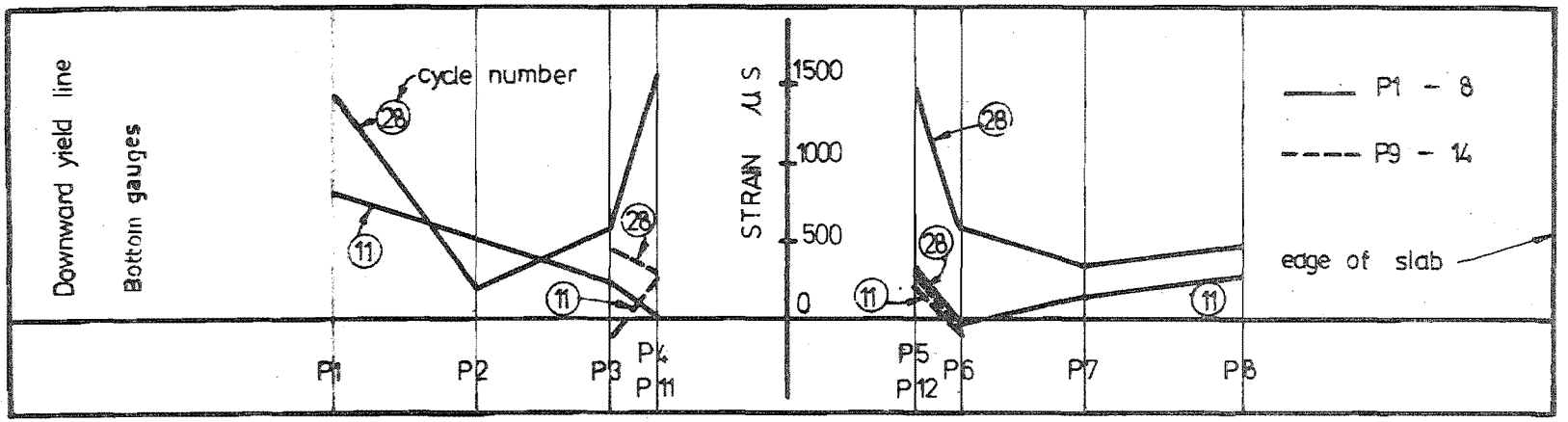

For gauge locations see figure 11·10

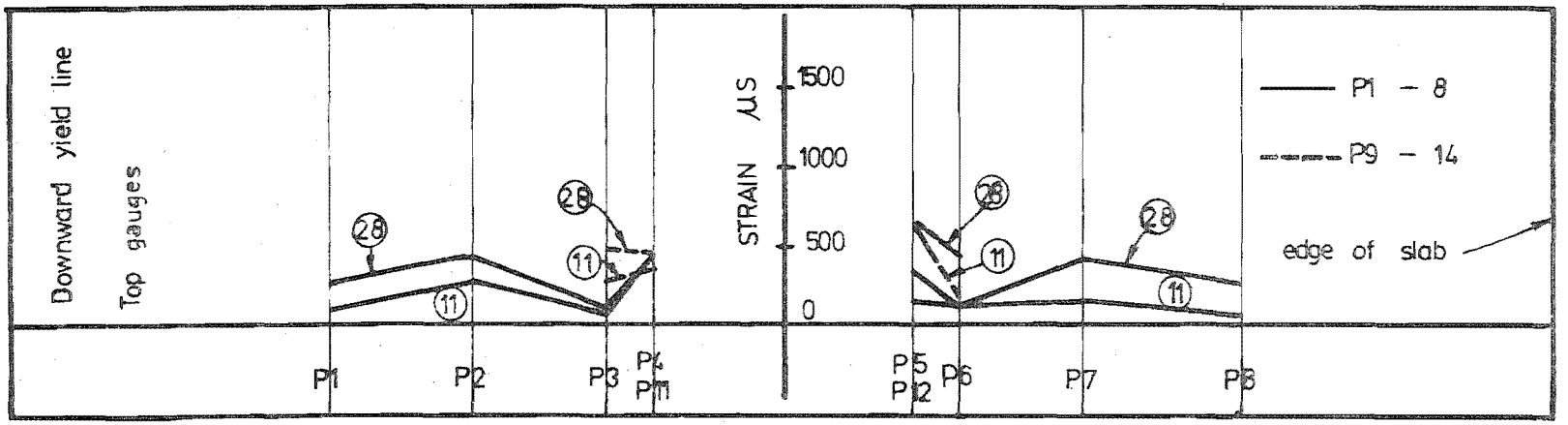

FIGURE 12.17 : STRAINS IN UNIT 2 TRANSVERSE REINFORCEMENT AT WALL TOES.

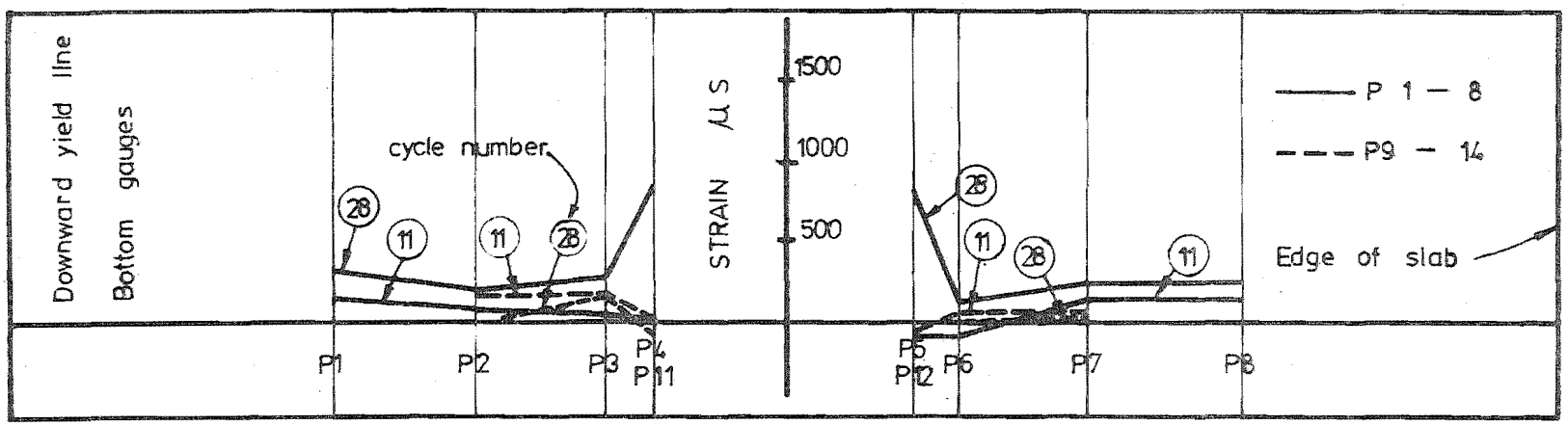

For gauge locations see figure 11·10

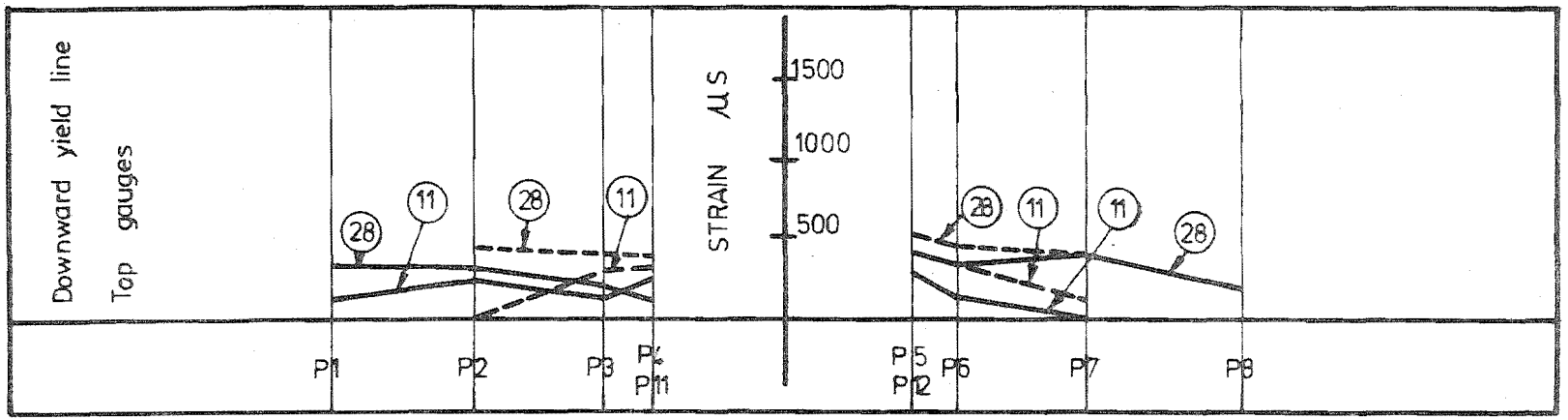

FIGURE 12.18 : STRAINS IN UNIT 3 TRANSVERSE REINFORCEMENT AT WALL TOES.

i) Two-way slab action results in a much more rapid reduction in moment in the transverse direction than indicated by the assumption of one-way action. With one exception (figure 12.17) transverse reinforcement stresses at localities distant from the walls were small.

ii) During later stages of the tests, visible shear deformations and increased tensile strains in both top and bottom transverse reinforcement at wall toes indicate that a "shear friction" mechanism is also present. This mechanism relies on aggregate interlock on either side of a full depth crack near the wall toe. A normal contact force, to increase the effectiveness of the mechanism, is provided by the horizontal portions of the slab stirrups which are strained as a result of a relative movement of the two rough surfaces. In unit 3, a limited increase in tensile steel strains at cycle 28 (figure 12.18), associated with shear deformation, occurred because the instrumented bar (Pfender gauges 1 - 8) was located between the embedded steel beam and the edge of the wall.

Although action of the transverse reinforcement became greater as deformations and damage increased, it remained ineffective in providing overall stiffness enhancement.

12.6 PERFORMANCE OF THE STRUCTURAL STEEL BEAM

12.6.1 Unit 3

Shear reinforcement, consisting of single structural steel sections, proved extremely effective in controlling shear deformations and, as discussed above, in reducing the participation of the special transverse reinforcement. However, substantial overall stiffening of the structure, that might have been expected, was not achieved.

In unit 3 at localities close to walls the web strains indicated almost pure shear at advanced stages of the loading (see figure 12.19 in which tensile strains are positive). From all readings shown, the highest principal stress was 158 MPa. Shear forces calculated assuming yield lines as shown in figure 11.8 lead to an approximate principal steel stress of 180 MPa. For this computation the beam is presumed to carry all shear forces associated with the longitudinal reinforcement yielding due to lateral loading as described in section 11.4.3. Approximate flange strains in the steel beam can only be inferred from strains in the transverse secondary reinforcement across wall toes. Reference to figure 12.18, noting that Pfender gauge positions 11 and 12 are above and below the embedded steel beam, confirms flexural strains to be small at localities near the walls.

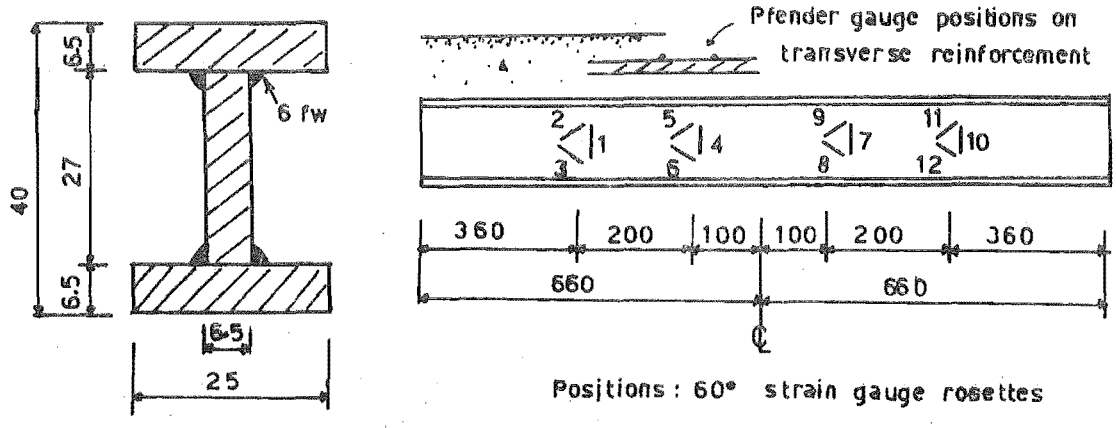

Cycle	Ductility	1	2	3	4	5	6	7	8	9	10	11	12
11	+ 5	152	-90	145	128	-146	188	152	299	-236	214	125	-105
12	- 5	391	133	-140	250	346	-237	331	-192	316	214	-114	78
29	+ 11	37	-195	294	42	-472	566	134	660	-526	283	208	-250
30	- 11	272	254	-348	93	648	-636	86	-553	648	128	-259	205

Measured Strains (μs)

FIGURE 12.19 : STRAINS IN THE STRUCTURAL STEEL BEAM OF UNIT 3.

12.6.2 Unit 4

The structural steel beam strains in unit 4 were much more difficult to assess than in unit 3. This was because the concrete beam, of unknown and changing shear stiffness, assisted in transmitting slab shears, which concentrated at wall toes, into the walls. However, it can be seen from the small flange strains in figure 12.20 (except gauge 14), and the even smaller cyclic flange strain changes, that flexural strains are relatively small. Distributions of strains along the steel member are very inconsistent. A particularly large disturbance occurred in the vicinity of gauges 4 - 6 (see figure 12.20) at cycle 11 due to a full depth shear crack similar to that causing the failure in unit 1 (see section 12.9.1). Large relative movements across the crack were not observed until the end of the test because of the presence of the embedded structural steel beam. Reduction of web strains to principal strains or principal stresses did not assist in observing any characteristic distribution patterns in the steel member.

12.7 BEAM REINFORCEMENT STRAINS IN UNIT 4

Strain distributions along the length of the concrete beam, which were measured at points shown in figure 11.11, are presented in figure 12.21. Noteworthy features include: very small strains occurred in the initial load cycle to 60% of the theoretical ultimate load, a confined area of yield near wall toes occurred in the first inelastic cycle and a considerable penetration of yielding into anchorage regions was observed after further inelastic cycling. It seems probable that larger longitudinal beam steel strains would have occurred, but for the horizontal shear failure of the beam (see section 12.9).

12.8 ELONGATION OF THE COUPLING SYSTEM

For each unit, a history of elongations (Table 12.I) at peak displacements were derived from wall deformations. In all cases the increase in wall separation was small and certainly insufficient to violate the relevant assumptions of model abstraction. As referred to in the previous section, a larger elongation might have been expected in unit 4 but for the horizontal shear failure of the beam.

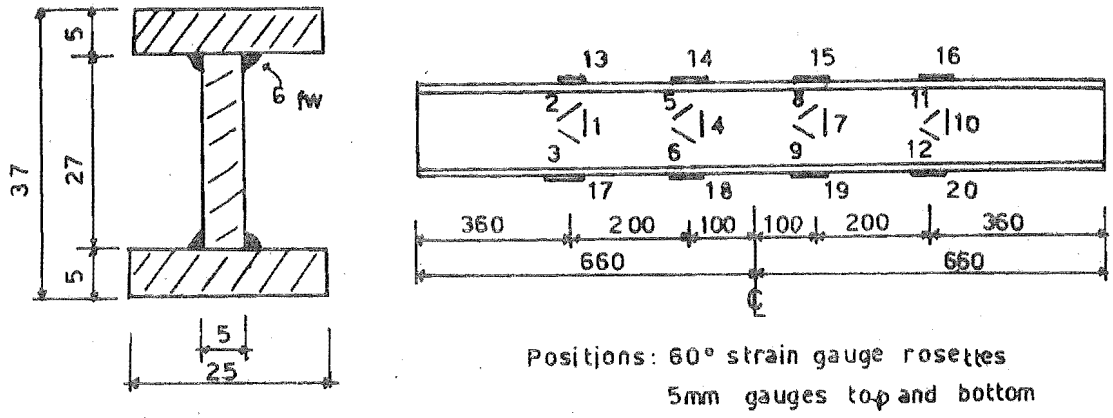

Cycle	Ductility	1	2	3	4	5	6	7	8	9	10	11	12
5	+3	480	305	120	432	232	462	856	265	-99	262	198	-374
6	-3	432	356	280	314	184	213	283	261	-126	246	134	-52
11	+5	1247	-265	+522	1040	146	1315	1402	-458	-263	203	291	-220
12	-5	554	621	557	428	267	194	92	191	-111	296	236	-58

Measured Web Strains (μs)

Cycle	Ductility	13	14	15	16	17	18	19	20
5	+3	-	484	-274	378	275	-84	231	228
6	-3	-	228	-48	332	185	-53	211	196
11	+5	-	746	-106	347	370	-147	188	163
12	-5	-	337	-88	261	309	-97	264	147

Measured Flange Strains (μs)

FIGURE 12.20 : STRAINS IN THE STRUCTURAL STEEL BEAM OF UNIT 4.

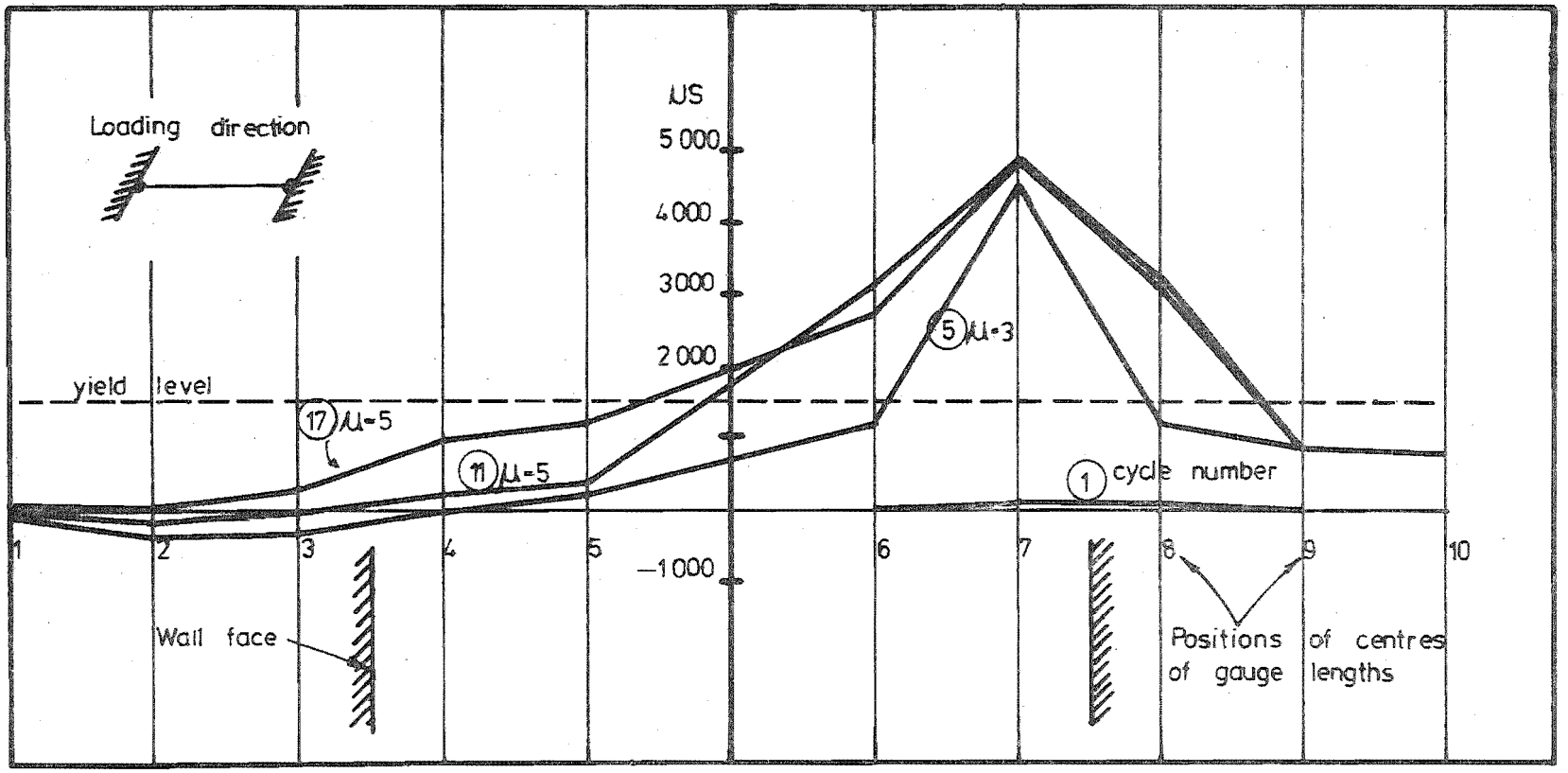

FIGURE 12.21 : STRAINS IN THE LONGITUDINAL BEAM REINFORCEMENT OF UNIT 4.

TABLE 12-I : COUPLING SYSTEM ELONGATION

Ductility	Cycle	Elongation in mm			
		Unit 1	Unit 2	Unit 3	Unit 4
3	5	1.0	0.3	0.9	2.2
5	11	1.6	3.1	3.0	3.5
7 (5 for unit 4)	17	3.1	3.5	3.5	4.8
9	23	3.1	3.3	5.8	-
11	29	-	3.8	6.2	-

12.9 STIRRUP BEHAVIOUR

12.9.1 Slab Tests

Strain measurement on the vertical legs of the shallow slab stirrups was somewhat limited by physical constraints. Generally, results of unsatisfactory consistency were obtained in units 1 and 2, which incorporated strain gauges on vertical stirrup legs, where differing sign strains with some large compressive strains were recorded.

The most important function of the stirrups in units 1 and 2 was to prevent a total punching shear failure by the horizontal legs acting as part of a shear friction mechanism. The horizontal portion of the stirrups provides a normal clamping force to enhance aggregate interlock and resist shear in an identical manner to the secondary transverse reinforcement as outlined in section 12.5. Stirrups within the central slab region were provided as conventional beam-type shear reinforcement and for confinement of the flexural reinforcement to prevent buckling when compressive yield occurred. No failures associated with these actions were observed in the specimens tested in this investigation.

Although punching shear was adequately controlled in all three slab units, each showed some minor concentrated shear deformation at the wall extremities, indicated by the shaded arrow in figure 12.26. This deformation engaged the transverse steel which resisted punching shear at the wall toes. In units 1 and 2 this transverse steel was an area of horizontal reinforcement (horizontal portions of stirrups and the transverse reinforcement) providing clamping, while in unit 3 the embedded steel beam provided the main control of sliding shear. The magnitude of this local deformation was observed to decrease progressively from unit 1 to unit 3.

As the unit 1 test progressed a shear failure occurred at the edge of the central double stirrup portion of the stirrup cage. It is

indicated with black arrows on the slab underside at a displacement ductility of 7 (figure 12.24) and after disassembly of the specimen (figure 12.26). This failure line, which is parallel to the walls, is approximately 270 mm from the wall centreline, while the double stirrups reduce to single stirrups (see figure 11.7a) at 150 mm from the wall centreline. The structural steel beam of unit 3 rendered the stirrups no longer necessary to control punching shear by their action in shear friction as in units 1 and 2.

12.9.2 Unit 4

Reliable strain measurements of unit 4 beam stirrups were obtained using mechanical gauges. Figure 12.22 shows the progressive yielding of the stirrups which reached large strain values after load cycling. A visible rising of the beam top, reaching a maximum mid-way between the wall faces, could be seen as the test progressed. Diagonal cracking of the beam was particularly severe as early as cycle 6 (figure 12.33). The initially inclined cracks tended to link together causing horizontal splitting of the beam adjacent to the top of the slab (see section 12.2.2 (iii)). The relative horizontal sliding of upper and lower portions of the beam may be seen by noting the angle of the stirrups in figure 12.34 and bending of the stirrups in figures 12.35 and 12.36.

The unit 4 stirrup reinforcement, which was provided for the full seismic shear associated with an ACI 318-71 effective beam width, was clearly inadequate to prevent a horizontal shear failure. The shear stress on the section computed from ideal strength with the ACI 318-71 effective beam width (section 12.10.2) was $v_u = 3.03$ MPa. The actual capacity of the stirrups was $v_s = 3.11$ MPa. The shear stress on the section at failure of the stirrups, computed from the maximum experimentally measured loads was $v_u = 5.21$ MPa.

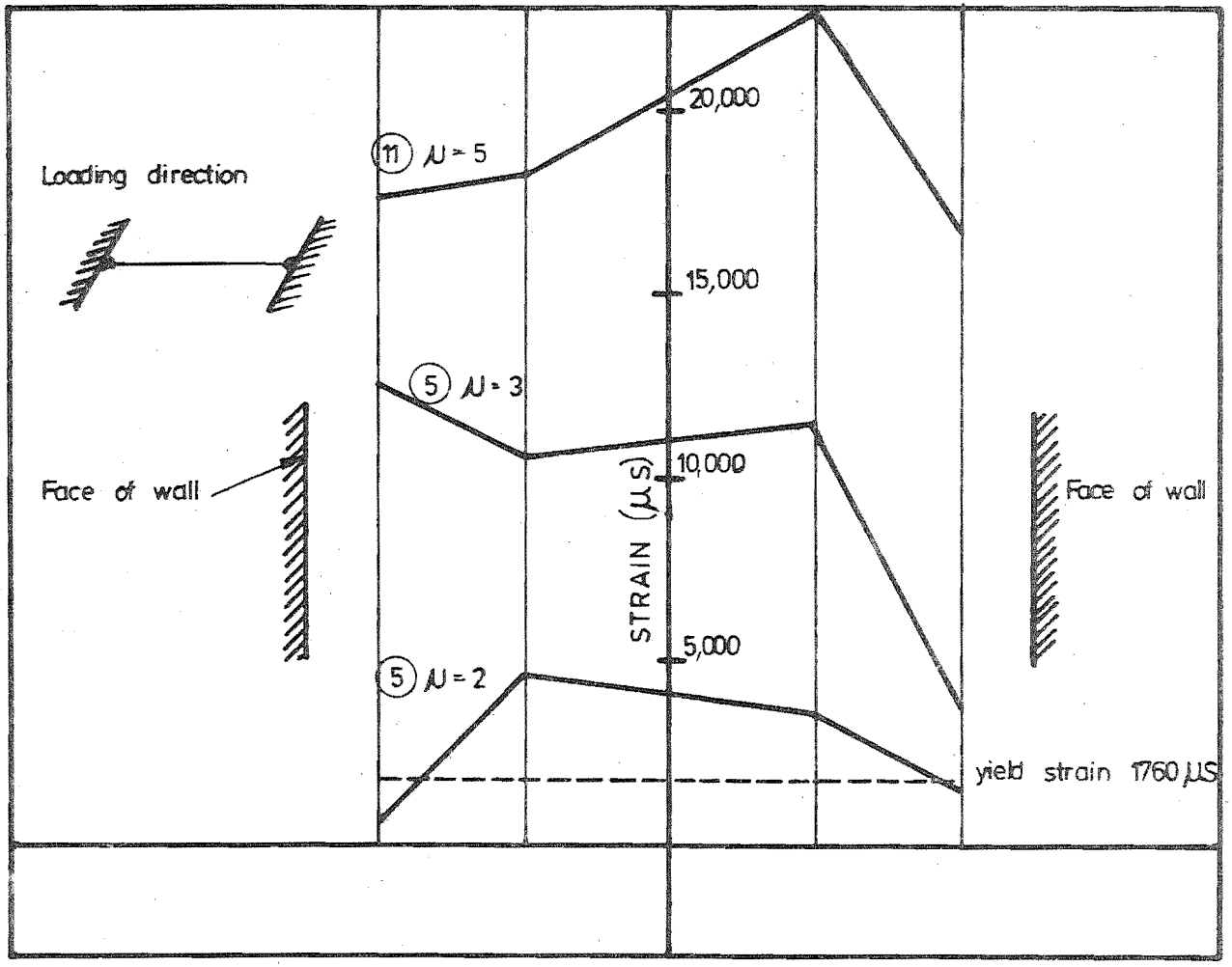

FIGURE 12.22 : STRAINS IN UNIT 4 BEAM STIRRUPS.

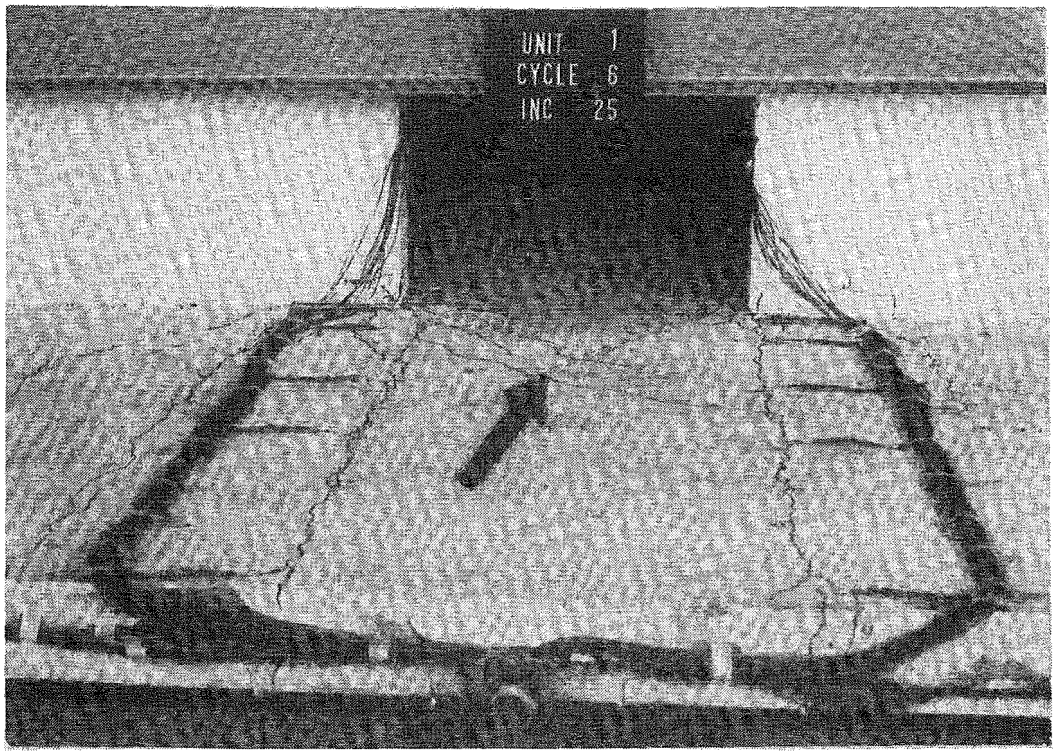

FIGURE 12.23 : UNIT 1 AT DUCTILITY 3.

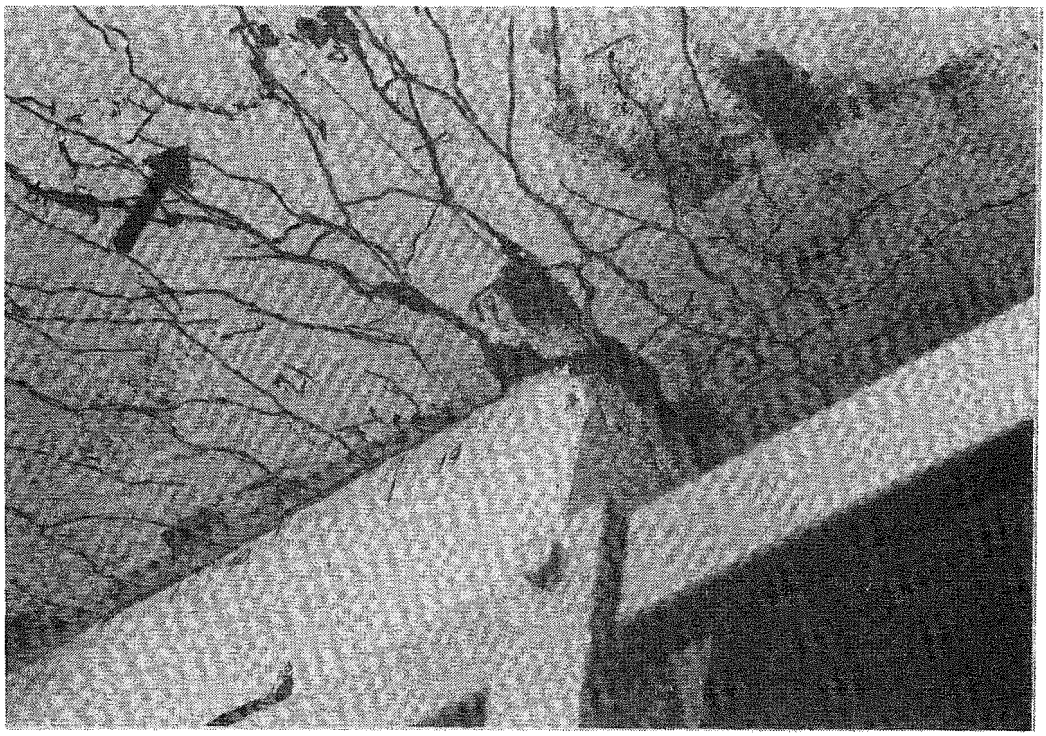

FIGURE 12.24 : UNIT 1 AT DUCTILITY 7.

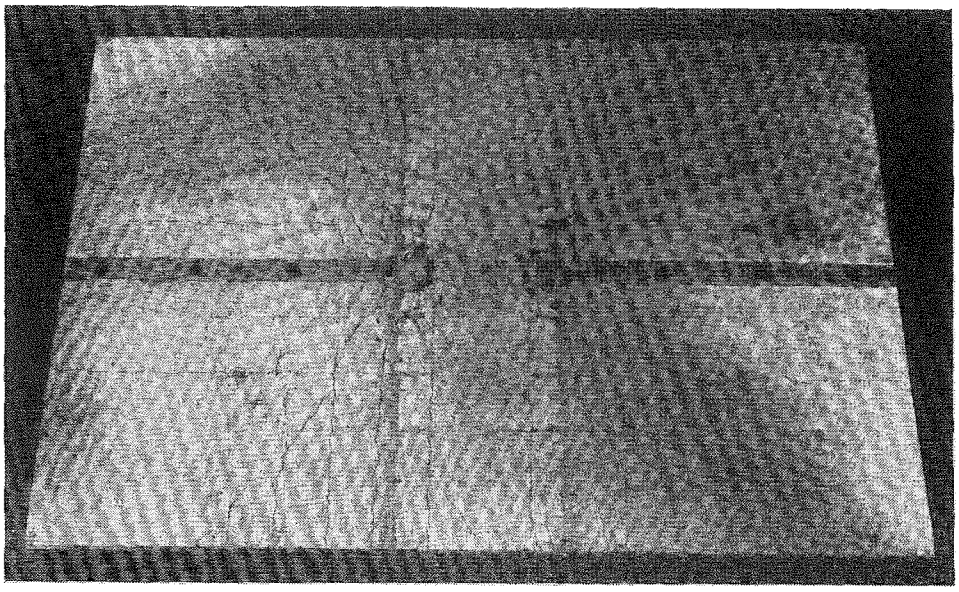

FIGURE 12.25 : UNIT 1 AFTER DISASSEMBLY.

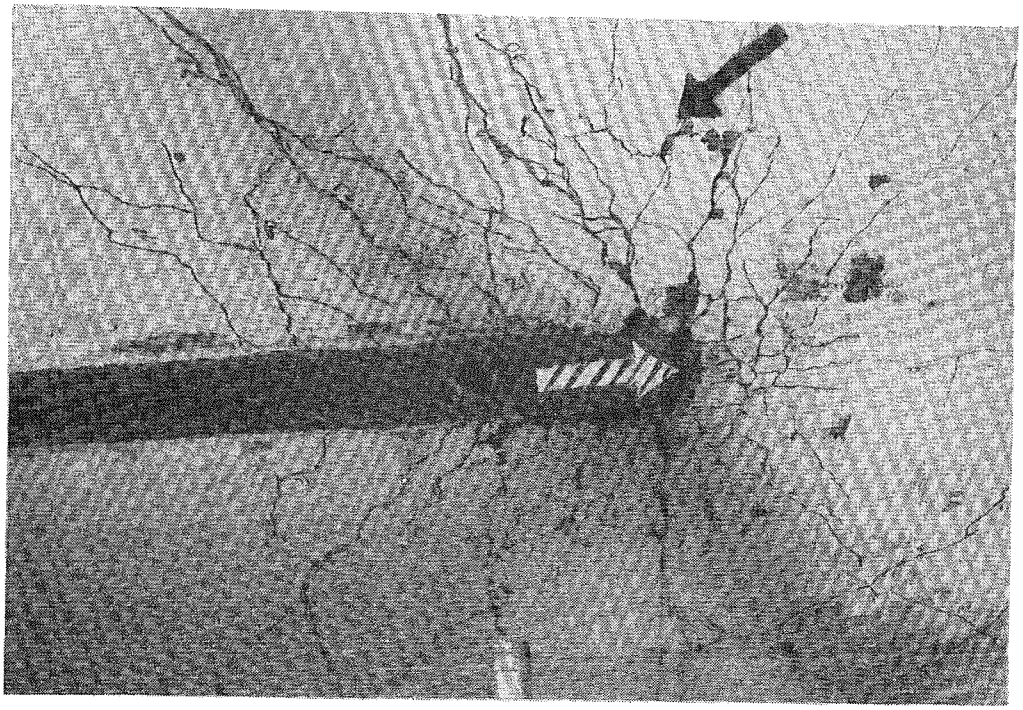

FIGURE 12.26 : PARTIAL FAILURE OF UNIT 1.

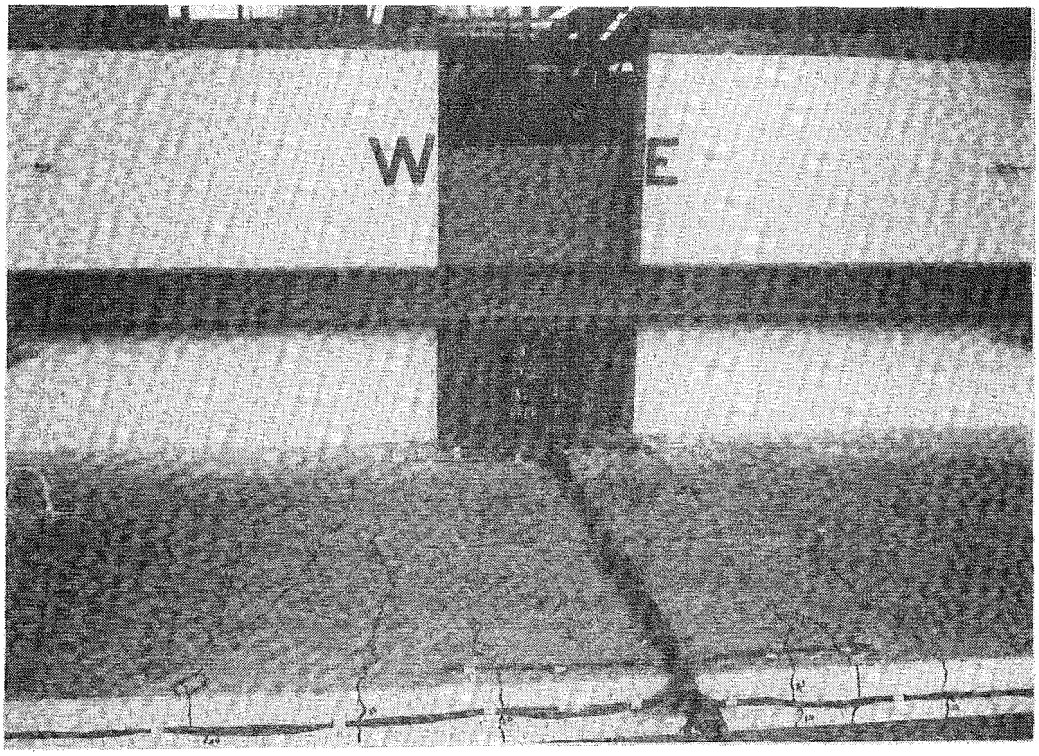

FIGURE 12.27 : UNIT 2 AT DUCTILITY 5.

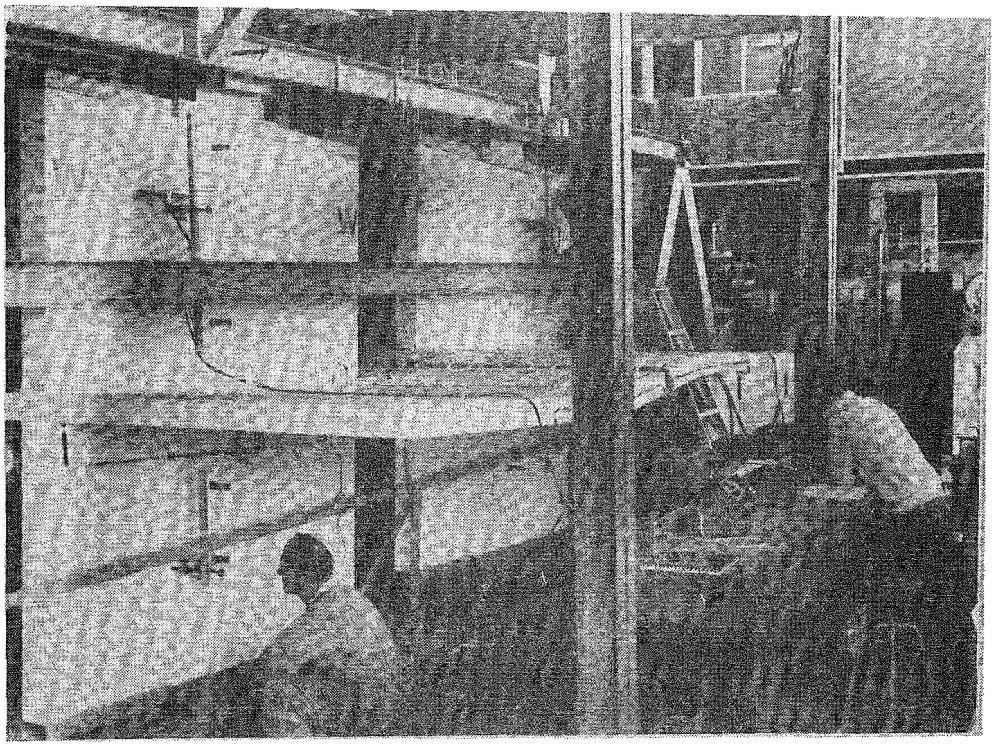

FIGURE 12.28 : UNIT 2 AT END OF TEST.

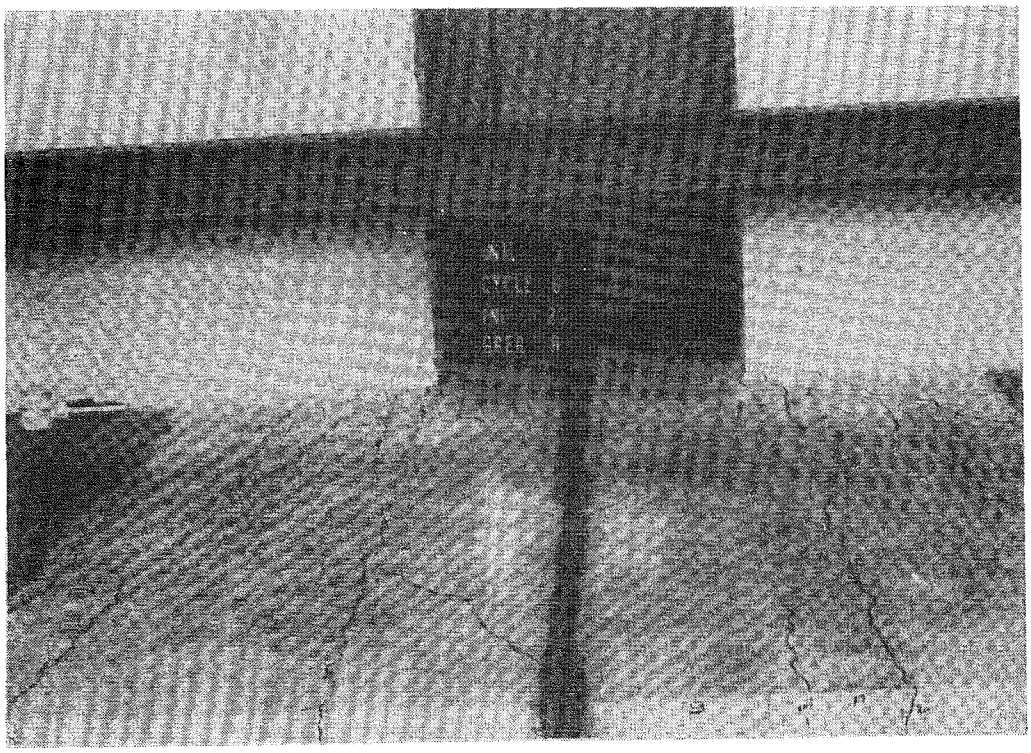

FIGURE 12.29 : UNIT 3 AT DUCTILITY 3.

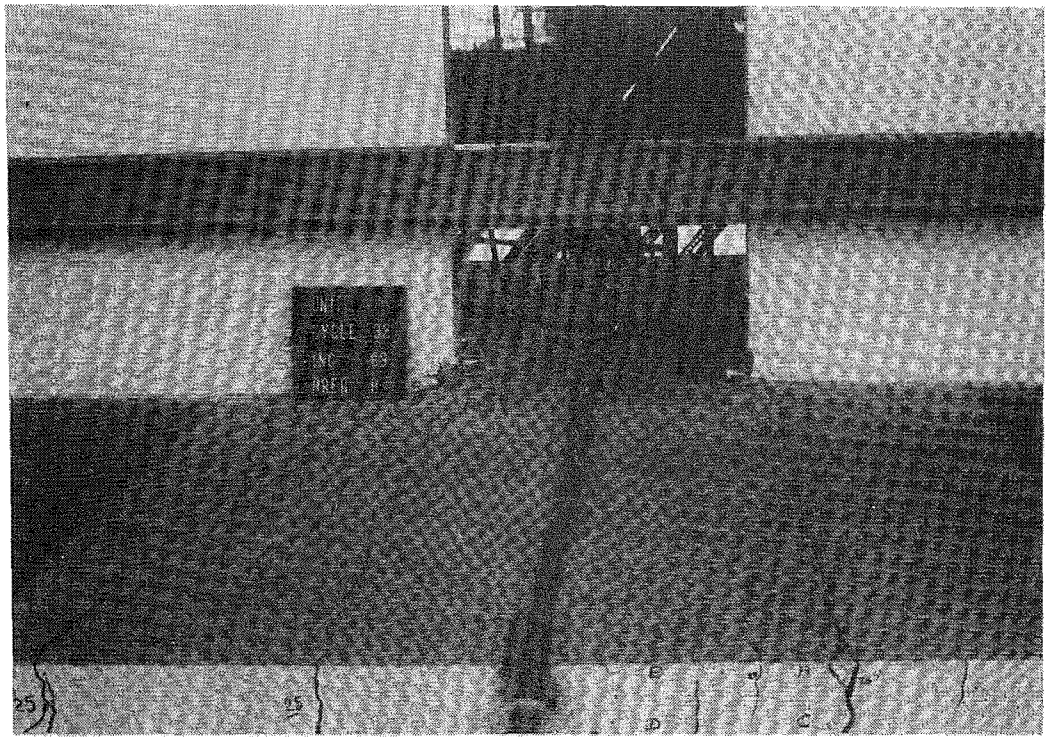

FIGURE 12.30 : UNIT 3 AT DUCTILITY 11.

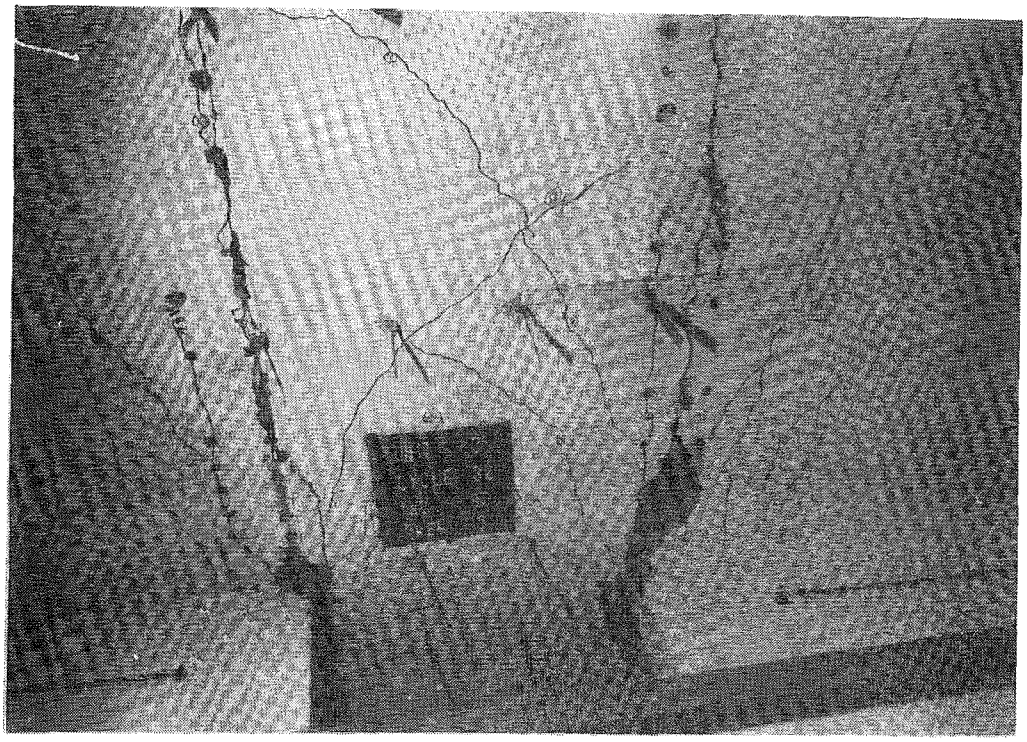

FIGURE 12.31 : UNIT 3 UNDERSIDE AT DUCTILITY 11.

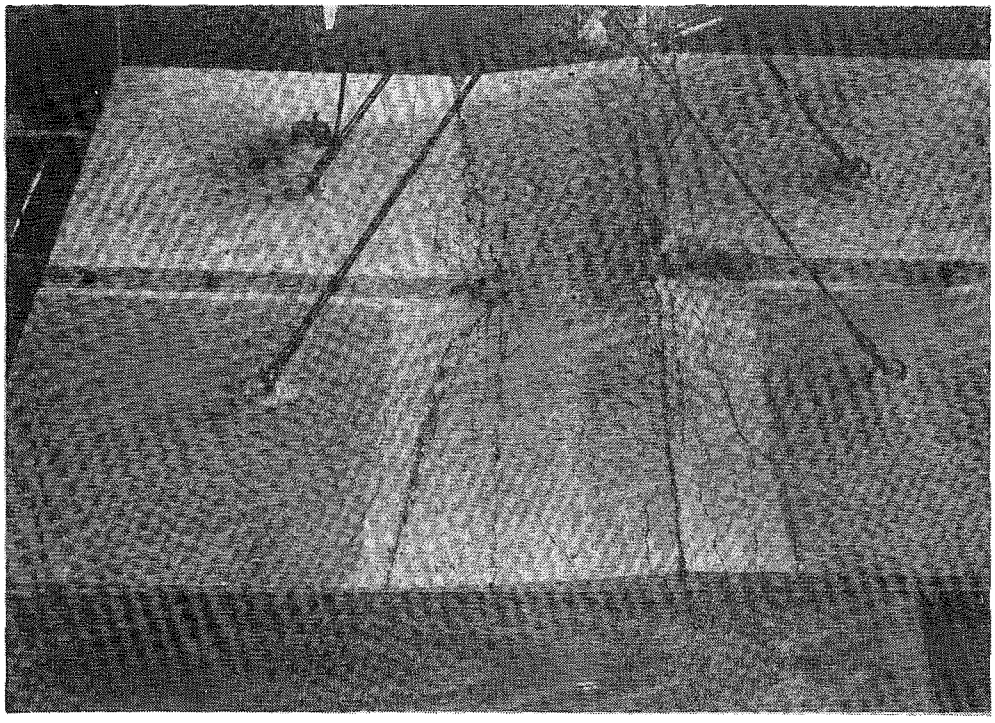

FIGURE 12.32 : UNIT 3 AFTER DISASSEMBLY.

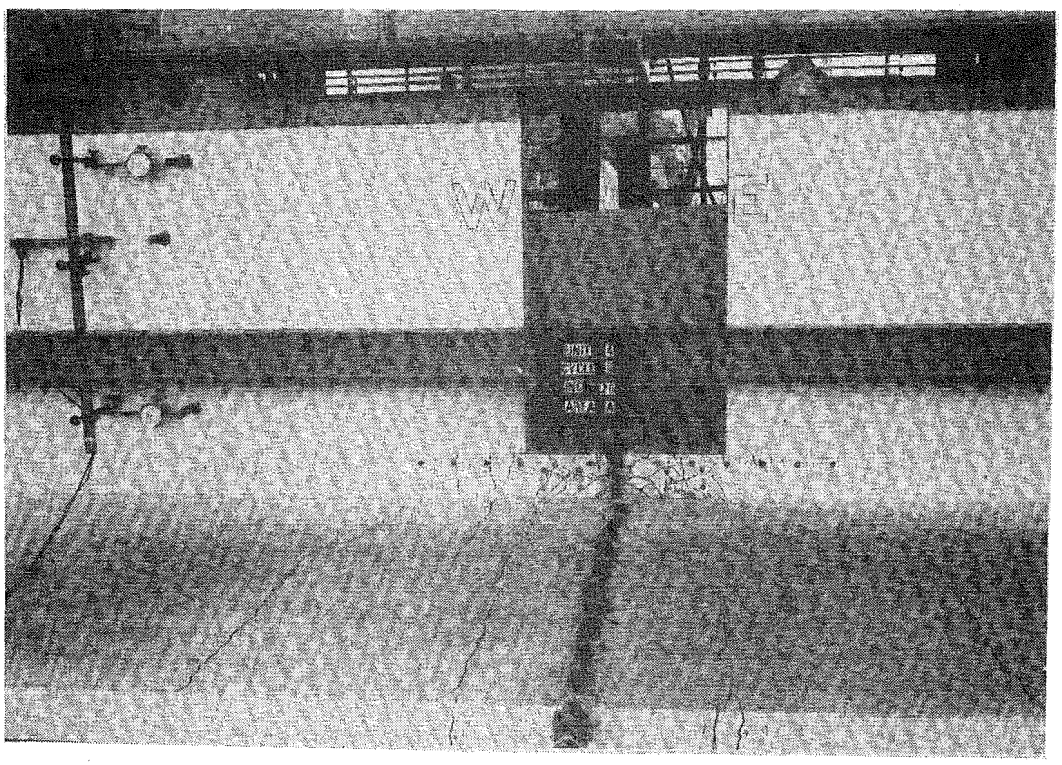

FIGURE 12.33 : UNIT 4 AT DUCTILITY 3.

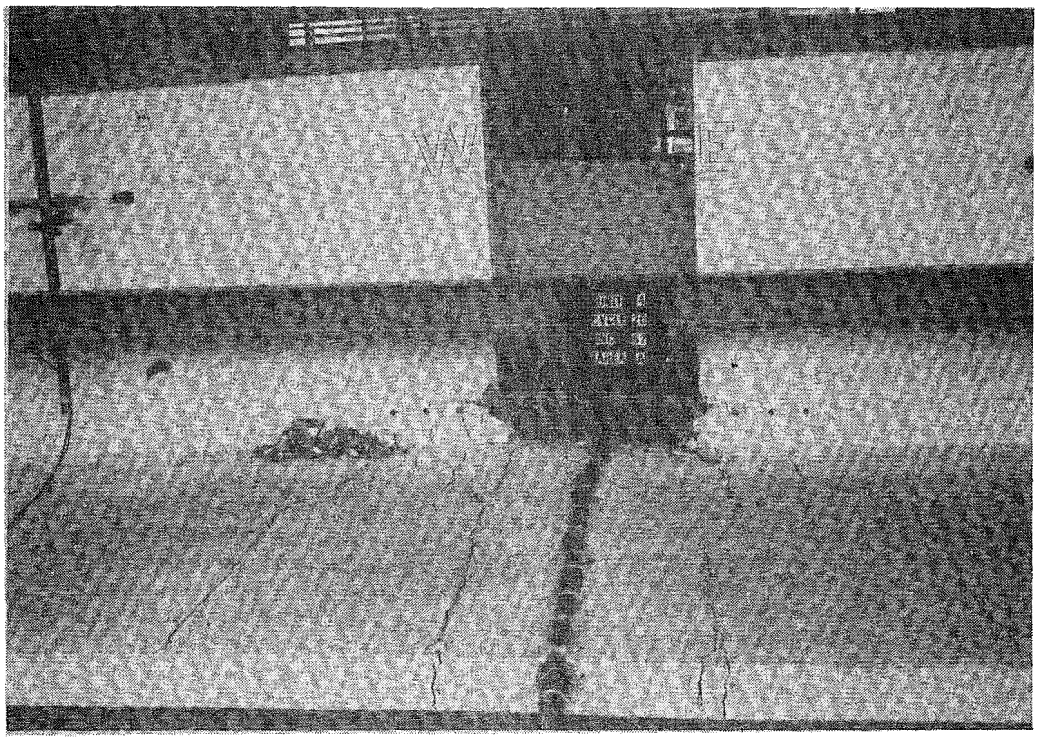

FIGURE 12.34 : UNIT 4 AT DUCTILITY 5.

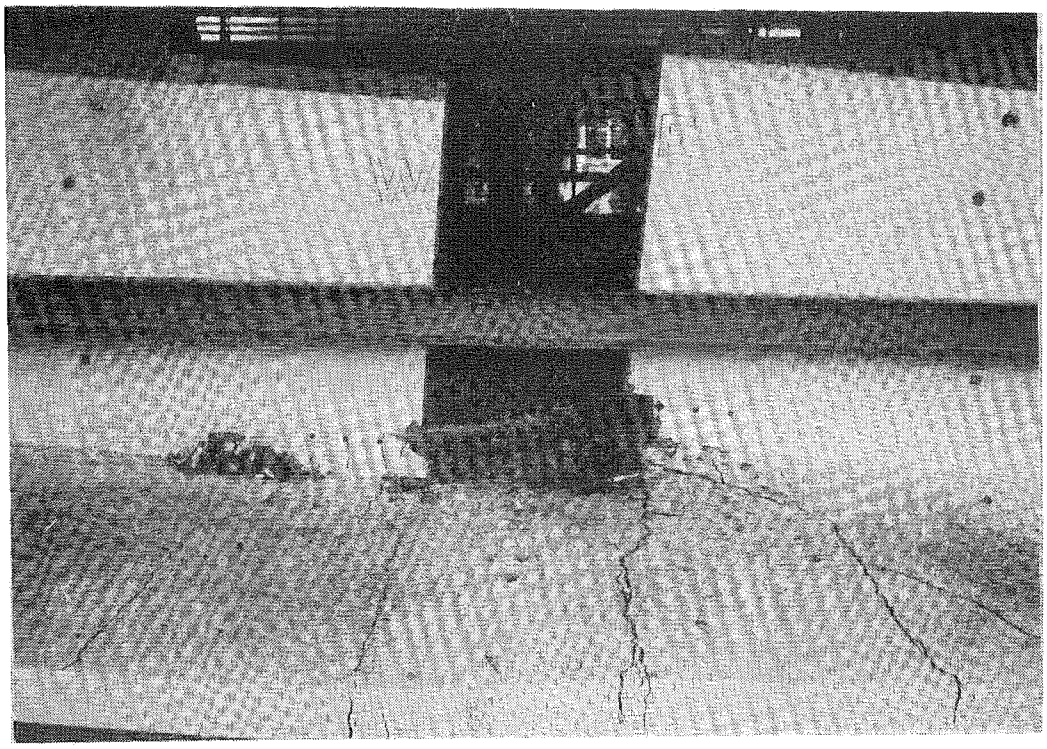

FIGURE 12.35 : UNIT 4 AT END OF TEST.

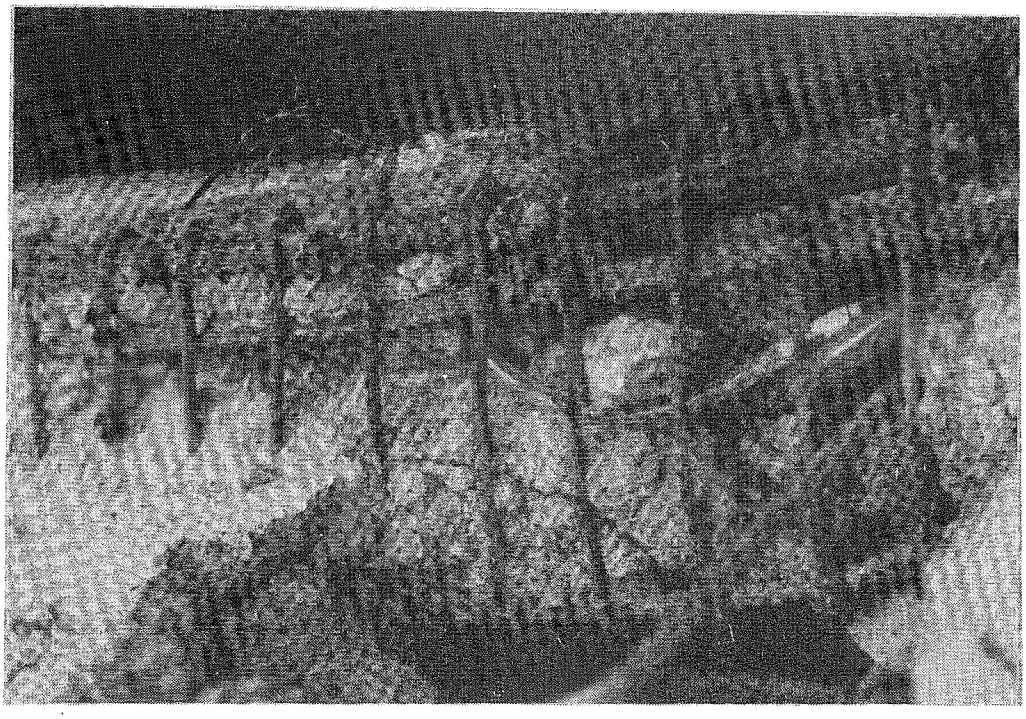

FIGURE 12.36 : VIEW OF UNIT 4 BEAM STIRRUPS AT END OF TEST.

12.10 EFFECTIVE SLAB WIDTHS

12.10.1 Slab Coupling

The usual way of expressing coupling stiffness, so that the result may be expected to relate to different configurations, is in terms of an effective slab width. Attempts were made to relate stiffnesses to assumed effective slab widths as shown by lines L1, L2 and L3 (figures 12.1 to 12.3). In each of these cases the width of the stirrup cage was taken because the horizontal portions of the stirrups provide considerable horizontal reinforcement in this region.

i) The relationship shown by L1 was based on a slab width of 600 mm, which in this case is approximately the door opening width, and was computed assuming 50% of the gross concrete moment of inertia of that width. This is equivalent to a width of half the stirrup cage width in the uncracked state.

ii) The relationship L2 was computed in the same way as L1 except that 20% of the gross moment of inertia of the concrete area was assumed. This corresponds to an effective width of 20% of the stirrup cage width.

iii) The relationship L3 was computed by considering only the steel within the stirrup cage.

It is apparent that the effective width in the first elastic cycle is much smaller than the values of all previous elastic theory predictions and it becomes extremely small on subsequent load cycling.

Comparison was made between these test results and the results of Szalwinski [75] which he obtained from a monotonic test of a slab coupling specimen. In his experimental study, Szalwinski measured a stiffness equivalent to an effective width of uncracked concrete of 260 mm while in his elastic finite element study he computed a width of 600 mm for the same specimen. These dimensions correspond to 68% and 158% of the corridor width, respectively. Considering that the door opening in Szalwinski's test was 65%, and the slab thickness 50% of the values for the tests reported here, his experimental effective widths are significantly higher. The large effective width computed in his elastic finite element study shows the effect of cracking in the reinforced concrete specimens.

For dynamic modelling purposes it is suggested that line L2 be used to estimate an initial slab stiffness while Clough's [37] degrading stiffness rule should be used to represent stiffness deterioration.

12.10.2 Unit 4

Effective widths of slabs were assessed for unit 4 and stiffness computations were based on an ACI 318-71 [78] effective T-beam with a 440 mm wide flange. This was considered with the following variations:

i) The relationship shown by L1 (figure 12.4) was derived from 50% of the moment of inertia of the gross section of the T-beam.

ii) The relationship shown by L2 was computed as in i) except that 20% of the moment of inertia of the gross concrete section was assumed.

The two plotted relationships (L1 and L2) provide an indication of the structural stiffness in the initial elastic cycles. Again considerable stiffness degradation occurred and a Clough [37] degrading stiffness model is suggested. The shear distortions in the beam are expected to have made a considerable contribution to the stiffness degradation.

12.11 DESIGN CONSIDERATIONS

12.11.1 Interpretation of Results for the Design of Slab Coupling

a) Longitudinal Reinforcement

Observed results indicate that, although yielding was observed in the longitudinal seismic reinforcement near the slab edges, the effectiveness of the outer bars reduced rapidly as load cycling continued. Therefore it is suggested that the minimum allowable longitudinal steel be used in the slab outside the corridor region which, in this case, was taken as a strip of slab parallel to the walls and equal to the width of the stirrup cage (approximately equal to door opening width). Longitudinal reinforcement placed inside the stirrup cage and within the corridor region defined above should provide fully effective coupling.

b) Stiffness

In most typical shear wall structures, it is considered that slab coupling will make only minor contributions to the structural response. A sensitivity study of the importance of the relative stiffness of walls and coupling elements of a 20-storey shear wall building [8] has shown coupling beams of a depth to span ratio of 0.08 (600 mm wide) to provide less than 25% of the total overturning moment. The conclusion reached was that coupling efficiency diminishes rapidly after the depth to span ratio falls below a certain value - approximately 0.2 for the 20-storey structure. Certainly for slab coupled shear wall structures of less than 10 floors, which are likely to be encountered in New Zealand, the beneficial coupling effect of the slab will be small, especially after the first large load cycle.

c) Shear Reinforcement

With the object of controlling punching shear in particular, the following types of shear reinforcement may be used:

i) The design of slab stirrups across the door opening is nominal when the slab section is considered as a beam, because shear stresses are low. Stirrups are provided mainly for confinement of the flexural steel across the corridor width.

ii) When these slab stirrups are continued behind the wall toe, they provide punching shear control by acting in shear friction. However, because the necessary clamping force can only be provided by a number of stirrups extending over a distance behind the wall toe, considerable deformations must occur at the wall toe before a sufficient number of stirrups are mobilised.

iii) The provision of additional horizontal reinforcement, concentrated at the wall toes provides the necessary normal force for a shear friction mechanism in a region closer to the wall toes. In unit 2 where horizontal transverse reinforcement was provided, shear deformations were significantly reduced in comparison with unit 1. In general, reduced shear deformations in the wall toe region will occur with increased quantities of transverse steel because the shear transfer is concentrated closer to the wall edge.

iv) The most promising suggestion is to provide shear strength and stiffness with a structural steel member in wall toe regions. For the unit 3 test, the total seismic shears summed across full width yield lines (see section 11.4.3) were considered to be carried by the steel section. The steel sections extended approximately one corridor width each side of the walls. Excellent punching shear control was observed.

In the writer's opinion, the use of structural steel for full seismic shear transfer, as in unit 3, to minimise damaging shear deformation in the wall toe region, is highly desirable. It is thought that the special transverse flexural reinforcement across the wall toes in unit 3 (section 11.4.4) could have been omitted without resulting in a significant change in behaviour.

12.11.2 Assessment of Beam-Slab Interaction

One of the more important remaining unidentified quantities in high-rise concrete structures, in both shear wall and frame structures, is the strength enhancement afforded by a slab cast monolithically with a beam. It is apparent that a substantial enhancement of the beam yield moments can result from slab interaction which, in unit 4, led to a failure of the beam stirrups. With the limitations of data from a single test only, the following design recommendations are made:

i) Longitudinal reinforcement in the slab outside the immediate corridor region should be kept to a minimum.

ii) Only the slab steel within corridor region (see section 12.11.1(a)) should be considered in the flexural design of the beam. The ACI 318-71 effective beam width recommendations are satisfactory for design of the flexural capacity for code loadings.

iii) Critical conditions which are given by either the tensile capacity of all of the slab steel or the maximum moment when the corresponding beam compression area crushes, whichever is least, should be used to compute the flexural capacity of the coupling system from which to derive maximum shears.

iv) A vertical sliding shear failure at the wall toe appears to be less critical than a failure due to horizontal shear in the beam because the slab has the capacity to transfer vertical shear to the wall toes and prevents large axial elongations of the beam. Further study is necessary to identify the interaction in a variety of typical cases. Suggested configurations include conventionally reinforced coupling beams of greater depth than unit 4 and deep (depth to span ratio near one) diagonally reinforced coupling beams [3,4]. For the diagonally reinforced coupling beam the longitudinal slab steel, acting as a tension member, is likely to increase the capacity significantly during maximum cycles only. This is because the slab steel may be expected to yield in tension for load cycling in either direction. Alternatively, a compression failure in the beam could occur before the slab steel yields.

CHAPTER THIRTEEN

A SUMMARY AND RECOMMENDATIONS FOR FUTURE RESEARCH

13.1 DYNAMIC RESPONSE STUDY

13.1.1 Program Reliability

During the course of this study it has been shown that unless the computer idealisation realistically models the actual structure and that the computational process is operating in a reliable manner, the quantitative results obtained from a dynamic "time history" analysis may be meaningless. The following program verification steps have been carried out:

i) The numerical integration schemes were checked against analytical solutions for a simple elastic structure.

ii) The stability and accuracy of Newmark's constant average acceleration ($\beta = \frac{1}{4}$) scheme were examined in a simple nonlinear single element structure to ensure that the scheme was operating satisfactorily for nonlinear problems.

iii) Five different nonlinear flexural elements were used in a two-element model in order to compare their accuracy and effects on numerical stability.

iv) A typical 10-storey cantilever shear wall was studied to check on the solution procedure when applied to larger problems.

A considerable portion of the research effort has been devoted towards ensuring the reliable operation of the developed program. It is suggested for future research projects that program verification could, in many cases, prove more valuable than a proliferation of new unproved algorithms.

13.1.2 Mathematical Modelling

A study of the characteristics of shear walls has been made and in order to select an appropriate mathematical model, a range of various types of model were considered. Elastic models, although widely accepted for design purposes, were considered unsuited to the computation of seismic responses. Nonlinear general purpose Finite Element models, capable of representing continua in detail, were also shown to be impracticable because of the excessive computational effort required. A study of

previous experimental work has shown a flexural model to be able to represent the behaviour of tall shear wall structures with an acceptable degree of accuracy during nonlinear portions of the response. Section analyses within these elements to determine structural stiffnesses during each time step of the analysis overcomes the difficulty of creating moment - curvature - axial load interaction curves for the walls. This approach also recognises the eccentricity of the instantaneous stiffness centroid and shows the resulting changes in structural geometry to be significant in coupled shear walls. The idealisation of materials is relatively simple but the numerical problems which are likely to be encountered with any practical stress-strain relationship have been satisfactorily dealt with by the numerical integration.

Modelling of shear deformations is probably the most significant remaining difficulty and hence opportunity for future research. Although errors in shear stiffness have been shown to have a minimal influence on the displacements of the ten-storey structure (see Chapter 9) the high shear forces computed in this and other studies are believed to be a direct result of the limitations of the shear model. A more accurate shear model, which allows for a reduction in shear stiffness after the occurrence of diagonal cracking ("stiff-soft" behaviour),is required if more accurate predictions of shear forces are to be made.

Now that the use of section idealisations in a full size dynamic analysis has been demonstrated to be a feasible proposition, improvement of the accuracy of modelling is considered to be the next logical step. Development of the mathematical model within a nonlinear static analysis, where behaviour can be closely checked against experimental results, is suggested. When modifications are proposed satisfactory numerical and physical verification is considered to be essential because considerable complexity is present and any benefits must be demonstrated to outweigh additional effort.

13.1.3 Numerical Integration

A study of different types of integration scheme has been made in order to establish which integration scheme is most suitable for a shear wall response study. Explicit integration of the equations of motion was investigated as a means of minimising the large amount of computation necessary when stiffness matrix changes are required. Although a short, stability bounded time step is required, explicit schemes were competitive

in the case of a two-dimensional frame structure and they should be useful if three-dimensional dynamic analyses are attempted. However, the higher natural periods encountered with shear wall structures made the use of an unconditionally stable implicit integration scheme essential in this study.

Efforts to examine the accuracy of the selected Newmark $\beta = \frac{1}{4}$ scheme concentrated on nonlinear response conditions. Measures to correct the equilibrium imbalance arising after changes in stiffness, which were derived and examined for effectiveness, include:

(a) Out-of-phase force application.

(b) Iteration on the excess force vector.

(c) Iteration on the total equilibrium imbalance.

The out-of-phase force application proved very economical because current corrections are lumped in subsequent time steps and very little additional computation is necessary. This method was seen to be identical to one cycle of iteration on the excess force vector and is therefore limited when major stiffness changes occur. Both the iteration on the excess force vector and iteration on the total equilibrium imbalance operated satisfactorily and were seen to be valuable techniques, particularly in problems where large translations of the section stiffness centroid are encountered - e.g. rocking foundations.

Stability limits were examined with the main objective being to ensure satisfactory results in subsequent analyses. Newmark's constant acceleration technique appeared to remain unconditionally stable in nonlinear examples. However, a convergence limit was encountered when iterative equilibrium correction was attempted and this led to a divergent solution in some problems. The approach suggested here was to monitor convergence when iteration is attempted or to restrict the iteration to one cycle and achieve satisfactory accuracy by refining the time step.

There is a pressing need for further research on numerical integration techniques, with particular emphasis on the convergence problem, so that the integration operators may be used for a wide variety of problems with greater confidence.

13.1.4 Structural Response Study

The potential benefit of the preceding preliminary investigation, derivation, implementation and verification has been demonstrated by a typical structural response study. To gain an appreciation of numerous

aspects of a response, a 10-storey coupled shear wall structure was selected for which a comprehensive set of results, describing the performance of the structure, has been presented. These show the following significant findings:

i) The wall deformations conform closely to first mode deformation shapes.

ii) Significant axial elongation of the wall centrelines was observed when yielding at the wall bases takes place.

iii) Coupling beams tend to yield before walls.

iv) Wall moments reveal significant higher mode effects and high wall shear forces were observed.

v) Only small vertical inertial forces in the walls were observed.

Sensitivity of the structure to changes in earthquake record and changes in design has been investigated for a limited number of cases. From these the following conclusions were drawn:

i) Significant differences in the magnitude of the maximum deformations were observed when different earthquake records were used but the sequence of plastification remained essentially unchanged.

ii) There appears to be little justification for arbitrarily increasing wall moment capacity to ensure that coupling beams yield prior to the walls. Wall geometry and relative stiffnesses of walls and coupling beams are thought to be more important. The use of high strength steel delays wall yielding.

iii) Curtailment of the flexural steel in walls according to the elastic bending moment diagram for lateral static loads is likely to result in wall yielding at the points of curtailment over the height. A linear reduction of moment capacity with height is recommended.

iv) Maximum deformations were relatively insensitive to changes in the strength of the walls and the inclusion of base flexibility. In this particular example, base flexibility was highly beneficial in reducing ductility demands within the structure.

v) Design shears in walls should be higher than those computed from code static loadings although the use of the maximum shear forces computed in this study would be excessive because of limitations of the shear model.

It has been demonstrated that the use of section idealisations in the dynamic analysis of typical size structures is practical to perform and allows a realistic representation of behaviour. A continuation of this study is desirable, where a wide range of structures are examined so that the general applicability of the above conclusions may be established.

13.2 EXPERIMENTAL STUDY OF SLAB COUPLING OF SHEAR WALLS

13.2.1 Slab Reinforcement Solutions and Coupling Stiffness

One example of experimental component testing, that of slab coupling between walls, has been undertaken with the dual outcome of load - deformation responses and recommendations for the design of the reinforcement:

i) A tendency towards a punching shear failure at the wall toe was observed in all cases and this should be controlled if surface damage and excessive stiffness degradation are to be avoided.

ii) Transverse flexural reinforcement, acting in shear friction, was seen to prevent a total punching shear failure although distortions became large in some cases.

iii) Structural steel sections provided beneficial shear stiffness in addition to preventing a punching shear failure.

iv) Longitudinal seismic steel placed across the slab width exhibited a high degree of participation at peak cycles although the effectiveness of the outer bars in resisting seismic actions was substantially reduced after repeated load cycling.

v) The slab stiffness was considerably lower than predicted by previous elastic studies and severe stiffness degradation was observed after cycling of the load. The suggested type of model for analysis purposes is a Clough degrading stiffness model [37].

The overall conclusion is that in most shear wall-slab structures constructed in New Zealand (typically 10-storeys) the floor slab coupling will make a negligible contribution to the overall response. Control of damage to the slab should be the designers main objective.

13.2.2 Composite Beam - Slab Action

It was confirmed that a considerable enhancement of coupling beam ultimate moments can result from the composite action of a monolithically cast slab. The unit 4 slab was found to enhance beam coupling moments to a much greater extent than is normally assumed and further testing is vital if accurate strength estimates of typical beam-slab components are to be obtained. Particular attention should be given to the provision of shear

reinforcement in the beam to prevent a non-ductile failure of the beam due to horizontal shear.

REFERENCES

1. Bertero, V.V., Mahin, S.A. and Hollings, J., "Response of a Reinforced Concrete Shearwall During the 1972 Managua Earthquake", Bulletin of N.Z. National Society for Earthquake Engineering, Vol. 7, No. 3, September 1974.

2. Penzien, J., "Predicting the Performance of Structures in Regions of High Seismicity", Second Canadian Conference on Earthquake Engineering, Hamilton, Ontario, June 1975.

3. Paulay, T., "Coupling Beams of Reinforced Concrete Shear Walls", Proceedings, Structural Division, ASCE, Vol. 97, No. ST3, March 1971, pp. 843-862.

4. Binney, J.R., "Diagonally Reinforced Coupling Beams", M.E. Report, University of Canterbury, Christchurch, New Zealand, Feb. 1972.

5. Fenwick, R.C. and Paulay, T., "Mechanisms of Shear Resistance of Concrete Beams", Journal of the Structural Division, ASCE, Vol. 94, ST10, Oct. 1968, pp.2235-2350.

6. O'Leary, A.J., "Shear, Flexure and Axial Tension in Reinforced Concrete Members", Ph.D. Thesis, University of Canterbury, Christchurch, New Zealand, 1970, 368pp.

7. Paulay, T., Park, R. and Phillips, M.H., "Horizontal Construction Joints in Cast In Place Reinforced Concrete", SP-42, American Concrete Institute, Detroit, 1974, pp.599-616.

8. Santhakumar, A.R., "Ductility of Coupled Shear Walls", Ph.D. Thesis, University of Canterbury, Christchurch, New Zealand, Oct. 1974, 385pp.

9. Spurr, D.D., "The Post-Elastic Response of Frame-Shear Wall Assemblies Subjected to Simulated Seismic Loading", Ph.D. Thesis, University of Canterbury, New Zealand. To be published.

10. Carpenter, J.E., Fiorato, A.E., Barney, G.B., Kaar, P.H., Oesterle, R.G., Russell, H.G. and Corley, W.G., "Structural Walls in Earthquake Resistant Structures, Experimental Investigation Progress Report", Report to National Science Foundation Grant No. G1-43880, Portland Cement Association, Old Orchard Road, Skokie, Ill., Aug., 1975.

11. Newmark, N.M., "A Method of Computation for Structural Dynamics", Journal of the Engineering Mechanics Division, ASCE, Vol. 85, No. EM3, Proc. Paper 2094, July, 1959, pp.67-94.

12. Sharpe, R.D., "The Seismic Response of Inelastic Structures", Ph.D. Thesis, University of Canterbury, Christchurch, New Zealand, Nov. 1974, 126 pp.

13. Symposium on Tall Buildings With Particular Reference to Shear Wall Structures, University of Southampton, April, 1966, Oxford, Pergamon Press, 1967, 607pp.

14. Phillips, D.V. and Zienkiewicz, O.C., "Finite Element Nonlinear Analysis of Concrete Structures", Proceedings of The Institute of Civil Engineers, Part 2, March 1976, pp.59-88.

15. Fintel, M., Derecho, A.T., Freskakis, G.N., Fugelso, L.E. and Ghosh, S.K., "Structural Walls in Earthquake Resistant Structures, Analytical Investigation Progress Report", Report to National Science Foundation Grant No. G1-43880, Portland Cement Association, Old Orchard Road, Skokie, Ill., Aug., 1975.

16. Blakeley, R.W.G., Cooney, R.C. and Megget, L.M., "Seismic Shear Loading at Flexural Capacity in Cantilever Shear Wall Structures", Bulletin of the New Zealand National Society for Earthquake Engineering, Vol. 8, No. 4, Dec. 1975.

17. Clough, R.W. and Benuska, K.L., "F.H.A. Study of Seismic Design Criteria for High-Rise Buildings", U.S. Department of Housing and Urban Development Report, Federal Housing Administration, Washington, HUD, TS-3, August, 1966.

18. Gormack, P.J., "Non-linear Finite Element Analysis of Shear Walls and Two Dimensional Reinforced Concrete Structures", M.E. Report, University of Canterbury, Christchurch, New Zealand, Feb. 1974, 111pp.

19. Cervenka, V., "Inelastic Finite Element Analysis of Reinforced Concrete Panels Under In-Plane Loads, Ph.D. Thesis, Dept. of Civil Engineering, University of Colorado, 1970, 241pp.

20. Cervenka, V. and Gerstle, K.H., "Inelastic Analysis of Reinforced Concrete Panels Under In-Plane Loads", Symposium on Inelasticity and Non-Linearity in Structural Concrete, University of Waterloo, Ontario, Canada, 1972, pp.333-343.

21. Franklin, H.A., "Non-Linear Analysis of Reinforced Concrete Frames and Panels", Ph.D. Thesis, University of California, Berkeley, California, March 1970, 259pp.

22. Aldstedt, E. and Bergan, P.G., "Large Deformation and Stability Analysis of Reinforced Concrete Frames Considering Material Non-Linearities", Symposium on Design and Safety of Reinforced Concrete Compression Members, Quebec, Canada, August 1974.

23. Paulay, T., "An Elasto-Plastic Analysis of Coupled Shear Walls", Proceedings, ACI Journal, Vol. 67, 1970, pp. 915-922.

24. Winokur, A. and Gluck, J., "Ultimate Strength Analysis of Coupled Shear Walls", Proceedings, ACI Journal, Vol. 65, Dec. 1968, pp. 1029-1036.

25. Gluck, J., "Elasto-Plastic Analysis of Coupled Shear Walls", Proceedings, Structural Division, ASCE, Vol. 99, No. ST8, Aug. 1973, pp. 1743-1760.

26. Bertero, V.V., "Research Needs in Limit Design of Reinforced Concrete Structures", Earthquake Engineering Research Center, Report No. EERC71-4, University of California, Berkeley, June 1971, 45pp.

27. Bertero, V.V., "Identification of Research Needs for Improving the Aseismic Design of Building Structures", Bulletin of N.Z. National Society for Earthquake Engineering, Vol. 9, No. 1, March 1976, pp.1 - 31.

28. MacLeod, I.A., "Lateral Stiffness of Shear Walls with Openings", Symposium on Tall Buildings, University of Southampton, April 1966, Pergamon Press, Oxford 1966, pp. 223-252.

29. Paulay, T., "The Coupling of Shear Walls", Ph.D. Thesis, University of Canterbury, Christchurch, New Zealand, 1969, 432pp.

30. Weaver, W. and Oakberg, R.G., "Analysis of Frames with Shear Walls by Finite Element Methods", Proceedings of the Symposium on Application of Finite Element Methods in Civil Engineering, Vanderbilt University, Nashville, Tennessee, Nov. 1969, pp. 567-600.

31. Girijavallabhan, C.V., "Analysis of Shear Walls by Finite Element Method", Proceedings of Symposium on Application of Finite Element Methods in Civil Engineering, Vanderbilt University, Nashville, Tennessee, Nov. 1969, pp.631-641.

32. Tottenham, H. and Brebbia, C., "Finite Element Techniques in Structural Mechanics", Chapter 8 Plasticity, Proceedings at Seminar at the University of Southampton, April 1970, Southampton University Press, pp.209-257.

33. Zienkiewicz, O. and Cheung, Y.K., "The Finite Element Method in Structural and Continuum Mechanics", McGraw-Hill Book Company, London, 1967, 272pp.

34. Zienkiewicz, O.C., Too, J. and Taylor, R.L., "Reduced Integration Technique in General Analysis of Plates and Shells", Int. J. Numerical Methods in Engineering, Vol. 3, 1971, pp.273-290.

35. Giberson, M.F., "Two Nonlinear Beams with Definitions of Ductility", Journal of the Structural Division, ASCE, Vol. 95, No. ST2, Proc. Paper 6377, February, 1969, pp.137-157.

36. Otani, S., "Inelastic Analysis of R/C Frame Structures", Journal of the Structural Division, ASCE, ST7, July 1974.

37. Clough, R.W., "Effect of Stiffness Degradation on Earthquake Ductility Requirements", Report No. 66-16, Structural Engineering Laboratory, University of California. Oct. 1966,67pp.

38. Turner, M.J.,Clough, R.W., Martin, H.C. and Topp, L.C., "Stiffness and Deflection Analysis of Complex Structures", Journal Aero. Sci. Vol. 23, No. 9, 1956.

39. Aoyama, H., "Moment-Curvature Characteristics of Reinforced Concrete Members Subjected to Axial Load and Reversal of Bending", Proceedings of the International Symposium on the Flexural Mechanics of Reinforced Concrete, Miami, Fla., Nov. 1964, pp. 183-212.

40. Cohn, M.Z. and Ghosh, S.K., "Ductility of Reinforced Concrete Sections in Bending", Symposium on Inelasticity and Non-Linearity in Structural Concrete, University of Waterloo, Ontario, Canada, 1972, pp.111-146.

41. Ghosh, S.K. and Cohn, M.Z., "Ductility of Reinforced Concrete Sections in Combined Bending and Axial Load", Symposium on Inelasticity and Non-Linearity in Structural Concrete, University of Waterloo, Ontario, Canada, 1972, pp.147-180.

42. Park, R., Kent, D.C. and Sampson, R.A., "Reinforced Concrete Members With Cyclic Loading", Journal of the Structural Division, ASCE, Vol. 98, No. ST7, Proc. paper 9011, July 1972, pp.1341-1360.

43. Kent, D.C., "Inelastic Behaviour of Reinforced Concrete Members with Cyclic Loading", Ph.D. Thesis, University of Canterbury, Christchurch, New Zealand, 1969, 246pp.

44. Thompson, K.J., "Ductility of Concrete Frames Under Seismic Loading", Ph.D. Thesis, University of Canterbury, Christchurch, New Zealand, 1969, 341pp.

45. Zienkiewicz, O.C. and Phillips, D.V., "Finite Element Nonlinear Analysis of Concrete Structures", The Institution of Civil Engineers, Proceedings, Part 2, March 1976, pp.59-88.

46. Fu, C.C., "On Stability of Explicit Methods for the Numerical Integration of the Equations of Motion in Finite Element Methods", International Journal for Numerical Methods in Engineering, Vol. 4, 95-107, (1972).

47. Gupta, K.K., "Dynamic Response Analysis of Geometrically Nonlinear Structures Subjected to High Impact", International Journal for Numerical Methods in Engineering, Vol. 4, 1972, pp.163-174.

48. Krieg, R.D. and Key, S.W., "Transient Shell Response By Numerical Time Integration", International Journal for Numerical Methods in Engineering, Vol. 7, 1973, pp. 273-286.

49. Hartzman, M. and Hutchinson, J.R., "Non-Linear Dynamics of Solids by the Finite Element Method", Computers and Structures, Vol. 2, 1972, pp.47-77.

50. Caughey, T.K., "Classical Normal Modes in Damped Linear Dynamic Systems", Journal of Applied Mechanics, ASME, Vol. 27, No. 2, Paper 59-A-62, June, 1960, pp. 269-271.

51. Wilson, E.L. and Penzien, J., "Evaluation of Orthogonal Damping Matrices" , International Journal for Numerical Methods in Engineering, Vol. 4, 5-10, 1972, pp. 5-10.

52. Nickell, R.E., "On the Stability of Approximation Operators in Problems of Structural Dynamics", International Journal of Solids and Structures, Pergamon Press, Vol. 7, 1971, pp.301-319.

53. MacNeal, R.H. and McCormick, C.W., "The NASTRAN Computer Program for Structural Analysis", Computers and Structures, Pergamon Press, Vol. 1, 1971, pp.389-412.

54. Dunham, R.S.,Nickell, R.E. and Stickler, D.C., "Integration Operators for Transient Structural Response", Computers and Structures, Pergamon Press, Vol. 2, 1972, pp. 1-15.

55. Bathe, K.J. and Wilson, E.L., "Linear and Nonlinear Earthquake Analysis of Complex Structures", Proceedings of the Fifth World Conference on Earthquake Engineering, Vol. 2, Rome, 1973, pp. 1796-1805.

56. Nickell, R.E., "Direct Integration Methods in Structural Dynamics", Journal of the Engineering Mechanics Division, ASCE, No. EM2, Proc. Paper 9652, April 1973, pp. 303-317.

57. Clough, R.W. and Wilson, E.L., "Dynamic Finite Element Analysis of Arbitrary Thin Shells", Computers and Structures, Pergamon Press, Vol. 1, 1971, pp.33-56.

58. Weeks, G., "Temporal Operators for Nonlinear Structural Dynamics Problems", Journal of the Engineering Mechanics Division, ASCE, Vol. 98, No. EM5, Proc. Paper 9260, October 1972, pp. 1087-1105.

59. Kanaan, K.A. and Powell, G.H., "General Purpose Program For Inelastic Dynamic Response Plane Structures", PB-221 260 NTIS (National Technical Information Service), U.S. Dept. Commerce, April 1973.

60. Bathe, K.J., Ekkehard, R., Wilson, E.L., "Finite Element Formulations for Large Deformation Dynamic Analysis", International Journal for Numerical Methods in Engineering, Vol. 9, 1975, John Wiley & Sons Ltd., pp. 353-386.

61. Archer, J.A., "Consistent Mass Matrix for Distributed Mass Systems", Journal of the Structural Division, ASCE, Vol. 89, No. ST4, Proc. Paper 3591, August, 1963, pp.161-178.

62. Argyris, J.H., "Continua and Discontinua", Proceedings of the Conference on Matrix Methods in Structural Mechanics, W.P.A.F.B., Dayton, Ohio, 1965, pp.11-190.

63. Taoka, G.T., Furumoto, A.S. and Chiu, A.N.L., "Dynamic Properties of Tall Shear Wall Buildings", Journal of the Structural Division, ASCE, ST2, Feb. 1974, pp. 305-317.

64. New Zealand Standard Model Building By-Law, "Basic Design Loads", NZSS 1900 Chapter 8, 1965, New Zealand Standards Institute, Wellington, New Zealand, 39pp.

65. Bertero, V.V. et al., "Rate of Loading Effects on Uncracked and Repaired Reinforced Concrete Members", Proceedings of the Fifth World Conference on Earthquake Engineering, Vol. 2, Rome, 1973, pp. 1461-1470.

66. Jennings, P.C., Housner, G.W. and Tsai, N.C., "Simulated Earthquake Motions for Design Purposes", Proceedings of the Fourth World Conference on Earthquake Engineering, Santiago, Chile, Vol. 1, January, 1969, pp.A1 145-160.

67. Nayar, K.K. and Coull, F., "Elastoplastic Analysis of Coupled Shear Walls", Journal of the Structural Division, ASCE, Vol. 102, No. ST9, Proc. Paper 12401, Sept. 1976, pp. 1845-1860.

68. Barnard, P. and Schwaighofer, J., "The Interaction of Shear Walls Connected Solely Through Slabs", Symposium on Tall Buildings, University of Southampton, April 1966, Pergamon Press, Oxford, 1966, pp. 157-173.

69. Qadeer, A. and Smith, B.S., "The Bending Stiffness of Slabs Connecting Shear Walls", ACI Journal, Proceedings Vol. 66, June 1969, pp. 464-473.

70. Michael, D., Discussion of "The Bending Stiffness of Slabs Connecting Shear Walls", by A. Qadeer and B.S. Smith, ACI Journal, Proceedings V66, No. 12, Dec. 1969, pp. 1021-1022.

71. Coull, A. and El Hag, A.A., "Effective Coupling of Shear Walls by Floor Slabs", ACI Journal, Proceedings V72, No. 8, August 1975, pp. 429-431.

72. Mirza, S. and Jaeger, L.G., "A Study of the Behaviour of Coupled Shear Wall Structures", First Canadian Conference on Earthquake Engineering, Vancouver, B.C., Canada, May 1971, pp. 252-268.

73. Simmonds, S.H., "Flat Slabs on Columns Elongated in Plan", ACI Journal, Proceedings V66, No. 12, Dec. 1970, pp. 967-975.

74. Schwaighofer, J. and Collins, M.P., "An Experimental Study of the Behaviour of Reinforced Concrete Coupling Slabs", ACI Journal, Proceedings V74, No. 3, March 1977, pp.123-127.

75. Szalwinski, C., "The Behaviour of Reinforced Concrete Coupling Slabs". M.Sc. Thesis, Department of Civil Engineering, University of Toronto, 1976, 144pp.

76. Rosman, R., "Approximate Analysis of Shear Walls Subjected to Lateral Loads", ACI Journal, Proceedings, Vol. 59, No. 8, August 1962, pp. 1055-1069.

77. Islam, S., "Limit Design of Reinforced Concrete Slabs", Ph.D. Thesis, University of Canterbury, Christchurch, New Zealand, 1973, 214pp.

78. ACI Standard 318-71, Building Code Requirements for Reinforced Concrete (ACI 318-71), American Concrete Institute, Detroit, 78pp.

79. Argyris, J.H., Dunne, P.C. and Angelopoulos, T., "Non-linear Oscillations Using the Finite Element Technique", Computer Methods in Applied Mechanics and Engineering 2, North Holland Publishing Company, 1973, pp.203-250.

80. Kelly, J.M., Skinner, R.I. and Heine, A.J., "Mechanisms of Energy Absorption in Special Devices for Use in Earthquake Resistant Structures", Bulletin of N.Z. Society for Earthquake Engineering, Vol. 5, No. 3, September 1972, pp.63-88.

81. Tuba, I.S. and Wright, W.B., Editors, "Pressure Vessel and Piping 1972 Computer Programs Verification", ASME, N.Y. 1972.

APPENDIX A

EQUILIBRIUM CORRECTION PROCEDURES FOR SINGLE DEGREE-OF-FREEDOM SYSTEMS

A.1 OUT-OF-PHASE EQUILIBRIUM CORRECTION

Definitions listed below generally agree with those used elsewhere and relate to the diagrams in this appendix. The time and iteration notation has been modified slightly from that used in Chapter 6 and although it is less general, it is simpler and conforms with the usual definitions for iteration in static problems.

Definitions

C - Damping coefficient

M - Mass

K_o - Initial tangent stiffness at the beginning of an increment

K_i - Tangent stiffness at i

K_{si} - Secant stiffness relating 0 and i

$\Delta U_{a,b,c}$ - Improved estimates of the incremental displacement

Δt - Time step

R - Externally applied force

F_i - Structural member force

F_o - Initial structural member force

Q - Dynamic force vector

In solving for an incremental displacement solution with Newmark's constant acceleration method, the first equation used is

$$\left[\frac{4}{\Delta t^2} M + \frac{2}{\Delta t} C + K_o\right] \Delta U_a = \Delta Q \qquad \text{(A-1)}$$

where ΔU_a, giving the displacement solution at 1 (figure A.1), is obtained. Because a nonlinear structural stiffness is present, repetition of the time step using an improved estimate of stiffness, the secant stiffness K_{s1}, should lead to an improved displacement solution ΔU_b.

$$\left[\frac{4}{\Delta t^2} M + \frac{2}{\Delta t} C + K_{s1}\right] \Delta U_b = \Delta Q \qquad \text{(A-2)}$$

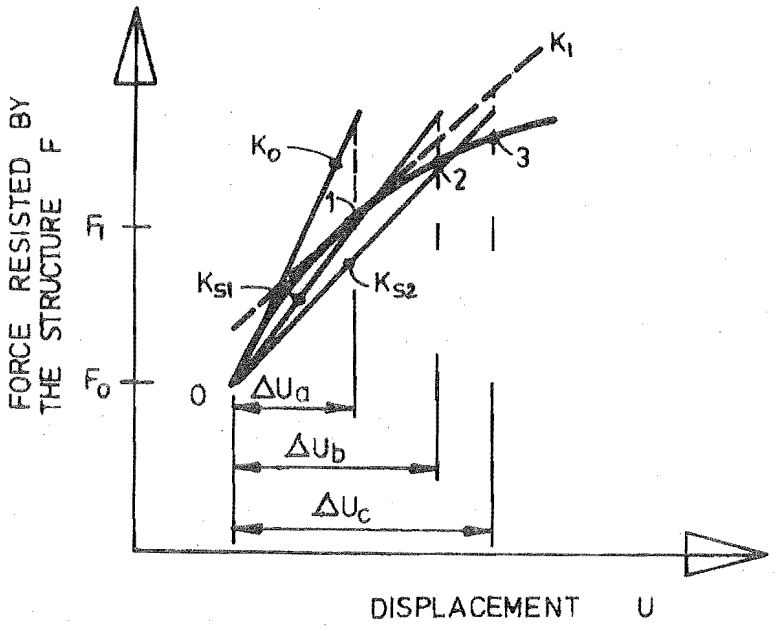

FIGURE A.1 : RESPONSE OF STRUCTURE DURING ITERATION.

This step is pure iteration within an increment. Subtracting equation A-2 from A-1 and defining

$$\Delta U_1 = \Delta U_b - \Delta U_a$$

leads to

$$\left[\frac{4}{\Delta t^2} M + \frac{2}{\Delta t} C + K_{s1}\right] \Delta U_1 = \Delta U_a (K_o - K_{s1}) \qquad \text{(A-3)}$$

Reference to figure A.2 shows the relationship between the out-of-balance force ΔR_1 and the correction term in equation A-3, which may be expressed as follows:

$$\Delta R_1 = \Delta U_a (K_o - K_{s1}) \qquad \text{(A-4)}$$

Although equation A-3 may be used directly and is compatible with most Finite Element models, it is convenient to use a direct evaluation of out-of-balance forces and equation A-5.

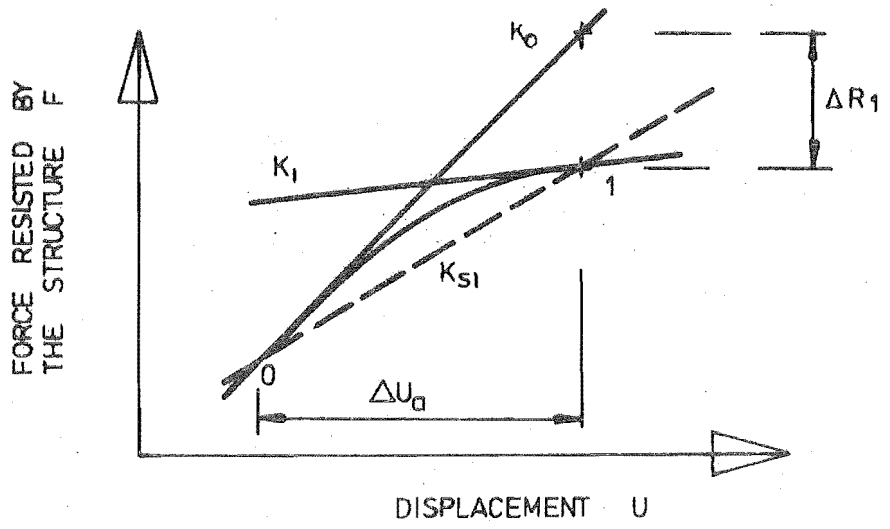

FIGURE A.2 : RELATIONSHIP BETWEEN STIFFNESS AND EXCESS FORCE

$$\left[\frac{4}{\Delta t^2} M + \frac{2}{\Delta t} C + K_{s1}\right]\Delta U_1 = \Delta R_1 \qquad \text{(A-5)}$$

In keeping with common practice in nonlinear analyses [79], it should be acceptable to replace K_{s1} in equation A-5 with K_o, K_1 or perhaps $\frac{1}{2}(K_o + K_1)$ if these are more convenient to use within the program. Usually a small error in stiffness is insignificant in comparison with damping and inertial forces when small displacement corrections are being made.

As a final step in deriving an out-of-phase correction, the procedure (A-5) may be incorporated into the subsequent increment. When point 1 (figure A-1) has been reached a new increment $\Delta U'_a$ may be calculated by using equation A-1 again:

$$\left[\frac{4}{\Delta t^2} M + \frac{2}{\Delta t} C + K_1\right]\Delta U'_a = \Delta Q' \qquad \text{(A-6)}$$

where $\Delta Q'$ is the incremental dynamic force for the new increment. Using a convenient modification of equation A-5, the equilibrium correction appropriate to the end of the step 0 - 1 (figure A.1) may be computed:

$$\left[\frac{4}{\Delta t^2} M + \frac{2}{\Delta t} C + K_1\right]\Delta U_1 = \Delta U_a (K_o - K_{s1}) \qquad \text{(A-7)}$$

Adding equations A-6 and A-7 gives

$$\left[\frac{4}{\Delta t^2} M + \frac{2}{\Delta t} C + K_1\right]\left(\Delta U'_a + \Delta U_1\right)$$

$$= \Delta Q' + \Delta U_a (K_o - K_{s1}) \qquad \text{(A-8)}$$

It can be seen that the incremental solution in equation A-8 contains the new incremental solution and a single cycle iteration on the previous increment.

A.2 ITERATION ON THE OUT-OF-BALANCE FORCE

By repeating the derivation above, the single cycle iteration may be extended to allow a number of iterations in an increment. Equation A-7 may be used as a recursive relation and a separate solution is obtained each iteration. Definitions in equation A-9 relate to figure A.1.

$$\left[\frac{4}{\Delta t^2}M + \frac{2}{\Delta t}C + K_i\right]\Delta U_i = (K_{i-1} - K_{si})\Delta U_j \qquad \text{(A-9)}$$

where $i = 1, 2 \ldots n$

and j takes values a, b, c ....

Variations on the use of K_i are possible.
It should be noted that equation A-9 applies after the initial incremental solution has been computed.

A.3 ITERATION ON THE TOTAL EQUILIBRIUM EQUATION

Instead of ensuring that individual increments satisfy incremental equilibrium, total equilibrium is examined and the appropriate corrections made.

The total external force is

$$R_G = -M\ddot{U}_g + P \qquad \text{(A-10)}$$

where P represents the initially applied loads.

The equilibrium imbalance after computing the initial incremental solution may be stated:

$$\Delta R_1 = R_G - M\ddot{U}_1 - C\dot{U}_1 - Fr_1 \qquad \text{(A-11)}$$

where Fr_1 is the internal force resisted
and $\ddot{U}_1$ and $\dot{U}_2$ are the values of acceleration and velocity computed at the end of the increment.

The complete equation may be written in a similar manner to equation A-9.

$$\left[\frac{4}{\Delta t^2} M + \frac{2}{\Delta t} C + K_i\right]\Delta U_i = R_G - M\ddot{U}_i - C_i\dot{U}_i - Fr_i \qquad \text{(A-12)}$$

where the definitions again relate to figure A.1.

Further practical details for a multi-degree-of-freedom system are described in Chapter 6.

APPENDIX B

EQUATION SOLVERS

B.1 ALGOL EQUATION SOLVER

```
PROCEDURE SYMS8L(NF,MF,A,B,MMAX,II);
VALUE NF,MF,MMAX,II;  REAL NF,MF,MMAX,II;
ARRAY A,B[*];
%
% PROGRAM TO SOLVE THE MATRIX EQUATION A*X=B.
% THE SEMI-BAND IS STORED AS A FULL RECTANGULAR MATRIX
% *** AND REQUIRES THE DIMENSIONS OF ARRAY A ***
% *** TO BE REVERSED COMPARED WITH THE FORTRAN VERSION ***
% *** TO ALLOW EFFICIENT PROCESSING ON THE B6700 ***
% *** ALSO MMAX IS THE LENGTH OF EACH COLUMN ***
% *** IN THE REVERSED ARRAY A ***
%
% II=1 REDUCES(A)TO ITS TRIANGULAR FORM
% II=2 DOES BACK SUBSTITUTION TO OBTAIN(X)
% II=3 DOES BOTH
%
BEGIN

  REAL N,M;
  REAL I,J,A1,L,C;
  N:=NF-1;  M:=MF-1; %ADJUST TO ALGOL UPPER BOUNDS
  IF BOOLEAN(II) THEN % II IS ODD
  BEGIN
    FOR I:=0 STEP 1 UNTIL N DO
    BEGIN
      A1:=1/A[I*MMAX];
      L:=I;
      FOR J:=1 STEP 1 UNTIL M DO
      BEGIN
        C:=A[J+I*MMAX]*A1;
        IF(L:=*+1)LEQ N THEN
        DO VECTORMODE (A[L*MMAX],AI=A[J+I*MMAX],FOR
          (M-J+1))BEGIN
          A:=A-C*AI;
          INCREMENT A,AI;
        END;
        A[J+I*MMAX]:=C;
      END OF J LOOP;
    END OF I LOOP;
  END OF TRIANGULAR REDUCTION;
%
% REDUCE THE VECTOR B=LDY WHERE Y IS STORED IN B
%
  IF II GTR 1 THEN
  BEGIN
    FOR I:=0 STEP 1 UNTIL N DO
    BEGIN
      C:=B[I];
      IF I LSS N THEN
      DO VECTORMODE(B[I+1],A[1+I*MMAX],FOR MIN(M,N-I))
      BEGIN
        B:=B-A*C;
        INCREMENT A,B;
      END;
      B[I]:=*/A[I*MMAX];
    END OF I LOOP;
%
% BACK SUBSTITUTE Y=UX WHERE X IS STORED IN Y
%
    FOR I:=(N-1)STEP -1 UNTIL 0 DO
    DO VECTORMODE(B[I+1],BI=B[I],A[1+I*MMAX],
      FOR MIN(M,N-I))
    BEGIN
      BI:=BI-A*B;
      INCREMENT A,B;
    END;
  END OF BACK SUBSTITUTION;
END OF SYMS8L.
```

B.2 COMPLEMENTARY FORTRAN VERSION

```
      SUBROUTINE SYMSOL (N,M,A,B,NMAX,II)
C     ***********************************************************************
C
C     PROGRAM TO SOLVE THE MATRIX EQUATION A*X=B.
C     THIS IS A VERSION OF SYMSOL FOR USE WHEN THE SEMI-BAND ONLY IS
C     STORED AS A FULL RECTANGULAR MATRIX.
C
C     II = 1 REDUCES (A) TO ITS TRIANGULAR FORM.
C     II = 2 CARRIES OUT THE BACK SUBSTITUTION METHOD TO OBTAIN (X).
C     II = 3  DOES BOTH.
C
C     ***********************************************************************
C
      DIMENSION A(NMAX,1),B(1)
C
      GO TO (100,101,100),II
C
C     M IS THE BAND-WIDTH OF MATRIX (A).
C
C     REDUCE MATRIX TO   A=LDU.
C
  100 DO 3 I=1,N
      DO 2 J=2,M
      C=A(J,I)/A(1,I)
      L=I+J-1
      IF(N.LT.L) GO TO 2
      JJ=0
      DO 1 K=J,M
      JJ=JJ+1
    1 A(JJ,L)=A(JJ,L)-C*A(K,I)
    2 A(J,I)=C
    3 CONTINUE
      IF(II.NE.3) RETURN
C
C     REDUCE THE VECTOR    B=LDY    WHERE Y IS STORED IN B.
C
  101 DO 5 I=1,N
      DO 4 J=2,M
      L=I+J-1
      IF(N.LT.L) GO TO 5
    4 B(L)=B(L)-A(J,I)*B(I)
    5 B(I)=B(I)/A(1,I)
C
C     BACK SUBSTITUTE    Y=UX    WHERE X IS STORED IN Y.
C
      I=N
    6 I=I-1
      IF(I.EQ.0) GO TO 8
      DO 7 J=2,M
      L=I+J-1
      IF(N.LT.L) GO TO 7
      B(I)=B(I)-A(J,I)*B(L)
    7 CONTINUE
      GO TO 6
    8 CONTINUE
      RETURN
      END
```

Classn:

THE NONLINEAR SEISMIC RESPONSE OF TALL SHEAR WALL STRUCTURES

R.G. Taylor

ABSTRACT: Details of preliminary investigations, derivations, implementation and verification of a time-history dynamic analysis for shear walls are presented. Problems encountered are described. The coupling of shear walls by slabs was investigated experimentally to provide information for design and dynamic response computation for slab - shear wall structures.

Department of Civil Engineering, University of Canterbury, Research Report No. 77-12, 1977.